Protein oxidation in human cells exposed to UVA photosensitising therapeutics

Melisa Guven

University College London

and

The Francis Crick Institute

PhD Supervisor: Dr. Peter Karran

A thesis submitted for the degree of

Doctor of Philosophy

University College London

September 2016

Declaration

I, Melisa Guven, confirm that the work presented in this thesis is my own. Where information has been derived from other sources, I confirm that this has been indicated in the thesis.

Abstract

Solar ultraviolet radiation (UV) comprising ≥ 95% UVA (320-400nm) and around 5% UVB (280-320nm), is a carcinogen. Nucleotide excision repair (NER) removes UVB-induced DNA lesions. Defective NER is associated with photosensitivity and an increased risk of sunlight-induced skin cancer. Some drugs including the immunosuppressant azathioprine and the fluoroquinolone antibiotics, cause photosensitivity and increase skin cancer risk. Azathioprine treatment results in the incorporation of 6-thioguanine (6-TG) into DNA where it interacts with UVA radiation to generate reactive oxygen species (ROS). ROS generated by DNA 6-TG+UVA or fluoroquinolone+UVA damage proteins, including those involved in NER. This protein damage results in NER inhibition. Replication protein A (RPA), the human single-stranded DNA binding protein essential for NER is particularly susceptible to damage by ROS. I investigated RPA oxidation in cultured human cells and identified several oxidised forms of RPA that are generated by 6-TG+UVA and fluoroquinolone+UVA treatments. Using cells expressing different levels of RPA, I examined the relationship between RPA oxidation and NER inhibition. My findings demonstrate that RPA is limiting for NER under oxidative stress conditions and that damage to RPA is the main contributor to oxidation-related NER inhibition. The vulnerability of NER to inhibition by oxidation links cutaneous photosensitivity, protein damage, and increased skin cancer risk and indicates that in addition to DNA damage itself, damage to DNA repair proteins may be an important factor in skin cancer risk.

The oxidative stress conditions generated by photosensitiser+UVA combinations also favour the formation of DNA-protein crosslinks (DPCs). I developed a sensitive and statistically rigorous proteomics-based method to study DPCs induced by oxidizing treatments. This novel approach provided a detailed analysis of the DPCs associated with 6-TG treatment and by the UVA activation of DNA 6-TG. It also provided the first demonstration that UVA activation of the fluoroquinolone antibiotic ciprofloxacin induces extensive DPC formation. Proteomic analysis identified more than 2000 cellular proteins that were crosslinked to DNA by 6-TG or by 6-TG+UVA. The proteins most susceptible to DNA crosslinking, were involved in control of gene expression and DNA repair and/or replication, including RPA. The findings indicate that DPCs are a significant product of photochemically-induced oxidative stress and may contribute to impaired DNA repair and an increased risk of permanent genetic damage.

Acknowledgement

Firstly, I'd like to express my deepest gratitude to my supervisor Dr Peter Karran for giving me the opportunity to work on this project and be a part of his lab full of wonderful people. His unwavering patience, guidance and support made the last four years a great learning experience. I even understand a bit of cricket now!

That's a lie, I still don't get it.

I'd like to thank my thesis committee members, Drs Mark Petronczki and Bram Snijders for their guidance and input during my PhD. I'd especially like to acknowledge Dr Snijders and Dr Karin Barnouin for their invaluable help and support with the mass spectrometry section of my thesis. I am also very grateful to Drs Luis Toledo and Jiri Lukas for providing me with the cell lines used in this thesis.

I would like to thank the past and present members of the Karran Lab for making it a wonderful place to work. Firstly, I'd like to thank Dr Reto Brem for his good humour, incredible patience, useful advice and lending me books that I still haven't returned. I would also like to thank Mr Peter Macpherson for always going out of his way to help me. Even though they all left the lab/abandoned me at different stages throughout my PhD, I'd like to thank Drs Lizzie McAdam-Gray, Matthew Peacock and Quentin Gueranger for teaching me, giving me advice and making me laugh even when science wasn't going my way.

I would like to express my gratitude to the Francis Crick Institute Cell Services, lab aides and admin staff for spoiling me with their help and hard work. I'd like to thank my fellow Clare Hall PhD students for helping me keep my sanity at times when it was very nearly lost.

Finally, I'd very much like to thank my parents and sister for being their amazing selves and putting up with me and supporting me my whole life. I know you wanted me to be a doctor, so this counts right?

Publications

Full versions of these publications are attached at the end of this thesis

*Guven, M., Brem, R., Macpherson, P., Peacock, M., and Karran, P. (2015). Oxidative Damage to RPA Limits the Nucleotide Excision Repair Capacity of Human Cells. J Invest Dermatol 135, 2834–2841.

**Guven, M., Barnouin, K., Snijders, A.P. and Karran, P. (2016). Photosensitized UVA-Induced Cross-Linking between Human DNA Repair and Replication Proteins and DNA Revealed by Proteomic Analysis. J Proteome Res. 15, 4612-4623.

*Brem, R., Guven, M. and Karran, P. (2016). Oxidatively-generated damage to DNA and proteins mediated by photosensitized UVA. Free Radic Biol Med. In press.

Reprinted with permission from Elsevier* and the American Chemical Society**

Table of Contents

Table of figures

List of tables

Abbreviations

•OH	Hydroxyl radical
$^1O_2$	Singlet oxygen
6-MP	6-mercaptopurine
6-TG	6-Thioguanine
6,4 Py:Py	6,4 pyrimidine-pyrimidone
8-oxo-dG	8-oxo-7,8-dihydro-2‘-deoxyguanosine
AA	Ascorbic acid
AcGFP	Green fluorescent protein
ALE/AGE	Advanced lipoxidation/glycation end products
AP	Apurinic/apyrimidinic
BCC	Basal cell carcinoma
BER	Base excision repair
BP-1	Biotin-1,3-cyclopentanedione
CM-H_2DCFDA	5-(and-6)-chloromethyl-2’,7’-dichlorodihydrofluorescein diacetate, acetyl ester
CPD	Cyclobutane-pyrimidine dimer
DBD	DNA binding domain
DPC	DNA-protein crosslinks
DSBs	Double strand breaks
dsDNA	Double-strand DNA
ELISA	Enzyme-linked immunosorbent assay
EMSA	Electrophoretic mobility shift assay
FA	Fanconi anaemia
FACS	Fluorescence-activated cell sorting
FCS	Foetal Calf Serum
FICZ	6-formylindolo[3,2-b]carbazole
GPX	Glutathione peroxidases
GR	Glutathione reductase
GSH	Glutathione
G^{SO2}	Guanine sulfinate
G^{SO3}	Guanine sulfonate

GSSG	Oxidised glutathione
H/L	Heavy/Light SILAC ratio
HPLC	High-performance liquid chromatography
HR	Homologous recombination
HU	Hydroxyurea
ICL	Interstrand crosslink
IR	Ionising radiation
MMR	Mismatch repair
MS	Mass Spectrometry
NAC	N-acetylcysteine
NER	Nucleotide excision repair
NHEJ	Non-homologous end joining
$O_2^{\bullet -}$	Superoxide anion
OB	Oligonucleotide binding
ORF	Open reading frame
PAGE	Polyacrylamide gel electrophoresis
Pen/Strep	Penicillin and streptomycin
PRX	Peroxiredoxins
PVDF	Polyvinylidene difluoride
RIPA	Radioimmunoprecipitation Assay
RNS	Reactive nitrogen species
ROS	Reactive oxygen species
SCC	Squamous cell carcinoma
SILAC	Stable isotope labelling by amino acids in cell culture
SOD	Superoxide dismutase
SSB	Single strand break
ssDNA	Single-strand DNA
TLS	Translesion synthesis
TRXR	Thioredoxin reductase
UV	Ultraviolet radiation
XP	Xeroderma pigmentosum

Chapter 1. Introduction

1.1 Oxygen and reactive oxygen species

Oxygen is essential for aerobic life. Paradoxically, it is also converted to reactive oxygen species (ROS), which can damage cellular components. As a consequence, cells have evolved powerful antioxidant defences and the existence of a plethora of these defences underlines the threat that ROS pose to cellular homeostasis. When the level of ROS production overwhelms antioxidant protection, cells succumb to oxidative stress, which can be detrimental to cellular function and is linked to cancer, premature aging, cardiovascular dysfunction and neurodegenerative diseases (Halliwell, 1998). More recently, the role of ROS in signalling and regulation of biological and physiological processes has been uncovered (Finkel, 2011). It has been shown to have a role in several cellular processes including cellular differentiation and tissue regeneration (reviewed in (Schieber and Chandel, 2014)).

Oxygen is in a triplet ground state and contains two unpaired electrons of parallel spin. This is unusual as most organic molecules exist in a singlet ground state with paired electrons of antiparallel spin. Quantum mechanical restrictions (Pauli exclusion principle) dictate pairing of electrons in the same orbital with antiparallel spins for reactions to occur. This means that reactions between singlet and triplet state molecules are rare and extremely slow (Halliwell, 1991). Whilst this restriction is protective against reactions between ground state oxygen and cellular components, the triplet state enables oxygen to react rapidly with radical species.

In respiring cells, molecular oxygen (O_2) is reduced to water with 4 electrons (e^-) at the end of the mitochondrial electron transport chain through cytochrome c oxidase (complex IV) (equation 1):

$$O_2 + 4H^+ + 4e^- \longrightarrow 2H_2O \qquad (1)$$

This mechanism is in place to restrict univalent reduction of O_2 that can result in the formation of reactive intermediates. Leakage of single electrons may occur from mitochondrial complexes I-III, however, resulting in partial reduction of O_2 to

superoxide ($O_2\bullet^-$), hydrogen peroxide (H_2O_2) and hydroxyl radical (•OH) (Figure 1.1) (Frei, 1994). The reduction potentials in Figure 1.1 explain the affinity of each ROS for electrons and their tendency to be reduced.

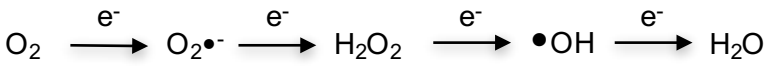

Reduction potential (V)	0.94	0.32	2.31
Half-life (seconds)	10^{-6}	10^{-5}	10^{-9}
***In vivo* concentration (M)**	10^{-10}	10^{-7}	10^{-15}

Figure 1.1: Univalent reduction of O_2 to H_2O and the characteristics of the intermediate products. Adapted from (Giorgio et al., 2007)

Free radicals contain one or more unpaired electrons (designated •) that render them generally more reactive than non-radical molecules. Radicals can react with non-radicals or with other radicals. The reaction between a radical and a non-radical generates a second radical species and reactions involving free radicals tend to be chain reactions (Halliwell, 1991). In order to terminate this chain reaction, a radical must form electron pairs with another free radical or be quenched by a free radical scavenger (Nordberg and Arner, 2001).

1.1.1 Hydroxyl radical

•OH is the most biologically reactive free radical. It can be produced due to exposure to ionising radiation, where most of the energy is absorbed by water in the cell. This breaks the single covalent bond between oxygen and hydrogen resulting in •H and •OH (Halliwell, 1991). The *in vivo* formation of •OH from the significantly less-reactive $O_2\bullet^-$ or H_2O_2 can also be catalysed by trace amounts of transition metals in the Haber-Weiss and Fenton reactions (equation 2 & 3):

$$Fe^{3+} + O_2\bullet^- \longrightarrow Fe^{2+} + O_2 \quad (2)$$

$$Fe^{2+} + H_2O_2 \longrightarrow Fe^{3+} + \bullet OH + OH^- \quad (3)$$

Normally, iron and copper are sequestered by binding to proteins, membranes or chelating agents (Halliwell and Gutteridge, 1984). Under certain conditions, however, transition metals are released from metalloproteins. For example, $O_2•^-$ can induce the release of iron from ferritin, a protein responsible for storing excess cellular iron (Biemond et al., 1984) and from [4Fe-4S] centres of dehydrases (Nordberg and Arner, 2001). The resulting •OH is extremely reactive and has a very short half-life of the order of nanoseconds. It can damage virtually any cellular molecule in its vicinity, limited only by its diffusion capacity (Bandyopadhyay et al., 1999).

1.1.1.1 Hydroxyl radical scavengers

Polyunsaturated fatty acids can exhibit a protective effect against •OH in diseases associated with free radical generation (Lipinski, 2011). This protective effect may reflect scavenging •OH mediated by C=C bonds. Further oxidation produces aldehydes and ketones - markers of oxidative stress (Lipinski, 2011). In addition, polyphenols, including salicylates can scavenge •OH and are protective against free radical injury *in vivo* (Kim et al., 2001; Lipinski, 2011).

Bioflavonoids are natural free radical scavengers. These benzo-γ-pyran derivatives inhibit •OH induced DNA damage by chelating copper or iron ions (Jun et al., 2007; Russo et al., 2000). The effects of these bioflavonoids can depend on the concentration of these ions. At low cupric ion concentrations, quercetin, a bioflavonoid, protects DNA from ROS mediated damage whereas at high concentrations it is carcinogenic (Jun et al., 2007).

1.1.2 Hydrogen peroxide

H_2O_2 is produced through various reactions including those catalysed by glucose oxidase, peroxisomal oxidases, cyclooxygenase and neutrophil NADPH (nicotinamide adenine dinucleotide phosphate) oxidase. Xanthine oxidase produces both $O_2•^-$ and H_2O_2 (Bandyopadhyay et al., 1999; Chance et al., 1979). $O_2•^-$ can also form H_2O_2 spontaneously or through superoxide dismutase (SOD) (Fridovich, 1983).

H_2O_2 is not a free radical and is not particularly reactive in a transition metal-free environment. It is, however, membrane-permeable (facilitated by some aquaporins) and its relatively long half-life allows it to diffuse significantly far away from its site of generation (Bienert et al., 2007; Halliwell and Gutteridge, 1984). H_2O_2 plays an important role in generating more reactive ROS including •OH, as well as hypochlorous acid (HOCl) in the phagosomes of neutrophils (Winterbourn et al., 2000).

H_2O_2 is a strong two electron oxidant, but a weak one electron oxidant. It is a more powerful two electron oxidant than HOCl or peroxynitrite ($OONO^-$), but is relatively unreactive with biological molecules because it has to overcome a high activation energy barrier (Winterbourn, 2013). As a one electron oxidant it has a low activation energy barrier and produces •OH due to its relatively weak O-O bond (Winterbourn, 2013). H_2O_2 can also react with keto acids, such as pyruvate. These reactions generate carbon dioxide (CO_2) that can react further with H_2O_2 to produce peroxymonocarbonate (HCO_4^-), which is ≥ 200x more reactive with thiols than H_2O_2 itself (Bakhmutova-Albert et al., 2010).

H_2O_2 has an important role in redox signalling, which most likely involves oxidation of protein thiols (Winterbourn, 2013). Under physiological and oncogenic conditions, H_2O_2 is involved in the transmission of growth signals, through epidermal growth factor, platelet derived growth factor and nerve growth factor, as well as through inactivation of some tyrosine and serine/threonine phosphatases (Finkel, 2000; Giorgio et al., 2007).

1.1.2.1 Antioxidant mechanisms against hydrogen peroxide

Catalases catalyse the breakdown of H_2O_2. They are found primarily in peroxisomes and convert H_2O_2 to a harmless mix of oxygen and water (equation 4) (Schrader and Fahimi, 2006). Catalases use NADPH (forming $NADP^+$) to improve efficiency as well as for protection against inactivation by preventing H_2O_2 from converting catalase into an inactive state through altering its heme group (Kirkman et al., 1999). This

protection may occur through electron tunnelling between NADPH and the heme group of catalase.

$$2H_2O_2 \xrightarrow{\text{catalase}} O_2 + 2H_2O \qquad (4)$$

Glutathione peroxidases (GPX) and peroxiredoxins (PRX) are present in several cellular compartments. GPX have an active site selenocysteine. Selenolate (Se^-) reacts with H_2O_2 to form selenenic acid (Se-OH), which then reacts with glutathione (GSH) to form selenylsulphide (Se-SG) (Nordberg and Arner, 2001). The active peroxidase selenolate is regenerated by reaction with a second GSH molecule. GPX can also react with other peroxides (ROOH) to produce alcohol as seen in equation (5).

$$ROOH + 2GSH \xrightarrow{\text{GPX}} H_2O + ROH + GSSG \qquad (5)$$

GSH is present in millimolar concentrations in cells and works as an antioxidant either *via* glutathione S-transferase or directly. The reaction of GSH not only protects protein thiols from hyperoxidation, but can also act as a regulatory post translational modification and alter protein structure and function (Dalle-Donne et al., 2007; Gallogly and Mieyal, 2007). Glutaredoxin can reduce the disulphide bonds formed between GSH and protein thiols.

Oxidized glutathione (GSSG) is reduced to GSH by glutathione reductase (GR) and NADPH (reviewed in (Deponte, 2013)). GR is a flavoenzyme and consists of a homodimer where each subunit binds FAD (flavin adenine dinucleotide) and NADPH. Both subunits together form the binding pocket for GSSG. The substrates of the reaction are NADPH and GSSG, and the products are 2GSH. There are two essential cysteines involved in the reaction. Initially, there is hydride transfer from NADPH to FAD, forming $FADH^-$. $NADP^+$ is then replaced with NADPH. GR (now GRH_2) then binds GSSG, where the SH group of one of the active site cysteines attacks GSSG to form an intermolecular disulphide bond. Following protonation, GSH can dissociate.

N-acetylcysteine (NAC) is a precursor of GSH and can act as a direct scavenger of •OH, H_2O_2 and $O_2•^-$. In addition, it can supplement the available pool of intracellular GSH under conditions of oxidative stress when GSH levels may be low (Santus et al., 2014).

PRX are thiol proteins (typical 2-Cys, atypical 2-Cys and 1-Cys) that react with H_2O_2 or $OONO^-$ to form protein sulfenic acid and organic hydroperoxides (equation 6) (Trujillo et al., 2007). The subsequent disulphide bond that forms between the two cysteines in typical and atypical 2-Cys PRX is regenerated by thioredoxin (TRX) (Hall et al., 2009). TRX is recycled using thioredoxin reductase (TRXR) and NADPH (see Section 1.1.6). The 1-Cys PRX are restored by GSH (Winterbourn, 2013). PRX are particularly abundant and are thought to be the major enzyme in charge of H_2O_2 disproportionation under steady state conditions. Inactivation of PRX through the reaction of the active site sulfenic acid with a peroxide to form sufinic acid can cause upregulation of catalase and GPX (Rhee et al., 2003).

$$\text{PRX-SH} + H_2O_2 \longrightarrow \text{PRX-SOH} + H_2O \qquad (6)$$

It is clear from the foregoing that there is redundancy in the antioxidant mechanisms targeting H_2O_2. Although catalases are restricted to peroxisomes, GPX and PRX can be co-localised. One of the proposed reasons for this redundancy is the requirement for the tight regulation of H_2O_2 due to its role in signalling and redox metabolism (Winterbourn, 2013). It is also important that antioxidant mechanisms targeting H_2O_2 are co-localised with SOD, as H_2O_2 is a product of the dismutation reaction (see Section 1.1.3.1).

1.1.3 Superoxide

$O_2•^-$ is formed by the acquisition of a single electron by molecular oxygen. In the cell, this usually occurs by leakage of an electron from complexes I and III in the electron transport chain. $O_2•^-$ has a single negative charge and an unpaired electron.

Despite its free radical nature, $O_2\bullet^-$ is not highly reactive. It is also unable to diffuse through lipid membranes. The reactions of $O_2\bullet^-$ with organic molecules such as proteins, lipids and nucleic acids are slow compared to its rate of conversion to H_2O_2 (Bielski et al., 1985). When it does react, it forms a substrate radical and hydroperoxyl radical ($HO_2\bullet$) (Sheng et al., 2014).

1.1.3.1 Antioxidant mechanisms against superoxide

There are two predominant forms of cellular SOD. CuZnSOD is located in the cytosol and MnSOD in the mitochondrial matrix. SOD-catalysed dismutation of $O_2\bullet^-$ is much more efficient than the corresponding spontaneous reaction (Nordberg and Arner, 2001). MnSOD is induced by oxidative stress. It is an essential enzyme and mice lacking MnSOD exhibit severe neurodegeneration and die soon after birth (Melov et al., 1998). The SOD reaction is shown in equation (7).

$$2H^+ + 2O_2\bullet^- \xrightarrow{\text{SOD/ spontaneous}} H_2O_2 + O_2 \qquad (7)$$

CuZnSOD overexpression in cultured mammalian cells results in higher levels of lipid peroxidation and hypersensitivity to oxidative stress. This can be alleviated by increasing catalase and GPX levels (Amstad et al., 1994). The most likely explanation for this behaviour is the increased production of H_2O_2 by overexpressed CuZnSOD (Giorgio et al., 2007). These findings illustrate the importance of rigorously controlling H_2O_2 production.

Superoxide reductase (SOR) is an iron metalloenzyme, which requires an external reductant to provide an electron in addition to two protons to produce H_2O_2 from one molecule of $O_2\bullet^-$ (equation 8) (reviewed in (Sheng et al., 2014)).

$$2H^+ + O_2\bullet^- + e^- \xrightarrow{\text{SOR}} H_2O_2 \qquad (8)$$

1.1.4 Singlet oxygen

Changing the valance electron spin state of triplet ground-state oxygen converts it to singlet oxygen ($^1O_2$), which has electrons with paired spins in the same molecular orbital. $^1O_2$ can be produced in many ways. Most commonly, it is produced through energy transfer from a sensitiser to ground-state O_2 (Ogilby, 2010). $^1O_2$ has a relatively long half-life of 1.7±1μs in H_2O. This increases to around 24 μs in D_2O, due to the higher density and stronger H-O bonds of D_2O (Jiménez-Banzo et al., 2008). $^1O_2$ can be quenched by sodium azide (NaN_3). These two properties are often used to infer the $^1O_2$-dependence of reactions.

$^1O_2$ can also be formed by peroxidases and the reaction of H_2O_2 with HOCl or $OONO^-$ (Di Mascio et al., 1994; Foote and Wexler, 1964). It can be produced by the reaction of ozone with organic and inorganic molecules, and is generated biologically by activated eosinophils and macrophages (Kanofsky and Sima, 1991; Kanofsky et al., 1988; Steinbeck et al., 1993). The ability of $^1O_2$ to oxidise target molecules can have beneficial effects in destroying pathogens, as well as a negative impact on healthy organisms.

When $^1O_2$ reacts with an organic molecule the initial product is a peroxide, which can then form •OH (Ogilby, 2010). When the rate constants for $^1O_2$ reactions as well as the cellular abundance of the targets is taken into account, $^1O_2$ is most reactive with proteins, followed by ascorbate, RNA and DNA (Davies, 2003). An interaction between $^1O_2$ and its target can result in energy transfer and a return to the triplet oxygen state, or a chemical reaction and alteration of the target.

1.1.4.1 Antioxidant mechanisms against singlet oxygen

The carotenoids, of which lycopene and β-carotene (Figure 1.2) are the most important, scavenge peroxyl radicals and $^1O_2$ and alleviate damage to cellular lipids by forming resonance stabilised carbon cantered radicals (Olson and Krinsky, 1995). Lycopene, found in many fruits and vegetables, has a large number of double bonds that delocalise unpaired electrons. This allows it to act as a strong $^1O_2$ quencher. It has been proposed that carotenoids act as antioxidants at low oxygen conditions,

but at high oxygen conditions can act as pro-oxidants by forming a carotenoid-peroxyl radical and oxidising unsaturated lipids (Valko et al., 2006).

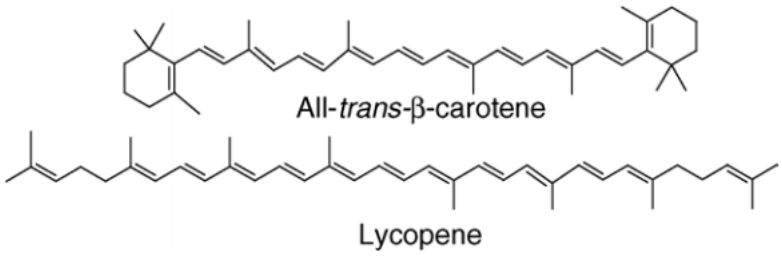

Figure 1.2: Chemical structures of β-carotene and lycopene (Valko et al., 2006)

1.1.5 Other reactive species

Nitric oxide (NO•), also a free radical, is similar to O_2•$^-$ in its low reactivity with biomolecules. It can cross cell membranes and has a role in signalling and redox regulation (Ignarro, 1990; Wink and Mitchell, 1998). NO• is produced together with L-citrulline from L-arginine, O_2 and NADPH by NO synthase (NOS). It acts as a type of radical scavenger and neutralises peroxyl and alkyl radicals to prevent lipid peroxidation (Rubbo et al., 2000). It can, however, react with O_2•$^-$ to produce the highly reactive $OONO^-$, that can nitrate aromatic amino acid residues of proteins and react with ceruloplasmin to release copper ions (Halliwell et al., 1997). Depending on the environmental conditions, $OONO^-$ can be protonated to form peroxonitrous acid (ONOOH). This can generate either •OH and •NO_2, rearrange to nitrate (NO_3) or react with CO_2 to form the very reactive nitrosoperoxycarbonate ($ONOOCO_2^-$) (Pavlovic and Santaniello, 2007).

Under conditions of high NO• production, it is removed from the cell by being conjugated to GSH to form S-nitroso-glutathione. This product is subject to cleavage by the TRX system (Nordberg and Arner, 2001).

1.1.6 Other antioxidants

Ascorbic acid is an important antioxidant but it is unable to exhibit its antioxidant effect in the presence of transition metal ions (Halliwell, 1991). Its antioxidant effect reflects its ability to form ascorbate radicals that terminate free radical chain reactions.

α-tocopherol (Toc) is a lipid soluble molecule present in cell membranes and plasma lipoproteins. It has an –OH group, where the hydrogen atom is donated to peroxyl and alkoxyl radicals formed through lipid (L) peroxidation (Halliwell, 1991). This reaction converts α-tocopherol into a radical, which has low reactivity with nearby fatty acid side chains, and terminates the chain reaction (equation 9-11). α-tocopherol radical may be converted back into α-tocopherol using GSH and ascorbic acid (AA) (equation 11) (Wefers and Sies, 1988). Low plasma content of α-tocopherol and ascorbate is associated with higher risk of myocardial infarction, due to their protection against lipid peroxidation of low density lipoprotein (LDL) (Gey et al., 1987).

$$LOO\bullet + TocH \longrightarrow Toc\bullet + LOOH \quad (9)$$

$$Toc\bullet + LOO\bullet \longrightarrow Toc\text{-}OOL \quad (10)$$

$$Toc\bullet + AAH^{-} \longrightarrow TocH + AA\bullet^{-} \quad (11)$$

TRX and TRXR are antioxidant oxidoreductase enzymes that together form the TRX system (Nordberg and Arner, 2001). TRX contains a –Cys-Gly-Pro-Cys active site that is essential for its function as a protein disulphide oxidoreductase (Holmgren, 1989). TRX is particularly important for acting as an electron donor to PRXs. TRX in its reduced form is able to reduce disulphide bonds in proteins and is restored using TRXR and NADPH. TRXR contains a selenocysteine and relies on NADPH and FAD to reduce the oxidised disulphide of TRX (Nordberg and Arner, 2001).

1.1.7 Lipid peroxidation

Free radicals can react with virtually all biomolecules. Reactions with cell membrane fatty acids generate acid radicals (L•) that propagate chain reactions (equation 12) (Nimse and Pal, 2015). These radicals can react with oxygen to form fatty acid

peroxyl radicals (LOO•) (equation 13) and generate lipid hydroperoxides (LOOH) (equation 14) and aldehydes (equation 15). Aldehydes can migrate from their original source to cause damage in other areas in the cell (Pryor and Porter, 1990).

$$LH + R\bullet \longrightarrow L\bullet + RH \quad (12)$$

$$L\bullet + O_2 \longrightarrow LOO\bullet \quad (13)$$

$$LOO\bullet + LH \longrightarrow LOOH + L\bullet \quad (14)$$

$$LOOH \longrightarrow LO\bullet + LOO\bullet + \text{aldehydes} \quad (15)$$

Lipid peroxidation is particularly relevant to the generation of atherosclerosis plaques through oxidation of LDL in cardiovascular disease (Steinberg, 1997).

1.1.8 Protein oxidation

Proteins can be directly modified by ROS or undergo secondary oxidation by lipid peroxides (eg. malondialdehyde) or reactive sugars (glycation or glyoxidation products) (Dunlop et al., 2009). Their high cellular abundance (70% of dry mass) and the reactivity of their side chains enhance their vulnerability to oxidation. These reactions can result in a chemically heterogeneous mixture of oxidation products, which are determined by the type of reactive species involved, steric constrictions imposed by the protein such as exposure of side chains, presence of metal atoms and the local redox environment. Protein oxidation can result in intersubunit crosslinking, dissociation of subunits, exposure of hydrophobic residues, aggregation, changes in mechanical properties, changes in binding to cofactors and metal ions and fragmentation of the backbone (Prinsze et al., 1990).

Certain extremophiles such as *Deinococcus radiodurans* exhibit resistance to cell killing by lethal treatments that induce both DNA and protein damage. It appears that this resistance is due to efficient proteome protection and preventing protein oxidation through non-enzymatic antioxidant protection rather than DNA protection (Green et al., 2011; Krisko and Radman, 2010). In addition, protein oxidation was identified as being responsible for elevated ultraviolet radiation (UV) induced

mutagenesis, highlighting the potential detrimental effect of protein oxidation on cellular viability (Krisko and Radman, 2013).

1.1.8.1 Protein modifications caused by •OH, $^1O_2$, H_2O_2 and O_2•$^-$

•OH is extremely reactive and results in extensive damage through its ability to modify all amino acid side chains. This results in a complicated set of modifications. The most common reaction involves H-abstraction from S-H and C-H bonds of amino acid side chains forming thiyl and alkyl radicals, respectively (Xu and Chance, 2007). Carbon centred radicals can react with oxygen to form peroxyl radicals, ranging from hydroperoxide, hydroxide and carbonyl products (Davies, 2003; Easton, 1997). Radicals formed from peroxides on tryptophan, tyrosine and histidine can result in backbone fragmentation (Davies, 2003; Pileni et al., 1979; 1978). Due to the radical nature and extreme reactivity of •OH, a propagating chain reaction can occur whereby a single •OH can modify up to 15 amino acids (Neuzil et al., 1993).

$^1O_2$ is reactive with proteins, particularly amino acids with electron rich aromatic or sulphur containing side chains (Davies, 2003). At physiological pH it reacts predominantly with histidine, tryptophan, methionine, cysteine and tyrosine in order of decreasing reactivity (Wilkinson et al., 1995). The reaction of free tryptophan with $^1O_2$ initially produces a hydroperoxide (ROOH), which can decompose through homolytic cleavage of the -O-O- bond to produce •OH, particularly in the presence of metal ions or UV light (Davies, 2003; Langlots et al., 1986). The hydroperoxide can also result in tryptophan ring-opening and protein:protein crosslinking or fragmentation. The ring opening produces *N*-formylkynurenine, which can further decompose to kynurenine. Both *N*-formylkynurenine and kynurenine are better photosensitisers than tryptophan, and can continue to cause $^1O_2$ formation through sustained UV light exposure (Pileni et al., 1978; 1979; Saito et al., 1977). Initially tryptophan can preferentially act as a physical quenching agent, however, the creation of these photosensitising decomposition products can result in propagating damage. The main product of peptide-bound tyrosine at room temperature after oxidation by $^1O_2$ is a hydroperoxide, which can also result in the formation of •OH and dityrosine protein:protein crosslinks (Langlots et al., 1986; Wright et al., 2002).

Reaction of histidine with $^1O_2$ causes the formation of endoperoxides. These can undergo further reactions with another histidine, an oxidised histidine or a lysine side chain to form protein:protein crosslinks (Krisko and Radman, 2010; Shen et al., 1996; 2000). Proteins which lack histidine have been shown to be less likely to form crosslinks (Montaner et al., 2007; Schäfer et al., 1998; Shen et al., 2000).

Oxidation of aromatic amino acids changes their hydrophobicity and can contribute to exposure of hydrophobic regions, which can result in unfolding, aggregation and non-specific interactions with other proteins (Mirzaei and Regnier, 2008). The protein:protein crosslinks caused by oxidised aromatic amino acids can also result in aggregation and loss of function (Souza et al., 2000). Under conditions of severe oxidative stress, oxidised proteins and lipids can form an aggregated complex called lipofuscin, which is challenging to remove and can cause further oxidation.

H_2O_2 does not generally react with proteins even at high concentrations (mM) (Halliwell and Gutteridge, 2007). It can react with and oxidise protein cysteine or methionine residues and low molecular weight thiols (glutathione). It can also oxidise proteins that have a transition metal centre and cause heme oxidation and release of iron, intensifying oxidative stress (Gutteridge, 1986).

$O_2\bullet^-$ is not generally reactive with proteins, although it can modify the iron-sulphur clusters of proteins, resulting in the release of ferrous iron (Fe^{2+}) and enzyme inactivation. Specific targets of this reaction include aconitase, which has an important role in metabolism (Halliwell and Gutteridge, 2007).

1.1.8.2 Protein carbonylation

Oxidation of protein side chains leads to the formation of aldehydes and ketones through protein carbonylation. Protein carbonyls cannot be repaired chemically or enzymatically and are therefore stable and effective markers of protein oxidation in cells. The level of protein carbonylation increases from one in nine to one in three proteins during oxidative stress (Stadtman and Levine, 2000). Lysine, arginine, threonine and proline are the most susceptible protein side chains for metal

catalysed oxidation (in the presence of Fe(II), H_2O_2 and a reducing agent) (Requena et al., 2001). $^1O_2$ can also react with aromatic amino acids and cause protein carbonylation. Protein carbonyls can react with lysine and arginine on the same or another protein, where further rearrangements may result in irreversible covalent crosslinking. In addition, nucleophilic side chains of cysteine, histidine and lysine can react with aldehydes generated by lipid peroxidation or with reactive carbonyls formed by reducing sugars, resulting in advanced lipoxidation/glycation end products (ALE/AGE) (Dalle-Donne et al., 2003).

1.1.8.3 Thiol oxidation

Thiol oxidation of cysteine can result in the formation of sufenic acid (R-S-OH), which can react with other thiols or glutathione to form a disulphide (R-S-S-R). Further oxidation of sulfenic acid leads to the formation of sulfinic acid (R-S(=O)-OH) and sulfonic acid (R-S(=O)$_2$-OH), which are generally stable and irreversible and can be inactivating modifications. Cysteine is also able to form a zwitterionic peroxy intermediate that can react with another cysteine to form two molecules of R-S-S(=O)-R (Ando and Takata, 1986; Berlett and Stadtman, 1997). Methionine oxidised by an oxidant [O] forms methionine sulfoxide (Dalle-Donne et al., 2003; Sysak et al., 1977) (equation 16). Further oxidation forms methionine sulfonate (R-S(=O)$_2$-CH_3).

$$\text{R-S-CH}_3 \xrightarrow{[O]} \text{R-S(=O)-CH}_3 \xrightarrow{[O]} \text{R-S(=O)}_2\text{-CH}_3 \qquad (16)$$

Cysteine oxidation has been shown to result in enzyme inactivation of a range of proteins with active site cysteines such as glyceraldehyde-3-phosphate dehydrogenase, glutathione reductase, and caspases through non-radical and radical reactions (Hampton et al., 2002; Morgan et al., 2002; Wright et al., 2002).

The reaction of weaker ROS such as H_2O_2 with cysteine is determined by whether cysteine is in its thiolate state. Stronger reactive species such as •OH, $^1O_2$ and ONOO- do not require this deprotonation and are likely to form higher cysteine oxyacids.

Some protein oxidation is important for regulation of enzymatic function and occurs almost exclusively through thiol oxidation. Modifications can be activating or inactivating and alter the binding of proteins to their substrates, interacting partners or cofactors (Kansanen et al., 2013; Korichneva, 2005). Although cysteine is considered to be the main residue for redox regulation, methionine when oxidised can result in protein conformational changes (eg. calmodulin) (Bigelow and Squier, 2011). The oxidation product of methionine, methionine sulfoxide, can be enzymatically reduced (Stadtman and Levine, 2000).

1.1.9 DNA oxidation

ROS and reactive nitrogen species (RNS) can result in >100 different types of oxidative DNA lesions. These include base modifications, single-strand (ss) and double-strand (ds) DNA breaks, DNA-protein crosslinks (DPCs) and deoxyribose oxidation (Dexheimer, 2013; Frei, 1994; Nordberg and Arner, 2001). Cellular DNA is subject to around 10^4 damaging oxidative reactions per day. Most of these lesions are removed. Persistent DNA lesions are potentially mutagenic due to erroneous base pairing during DNA replication. The accumulation of mutations over time contributes to various pathological conditions. DNA damage and repair will be discussed in detail in Section 1.3.

1.2 Solar radiation

Radiation from the sun enables life on Earth. Solar radiation has played a pivotal role in evolution. Its benefits range from a contribution to the provision of temperatures that support life, to being an essential component of photosynthesis. However, solar UV radiation also has detrimental effects on biological systems.

1.2.1 The solar radiation spectrum

The electromagnetic spectrum is divided into wavelength segments of UV, visible and infrared radiation. The most biologically damaging solar wavelengths lie in the UV region of the spectrum. For this reason, the effects of UV radiation have been

extensively studied and the biological effects of visible and infrared radiation are less well characterised. For the purpose of this thesis I will focus mainly on UV radiation.

UV radiation is divided into UVA, UVB and UVC in order of decreasing wavelength (Figure 1.3). Oxygen produced by photosynthesis splits and recombines to form the stratospheric ozone layer. The ozone layer absorbs UV wavelengths less than 310nm and effectively removes all UVC and 95% of UVB radiation from incident sunlight. UVA is not absorbed (de Gruijl and van der Leun, 2000). UV is required for the synthesis of vitamin D. It is important for regulation of hormones through circadian rhythm and is used in the treatment of skin disorders (Beersma and Gordijn, 2007).

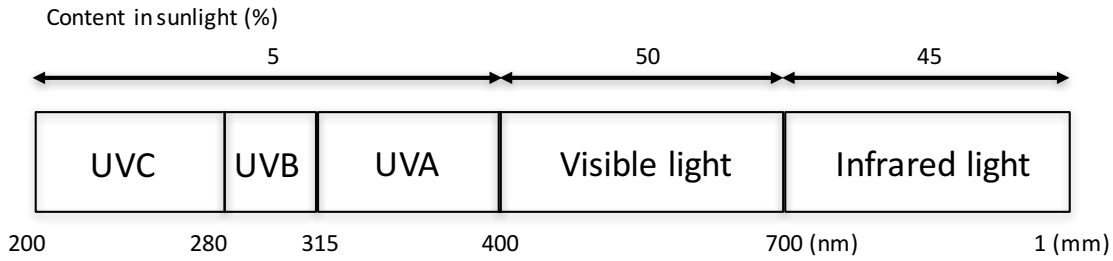

Figure 1.3: Solar radiation spectrum
Adapted from (Svobodova et al., 2006)

1.2.1.1 The skin anatomy

The skin is the major target for the biological effects of solar radiation. It is the largest organ with many essential functions, including protection against the external environment. The skin has three layers: epidermis, dermis and hypodermis (Figure 1.4). The epidermis contains squamous keratinised epithelium made up of 80% keratinocytes, and other cell types including melanocytes (1-2%) for pigment production and Langerhans immune cells (Svobodova et al., 2006). Depending on the location, the epidermis contains 4-5 layers of cells where the outermost layer is called the *stratum corneum* and the innermost layer is called the *stratum basale.* The innermost basal layer separates the dermis from the epidermis and is the layer of stem cells with the ability to migrate outwards and differentiate into keratinocytes. The *stratum corneum* contains several layers of keratinised dead cells lacking nuclei and other organelles. Each melanocyte in the basal layer is associated with 30-40

keratinocytes and one Langerhans cell. They contain melanosomes in which they produce the photoprotective melanin pigment that is distributed to the associated keratinocytes (Svobodova et al., 2006). Melanosomes persist in the various layers of the skin until they are shed by epidermal turnover that occurs every 4-5 weeks (Borovanský and Elleder, 2003). Fibroblasts are the most common cells in the dermis. The dermis contains collagen and elastin fibres, which gives skin its elasticity.

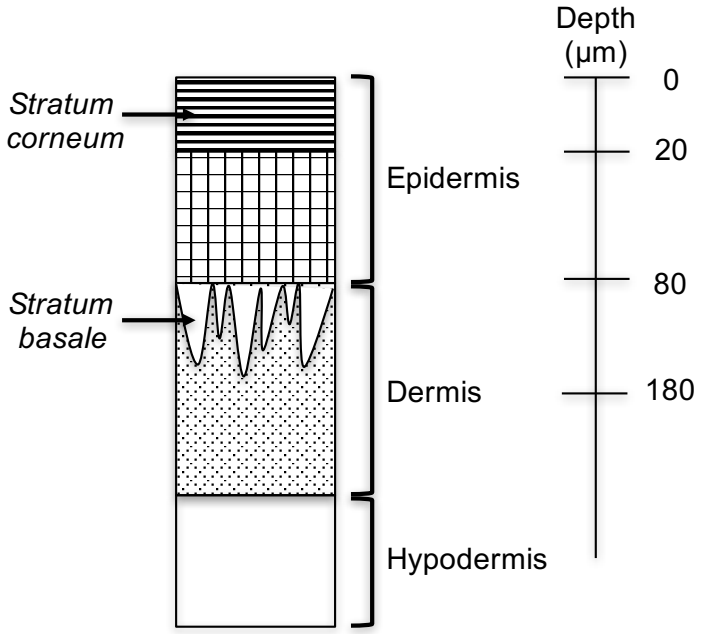

Figure 1.4: Skin anatomy
Adapted from (Svobodova et al., 2006)

1.2.1.2 Sun, tanning and skin cancer

Skin pigmentation is regulated by over 125 genes (Brenner and Hearing, 2008). Each individual has a genetically determined constitutive skin pigmentation. In addition, facultative pigmentation occurs upon exposure to external stimuli such as UV radiation. Upon exposure to UV, oxidation and polymerisation of melanin precursors in the skin causes immediate (within minutes) pigment darkening (Polefka et al., 2012). Within an hour of exposure, UVA detection by the photoreceptor rhodopsin stimulates signalling that results in activation of melanin synthesis in melanosomes that have migrated to the outer epidermal layer (Moan et al., 2012; Natarajan et al., 2014a; Wicks et al., 2011). Pigment darkening continues for several hours until *de*

novo melanin synthesis stimulates delayed tanning that lasts for several days (Yamaguchi et al., 2007).

Melanin precursors are cytotoxic to melanocytes (Svobodova et al., 2006). Dihydroxyphenylalanine and indolic precursor autooxidation can result in the formation of ROS and generate products such as dihydroxyindole, which can insert itself between DNA bases and act as a mutagen (Svobodova et al., 2006). This DNA binding is enhanced by UV exposure (Hussein, 2005). Even though melanin acts in a protective manner against damage caused by solar radiation, melanogenesis is a pro-oxidative process and its activation and long term progression can be detrimental (Urabe et al., 1994).

The hyperpigmentation that occurs in sun exposed regions of the skin through the accumulation of melanosomes can be shed through desquamation during the de-tanning response (Natarajan et al., 2014a; 2014b). However, this is not specific to sun exposed regions but is a constitutive process that occurs in the entire skin. IFN-γ (interferon-γ) is proposed to be responsible for acting as a transient molecular switch to downregulate expression of melanogenic genes and impede maturation of melanosomes without altering melanocyte biology. IFN-γ is a good candidate for this type of response as it can be produced by immune cells in the vicinity of injury from UV exposure. IFN-γ is also strongly associated with predisposition to melanomagenesis (Zaidi et al., 2011). Therefore, the de-tanning response can be harmful as well.

UV radiation is firmly implicated in the three major types of skin cancer: basal cell carcinoma (BCC), squamous cell carcinoma (SCC) and melanoma. Keratinocyte-derived BCCs are the most common, followed by SCCs (in a ratio of approximately 4:1) (Stockfleth and Ulrich, 2009). Melanomas, which are derived from melanocytes, are less frequent but are the most dangerous due to their tendency to metastasize (de Gruijl and van der Leun, 2000). Fair skin, proximity to the equator, increasing altitude and increasing exposure (particularly 11am-1pm), are risk factors for UV-mediated carcinogenesis (Diffey, 2002; Rigel, 2008). The risk of developing SCC increases with lifelong accumulated exposure to solar radiation (Vitasa et al., 1990). On the other hand, the risk of developing BCCs and cutaneous malignant melanoma

is more related to childhood and adolescence sun exposure and intermittent excessive exposure (sunburn) (Holman and Armstrong, 1984; Kricker et al., 1995).

1.2.1.3 UVA

UVA comprises 95% of solar UV radiation that reaches the earth surface. Its comparatively longer wavelengths enable UVA to penetrate deep into the epidermis and dermis. It is also 1000-fold more efficient than UVB at inducing pigment darkening in the epidermis (Clydesdale et al., 2001). Around 80% of UVA reaches the dermo-epidermal junction and around 10% can reach the hypodermis (Verschooten et al., 2006). On a sunny summer's day, at midday in south-east England, skin is exposed to 10kJ/m^2 of UVA in less than 10 minutes (Attard and Karran, 2012). This can result in DNA and protein damage. Extensive exposure to UVA can result in skin photoaging, necrosis of endothelial cells and damage to dermal blood vessels.

UVA induces the production of ROS *via* interactions with endogenous cellular photosensitisers. UVA-induced ROS stimulate detoxification responses in keratinocytes and melanocytes. Activation of the mitogen activated protein kinase (MAPK) signalling pathways and subsequent formation of the AP-1 (activator protein-1) transcription factor, increases scavenging enzyme levels (Natarajan et al., 2014a). UVA dependent activation of NF-κB and Nrf modulates inflammatory and antioxidant responses, respectively (Bickers and Athar, 2006).

1.2.1.4 UVB

UVB is less penetrative than UVA and mainly targets the epidermal basal cell layer of the skin (Svobodova et al., 2006). Around 70% of UVB is blocked by the *stratum corneum* (Svobodova et al., 2006). Proteins and DNA absorb maximally in the UVC and UVB regions of the spectrum, with absorbance maxima around 280nm and 260-265nm, respectively. High energy UVB and UVC photons cause significant DNA damage. The two most common DNA modifications are cyclobutane-pyrimidine dimers (CPDs) and pyrimidine-pyrimidone (6,4) photoproducts (6,4 Py:Py) that occur

between adjacent pyrimidine residues (Brash, 1988). These photoproducts are removed by nucleotide excision repair (NER). Mutations at persistent dipyrimidine photoproducts are implicated in skin cancer development.

UVB induces ROS and RNS. UVB can also modify endogenous photosensitisers and alter their absorption, which can make them more or less vulnerable to UVB or UVA radiation and $^1O_2$ production. $^1O_2$ is generated by irradiation of vitamin B molecules and unsaturated fatty acids can change their absorption spectra, increase $^1O_2$ production and can cause lipid peroxidation (Regensburger et al., 2012). This production of ROS and RNS also depletes skin antioxidants, which decreases the skin's protection against free radical damage.

1.2.1.5 Ageing

UV stimulates cytokine release into the dermal microenvironment. This results in inflammation and the production of ROS. Recruited immune cells secrete elastases and proteases, which in turn upregulate matrix metalloproteases (MMPs). The result of this cascade is matrix degradation (Cavarra et al., 2002). Fibroblast AP-1 also increases MMP production that stimulates collagen breakdown. Concomitantly, TGF-β downregulates Type 1 procollagen expression. Collagen depletion following repeated UV injury can result in a visible solar scar (Helfrich et al., 2008; Schroeder and Krutmann, 2010). Oxidative stress can also induce higher elastin levels in dermal fibroblasts which may contribute to the elastolytic changes characteristic to photoaged dermis (Svobodova et al., 2006). Daily sub-erythemic UVA exposure for one month is sufficient to cause sufficient damage to dermal collagen and elastin to be apparent as photoaging (Matsumura and Ananthaswamy, 2004).

1.2.1.6 Immunosuppression

UVA (360-380nm) and UVB (around 300nm) can be immunosuppressive. This may exacerbate the development of skin cancers (Damian et al., 2011; Halliday et al., 2011). It can also cause UV-induced expression of latent viruses (HSV and HPV) (Norval, 2006). The likely advantage of this immunosuppression is in preventing an

immune response against neo-antigens produced by UV-mediated modifications of skin cell molecules (de Gruijl and van der Leun, 2000). UVA and UVB can also act in a synergistic way, whereby UVA can sensitise cultured human cells to UVB mediated killing and enhance UVB mediated immune suppression (Kuchel et al., 2002; Tyrrell et al., 1984). UV radiation is therefore particularly dangerous. It is a complete carcinogen that not only initiates carcinogenesis by mutation, but also acts as a cancer promoter by dampening the immune response (Bickers and Athar, 2006).

1.2.1.7 Signalling

Keratinocytes, fibroblasts, melanocytes and Langerhans cells express the aryl hydrocarbon receptor (AhR) - a cytosolic ligand-activated transcription factor (Abel and Haarmann-Stemmann, 2010). Tryptophan absorbs UVB and the resulting photoproduct, 6-formylindolo[3,2-*b*]carbazole (FICZ), activates AhR signalling. AhR-activated signalling is a part of the UV stress response (Fritsche et al., 2007). Upon ligand binding, AhR translocates to the nucleus and activates the expression of genes containing a xenobiotic response element. These include genes involved in oxidative stress, skin tanning response, circadian rhythm and inflammation (Abel and Haarmann-Stemmann, 2010; Agostinis et al., 2007; Jux et al., 2011; Oberg et al., 2005). FICZ is discussed further in Chapter 4.

1.2.1.8 Visible light

Visible wavelengths account for around 50% of the total solar spectrum and nearly 20% of visible light can penetrate the hypodermis (Svobodova and Vostalova, 2010). Studies of *ex vivo* skin explants exposed to UVA, UVB and visible light have shown that the relative contribution to ROS generation was around 46%, 4% and 50% respectively (Zastrow et al., 2009). Visible light also induces inflammatory cytokines and MMPs. Cellular photosensitisers for visible light include β-carotene (464 nm), porphyrins (400–410 nm), bilirubin (420–490 nm), melanin, and its precursors (300–700 nm) (Mahmoud et al., 2008). Visible light exposure also oxidises DNA bases but does not induce CPD or 6,4 Py:Py formation (Dupont et al., 2013). Overall, it is

responsible for <10% of the DNA damage caused by solar radiation (Dupont et al., 2013).

1.2.1.9 Infrared radiation

Infrared radiation is split into ranges of infrared A (700–1400nm), B (1400–3000nm) and C (3000nm–1mm). Infrared B and C interact with thermosensitive receptor molecules in tissues. Vibrational energy from infrared B and C generates heat and provides the sensation of warmth in sunlight-exposed skin (Svobodova and Vostalova, 2010). Infrared A makes up 30% of infrared radiation and more than half of incident infrared A can reach the dermis and 10% the hypodermis (Svobodova and Vostalova, 2010). Infrared radiation can be a source of free radicals and generate ROS, albeit with around a quarter of the potency of UV (Darvin et al., 2011; Zastrow et al., 2009). Infrared is not strongly absorbed by melanin and other skin chromophores, including DNA. It does contribute to photoaging, may promote carcinogenesis and has a detrimental effect on mitochondrial integrity (Krutmann and Schroeder, 2009; Schroeder et al., 2008; Zastrow et al., 2009). The last point may be due to the disruption of the electron transport chain and ROS production following infrared absorption by cytochrome c oxidase (Krutmann and Schroeder, 2009).

1.2.2 Types of photosensitising reactions

UV photons can be directly absorbed by cellular chromophores such as DNA. The absorbed energy causes chemical reactions that result in damaged bases. In a second mechanism, endogenous or exogenous photosensitisers absorb UV photons and attain a singlet excited state. The excited photosensitiser can lose the energy as heat, emit fluorescence or undergo intersystem crossing to generate a relatively long-lived (micro/milliseconds compared to nanoseconds) triplet excited state. The triplet state allows efficient transfer of charge or energy to other molecules. Energy transfer to molecular oxygen generates $^1O_2$ (Figure 1.5).

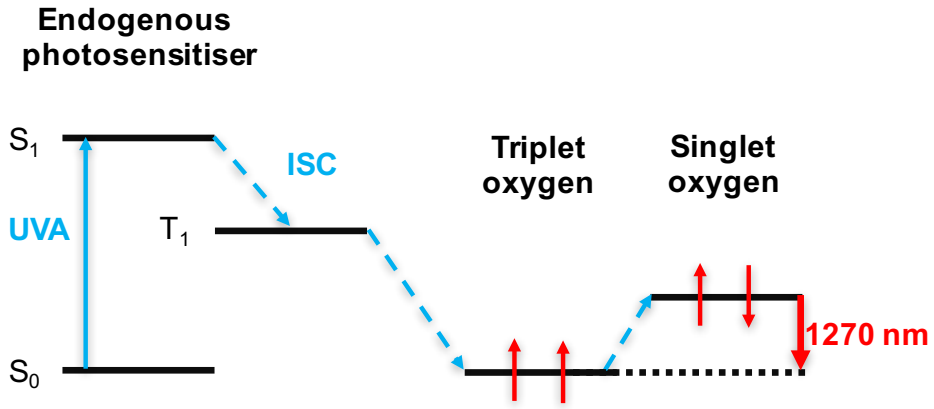

Figure 1.5: Photosensitisation reaction and production of singlet oxygen
UVA exposure converting endogenous photosensitiser from singlet (S_0) to excited singlet state (S_1) to triplet state (T_1) *via* intersystem crossing (ISC). The triplet state can transfer energy to triplet oxygen to form singlet oxygen, which exhibits luminescence at 1270nm.

Cellular UV chromophores include nucleic acids, NADH/NADPH, carotenoids, melanin precursors, collagen crosslinks, ALE/AGE, as well as amino acid side chains and prosthetic groups such as flavins and heme (Lamore et al., 2010; Wondrak et al., 2003).

Photosensitisers absorb UV radiation to generate an excited state, which can react with a substrate to produce a radical or radical ion in the sensitiser and substrate (Davies, 2003). The sensitiser can then undergo another reaction with O_2 to form $O_2^{\bullet -}$. This is known as Type I photosensitisation. Type II photosensitisation occurs when energy is transferred from an excited chromophore to ground state triplet oxygen to form $^1O_2$. $^1O_2$ can then result in protein oxidation. A less common reaction involves $O_2^{\bullet -}$ formation that can dismutate to H_2O_2, which can form •OH in the presence of iron and copper as mentioned previously (Svobodova et al., 2006). These two types of reactions are summarised in Figure 1.6.

In general, cells are not exposed to UV light wavelengths below 290nm. Most amino acid side chains absorb at wavelengths around 230nm (Davies, 2003). In addition, the peptide bond (-C(=O)-NH-) displays weak absorbance at 210-220nm. The formation of $^1O_2$ by protein absorption of solar UV is therefore limited. The aromatic amino acids (tryptophan in particular) do absorb longer wavelengths and are more effective in their ability to form $^1O_2$.

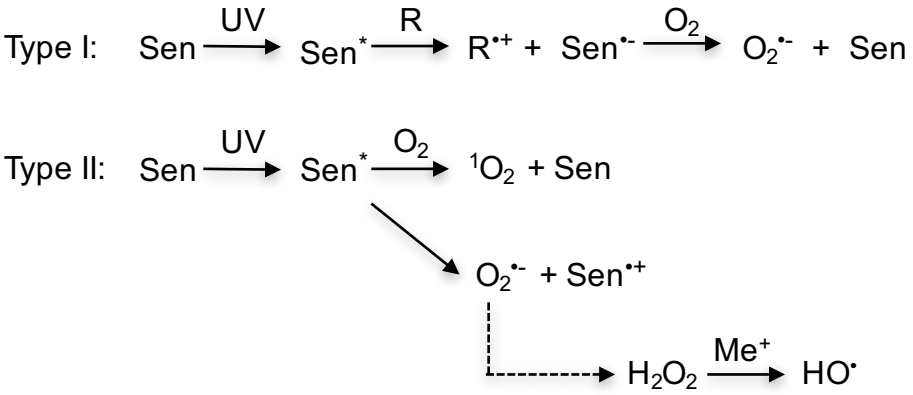

Figure 1.6: Photosensitiser mediated ROS formation
Sen, photosensitiser; Sen*, excited photosensitiser, R, DNA base or aromatic amino acid; Me+, metal cation. Adapted from (Svobodova et al., 2006).

1.2.3 Photosensitisers and their mechanism of photosensitisation

Photosensitising drugs predispose individuals to phototoxic effects. A drug that is absorbed into the skin either locally or in the systemic circulation can absorb UVA and result in phototoxic reactions.

Many commonly-prescribed drugs are photosensitizers. The work I describe in this thesis concerns the properties of three photosensitizers: 6-thioguanine (6-TG, a metabolite of the immunosuppressant azathioprine) and the antibiotics ciprofloxacin and ofloxacin (Figure 1.7). All three drugs are on the 2015 WHO Model List of Essential Medicines. Ciprofloxacin and the active enantiomer of ofloxacin (levofloxacin) are the most widely-prescribed fluoroquinolones in the United Kingdom (www.hscic.gov.uk).

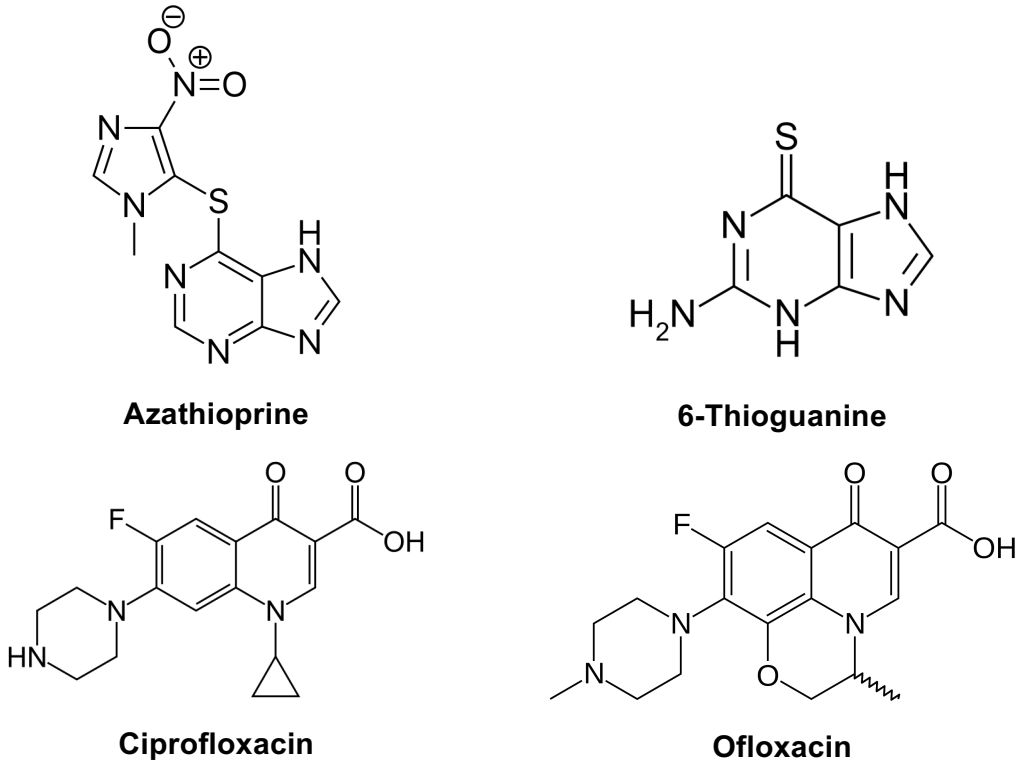

Figure 1.7: Chemical structures of azathioprine, 6-thioguanine, ciprofloxacin and ofloxacin

1.2.3.1 6-Thioguanine

Thiopurines 6-mercaptopurine (6-MP), 6-TG and azathioprine are immunosuppressants that are also used in the treatment of cancer and inflammatory disorders (Elion, 1989). More specifically, they are used in the treatment of acute leukaemia in children and are prescribed for colitis, psoriasis and rheumatoid arthritis (Attard and Karran, 2012). For many years, azathioprine was the standard immunosuppressant to prevent graft rejection in organ transplant patients. Although it has been to some degree superseded by a new generation of immunosuppressants, azathioprine remains the main immunosuppressant drug for many transplant patients. It is increasingly prescribed for chronic inflammatory disorders such as colitis. In fact, azathioprine prescriptions have been increasing steadily in the past five years in England, with 866,200 prescriptions dispensed in 2015 (NHS Digital, Prescription Cost Analysis). Azathioprine, 6-MP and 6-TG are prodrugs that are metabolised into deoxythioGTP (Figure 1.8), which can be used as a substrate for DNA replication. Since thiopurines act systemically and are taken

continuously, the DNA of patients taking these drugs contains measurable levels of 6-TG.

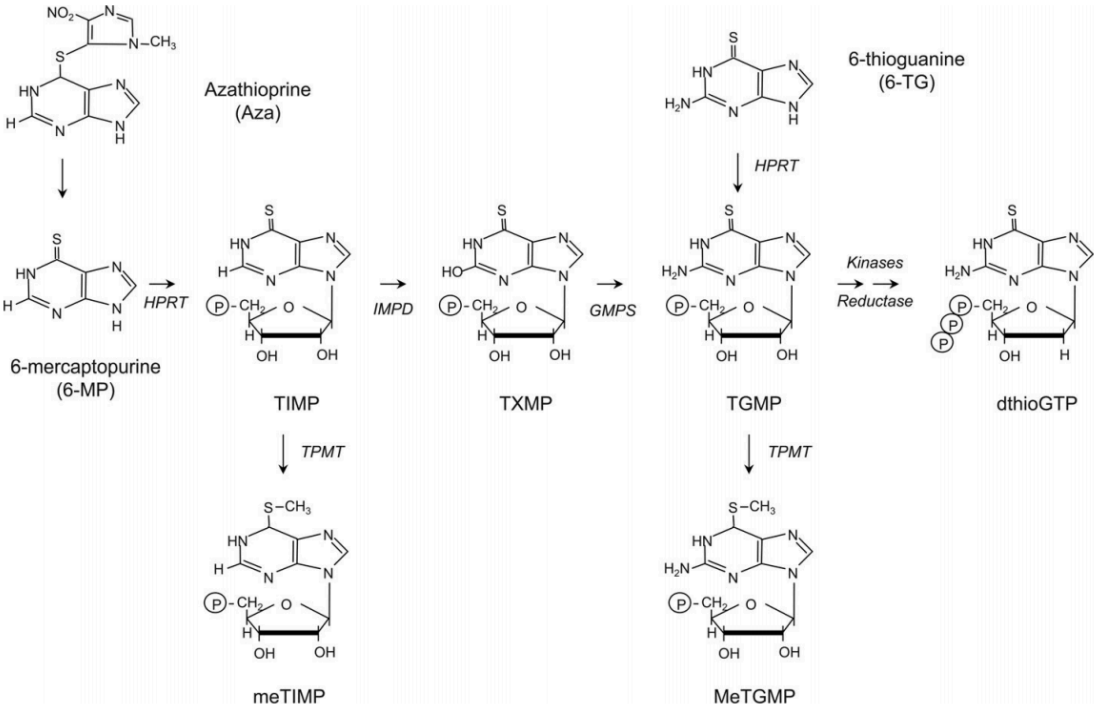

Figure 1.8: Thiopurine metabolism (Karran, 2006)
Following transporter mediated uptake, 6-MP and 6-TG are converted by hypoxanthine phosphoribosyltransferase (HPRT) to thioinosine and thioguanosine monophosphate, TIMP and TGMP, respectively. TIMP and TGMP are substrates for thiopurine methyltransferase (TPMT), which forms S-methylmercaptopurine (me6-MP, meTIMP) or S-methylthioguanine (me6-TG, meTGMP). This methylation prevents further metabolism and incorporation into DNA. meTIMP also inhibits *de novo* purine synthesis. While TGMP is converted directly to deoxynucleoside triphosphate by deoxynucleotide kinases followed by reductases, TIMP requires inosine monophosphate dehydrogenase (IMPD) to form thioxanthine monophosphate and is then converted to thioguanosine monophosphate (TGMP) by guanine monophosphate synthetase (GMPS). Deoxythioguanine-5'-triphosphate (dthioGTP) can be incorporated into DNA by replicative DNA polymerases.

The therapeutic mechanism of thiopurines is still not fully elucidated. They are selectively toxic towards rapidly proliferating leukaemia cells and activated T cells involved in graft rejection. One suggested mechanism is *via* meTIMP-mediated inhibition of phosphoribosylpyrophosphate amidotransferase. This is the first enzyme in *de novo* purine biosynthesis and it has been proposed that proliferating cells are likely to be particularly susceptible to the resulting purine starvation (Bökkerink et al.,

1993). meTIMP is not formed through 6-TG metabolism, however, and its toxicity clearly implies the existence of an alternative pathway, most likely related to its incorporation into DNA.

Around 0.01-0.03% of the DNA guanine in circulating peripheral blood lymphocytes and skin of azathioprine patients is replaced by 6-TG (Cuffari et al., 2004). Unlike the oxygen atoms of canonical DNA bases, the thiol group of DNA 6-TG is susceptible to chemical methylation - most likely by the cellular methyl group donor S-adenosylmethionine (Swann et al., 1996). Its methylation product (6-meTG) pairs with thymine during replication and the resulting base pairs are processed by the mismatch repair (MMR) system that corrects replication errors. This processing is incomplete and results in the formation of ssDNA breaks (SSB), cell cycle arrest and cell death (Karran, 2001; Swann et al., 1996; Yan et al., 2003). 6-TG cytotoxicity is partly MMR-independent, as MMR-deficient cells are sensitive to high 6-TG concentrations (Karran et al., 2003).

Organ transplant patients have high rates of malignancy. Cancer is the reported cause of death in 25% of kidney transplant patients 10 years after transplantation (Bustami et al., 2004). Although immunosuppression probably plays a part in this susceptibility, comparison with cancer incidence among HIV infected individuals suggests that additional factor(s) influence malignancy in transplant patients (Grulich et al., 2007). Whereas cancers with a known viral aetiology are significantly overrepresented in both HIV positive and transplant patients, skin cancer is by far the most common malignancy among the latter but not the former group. The frequency of SCCs in organ transplant patients is around 100-fold higher than the population average (Euvrard et al., 2003). SCCs account for 90% of the skin cancers in these patients, reversing the normal BCC:SCC ratio. This is not specific to thiopurine use in organ transplant patients. The ongoing and past use of thiopurines for the treatment of inflammatory bowel disease is associated with an increased risk of developing non-melanoma skin cancer even prior to the age of 50 years (Long et al., 2010; Peyrin-Biroulet et al., 2011; Setshedi et al., 2012).

Sun exposure is clearly a factor in transplant associated skin cancer. Tumours develop almost exclusively on sun-exposed regions of the body. They are more

frequent in geographical regions with the most sunshine. In Australia, the cumulative risk of non-melanoma skin cancer 10 years after receiving a transplant is 50%, compared to 10% in the Netherlands (Hartevelt et al., 1990; Ramsay et al., 2002). Facial tumours in British and French organ transplant patients occur preferentially on the right and left sides of the face, respectively, consistent with glass filtered UV exposure during driving (predominantly UVA as UVB is blocked by glass) (Atkar et al., 2013). The likely involvement of UVA in the effects of azathioprine is strengthened by the observation that azathioprine patients exhibit increased sensitivity to erythema and photochemical damage when exposed to UVA but not UVB (Hofbauer et al., 2012; Perrett et al., 2008).

Canonical DNA bases absorb maximally in the UVC region of the spectrum. The substitution of the guanine oxygen atom with sulphur in 6-TG shifts its absorption maximum to the UVA wavelength of 340nm (O'Donovan et al., 2005). DNA 6-TG is a Type I and Type II UVA photosensitiser and a source of $^1O_2$ (Hemmens and Moore, 1986). UVA and DNA 6-TG have synergistic toxicity and mutagenicity (Attard and Karran, 2012). Therefore, UVA activation of normally harmless levels of skin DNA 6-TG is potentially dangerous.

Several consequences of the synergism between DNA and UVA have been reported. DNA 6-TG has a low oxidation potential and is readily oxidised to guanine sulfinate (G^{SO2}) and guanine sulfonate (G^{SO3}). These bulky DNA lesions remain in DNA for over 24 hours after irradiation (Karran, 2006). They block DNA and RNA polymerases and require an error-prone DNA polymerase for bypass, entailing a potential risk of mutation (Brem et al., 2009; Zhang et al., 2007). DNA 6-TG and UVA-mediated replication and transcription inhibition triggers a cell cycle checkpoint response through ATR (ataxia telangiectasia and Rad3 related) and Chk1 (checkpoint kinase 1) phosphorylation (Brem et al., 2010; 2009; Zhang et al., 2007). DNA 6-TG and UVA also induces collateral DNA damage in the form of DNA 8-oxo-dG (8-oxo-7,8-dihydro-2‘-deoxyguanosine), some of which is derived from the oxidized dNTP pool (Cooke et al., 2008).

UVA activation of DNA 6-TG increases the vulnerability of DNA near the replication fork to breakage. Cells deficient in homologous recombination (HR), the pathway that

repairs DNA double strand breaks (DSB) during S phase, are hypersensitive to UVA-activated DNA 6-TG. Consistent with a particular S phase sensitivity, cells with a deficiency in non-homologous end joining (NHEJ) which repairs DSBs outside of S phase are not hypersensitive to UVA-activated DNA 6-TG (Brem et al., 2010).

6-TG also causes interstrand crosslinks (ICL) between DNA 6-TG and canonical DNA bases in a UVA-dependent and -independent manner (Brem and Karran, 2012). This reaction is the consequence of 6-TG mediated antioxidant depletion and the presence of DNA embedded 6-TG that serves as a target for ROS-mediated crosslinking (Brem and Karran, 2012). Cells defective in the Fanconi anaemia (FA) pathway (see Section 1.2.3.5), which processes ICLs by HR, are sensitive to both 6-TG and to UVA-activated DNA 6-TG.

UVA-activated DNA 6-TG causes protein damage. $^1O_2$ mainly targets tryptophan, histidine, methionine, cysteine and tyrosine *in vitro*, and carbonyls are formed through oxidation of aromatic amino acids (Oleinick et al., 2009; Silvester et al., 1998). The subunits of the homotrimeric PCNA (proliferating cell nuclear antigen) complex become crosslinked *via* a His-Lys covalent bond in cells treated with 6-TG and UVA (Montaner et al., 2007). 6-TG mediated damage impairs proteins from various DNA repair pathways, including non-homologous end joining (NHEJ) by protein-protein crosslinking of Ku70 and Ku 80, base excision repair (BER) of 8-oxo-G by oxidation of OGG1 and MYH, and nucleotide excision repair (NER) (Gueranger et al., 2014). Ku was originally identified as an oxidised protein in a screen for protein carbonyls and Ku80 was shown to contain sulfenic acid, suggesting that the same protein can be oxidised in several ways (Leonard et al., 2009).

1.2.3.2 Ciprofloxacin

The first developed quinolone antibiotic, nalidixic acid, did not have a wide clinical use. In contrast, the fluoroquinolones that have a fluorine in the 6-position, are the most widely prescribed family of antibiotics. They have an improved half-life, absorption and antibacterial efficacy (Domagala, 1994). Fluoroquinolones prevent bacterial growth by inhibiting DNA gyrase and topoisomerase IV, which have crucial

roles in replication (Higgins et al., 2003; Maxwell, 1992). UVA and UVB photosensitising activity is a side effect of several fluoroquinolones and their photoactivation generates ROS (Hooper and Wolfson, 1985).

Absorbance of UVA and UVB radiation by ciprofloxacin results in the production of $^1O_2$ along with $O_2\bullet^-$, H_2O_2 and •OH. In the presence of DNA these cause SSB and cyclobutadithymine (T<>T) CPDs through Type I and Type II photosensitised reactions (Agrawal et al., 2007; Lhiaubet-Vallet et al., 2007; Spratt et al., 1999). Cultured rat epithelial cells exhibit a significant increase in DNA 8-oxo-dG when treated with lomefloxacin or ciprofloxacin in combination with UVA (Rosen et al., 1997). Production of DNA 8-oxo-dG and SSB by UVA-activated ciprofloxacin is suppressed by NaN_3 ($^1O_2$ scavenger) and *N-tert*-butyl-α-phenylnitrone (BPN, radical scavenger) and is amplified by D_2O, implicating $^1O_2$ and radicals in their formation (Spratt et al., 1999).

1.2.3.3 Ofloxacin

The fluoroquinolone ofloxacin is a racemic mixture of 50% levofloxacin (the biologically active component) and the R-enantiomer dextrofloxacin. The usage of ofloxacin is increasing worldwide for the treatment of urinary tract infections (Dwivedi et al., 2014). Ofloxacin produces $^1O_2$, $O_2\bullet^-$ and •OH when exposed to UVA, UVB or sunlight (Ray et al., 2006; Viola et al., 2004). Cellular damage caused by UVA-activated ofloxacin includes oxidation of pyrimidine and purine bases through both Type I and Type II mechanisms (Dwivedi et al., 2014; Lhiaubet-Vallet et al., 2003).

The S-stereoisomer of ofloxacin, levofloxacin, is more damaging to cellular macromolecules than ofloxacin (Lhiaubet-Vallet et al., 2003). It decreases HaCaT cell viability, induces micronuclei and lipid peroxidation and causes G2/M cell cycle arrest (Dwivedi et al., 2012). UVA-activated ofloxacin can destroy the actin filament network and cause the release of cytochrome c, caspase-3 activation and apoptosis (Ouédraogo et al., 1999). These effects are quenched by antioxidants DABCO (1,4-diazabicyclo[2.2.2]octane), NaN_3, D-mannitol and N-acetyl cysteine (NAC) (Dwivedi et al., 2012).

Ofloxacin forms T<>T CPDs much less efficiently than ciprofloxacin. Neither induces 6,4 Py:Pys (Peacock et al., 2014; Sauvaigo et al., 2001). Consistent with this difference, UVA-activated ciprofloxacin blocks replication more efficiently than ofloxacin (Peacock et al., 2014). Both treatments cause extensive protein carbonylation, PCNA protein-protein crosslinking and inhibit NER (Peacock et al., 2014).

UVA-activated ciprofloxacin and ofloxacin induce benign skin tumours and a few cases of SCCs and solar keratosis in Skh-1 hairless mice (Mäkinen et al., 1997). UVA-activated ciprofloxacin depletes antigen presenting Langerhans cells and suppresses local but not systemic immunity in mice (Sun et al., 2001). In the treatment of ocular infections, ofloxacin and ciprofloxacin cause phototoxic reactions resulting in decreased viability of lens epithelial cells and photopolymerisation of α-crystallin (Zhao et al., 2010).

Photodegradation also compromises the antibiotic efficacy of ofloxacin and reduces its ability to bind DNA gyrase (Singh et al., 2016). Although short term treatment with fluoroquinolones is unlikely to significantly increase skin cancer risk, their long term prophylactic use by immunosuppressed organ transplant patients may be more of a cause for concern (Green et al., 2011).

1.3 DNA damage and repair

Since the ~10^{13} cells in the human body sustain tens of thousands of DNA lesions of various types every day, they have evolved highly coordinated strategies to cope with DNA damage. These are known collectively as the DNA damage response (DDR) (Jackson and Bartek, 2009). DDR can trigger DNA repair, cell cycle arrest or cell death pathways. The genetic conditions xeroderma pigmentosum (XP), ataxia-telangiectasia and FA are all defective in different aspects of DDR.

Hydrolytic reactions are a source of endogenous DNA damage. Spontaneous hydrolysis of the N-glycosyl bond between DNA bases and deoxyribose, generates

an AP (apurinic/apyrimidinic) site (Lindahl, 1993). Around 10,000 AP sites are created per cell per day (Lindahl and Nyberg, 1972). AP sites are themselves vulnerable to hydrolysis, producing DNA strand breaks (Sugiyama et al., 1994).

Deamination of exocyclic amino groups is another source of spontaneous DNA base damage. Deamination of cytosine to uracil occurs around 100-500 times per cell per day (Krokan et al., 2002). Deamination of adenine and guanine to hypoxanthine and xanthine, respectively, occurs at slower rates (Kow, 2002).

DNA modification by endogenous alkylating agents targets the O and N atoms of nucleobases. These reactions can be stimulated by methyl donor S-adenosylmethionine, nitrosated amines and methyl radicals formed through lipid peroxidation (Dexheimer, 2013).

Mismatches, insertions and deletions are introduced by polymerase errors during DNA replication, at a rate ranging from 10^{-4} to 10^{-6} (McCulloch and Kunkel, 2008). These misincorporations are normally removed by their 3'-5' exonuclease activity, lowering the error rate to 10^{-8}, which means one mutation for 100 million base pairs replicated without the involvement of repair enzymes. Other types of endogenous DNA damage include incorrect incorporation of non-canonical nucleosides such as 8-oxo-dG and dU, erroneous DNA repair and abortive topoisomerase activity resulting in a covalent crosslink with DNA (Bridges, 2005; McClendon and Osheroff, 2007; Pourquier and Pommier, 2001; Shimizu et al., 2003).

Exogenous sources of DNA damage include UV radiation as well as ionising radiation from natural (cosmic and gamma radiation) and artificial sources (X-ray and radiotherapy), which can result in DSBs and ROS mediated DNA lesions (Dexheimer, 2013).

1.3.1 UVB mediated DNA damage

Nucleic acids absorb UVB. In skin, aromatic amino acids in the *stratum corneum* absorb a significant amount of UVB to protect DNA in living skin cells (Hussein, 2005).

UVB induces CPDs and 6,4 Py:Pys (Figure 1.9), which account for the vast majority of UVB mediated photoproducts in double-stranded DNA (dsDNA). All four possible CPDs, T<>T, C<>T, T<>C and C<>C have been identified in irradiated naked and cellular DNA. The cyclobutadithymine (T<>T) is the most common UVB-induced photoproduct (Cadet et al., 2005).

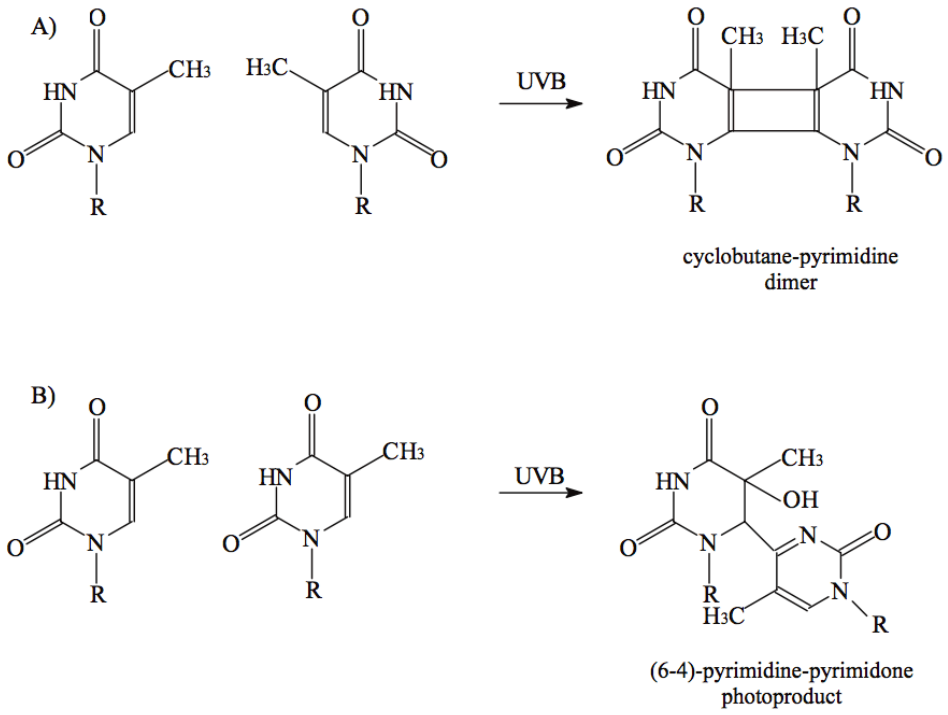

Figure 1.9: UVB mediated DNA damage (Svobodova et al., 2006)
Formation of **(A)** cyclobutane pyrimidine dimers and **(B)** 6,4 pyrimidine-pyrimidone photoproducts upon UVB absorption.

For UVB, the ratio between CPDs and 6,4 Py:Pys is around 4:1 (Douki and Cadet, 2001; Perdiz et al., 2000). In mammalian cells and explanted human skin the T<>T CPD to 6,4 T:T ratio is 10:1 (Douki and Cadet, 2001; Douki et al., 2003b; Mouret et al., 2006). The yield of T<>C CPDs is comparable to that of 6,4 T:C (1:1.1).

Failure to remove these DNA lesions can result in mutation. Because 6,4 Py:Pys induce a more severe structural distortion, they are repaired more efficiently than CPDs (see section 1.3.3.4). As CPD repair is less efficient, these lesions are likely to be the main contributor to mutations in human cells. Mutation analysis indicates

that T<>C and C<>C CPDs are the most mutagenic, and C→T transitions in bipyrimidine sites and CC→TT tandem mutations are the predominant mutations in skin tumours (Ichihashi et al., 2009; Ikehata et al., 2003; Reid and Loeb, 1993; Skinner and Turker, 2008).

UV also causes mutations in mitochondrial DNA, including the 4977bp common deletion and/or 3895bp deletion. Mitochondrial DNA is particularly susceptible to damage owing to the absence of histones and only minimal protection from DNA repair (Reimann et al., 2008).

1.3.2 UVA mediated DNA damage

UVA induces CPDs in cellular DNA (Tyrrell, 1973). Importantly, it is also a source of ROS including $^1O_2$. Guanine has the lowest ionisation potential of the canonical DNA bases and the most susceptible to both Type I and Type II oxidation, followed by adenine and pyrimidines (Svobodova et al., 2006).

Following a type I reaction, in which an excited chromophore carries out a one electron oxidation of DNA, a radical cation intermediate is generated, which can undergo hydration or deprotonation (Svobodova et al., 2006). Guanine is the main target of this type of oxidation. Hydration of a guanine radical cation results in a radical intermediate, which under reducing conditions forms 2,6-diamino-4-hydroxy-5-formamidoguanine (FapyGuanine) through a ring opening reaction. Under oxidising conditions or in the presence of molecular oxygen, it forms 8-oxo-7,8-dihydroguanine (8-oxo-G) or 8-oxo-dG as seen in Figure 1.10 (Svobodova et al., 2006). UVB can also result in the formation of 8-oxo-dG, but the yield of this product is 2-3 orders of magnitude lower than the amount of CPDs or 6,4 Py:Pys generated (Kielbassa et al., 1997).

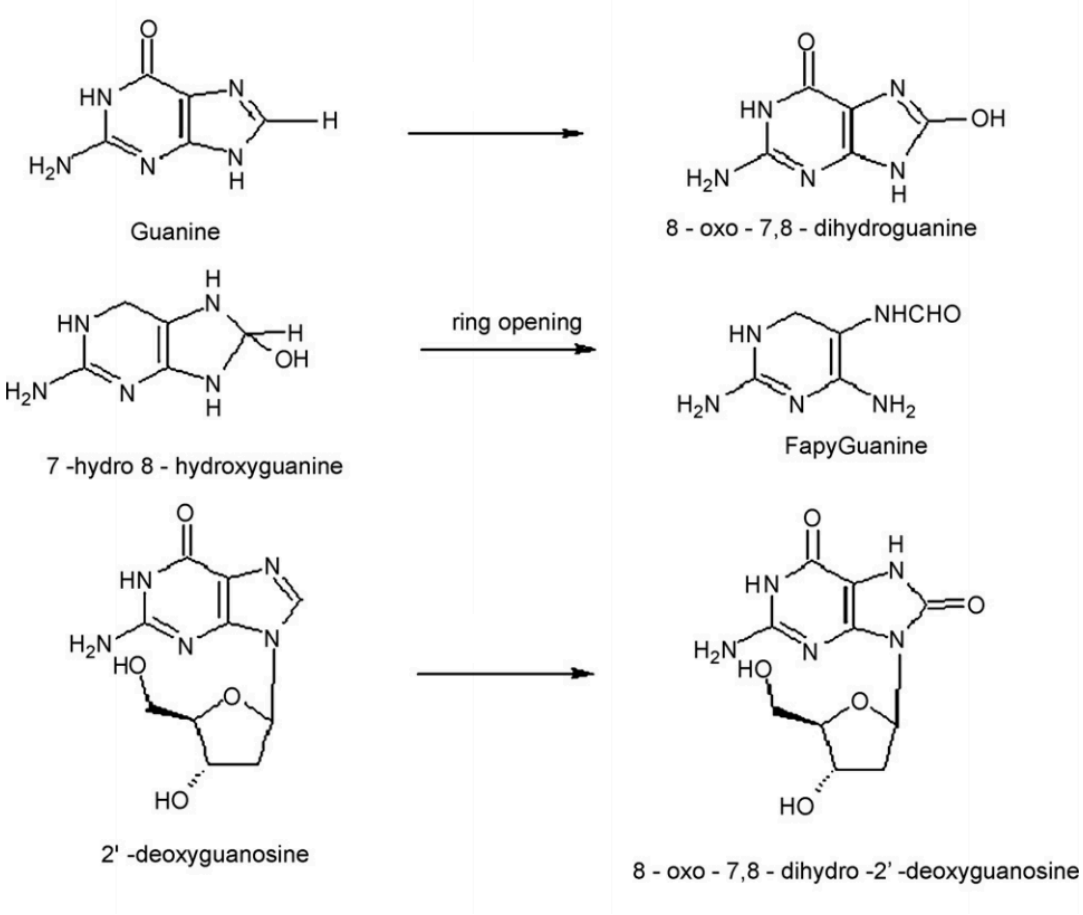

Figure 1.10: DNA oxidation products (Malayappan et al., 2007)
Oxidised guanine forming 8-oxo-7,8-dihydroguanine (8-oxo-G), 2,6-diamino-4-hydroxy-5-formamidoguanine (FapyGuanine) and 8-oxo-7,8-dihydro-2'deoxyguanosine (8-oxo-dG).

$^1O_2$ has a strong affinity for molecules with double bonds. Following Type II reactions, $^1O_2$ generates endoperoxides through a cycloaddition reaction of the imidazole ring. The 8-hydroxyperoxyguanine produced by this reaction decomposes to 8-oxo-dG (Pattison and Davies, 2006; Svobodova et al., 2006). Nucleobase damage by UVA occurs more frequently than the formation of SSB and DPCs (Melnikova and Ananthaswamy, 2005). On its own $^1O_2$ is not able to cleave the DNA backbone. However, 8-oxo-dG is 100-fold more reactive with $^1O_2$ than guanosine and its secondary oxidation can promote the formation of SSBs as well as UVA mediated formation of •OH (Cadet et al., 2012). UVA-mediated •OH formation is likely to be responsible for around a quarter of 8-oxo-dG produced, subject to the wavelength of incident UVA and cell type (Svobodova et al., 2006).

Surprisingly, UVA irradiation of human skin induces more CPDs than 8-oxo-dG (9:1 ratio) (Courdavault et al., 2004; Douki et al., 2003a; Mouret et al., 2006). This ratio depends on the cell type. Melanocytes incur higher levels of oxidative stress, which reduces the ratio to 1.4:1 (Ikehata et al., 2008; Kappes et al., 2006). Studies have shown that ketone compounds in UVA irradiated cells cause DNA triplet transfer photosensitisation, and result in the formation of a majority of CPDs (90%) as T<>T followed by T<>C and C<>T (Douki et al., 2003b; Sauvaigo et al., 2001).

1.3.3 DNA repair pathways

1.3.3.1 Base excision repair (BER)

BER is initiated by lesion-specific DNA glycosylases. Enzymes targeting uracil in ss and dsDNA, alkylated purines and oxidised, ring-fragmented or saturated pyrimidines have been characterized (Jacobs and Schär, 2012).

DNA glycosylases (Table 1.1) flip the target base to an extra-helical position to facilitate cleavage of the *N*-glycosyl bond, which generates an AP site (Huffman et al., 2005; Lindahl, 1974). Monofunctional DNA glycosylases have glycosylase activity only (e.g., UNG) and generate an AP-site. AP sites created by monofunctional glycosylases can be processed by AP endonuclease 1 (APE1), which hydrolyses the phosphodiester backbone 5' of the AP site generating a SSB with a 3'-OH and 5'-deoxyribose phosphate (Hitomi et al., 2007). All uracil removing DNA glycosylases are monofunctional, while most glycosylases specialised in the removal of oxidised bases (eg. NTHL1, NEIL1-3) are bifunctional (Krokan and Bjørås, 2013). Bifunctional glycosylases have both glycosylase and lyase activity, which enables them to cleave the DNA strand (Jacobs and Schär, 2012). Their cleavage product, however, differs from that of APE1.

Table 1.1: Mammalian DNA glycosylases and their substrates
U, uracil; A, adenine; T, thymine; C, cytosine; G, guanine; ss, single stranded; ds, double stranded; hm, hydroxymethyl; FU, fluorouracil; ε, etheno; fC, formylcytosine; 5-caC, 5-carboxylcytosine; 8-oxo-G, 8-oxo-7,8-dihydroguanine; Tg, thymine glycol; Fapy, 2,6-diamino-4-hydroxy-5-N-methylformamidopyrimidine; me, methyl; h, hydroxyl. Adapted from (Jacobs and Schär, 2012).

Type of base lesion	Name	Physiological substrates	Mono or Bi functional
Uracil in ssDNA and dsDNA	Uracil-N glycosylase (UNG)	U, 5-FU (ss and ds DNA)	Mono
	Single-strand-specific monofunctional uracil DNA glycosylase 1 (SMUG1)	U, 5-hmU, 5-FU (ss and ds DNA)	Mono
Pyrimidine derivatives in mismatches	Methyl-binding domain glycosylase 4 (MBD4)	T, U, 5-FU, εC, opposite G (dsDNA)	Mono
	Thymine DNA glycosylase (TDG)	T, U, 5-FU, εC, 5-hmU, 5-fC, 5-caC, opposite G (dsDNA)	Mono
Oxidative base damage	8-oxo-G DNA glycosylase 1 (OGG1)	8-oxo-G, Fapy, opposite C (dsDNA)	Bi
	MutY homolog DNA glycosylase (MYH)	A opposite 8-oxo-G, C or G, 2-hA opposite G (dsDNA)	Mono
Alkylated purines	Methylpurine glycosylase (MPG)	3-meA, 7-meG, 3-meG, hypoxanthine, εA (ss and dsDNA)	Mono
Oxidized, ring-fragmented or -saturated pyrimidines	Endonuclease III-like 1 (NTHL1)	Tg, FapyG, 5-hC, 5-hU (dsDNA)	Bi
	Endonuclease VIII-like glycosylase 1 (NEIL1)	Tg, FapyG, FapyA, 8-oxo-G, 5-hU, 5-hC (ss and dsDNA)	Bi
	Endonuclease VIII-like glycosylase 2 (NEIL2)	As NTHL1 and NEIL1	Bi
	Endonuclease VIII-like glycosylase 3 (NEIL3)	FapyG, FapyA (prefers ssDNA)	Bi

The ends that are generated need to be modified to 3'-OH and 5'-phosphate to permit ligation to complete repair. Removal of damaged bases by a bifunctional DNA glycosylase results in an unsaturated hydroxyaldehyde at the 3' end and a 5'phosphate, or 3' phosphate and 5' phosphate ends (Svilar et al., 2011). The 3' end of the former is processed by APE1 to form a 3' OH end, and the 3' end of the latter is processed by polynucleotide kinase/phosphatase (PNKP), which is a bifunctional enzyme with 5' kinase and 3' phosphatase activities.

Two BER pathways are characterized as short and long patch. In short patch BER (80-90% of all BER), AP site repair involves replacement of a single nucleotide by DNA polymerase β, which also removes the 5'-deoxyribose phosphate generated by APE1 (Beard and Wilson, 2006). DNA ligase I or DNA ligase III and XRCC1 ligate the DNA ends to complete repair. Long patch BER is initiated when the terminus created by APE1 or lyase cannot be removed by DNA polymerase β. In this case elongation from the 3'-OH by DNA polymerase/PCNA displaces the 5'-blocking lesion in a flap structure. The flap is then removed by FEN1 (flap endonuclease-1) and the nick is sealed by DNA ligase I.

DNA glycosylase OGG1 (8-oxo-G DNA glycosylase I) removes miscoding 8-oxo-G from dsDNA (Jacobs and Schär, 2012). MYH (MutY homolog DNA glycosylase) is unique in that it works during replication to remove adenine bases misincorporated opposite a template 8-oxo-dG. The removal of adenine and replacement with cytosine prevents the G→T transversion mutations that are the hallmark of oxidation damage to DNA (Besaratinia et al., 2004). In addition, formation of 8-oxo-G in the nucleotide pool results in hydrolysis by MTH to avoid the misincorporation of oxidised guanine opposite adenine in the template strand.

1.3.3.2 Mismatch repair (MMR)

MMR prevents mutation by correcting mispairs that have evaded proofreading by replicative polymerases. By removing the small loops that occur through polymerase slippage during replication of repetitive sequences, MMR also prevents insertion/deletion mutations (Kroutil et al., 1996).

MMR has three stages: recognition of mismatches, excision of the newly-synthesized strand containing the error and a resynthesis step in which the gap left by excision is filled (reviewed in (Kunkel and Erie, 2015)). Human mismatch recognition is initiated by MutSα, a heterodimer of the hMSH2 and hMSH6 proteins that recognises single base mismatches (eg. T:G) and small loops of one or two nucleotides. MutSβ, a hMSH2 and hMSH3 heterodimer, recognises larger insertion/deletion loops and one or two base insertion/deletion mismatches. In the majority (90%) of cases, excision is initiated by MutLα, (hMLH1 and hPMS2). MutSα binds the mismatch and its ATP activated state interacts with the MutLα heterodimer (Friedhoff et al., 2016). PCNA is then loaded by replication factor C (RFC), which activates the PCNA and ATP-dependent endonuclease activity of MutLα and allows it to generate a single-stranded incision (Kadyrov et al., 2006). Strand incision allows access of exonuclease 1 (Exo1) that degrades the error-containing strand in a 5' to 3' direction (Tran et al., 2004). The gap that this creates is filled by DNA polymerase δ, PCNA and replication protein A (RPA), followed by DNA ligase I mediated ligation.

1.3.3.3 Double-strand break repair

DSBs are particularly hazardous and a single unrepaired DSB can result in cell death (Jeggo and Löbrich, 2007). In human cells, DSBs are repaired by homologous recombination (HR) and non-homologous end joining (NHEJ). HR uses the genetic information from the undamaged sister chromatid as a template for repair and is generally error-free. NHEJ ligates the two ends of the DSB in a way that requires limited or no sequence homology, making it a more error-prone mechanism (Raynard et al., 2008). NHEJ is utilised in all phases of the cell cycle, while HR takes place in late S and G2 phases. A very brief overview of the two processes is outlined below and in Figure 1.11.

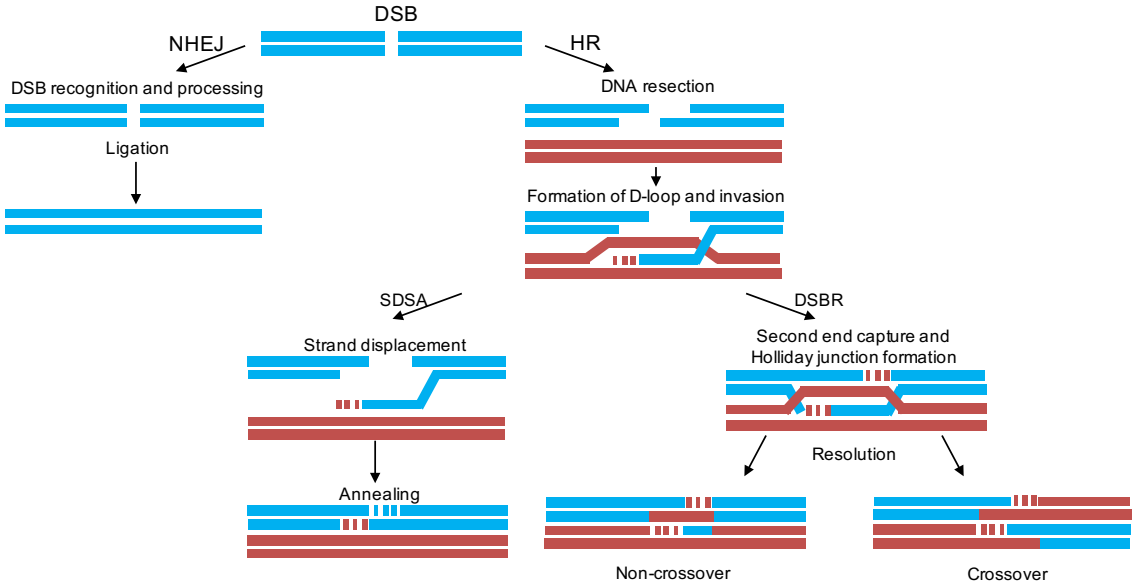

Figure 1.11: Repair of double strand breaks
Double strand breaks (DSBs) are repaired through homologous recombination (HR) and non-homologous end joining (NHEJ) in mammalian cells. From the formation of the displacement (D-loop) the HR pathway branches in two, synthesis-dependent strand annealing (SDSA) and double strand break repair (DSBR). A non-crossover outcome results from SDSA without a change in the template DNA, while DSBR can also result in a crossover.

Homologous recombination follows three stages: presynapsis, synapsis and postsynapsis. The heterotrimeric MRN complex (Mre11 3' to 5' endo/exonuclease-Rad50-Nbs1), along with CtIP, instigate a 5'-end resection to generate 3'-overhangs on both sides of the DSB. This also requires the collective involvement of the BLM helicase and Exo1 exonuclease. The exposed ssDNA generated by the resection is protected by ssDNA binding protein RPA. The Rad51 recombinase then replaces RPA in a reaction that activates ATM and histone γH2A.X phosphorylation (Lukas et al., 2011). This nucleoprotein filament initiates a homology search of the sister chromatid to generate a template for repair. The DNA is then synthesised by DNA polymerase η from the 3' end of the invading strand (McIlwraith et al., 2005). The nicks are ligated by DNA ligase I, resulting in the formation of a Holliday junction. This structure can be resolved through dissolution by BLM-TopIIIα, GEN1/Yen1 or Slx1/Slx4 mediated symmetrical cleavage or endonuclease Mus81/Eme1 mediated asymmetrical cleavage (Ip et al., 2008; Mimitou and Symington, 2009; Seki et al., 2006).

Binding of the Ku70/Ku80 heterodimer to both termini of a DSB instigates recruitment of DNA-PKcs, the catalytic subunit of DNA-dependent protein kinase, to initiate NHEJ (Walker et al., 2001). Autophosphorylation of the DNA end-associated DNA-PKcs tethers the broken ends to facilitate ligation (DeFazio et al., 2002). DSB frequently require modification before ligation by DNA ligase IV/XRCC4/XLF (Ahnesorg et al., 2006). Overhanging terminal ssDNA can be converted to dsDNA by DNA polymerase (Pol μ and Pol λ) or removed through resection by Artemis (Lieber et al., 2008). Artemis is specific to NHEJ and has both a DNA-PK independent 5' to 3' exonuclease activity and a DNA-PK phosphorylation dependent endonuclease activity (Jeggo and O'Neill, 2002). BER enzymes APE1, Tdp1 and PNKP, as well as exonucleases Exo1 and WRN may also participate in end modification process (Chappell et al., 2002; Perry et al., 2006). Since end processing can result in a gain or loss or mispairing of nucleotides, NHEJ is a more error-prone process than HR.

1.3.3.4 Nucleotide excision repair (NER)

NER occurs through two partly-overlapping pathways. Global genome NER (GG-NER) is initiated by the interaction between a DNA repair protein complex and a helix-distorting DNA lesion. Transcription coupled NER (TC-NER) is triggered by RNA polymerase II stalling at a lesion on the template strand during transcription. Both pathways are outlined in Figure 1.12.

Lesion recognition in GG-NER is performed by a complex of the xeroderma pigmentosum complementation group C protein (XPC) with the RAD23B and centrin 2 (CETN2) proteins (Nishi et al., 2005). The XPC/RAD23B/CETN2 complex recognizes a wide spectrum of DNA lesions. Studies in fission yeast led to the development of a model in which XPC binds the ssDNA exposed by disrupted base pairing through inserting its C-terminal double β-hairpin between the dsDNA and ssDNA (Min and Pavletich, 2007).

By comparison to other lesions, including 6,4 Py:PYs, CPDs are surprisingly poor substrates for recognition by XPC/RAD23B/CETN2 (Reardon and Sancar, 2003).

Their recognition is facilitated by the UV-DDB (ultraviolet radiation-DNA damage-binding protein) complex. This comprises the DDB1 and DDB2 proteins which bind UV-induced DNA lesions. UV-DDB binds the CRL complex (cullin 4A (CUL4A), regulator of cullins 1 (ROC1) E3 ubiquitin ligase) and DDB1 links the CRL complex and DDB2 (Marteijn et al., 2014). It is generally thought that DDB2-generated kinks in the DNA to allow XPC to bind the exposed ssDNA lesion (Scrima et al., 2008).

Following XPC binding, TFIIH (transcription initiation factor IIH) complex is recruited to the lesion. TFIIH can switch between its roles in transcription and repair by dissociating from the trimeric CAK transcription subcomplex (CDK-activating kinase) upon binding to XPC (Coin et al., 2008). Two of the ten TFIIH subunits are helicases encoded by the XPB and XPD genes (also ERCC3 and ERCC2, respectively) with complementary polarities. The ATPase activity of XPB is important for the DNA/TFIIH association. The 5' to 3' helicase activity of XPD is essential for NER (Coin et al., 2007). The XPD helicase detects helicase-blocking damage and verifies the presence of lesions. It contains an Fe-S cluster that may be important in this verification process (Mathieu et al., 2013; Sugasawa et al., 2009). The XPA protein, not a part of TFIIH, is also involved in lesion verification (Camenisch et al., 2006).

Lesion excision is carried out by structure specific endonucleases XPF-ERCC1 and XPG (ERCC5), which cleave DNA 5' and 3' of the damaged site, respectively (Fagbemi et al., 2011). XPA interacts with nearly all NER proteins and is particularly important in recruiting XPF-ERCC1 (Tsodikov et al., 2007). RPA, an interacting partner of XPA, protects ssDNA from endonucleases and assists in the correct orientation of XPF-ERCC1 and XPG (de Laat et al., 1998). XPG needs to be present to allow XPF-ERCC1 mediated 5' incision. Once this 5' incision takes place, DNA synthesis can begin. The synchronisation of excision/resynthesis by RPA and XPG counteracts the accumulation of 22-35 nucleotide ssDNA gaps and onset of DNA damage signalling (Mocquet et al., 2008; Overmeer et al., 2011). The gap is filled by the coordinated action of PCNA and RFC, together with DNA Pol ε and DNA ligase I in replicating cells or DNA Pol κ/δ and XRCC1–DNA ligase III in non-replicating cells (Moser et al., 2007; Ogi et al., 2010).

UV induced lesions during S phase causing stalled replication forks and long stretches of RPA bound ssDNA result in ATRIP (ATR-interacting protein), TOPBP1 (topoisomerase 2-binding protein 1) and 9-1-1 complex binding to RPA (Bartek and Lukas, 2007). This results in ATR activation and γH2A.X phosphorylation. NER intermediates with a single bound RPA heterotrimer may not be sufficient to generate ATR signalling (MacDougall et al., 2007). When there is a shortage of NER factors during high damage load, when two NER reactions collide, when repair synthesis is inhibited or when 3' incision does not take place, Exo1 (5'-3') can be recruited instead of XPG and generate longer regions of ssDNA (Sertic et al., 2011). This can form a ssDNA gap of up to 1kb that is covered by RPA, which can cause a reaction similar to DSB signalling and recruit ATRIP/ATR and phosphorylate γH2A.X.

Despite the help provided by UV-DDB, the removal of CPDs is still relatively inefficient. Persistent CPDs interfere with replication and transcription. Stalled replication forks can result in DSBs and activate cell cycle checkpoints. During replication, alternative DNA polymerases or template switching can be used for lesion bypass. To date RNA polymerases with the ability to carry out transcriptional lesion bypass of helix distorting adducts have not been identified.

The TC-NER pathway removes transcription-blocking DNA lesions and is initiated by stalled RNA polymerase II. Transcription stalling induces recruitment of Cockayne syndrome proteins CSA (Cockayne syndrome WD repeat protein A) and CSB (Cockayne syndrome protein B). The lesion is made available for repair by RNA polymerase II backtracking. Additional factors involved in TC-NER initiation include: UV-stimulated scaffold protein A (UVSSA), ubiquitin-specific-processing protease 7 (USP7), XPA-binding protein 2 (XAB2) and high mobility group nucleosome-binding domain-containing protein 1 (HMGN1) (Marteijn et al., 2014). Cockayne syndrome is a severe neurodevelopmental disorder with symptoms that include photosensitivity, growth abnormalities, premature aging and likely death within the first decade of life (Brooks, 2013). Around 80% of Cockayne syndrome cases occur due to mutations in CSB, which not only has a role in TC-NER but also BER, mitochondrial function and transcriptional regulation (Brooks, 2013). It has been proposed that the neurodevelopmental problems occur as a result of imperfect gene regulation as opposed to DNA repair defects (reviewed in (Brooks, 2013), (Wang et al., 2016)).

CSB also has an important role in regulating transcriptional response to UV irradiation (Proietti-De-Santis et al., 2006).

In the context of chromatin, DNA needs to be made accessible to NER repair factors through histone tail modifications and histones need to be shifted along DNA by ATP-dependent chromatin remodelling enzymes (Schärer, 2013). This chromatin rearrangement during NER led to the proposal of the “access-repair-restore” model (Smerdon, 1991; Smerdon and Lieberman, 1978). There are several candidates for chromatin remodelling in NER, such as the SWI/SNF family of proteins, but the exact mechanism by which this occurs is not clear (Zhao et al., 2009).

Mutations in NER cause xeroderma pigmentosum (XP), an inherited disorder characterized by UV-sensitivity, susceptibility to UV mutagenesis and skin cancer predisposition. There is significant clinical heterogeneity in XP. Patients who have defects in exclusively GG-NER proteins XPC and XPE have >1000-fold increase risk of sun-related skin cancer, skin hypo/hyper pigmentation and a substantially increased risk of developing internal tumours (Marteijn et al., 2014). Mutations in proteins that are involved in both TC and GG-NER can exhibit additional symptoms. XPD mutations can range from XP to a combination of XP and Cockayne syndrome, as well as Cerebro-oculo-facio-skeletal syndrome (COFS). Mutations in genes encoding XPD, XPB and TTDA can result in trichothiodystrophy, a disorder of sulphur metabolism that displays similar symptoms to Cockayne syndrome with the addition of brittle hair and nails and scaly skin (Kraemer et al., 2007). These overlapping symptoms reflect effects on transcription and gene expression during hair, nail and skin differentiation. XPF-ERCC1 is involved in NER, interstrand crosslink repair (ICL) and DSB repair. As a consequence, *XPF* or *ERCC1* mutations can result in XP, severe Cockayne syndrome, COFS and/or FA features (Jaspers et al., 2007; Kashiyama et al., 2013).

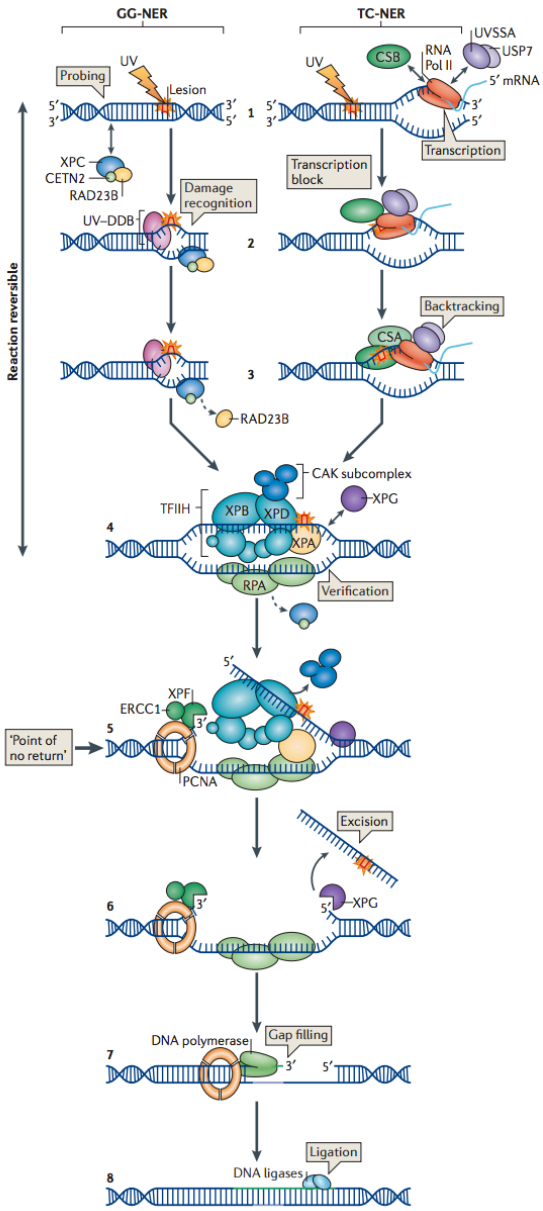

Figure 1.12: Outline of nucleotide excision repair (Marteijn et al., 2014) In GG-NER (global genome nucleotide excision repair), XPC in complex with RAD23 homologue B (RAD23B) and centrin 2 (CETN2) recognise helix distorting lesions **(left, 1)** and are aided by UV–DDB (ultraviolet (UV) radiation–DNA damage-binding protein) complex **(left, 2)**. Upon XPC binding, RAD23B dissociates **(left, 3)**. UV-stimulated scaffold protein A (UVSSA), ubiquitin-specific-processing protease 7 (USP7) and Cockayne syndrome protein CSB transiently interact with RNA Pol II throughout transcription elongation **(right, 1)**. This interaction is stabilised by RNA Pol II stalling at a lesion **(right, 2)**, which initiates TC-NER (transcription-coupled NER). This forms Cockayne syndrome WD repeat protein CSA–CSB complex. There is some backtracking by RNA Pol II to reveal the lesion **(right, 3)**. At this point the two pathways both recruit the TFIIH (transcription initiation factor IIH) complex, where upon binding the CAK (CDK-activating kinase) subcomplex dissociates from TFIIH **(4)**. XPG is a structure specific endonuclease that is recruited to the pre-incision complex. TFIIH helicase activity (XPD) exposes the lesion further and contributes to lesion verification, along with XPB and XPA. Single stranded DNA binding protein replication protein A (RPA) binds and protects the undamaged strand. XPF-ERCC1 structure specific endonuclease is recruited by XPA and RPA to 5' of the lesion **(5)**. Following incision by XPF-ERCC1 the process is no longer reversible and is followed by XPG incision of the damaged DNA at the 3' end, producing a 22-30 nucleotide excision product **(6)**. Proliferating cell nuclear antigen (PCNA) is recruited, followed by DNA Pol δ, DNA Pol κ or DNA Pol ε for DNA synthesis **(7)** and the nick is sealed by DNA ligase I or III **(8)**.

1.3.3.5 Interstrand crosslink repair (ICL)

ICLs inhibit DNA separation. As a consequence, they block replication and transcription and are highly toxic. They are induced by a range of chemotherapeutic drugs, particularly those used in the treatment of leukaemias. The repair of ICLs is defective in Fanconi anaemia (FA), a rare genetic disorder that causes reduced fertility, congenital abnormalities, bone marrow failure and increased predisposition to haematological and squamous cell cancers (Deans and West, 2011). FA cells are extremely sensitive to the toxic effects of ICL-inducing agents. Following exposure they exhibit high levels of chromosome breakage and fusion of the broken arms of non-homologous chromosomes (radial chromosomes) (Deans and West, 2011). These radial chromosomes are considered a hallmark of ineffectively processed ICLs. The FA pathway contains 19 gene products (Ceccaldi et al., 2016). Seven FA gene products (FANCA, FANCB, FANCC, FANCE, FANCF, FANCG and FANCL) form a multiprotein assembly known as the FA core complex. Most of the mutations identified in FA patients are FANCA (65%), FANCC (15%) or FANCG (10%) (Fanconi Anaemia Mutation Database). Patients with BRCA2/FANCD1 or PALB2/FANCN mutations have increased susceptibility to cancer development and particularly medulloblastoma in the case of FANCD1.

The FANCM protein recognises ICLs during S phase (Niedernhofer, 2007). Subsequent recruitment of the FA core complex results in the monoubiquitination of FANCD2-FANCI – a process that depends on the simultaneous presence of all FA complex components. Although the consequences of these protein modifications have not been fully clarified, a proposed mechanism suggests that monoubiquitination stabilises the otherwise transient interaction of FANCD2-FANCI with damaged DNA (Deans and West, 2011).

Subsequent processing of the ICL involves proteins from HR, NER and translesion synthesis (TLS) pathways. A variety of nucleases and polymerases are recruited to the damaged region. Multiple nuclease recruitment may reflect different types of ICLs (different levels of DNA distortion) or different requirements depending on the cell cycle phase.

HR factors are recruited to the damaged area to stabilise the fork. Fanconi associated nuclease (FAN1) can interact with monoubiquitinated FANCD2 and can degrade ssDNA or dsDNA through its 5'-3' exonuclease and 5'-flap endonuclease activity. The coordinated action of the recruited FAN1 and MUS81-EME1 3'-flap endonuclease allows unhooking of the ICL (Deans and West, 2011). Once the translesion polymerase is recruited, the replicative polymerase stalls to allow the exchange to the translesion polymerase (Zhuang et al., 2008). Although there are several translesion polymerases, REV1 and Pol ζ seem to be essential for ICL repair and are error-prone and mutagenic (Räschle et al., 2008). After sufficient extension past the lesion, the replicative polymerase is reinstated (Huang et al., 2006). The translesion synthesised area will still be a substrate for DNA repair. Once the FA complex dissociates, deubiquitinating enzyme ubiquitin-specific peptidase 1 (USP1) can deactivate the pathway. Exposure of ssDNA during these processes results in RPA binding to ssDNA and the stimulation of cell cycle checkpoints by ATR-Chk1 signalling cascade.

1.3.3.6 Translesion synthesis (TLS)

Genomic DNA is normally replicated by DNA polymerase α, δ and ε, where Polα initiates DNA synthesis with an RNA primer, while DNA Polδ and ε elongate the primers. Polδ and ε are high fidelity enzymes that have 3'-5' exonuclease activity to remove base substitution errors (McCulloch and Kunkel, 2008). Replicative DNA polymerases have limited ability in replicating opposite damaged bases and therefore are exchanged with translesion bypass polymerases (Schmitt et al., 2009). TLS polymerases include Y-family polymerases POLη, POLι, POLκ and REV1, and B-family polymerase POLζ (Waters et al., 2009). None of these have proofreading exonuclease activity.

A deficiency in POLη results in XP-V and increased risk of SCCs (Masutani et al., 1999). Polη is able to bypass T<>T CPDs, the most common lesion caused by UV radiation, exhibiting high efficiency and fidelity. The mutation results in loss of specific contacts made by Polη with T<>T (Silverstein et al., 2010). This results in DSB formation where replication forks stall and collapse at sites of UV radiation induced

damage on the template strand (Limoli et al., 2002). Polη does not exhibit as high fidelity when bypassing 6,4 T:T and generally incorporates one G (Szüts et al., 2008). POLι is better at inserting the correct bases across from this lesion, however, it is extremely mutagenic when faced with T<>T or undamaged DNA (Johnson et al., 2000). REV1 is also involved in bypass of UV-mediated damage in cells and may have a role in interacting with monoubiquitinated PCNA and Y-family polymerases to regulate DNA polymerase switching (Jansen et al., 2009)

Chapter 2. Materials & Methods

2.1 Chemicals and reagents

All chemicals and reagents were obtained from Sigma-Aldrich, unless otherwise stated.

Standard solutions of 1M Tris-HCl, 0.5M Ethylenediaminetetraacetic acid (EDTA), 1M $MgCl_2$, 5M NaCl, 10x Tris-Borate-EDTA (TBE), phosphate-buffered saline (PBS), 10x tris-buffered saline (TBS) and 20x saline sodium citrate (SSC) were sourced from The Francis Crick Institute Central Services.

2.2 Cell culture

2.2.1 Cell maintenance

DMEM (Dulbecco's Modified Eagle Medium) and RPMI (Roswell Park Memorial Institute) 1640 Medium were obtained from Thermo-Fisher (Gibco™). Penicillin and streptomycin (Pen/Strep), were obtained from The Francis Crick Institute Central Services. Foetal Calf Serum (FCS) and Dialysed FCS were obtained from Thermo-Fisher. Sterile plastic equipment was obtained from Becton Dickinson, Corning and Fisher Scientific.

The cell lines and cell culture conditions are specified in Table 2.1. RPA16 and RPA21 cells were grown in medium containing G418 (200μg/ml), which was removed during experiments. All cells were grown at 37°C in a humidified atmosphere containing 5 or 10% CO_2. Cells were counted using a haemocytometer or Cellometer® Auto T4 (Nexcelom Bioscience).

Table 2.1: Cell lines used and their individual cell culture methods

Cell Line	Organism	Cell Type	Cell Culture Method
HeLa	Human	Epithelial	DMEM 10% FCS, Pen/Strep, 10% CO_2
U2OS	Human	Epithelial	DMEM 10% FCS, Pen/Strep, 10% CO_2
RPA16	Human	Epithelial	DMEM 10% FCS, Pen/Strep, 10% CO_2, G418
RPA21	Human	Epithelial	DMEM 10% FCS, Pen/Strep, 10% CO_2, G418
GM8339	Human	Fibroblast	DMEM 10% FCS, Pen/Strep, 5% CO_2
CCRF-CEM	Human	T leukemic lymphoblast	RIPA 1640 10% Dialysed FCS, Pen/Strep, 5% CO_2
GM03467 Lesch-Nyhan	Human	Fibroblast	DMEM 15% FCS, Pen/Strep, 5% CO_2

2.2.2 Drug treatments

6-thioguanine (6-TG): Stock solution of 1mM 6-TG dissolved in 0.1mM NaOH was filter sterilised. It was added to cells at around 50% confluency. Cells were incubated with 6-TG for 24 hours for all experiments, except when measuring 6-TG incorporation where the incubation was 48 hours.

Ciprofloxacin and ofloxacin: Stock solution of 50mM fluoroquinolone dissolved in 0.1mM NaOH was filter sterilised. Cells were treated in medium (with FCS) for 1 hour at 37°C.

6-formylindolo[3,2-b]carbazole (FICZ): FICZ was purchased from Enzo (Plymouth Meeting, PA). Stock solution of 200μM dissolved in dimethyl sulfoxide (DMSO) was filter sterilised. Cells were treated in medium (with FCS) for 2 hours at 37°C.

For irradiation, treated cells were rinsed in PBS and adherent cells irradiated through a thin layer of PBS (5 ml per 100mm dish).

2.2.3 Antioxidant treatments

Antioxidants ascorbic acid (1M stock, in water), N-acetyl cysteine (200mM stock, in water) and allopurinol (200mM stock, in 0.1M NaOH) were present throughout 6-TG treatment.

2.2.4 UVA irradiation

Cells were irradiated in PBS using a UVH 253 lamp (UV Light Technology Limited) with a low range cut off at 320nm, high range cut off at 400nm and maximum emission at 365nm. The standard dose rate was 0.1kJ/m^2/s measured using a UVA dosimeter (UV Light Technology Limited). The irradiation chamber includes a temperature control unit that maintains a temperature range of 10-15°C during irradiation.

2.2.5 UVC irradiation

UVC irradiation (254nm) was performed using a Stratalinker UV Crosslinker (Stratagene). The machine was calibrated to deliver 10J/m^2/s. For experiments with combined UVA and UVC irradiation, drug treatment preceded UVA, which preceded UVC irradiation.

2.3 Biochemical techniques

2.3.1 CM-H_2DCFDA (5-(and-6)-chloromethyl-2',7'-dichlorodihydrofluorescein diacetate, acetyl ester) assay

Treated cells ($8x10^6$) were washed with PBS and resuspended in 1.5ml PBS. CM-H_2DCFDA (Thermo Fisher) was added at a final concentration of 7.5μM and the cells incubated at 37°C for 20 minutes. They were transferred to 100mm dishes and UVA irradiated. Following washing and resuspension in PBS, FACS (fluorescence-activated cell sorting) analysis was carried out using a Beckton Dickinson FACScan. The fluorescence intensity and frequency distribution data were collected and analysed using BD CellQuest™ Pro v3.3 software.

2.3.2 Cell extracts

2.3.2.1 RIPA and non-denaturing extracts

Cells (generally $8x10^6$) were suspended in three pellet volumes of extraction buffer, either RIPA (Radioimmunoprecipitation assay) buffer or non-denaturing buffer (Table 2.2 for chemicals and concentrations). Following 20 minutes on ice, cells were disrupted by vortexing. Extracts were centrifuged at 20,000g for 20 minutes.

Pellets were discarded and supernatant protein concentrations were measured by Bradford assay (Bio-Rad). Supernatants were stored in aliquots at -80°C.

Table 2.2: Components of the radioimmunoprecipitation assay (RIPA) and non-denaturing lysis buffers

RIPA buffer		**Non-denaturing lysis buffer**	
Chemical	**Final Concentration**	**Chemical**	**Final Concentration**
Tris-HCl (pH 7.5)	50mM	**Tris-HCl (pH 7.5)**	20mM
NaCl	150mM	**NaCl**	137mM
Sodium Dodecyl Sulphate (SDS)	0.1%	**Glycerol**	10%
Sodium Deoxycholate	0.5%	**Nonidet P-40 (NP-40)**	1%
Triton x100	1%	**EDTA**	2mM
cOmplete Protease Inhibitor Cocktail Tablets	1 tablet	**cOmplete Protease Inhibitor Cocktail Tablets**	1 tablet

2.3.2.2 Benzonase treatment

Benzonase treatment of RIPA extracts was as follows: $MgCl_2$ and benzonase were added to reach a final concentration of 2mM and 2.5U/µl, respectively. Digestion was allowed to proceed for 15 min at room temperature. Digested extracts were then centrifuged at 20,000g for 20 min.

Sodium deoxycholate has a negative impact on benzonase activity but benzonase retains 60% activity at 0.5% concentration of sodium deoxycholate. SDS partially inactivates benzonase. Therefore, high benzonase concentrations were used to allow benzonase to retain its activity.

2.3.3 Polyacrylamide gel electrophoresis (PAGE)

10-well, 10% polyacrylamide NuPAGE® Bis-Tris Precast Gels (Life Techonologies, Thermo Fisher) were electrophoresed in X-cell SureLock Mini Cells. Cell extracts

(20µg protein) were mixed with loading buffer (β-Mercaptoethanol (1%), Dithiothreitol (DTT, 20mM), Bromophenol blue (0.004%), Glycerol (6%), SDS (2%), Tris-HCl (50 mM, pH 7.5)). Extracts were heated for 10 minutes at 95°C. Each gel was run with Amersham ECL Full-Range Rainbow Molecular Weight Markers (GE Healthcare Life Sciences).

2.3.4 Immunoblot

Following protein gel electrophoresis, proteins were transferred to PVDF (polyvinylidene difluoride) membranes (Immobilon-P, Milipore) overnight at 4°C using a Bio-Rad wet transfer apparatus. After transfer, membranes were washed at room temperature with water and TBS-T (TBS+0.1% Tween 20). Membranes were blocked for 1 hour with 10% (w/v) non-fat powdered milk in TBS-T. They were then incubated for 2 hours at room temperature with primary antibodies (Table 2.3 for dilutions and suppliers) diluted in 5% milk in TBS-T. After washing with TBS-T, membranes were incubated with the appropriate secondary antibody (Table 2.3 for dilutions and suppliers) at 1:5000. Proteins were visualised using Amersham ECL Western Blotting Detection Reagent (GE Healthcare Lifesciences) and Amersham Hyperfilm ECL (GE Healthcare Lifesciences).

Table 2.3: The antibodies used in this work, their suppliers and dilutions- all dilutions in 5% milk in TBS-T (TBS+0.1% Tween 20); HRP, horseradish peroxidase

Antibody	Supplier	Dilution
XPA	Abcam	1:1000
XPD	Abcam	1:1000
RPA14	Abcam	1:1000
RPA32	Abcam	1:1000
RPA70	Abcam	1:1000
β-Tubulin	Abcam	1:1000
PCNA	Santa Cruz	1:1000
MSH2	Santa Cruz	1:500
Goat Anti-Mouse HRP	Bio-Rad	1:5000
Goat Anti-Rabbit HRP	Bio-Rad	1:5000

2.3.5 Electrophoretic mobility shift assay (EMSA)

2.3.5.1 ^{32}P labelling of oligonucleotides

A 51 nucleotide oligonucleotide (5'GGGGACCACTTTGTACAAGAAAGCTGGGTCTCACATCAATGCACTTCTCCT 3') (0.2pmol/µl) was mixed with T4 Kinase Buffer, T4 polynucleotide kinase (2U/µl final concentration) (both New England Biolabs), and 3µl γ-[^{32}P]-ATP (Amersham Pharmacia) in a final volume of 10µl. Following incubation for 40 min at 37°C, the labelled oligonucleotide was recovered using a G50 spin column (Amersham Pharmacia) and stored at 4°C.

2.3.5.2 RPA-DNA binding and PAGE

Cell extracts (25µg) were incubated in a total volume 20µl containing 2µl γ^{32}P-labelled oligonucleotide (80fmol) and 1µl Poly(dA-dT) for 30 minutes at 37°C. For the supershift analysis, anti-RPA32 antibody was also present (1:50 dilution). Following incubation, 4µl of loading buffer (50mM Tris-HCl pH8, 10% glycerol, 2mM EDTA, bromophenol blue) was added to each sample. Samples were electrophoresed at 80V on 12.5% polyacrylamide gels in 0.5x TBE. Gels were fixed in 10% glycerol for 30 minutes and dried. They were then exposed to a Storage Phosphor Screen and imaged using a Typhoon scanner (both GE Healthcare Lifesciences).

2.3.6 Immunoprecipitation

Anti-RPA32 antibody (1:50 dilution) in TBS-T was combined with 1.5mg Dynabeads® Magnetic Beads (Thermo Fisher) and incubated with constant rotation for 10 min at room temperature. Beads were recovered and unbound antibody was removed by extensive washing with TBS-T.

Extracts (500µg protein) in 200µl TBS-T were incubated with coated beads for 30 minutes at room temperature with rotation. The supernatant protein was retained. Following extensive washing with TBS-T, beads were transferred to a new tube in

TBS-T, heated for 10 minutes at 95°C and the released protein was analysed by gel electrophoresis and immunoblotting (see Sections 2.3.3 and 2.3.4).

2.3.7 Cell viability assay

Treated cells were diluted in medium and 1000 cells were added per well into a 96-well plate. Each cell treatment was plated in triplicate. Once the untreated cells reached 70% confluency (4 days), 10µl tetrazolium MTT reagent (3-(4,5-dimethylthiazolyl-2)-2,5-diphenyltetrazolium bromide) was added to each well and incubated for 4 hours at 37°C. Excess MTT reagent was removed and replaced with 100µl DMSO to dissolve the formazan generated by metabolically active cells. The dissolved formazan was quantified by absorbance at 540nm.

2.3.8 6-TG incorporation

6-TG was measured as previously described (Zhang et al., 2007). Cells were grown for 48 hours in 6-TG containing medium. DNA was purified from cells using the Wizard® Genomic DNA Purification Kit (Promega), with an additional overnight proteinase K digestion step. The DNA concentration was measured by NanoDrop. Purified DNA was denatured and digested with Nuclease P1 at 50°C for 1 hour. The pH was adjusted to pH 8.0 and two units of shrimp alkaline phosphatase (SAP) and 10x SAP buffer were added to a total volume of 120µl. Digestion was continued for a further hour at 37°C.

6-TG was analysed by high-performance liquid chromatography (HPLC) on a Waters dC18 (Atlantis 3µm, 150 × 2.1mm) column using a Waters 2695 Alliance system equipped with a photodiode array and Waters 474 dual monochromator fluorescence detector. Absorbance at both 280 and 342nm were measured to detect guanine and 6-TG, respectively. 6-TG eluted around one minute after guanine. The percentage substitution of G by 6-TG was calculated from the areas under the respective peaks using standard curves.

2.3.9 Enzyme-linked immunosorbent assay (ELISA)

6,4 pyrimidine-pyrimidone (6,4 Py:Py) induction and persistence in cellular DNA can be detected by ELISA. The experiment was performed according to instructions specified by Cosmo Bio Co. The ELISA was conducted in 96-well plates, which were coated in protamine sulphate (0.003% in distilled water, dried overnight).

Genomic DNA was extracted from treated cells using QiaAMP DNA Mini Kit (Qiagen) and quantified using a NanoDrop spectrophotometer (NanoDrop Technologies). DNA was diluted in PBS at 4µg/ml, heated to 100°C for 10 minutes and left on ice for 15 minutes. 200ng denatured DNA was added to triplicate wells in 96-well plates. Plates were dried overnight at 37°C without the lid to allow evaporation and washed with PBS-T (0.05% Tween-20 in PBS).

The summary of this experiment is presented in
Figure **2.1**. 150µl/well of 2% FCS in PBS was distributed for blocking and incubated and then washed off. All incubations were performed for 30 minutes at 37°C. All washes were performed 5x with 150µl/well PBS-T. 100µl/well of anti-6,4 Py:Py antibody (diluted in PBS at 1:1500, Cosmo Bio Co) was added, incubated and washed off. Each well was then incubated with 100µl/well F(ab')2-Goat anti-Mouse IgG (H+L) Secondary Antibody (Biotin conjugate, Thermo Fisher, 1:2000 dilution), and washed off. 100µl/well of Peroxidase-Streptavidin conjugate (1:10,000 dilution) was added, incubated and washed off. 150µl/well of citrate phosphate buffer (5.1g citric acid monohydrate and 7.3g Na_2HPO_4 in 1000ml distilled water, pH5) was added. This buffer was kept on the plate until a mixture of 8mg o-Phenylene diamine, 4µl hydrogen peroxide and 20ml citrate phosphate buffer was prepared. 100µl/well of this solution was added and checked regularly for the yellow colour to appear. Once a discernible difference between different treatments could be seen, the reaction was stopped with 50µl/well 2M H_2SO_4. The absorbance was measured at 492nm in a plate reader.

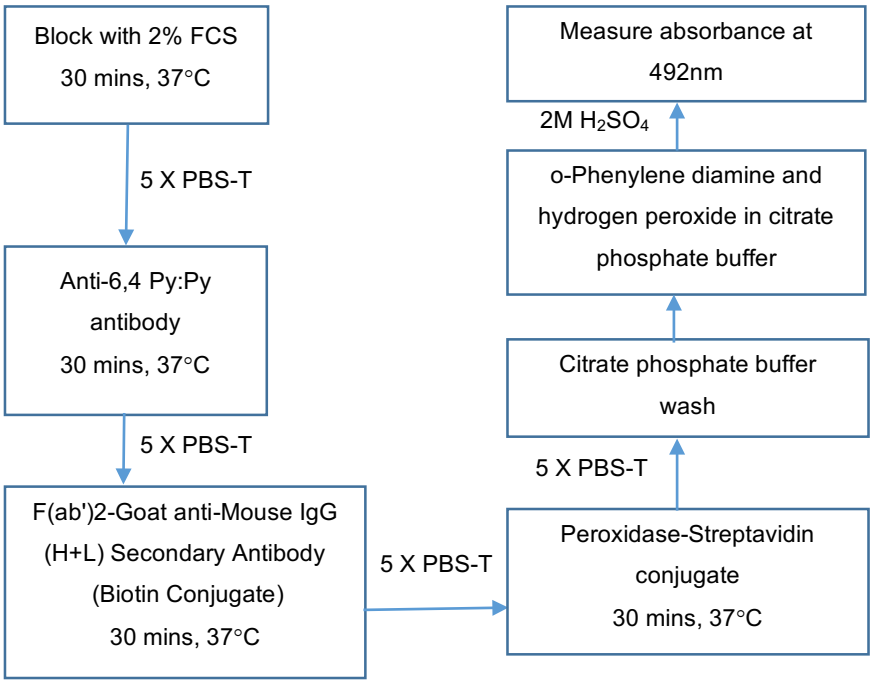

Figure 2.1: Summary of 6,4 pyrimidine-pyrimidone detection by ELISA
The experimental instructions were specified by Cosmo Bio Co.

2.3.10 Protein sulfenate derivatisation and detection

RIPA cell lysates were incubated with 1mM biotin-1,3-cyclopentanedione (BP-1) probe (Kera-FAST) and N-ethylmaleimide (20mM) – the latter to block free thiols. BP-1 contains a sulfenate reactive group linked to biotin (Qian et al., 2011). The proteins were precipitated by the addition of four volumes of acetone. The precipitate was dissolved in 2% SDS and the protein concentration measured using the BCA assay (Thermo Scientific). BP-1-reacted proteins were enriched by binding to M280 Streptavidin Dynabeads (Invitrogen) at 4°C overnight. Beads were then washed three times with 4 volumes of 0.1% SDS to remove non-specifically associated protein. Washed beads were then resuspended sequentially in, 2M Urea, 1M NaCl, 0.1% SDS/10mM DTT, and PBS (for 30 minutes each). The beads were then boiled (95°C) in PAGE loading buffer (see Section 2.3.3) and detached proteins analysed by western blotting (see Section 2.3.4).

2.4 Mass spectrometry (MS)

2.4.1 Cells and UV irradiation

For SILAC (stable isotope labelling by amino acids in cell culture) experiments, CCRF-CEM cells were grown in SILAC RPMI 1640 Medium (Thermo Fisher) supplemented with 10% dialysed FCS and a combination of either 100 mg/L light (^{14}N, ^{12}C) or heavy (^{15}N, ^{13}C) lysine and arginine (CK Isotopes). After growth for 7 days in this medium, light or heavy labelling of proteins was confirmed by MS.

CCRF-CEM cells were incubated for 24 hours with 6-TG or 1 hour with ciprofloxacin, and UVA irradiated in PBS.

For hydroxyurea (HU) treatment, the medium was supplemented with 3 mM HU for 6 hours prior to 6-TG addition and throughout growth in 6-TG. DNA was extracted and 6-TG incorporation was quantified (see Section 2.3.8). ROS levels were determined by FACS using the CM-H_2DCFDA assay (Thermo Fisher) as in Section 2.3.1.

2.4.2 Sample preparation

2.4.2.1 Chromatin preparation

Following treatment, 10^6 isotopically-labelled control and/or treated cells were mixed and resuspended in 200µl Buffer 1 (Table 2.4 for chemicals and concentrations). Nuclei were harvested by centrifugation at 10,000g for 20 minutes at 4°C.

Chromatin was released from the nuclear pellet by resuspension in 200µl Buffer 2 (Table 2.4) and harvested by centrifugation at 10,000g for 20 minutes at 4°C. The chromatin pellet was then washed three times with four volumes of the same high-salt buffer and extensively sheared by passage through 19G, 25G and 27G needles (20 times per needle). The DNA concentration was measured by NanoDrop. 10µg DNA was applied to a HyBond-N^+ membrane using a slot blot apparatus (GE Healthcare) and crosslinked to the membrane by UVC irradiation from a Stratalinker

(Stratagene). Membranes were then washed sequentially with 2xSSC, 8M urea and water. Membrane areas containing chromatin were excised with sterile scalpels (Swann Morton).

Table 2.4: Components of Buffer 1 and Buffer 2 for chromatin extract preparation

Buffer 1		**Buffer 2**	
Chemical	**Final Concentration**	**Chemical**	**Final Concentration**
Tris-HCl pH7.4	10mM	**Sodium phosphate pH 7.4**	25mM
MgCl2	2.5mM	**MgCl2**	5mM
NP-40	0.5%	**NaCl**	500mM
DTT	1mM	**EDTA**	1mM
cOmplete Protease Inhibitor Cocktail Tablets	1 tablet	**Triton-X**	0.5%
		DTT	1mM
		Glycerol	10%
		cOmplete Protease Inhibitor Cocktail Tablets	1 tablet

Further sample preparation for MS analysis was carried out by my collaborator Karin Barnouin. Excised membrane samples were treated with 10mM DTT at 50°C for 30 minutes and then alkylated with 55mM iodoacetamide for 30 min at room temperature in the dark. Alkylation was stopped by the addition of 10mM DTT and further incubation for 10 minutes at room temperature. The membrane fragments were washed three times with 10mM triethylammonium bicarbonate (TEAB) and immersed in trypsin (12.5ng/ul) for overnight digestion at 37°C. DTT, iodoacetamide and trypsin were all prepared in 10mM TEAB.

2.4.2.2 RIPA extract

DNA-free whole cell RIPA extracts (Table 2.2, 20µg of protein) were separated by SDS-PAGE (see Section 2.3.3) until the dye front had migrated 1-2cm into the gel. The gel was stained with Coomassie protein stain (Instant Blue, Expedeon). Gel bands were excised and trypsin digested using a Perkin Elmer Janus liquid handling system.

2.4.2.3 Immunoblotting

Chromatin extracts were applied to HyBond-N^+ membranes that were blocked for 1 hour with 10% (w/v) non-fat powdered milk in TBS-T. They were then incubated for 2 hours at room temperature with primary antibodies for MSH2, MSH6, PCNA and RPA70 (Table 2.3, dilutions and suppliers) in 5% milk in TBS-T. Following washing with TBS-T, they were incubated with the appropriate HRP secondary antibody (1:5000). Immunoreactive proteins were detected using Amersham ECL Western Blotting Detection Reagent (GE Healthcare Lifesciences) and visualised using Amersham Hyperfilm ECL (GE Healthcare Lifesciences).

2.4.3 MS and analysis

MS was performed by my collaborator K. Barnouin. Tryptic peptides were analysed by LC-MS using an Ultimate 3000 uHPLC system, which was connected to either a Q-Exactive or Orbitrap Velos Pro mass spectrometer (Thermo Fisher Scientific). Acquisition was in data-dependent mode. The data were searched against human Uniprot (UniProt KB2012_08 taxonomy human 9606 canonical with contaminants 20120921) using the Andromeda search engine and MaxQuant (version 1.3.0.5) (Cox and Mann, 2008). A false discovery rate of 0.1% was used to generate protein identification tables. The data were uploaded into Perseus version 1.4.0.11 (MaxQuant) for statistical analyses. K. Barnouin also used the data visualization package ggplot2 (Wickham, 2009). I used Prism 6.0 to generate all of the scatterplots presented in Chapter 5 of this thesis.

Chapter 3. Oxidative damage to proteins caused by 6-TG+UVA

3.1 Introduction

Previous studies have shown that antioxidant defences of cultured human cells are not sufficient to prevent the extensive protein damage caused by 6-thioguanine (6-TG) photoactivation (Gueranger et al., 2014; 2011; Montaner et al., 2007). Photoactivation of DNA-6-TG compromises DNA break joining, base excision repair (BER) and nucleotide excision repair (NER). *In vitro* DNA repair assays, which monitor excision of a platinum-DNA adduct by extracts prepared from treated cells (Lainé et al., 2006), implicated protein oxidation in DNA repair inhibition (Gueranger et al., 2014; Peacock et al., 2014). The use of purified NER proteins to complement repair–deficient extracts indicated that replication protein A (RPA) might be a target for inactivation by photoactivated DNA 6-TG. In this chapter, I describe my findings that confirm that RPA is indeed susceptible to oxidative damage.

3.1.1 Replication protein A

The use of genetic information encoded in DNA, requires unwinding of duplex DNA and exposure of single stranded DNA (ssDNA). In this state DNA is highly vulnerable to damage, as well as to the formation of spontaneous duplex DNA. ssDNA binding proteins exist in bacteria, archaea and eukaryotes, and all contain the oligonucleotide binding (OB) fold for ssDNA binding and oligomerisation (Flynn and Zou, 2010).

RPA is the primary eukaryotic ssDNA binding protein. It is required for all aspects of DNA metabolism that involves a ssDNA intermediate. These include DNA replication, recombination, repair, telomere maintenance and DNA damage response. RPA is a heterotrimer of 70, 32 and 14kDa subunits (RPA70, RPA32 and RPA14, respectively) that are encoded by three separate genes (Wold, 1997). RPA70 is the major DNA binding subunit and has four domains (Figure 3.1). The domains include an N-terminal regulatory, protein–protein interaction domain (amino acids 1–110, DBD-F) and three DNA binding domains (DBD): DBD-A (amino acids 181–290),

DBD-B (amino acids 301–422), and DBD-C (amino acids 436–616) (Liu and Huang, 2016). RPA32 contains the DBD-D domain and DBD-E is present in RPA14 (Brill and Bastin-Shanower, 1998). The trimerisation occurs through interactions between domains DBD-C, D and E (Bochkareva et al., 2002). RPA32 contains an additional C-terminal winged helix domain for RPA interaction with other proteins and an N-terminal domain which becomes phosphorylated after DNA damage (Binz et al., 2004; Oakley and Patrick, 2010). DBD-E has a very weak interaction with DNA and mainly participates in trimerisation (Bochkarev et al., 1999).

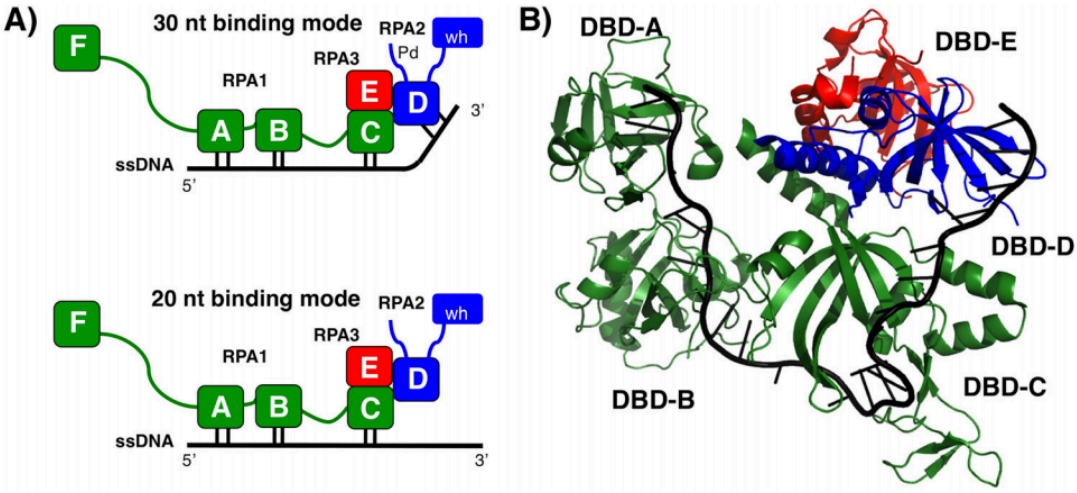

Figure 3.1: Structure and binding of RPA (Chen and Wold, 2014)
(A) RPA binding to ssDNA by DNA binding domains (DBD) A-F, also showing the winged helix domain (wh) and the phosphorylation domain (Pd). Longer ssDNA binding (30nt) involves DBD-D. **(B)** The structure of *Ustilago maydis* RPA bound to ssDNA (black). RPA1 (RPA70, green), RPA2 (RPA32, blue) and RPA3 (RPA14, red) (Fan and Pavletich, 2012).

RPA binds ssDNA 1000-fold more efficiently (nM affinity) than to dsDNA. It binds preferentially to longer ssDNA sequences and prefers polypyrimidine sequences to polypurines (Kim et al., 1994). The proposed dynamic binding mechanism involves an initial weak binding step by DBD-A and DBD-B to an 10-20 nucleotide segment. Subsequent conformational changes allow binding of DBD-C, which in turn permits DBD-D access for binding to ssDNA substrates of 28-30 nucleotides (Bastin-Shanower and Brill, 2001).

The long linker connecting the DBD-F protein interaction and DNA binding DBD-A domains confers some structural and dynamic autonomy on these functions and binding of ssDNA does not affect the protein interactions of RPA (Brosey et al., 2015). The DNA binding domains (A and B) are connected by a short linker reflecting the high degree of coordination required for the initial binding of ssDNA. The combination increases binding affinity by around a 100-fold compared to each separate domain.

The binding of RPA to DNA appears to depend on free RPA concentration. It was shown that *Saccharomyces cerevisiae* RPA remains tightly associated with ssDNA in the absence of free RPA (Gibb et al., 2014). When free RPA becomes present in solution, RPA undergoes dissociation from DNA and exhibits rapid exchange between free and bound RPA, which may occur through a partially dissociated intermediate. This may allow other proteins to replace RPA. Gourdin *et al.* have shown that RPA exhibits differential binding to ssDNA under different conditions. They speculate that transient RPA binding to DNA during replication and the pre-incision steps of RPA prevents checkpoint activation (Gourdin et al., 2014). RPA binding during replication stress or in the post-incision steps of NER is more stable and can activate ATR (ataxia telangiectasia and Rad3 related) and ATRIP (ATR-interacting protein).

A critical step of NER involves RPA70 binding the N-terminal region of XPA (xeroderma pigmentosum group A), while RPA32 binds its central region (Saijo et al., 2011). These interactions allow the recruitment of the XPF-ERCC1 and XPG endonucleases. XPG interacts with RPA directly (Saijo et al., 1996). RPA interacts with uracil-DNA glycosylase (UNG) and also facilitates long patch BER (DeMott et al., 1998; Nagelhus et al., 1997). Exonuclease 1-mediated excision during MMR is stimulated by RPA, which also protects the ssDNA generated by the excision (Genschel and Modrich, 2003). RPA has an important role in protecting ssDNA and removing secondary structures formed by ssDNA in homologous recombination (HR) and interacts with RAD51 and 52 (San Filippo et al., 2008).

Some genotoxic treatments may disrupt the interaction between RPA and XPA that is required for NER (Jiang et al., 2012). This disruption can occur through RPA32 hyperphosphorylation, which can promote the interaction of RPA with other factors

(Deng et al., 2009; Shi et al., 2010). The association of RPA with ssDNA is more favourable than its binding to XPA and there is some overlap in the XPA interaction site and the DNA binding site of RPA70 (Daughdrill et al., 2003). ssDNA at collapsed DNA replication forks will sequester RPA and prevent it from binding XPA. The presence of a common surface of RPA involved in interacting with UNG2 (BER), Rad52 (HR) and XPA also results in competition between the different repair pathways for RPA (Mer et al., 2000). In the case of ultraviolet radiation (UV) and NER, it is proposed that at low DNA damage levels and few double strand breaks (DSBs), RPA associates with XPA for NER. At higher levels of DNA damage, DSBs at stalled DNA replication forks will compete with XPA, potentially aided by RPA hyperphosphorylation and sequester RPA (Wu et al., 2005). Consistent with this model, in the absence of translesion polymerase Polζ or in cells treated with hydroxyurea, persistently arrested replication forks sequester RPA (Tsaalbi-Shtylik et al., 2014). This is accompanied by inhibition of NER in *trans*. Therefore, free RPA levels have a significant regulatory role in the cell. Persistent fork stalling and the absence of free RPA can result in cell death (Tsaalbi-Shtylik et al., 2014).

Loss of any of the RPA subunits is lethal and non-lethal mutations result in genomic instability (Chen and Wold, 2014). Depletion of RPA can result in spontaneous DNA damage and G2/M checkpoint activation through ATM (ataxia telangiectasia mutated) (Halliwell, 1991; Haring et al., 2010; Santocanale et al., 1995). It has also been shown that depletion of RPA70 results in genome instability, activates the Fanconi anaemia (FA) pathway through chromatin association of the FA core complex and causes FANCD2 ubiquitination through ATR (Jang et al., 2016). Haploinsufficiency of RPA in mice results in lymphoid tumours and shortened life span (Hass et al., 2010; Wang et al., 2005).

Replication fork stalling during replication stress increases the levels of exposed ssDNA. Under normal conditions, RPA stabilisation of stalled forks and activation of ATR, resolves the stalled fork and allows continuation of replication. Toledo *et al.* showed that replication stress-induced depletion of RPA can cause exposed ssDNA to convert to DSBs (Toledo et al., 2013). This results in replication catastrophe and cell death. Overexpression of RPA enables cells to tolerate higher levels of replication stress. The activation of ATR by RPA and cell cycle arrest prevents new

origin activation and therefore inhibits further generation of ssDNA to alleviate RPA exhaustion.

3.1.2 Antioxidant allopurinol

Allopurinol is a xanthine oxidase inhibitor (Elion et al., 1966). It is also an antioxidant and prevents radiation-induced lipid peroxidation by •OH, ClO_2 and HOCl (Das et al., 1987; England et al., 1986; Moorhouse et al., 1987). Allopurinol protects against 6-thioguanine (6-TG) toxicity by acting as a reactive oxygen species (ROS) scavenger and improving cell viability at high (mM) allopurinol concentrations (Brem and Karran, 2012). It also confers significant protection against the inflammatory effects of fluoroquinolone+UVA combinations in mice (Wagai and Tawara, 1991).

3.1.3 Aims

My aims at the outset were to investigate:

- Proteins affected by 6-TG+UVA treatment,
- The impact of antioxidants on ROS production and protein damage,
- The impairment of RPA by 6-TG+UVA and ciprofloxacin+UVA treatments.

3.2 Results

3.2.1 Production of intracellular ROS by 6-TG+UVA

I initially examined the production of ROS in cells treated with UVA, 6-TG and combined 6-TG and UVA using the CM-H_2DCFDA probe. CM-H_2DCFDA passively diffuses into cells where it undergoes cleavage by intracellular esterases and reaction with proteins that increase its retention in the cell. Oxidation by intracellular ROS then converts the reduced fluorescein derivative to its oxidised fluorescent form that is trapped inside the cell and can be detected by fluorescence-activated cell sorting (FACS) (Figure 3.2).

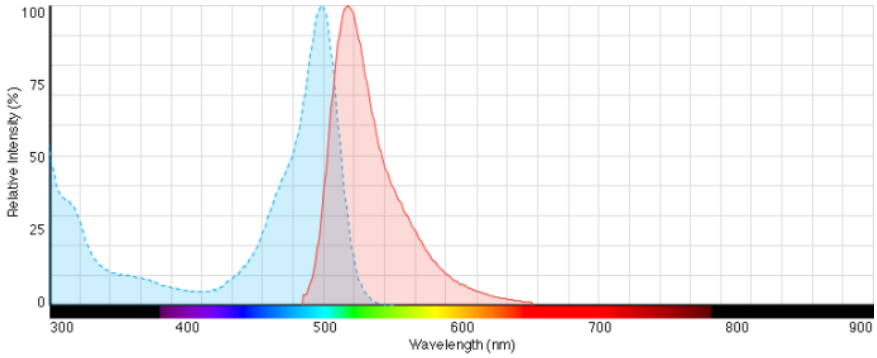

Figure 3.2: The fluorescence spectra of CM-H_2DCFDA (Thermo Fisher)
Following passive diffusion into cells, the reaction of CM-H_2DCFDA with ROS results in the production of the fluorescent form of the probe, which exhibits excitation (blue) at around 492-495nm and emission (red) at around 517-527nm.

To examine ROS production by 6-TG+UVA, HeLa cells were grown in the presence of 6-TG for 24 hours to allow 6-TG incorporation into DNA. They were then incubated with CM-H_2DCFDA and irradiated with UVA. The fluorescence intensity and frequency distribution was determined by FACS analysis. In addition, I examined the effect of allopurinol on ROS levels.

Figure 3.3 (A) shows that:

- Allopurinol has a small effect on steady-state ROS in untreated cells,
- A low dose of UVA induces detectable ROS,
- Allopurinol measurably reduces the ROS induced by UVA but does not fully restore it to background level.

Figure 3.3 (B) confirms previous findings that treatment with 6-TG+UVA results in a highly significant increase in ROS levels in comparison to UVA alone (O'Donovan et al., 2005). The FACS signal for this combination is close to the maximum detection capacity of this assay. Allopurinol afforded significant protection against ROS induced by 6-TG+UVA, but did not restore untreated steady state levels.

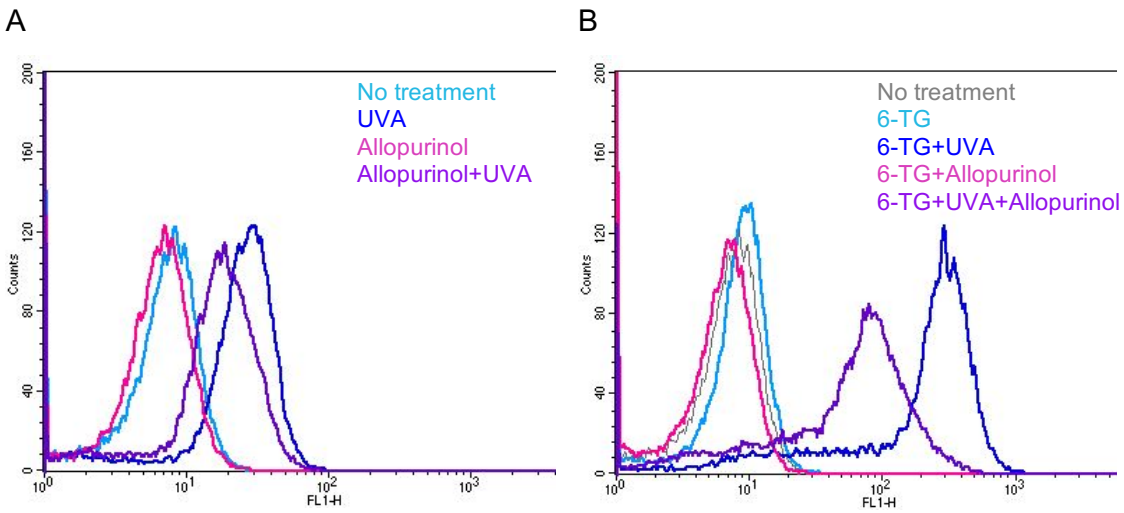

Figure 3.3: FACS analysis of intracellular ROS
HeLa cells were treated with 6-TG and incubated for 20 minutes with 7.5μM CM-H_2DCFDA. They were then irradiated with UVA, washed and resuspended in PBS for FACS analysis. The fluorescence intensity (FL1-H log 10) vs frequency distribution (counts) is shown. 1μM 6-TG for 24 hours, 1mM allopurinol for 24 hours, 20kJ/m^2 UVA.

3.2.2 Protein damage to NER proteins

I investigated the effect of 6-TG+UVA and allopurinol treatment on proteins of the NER pathway. Immunoblotting of cell extracts indicated that 6-TG+UVA treatment caused a decrease in the recovery of XPD, XPA and RPA, three essential NER proteins (Figure 3.4). Neither UVA nor 6-TG alone affected the extractable amounts of these proteins. The addition of the antioxidant allopurinol restored levels of both XPA and RPA70 but not XPD. This loss could be due to various forms of protein oxidation that results in precipitation as well as loss *via* the formation of DNA-protein crosslinks.

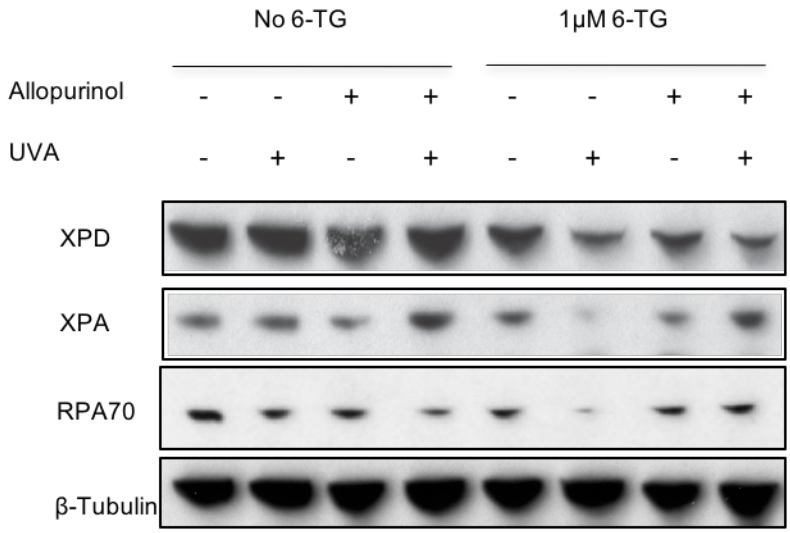

Figure 3.4: Effects of 6-TG+UVA and allopurinol on NER proteins
HeLa cells were treated with 1μM 6-TG for 24 hours, 1mM allopurinol for 24 hours and 20kJ/m^2 UVA as indicated. Extracts (20μg) were analysed by western blotting and probed with antibodies against XPD, XPA, RPA70 and β-tubulin as specified.

Previous findings from our laboratory had indicated that protein oxidation, and in particular RPA damage, is associated with NER inhibition in cells treated with 6-TG+UVA (Gueranger et al., 2014; Peacock et al., 2014). As treatment with 6-TG+UVA inhibits DNA replication and causes replication fork stalling, I examined whether recruitment of RPA to exposed ssDNA at stalled replication forks (chromatinisation) might decrease RPA70 levels recovered in the low-salt RIPA extracts. I treated cells with 6-TG+UVA, with and without benzonase digestion and

tested RPA70 levels over time. Benzonase digests DNA to completion and releases bound proteins. Figure 3.5 shows that following UVC treatment, an efficient inducer of replication arrest, RPA70 recovery was visibly diminished after 30 minutes. Benzonase digestion largely restored pre-treatment levels, consistent with the expected recruitment of RPA70 to newly-exposed regions of ssDNA. 6-TG+UVA treatment also resulted in RPA chromatinisation, although to a lesser extent than UVC. RPA70 recovery was diminished immediately after treatment and continued to decline slowly over time.

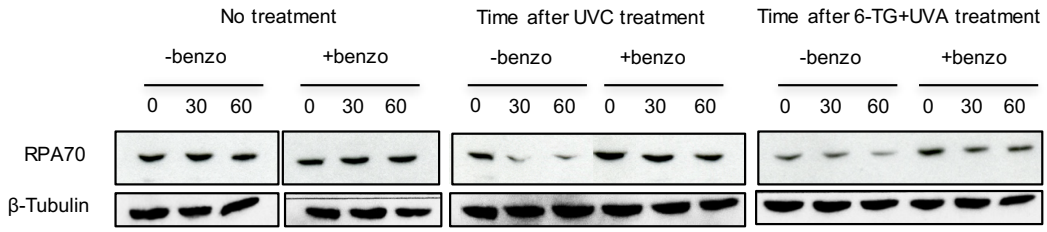

Figure 3.5: Chromatinisation of RPA with UVC and 6-TG+UVA treatment
Cells were treated with 1μM 6-TG for 24 hours and irradiated with 10J/m^2 UVC and 20kJ/m^2 UVA and treated with benzonase where indicated. Extracts prepared at 0, 30 and 60 minutes after treatment were analysed by western blotting (20μg) and probed with antibodies against RPA70 and β-tubulin as specified.

To examine the impact of 6-TG+UVA treatment on RPA function, I carried out an electrophoretic mobility shift assay (EMSA). Extracts of HeLa cells were incubated with a [^{32}P] end-labelled 51-mer oligonucleotide and the products analysed by polyacrylamide gel electrophoresis (PAGE). Figure 3.6 (A and B) shows that RPA binding to ssDNA can be detected by reduced oligonucleotide mobility (*). The supershift assay (**) in which an antibody against RPA32 was included in the incubations, confirms that binding is by RPA. RPA binding activity was lower in extracts of cells treated with both UVA and 6-TG although neither alone had a substantial effect. UVC treatment also causes a decrease in RPA binding most likely reflecting RPA recruitment to sites of DNA damage and exposed ssDNA regions. The decrease in RPA binding is, however, more pronounced in extracts from cells treated with combined 6-TG+UVA despite the similar levels of chromatinisation of RPA after UVC (Figure 3.5) .

I conclude that RPA recruitment to chromatin can only partly explain the considerable loss of RPA activity and NER inhibition in extracts from 6-TG+UVA treated cells. I therefore examined other potential contributors to loss of NER activity.

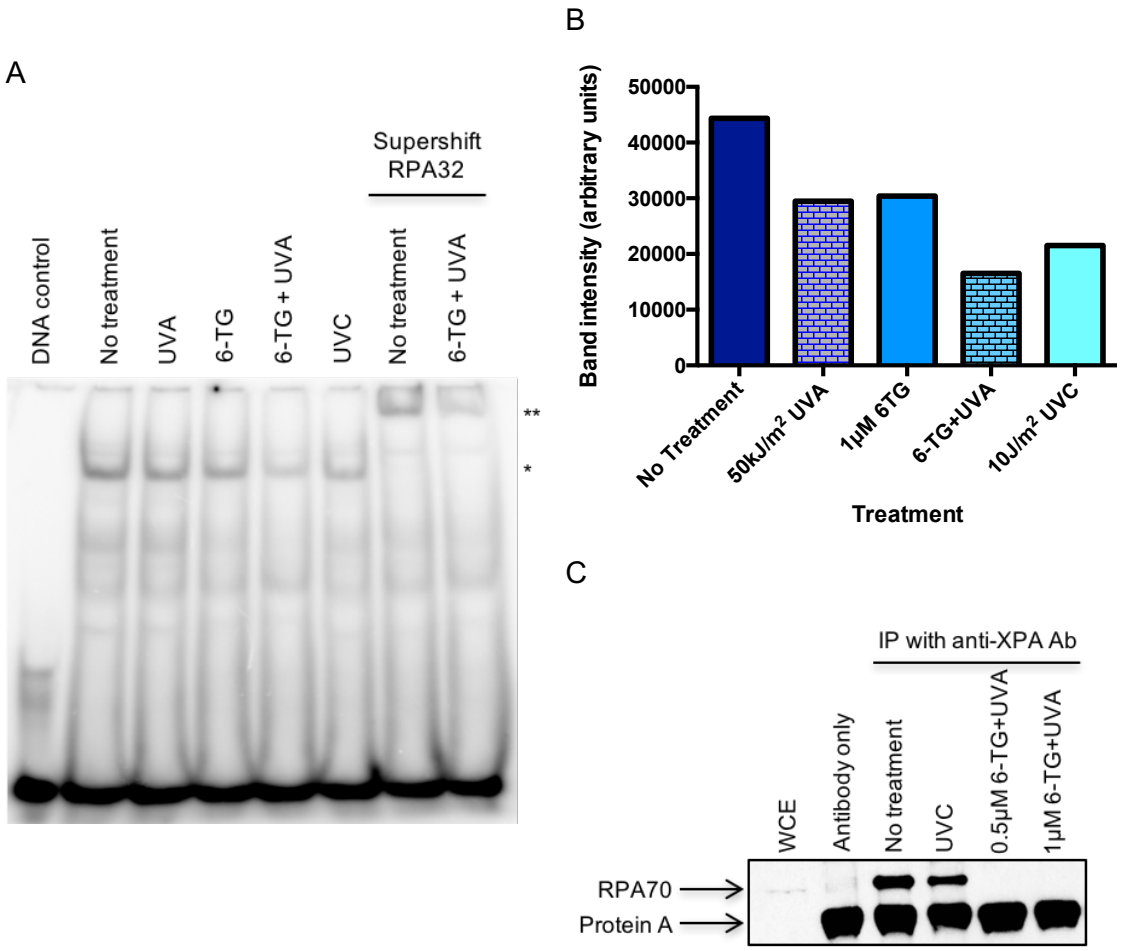

Figure 3.6: The effect of 6-TG+UVA on RPA binding to ssDNA and XPA
Extracts (25μg) prepared from HeLa cells treated with 1μM 6-TG for 24 hours and irradiated with 10J/m^2 UVC and 20kJ/m^2 UVA, as indicated **(A)** were incubated with a 51nt [^{32}P] end-labelled oligonucleotide. Products were separated on a 12.5% polyacrylamide gel and imaged using a phosphor screen. For the supershift assay, the extracts were supplemented with anti-RPA32 antibody. *DNA:RPA, **DNA:RPA:Antibody. **(B)** Band intensities for representative example were measured using ImageJ software. **(C)** Immunoprecipitation (IP). Extracts enriched for XPA using protein A dynabeads bound to anti-XPA antibody (Ab) were analysed by western blotting and probing with anti-RPA70 Ab. WCE, whole cell extract.

Efficient NER requires an interaction between RPA and XPA (Saijo et al., 2011). I therefore conducted an immunoprecipitation assay (IP), in which anti-XPA antibodies were used to enrich HeLa cell extracts for XPA. By probing with an anti-RPA70

antibody, I tested for the interaction between the two proteins. An interaction between XPA and RPA70 was detected in both untreated and UVC-treated extracts (Figure 3.6 (C)). UVC slightly reduced the amount of XPA detected – possibly reflecting RPA recruitment to stalled replication forks. In contrast, 6-TG+UVA abolished the RPA:XPA interaction. This could be due to chromatinisation, however, at 0.5μM 6-TG, chromatinisation is limited (Figure 3.7 (A)) yet it still abolishes RPA:XPA binding. Therefore, the lack of interaction may be due to RPA, XPA or both proteins being damaged and unable to interact with each other. These findings also support the conclusion that, in addition to chromatinisation, damage to RPA or its interacting proteins, induced by 6-TG+UVA contributes to loss of ssDNA binding and inhibition of NER.

3.2.3 RPA32 modification by 6-TG+UVA

I also examined the effect of 6-TG+UVA on the smaller RPA subunits, RPA32 and RPA14. The western blots shown in Figure 3.7 (A) confirm the 6-TG and UVA-dependent reduction in recovery of RPA70. They also demonstrate a concomitant 6-TG+UVA-dependent decrease in the yield of RPA14. More strikingly, they reveal modifications of RPA32 that generate prominent bands at around 100 and 45-50kDa. To examine whether these new RPA32 species were simply a consequence of damaging and lethal treatments, I investigated the effects on RPA32 of high doses of ionising radiation (IR), UVC and hydroxyurea (HU). Figure 3.7 (B) shows that none of these treatments induced detectable RPA32 modification. Allopurinol, but not N-acetylcysteine (NAC) or ascorbic acid (AA), provided some protection against RPA32 modification (Figure 3.7 (C)).

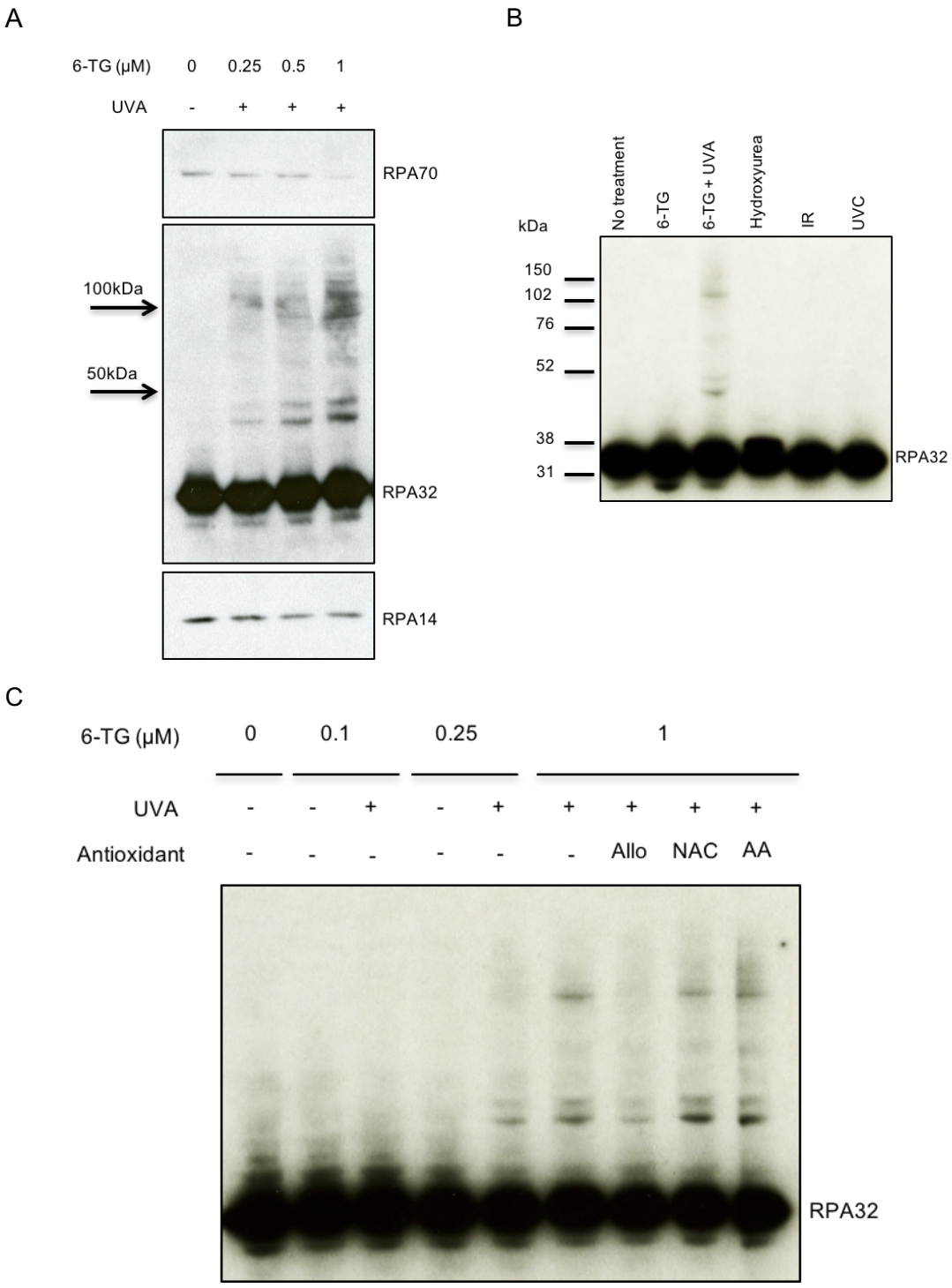

Figure 3.7: Crosslinking of RPA32
(A) Extracts from HeLa cells treated with 6-TG for 24 hours at the indicated concentration and 20kJ/m^2 UVA. **(B)** Extracts treated with 1μM 6-TG, 20kJ/m^2 UVA, 3mM hydroxyurea for 3 hours, 20Gy ionising radiation (IR), 100J/m^2 UVC. **(C)** as in (A) with the addition of 1mM allopurinol (Allo), ascorbic acid (AA) and N-acetylcysteine (NAC) as specified. The extracts were analysed by western blot (20μg) using antibodies against RPA70, 32 and 14. Unmodified RPA32 serves as the loading control.

3.2.4 RPA32 modification by ciprofloxacin and UVA

Since the findings with antioxidants were equivocal, I investigated the role of ROS in RPA32 modification by a different approach. The fluoroquinolone antibiotic ciprofloxacin is also a UVA photosensitizer that generates ROS that are detected by the CM-H_2DCFDA assay (Figure 3.8 (A)). Ciprofloxacin on its own results in a modest increase in intracellular ROS, while the combined treatment of ciprofloxacin and UVA result in a significant increase in intracellular ROS in a concentration dependent manner. Figure 3.8 (B) shows that ciprofloxacin+UVA (Cip+UVA) generates modified RPA32 species that are closely similar to those produced by 6-TG+UVA.

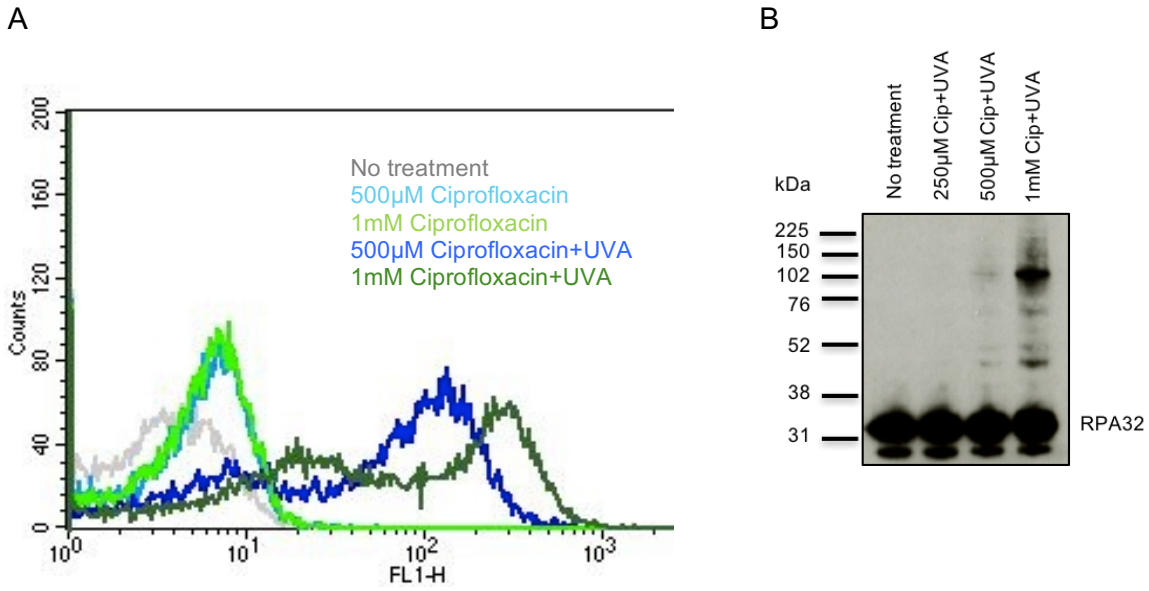

Figure 3.8: ROS production and RPA32 modification by ciprofloxacin+UVA
(A) HeLa cells were treated with ciprofloxacin for 1 hour and incubated for 20 minutes with 7.5μM CM-H_2DCFDA. They were then irradiated with 20kJ/m^2 UVA, washed and resuspended in PBS for FACS analysis. The fluorescence intensity (FL1-H log 10) vs frequency distribution (counts) is shown. **(B)** Extracts were prepared from HeLa cells treated with ciprofloxacin for 1 hour and irradiated with 20kJ/m^2 UVA. Extracts (20μg) were analysed by western blotting with antibodies against RPA32. Unmodified RPA32 serves as the loading control.

In summary, 6-TG+UVA results in reduced RPA70 recovery and impedes ssDNA binding and potentially interaction with XPA, necessary for NER. RPA32 is also damaged by 6-TG+UVA and Cip+UVA treatments. This damage is most likely through the formation of protein-protein crosslinks formed in a ROS dependent manner. This RPA32 modification was investigated further in Chapter 4.

Chapter 4. Photosensitiser+UVA mediated damage to RPA

4.1 Introduction

Following the results of the previous chapter, the damaging effects of photosensitising treatments on replication protein A (RPA) were further investigated. In addition to the existing photosensitisers used, I studied the effects of an endogenous photosensitiser that is described below, as well as examining the way in which oxidised proteins are removed from the cell.

In this chapter, I describe the protective effects of RPA overexpression against the damaging effects of photosensitising treatments, forms of oxidised RPA and their removal, as well as the surprising finding that this abundant and essential protein is limiting for nucleotide excision repair (NER).

4.1.1 Formylindolo[3,2-*b*]carbazole (FICZ)

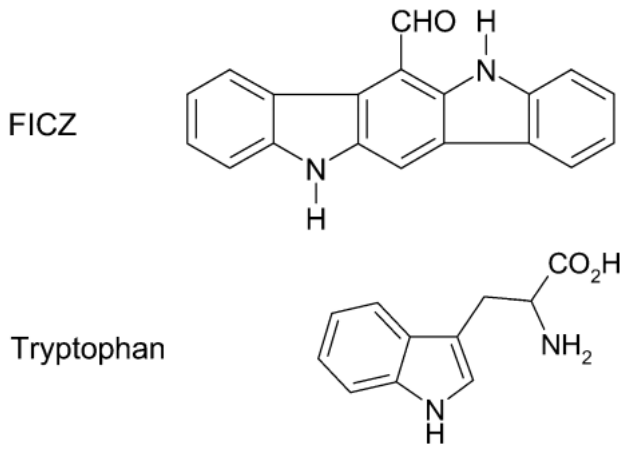

Figure 4.1: Chemical structure of tryptophan and 6-formylindolo[3,2-*b*]carbazole (FICZ) (Oberg et al., 2005)

Along with various established endogenous photosensitisers of ultraviolet radiation (UV), exposure of these chromophores to solar UV and the resulting production of

reactive oxygen species (ROS) can cause the formation of other photosensitisers in human skin. The L-tryptophan-derived photoproduct FICZ (Figure 4.1) exhibits nanomolar photodynamic activity through photoexcitation by UVA or blue light irradiation (Park et al., 2015). Combined FICZ and UVA treatment was shown to induce oxidative and proteotoxic stress response genes in keratinocytes, impair mitochondrial transmembrane potential and form ROS that result in protein peroxides (Park et al., 2015). The ROS generated by FICZ and UVA include singlet oxygen ($^1O_2$) and superoxide ($O_2^{\bullet -}$). Oxidation of a target protein by FICZ and UVA was also observed and the oxidation was inhibited through the presence of $^1O_2$ quencher sodium azide (NaN_3) (Park et al., 2015). It also resulted in a decrease in cell viability *via* caspase 3 activation, which was prevented by NaN_3.

4.1.2 Degradation of oxidised proteins

Oxidatively damaged proteins are targeted for proteolytic degradation to their constitutive amino acids. The limited efficiency of this process results in accumulation of misfolded and oxidised proteins over time in cells (especially post-mitotic cells) and tissues resulting in age-related diseases including atherosclerosis, neurodegeneration and cataractogenesis (Dunlop et al., 2009). Oxidatively damaged proteins are degraded by either the proteasome or through lysosomal pathways.

4.1.2.1 Proteasomal degradation

The proteasome has several isoforms but each isoform contains the catalytic core subunit, the 20S subunit. The different substrate specificities of its catalytically active subunits result in the cleavage of 10-15% of the peptide bonds in proteins, the remainder of which is carried out by cytosolic exo- and endo-peptidases (Reits et al., 2004). The 20S proteasome associates with one or two of the regulatory 19S (PA700) particles to form the 26S proteasome, which is ATP and ubiquitin dependent (Dunlop et al., 2009). The role of the 19S particle is to bind polyubiquitinated proteins, remove the ubiquitin and transport the particle into the 20S core (Strickland et al., 2000). The 20S proteasome can also degrade proteins without the conjugation of ubiquitin (Jariel-Encontre et al., 2008).

It appears that degradation of oxidatively damaged proteins does not require ATP or polyubiquitination, as shown by (1) lack of effect of inhibition of ubiquitination on degradation of oxidised proteins, (2) low efficiency of 26S degradation of oxidised proteins, (3) disassembly of the 26S proteasome and release of 19S and (4) inactivation of the ubiquitinating system under oxidative stress (Davies, 2001; Reinheckel et al., 1998; Shang and Taylor, 1995). Instead of ubiquitination, the exposure of hydrophobic structures appears to be responsible for proteasomal substrate recognition (Lasch et al., 2001). The ability of the proteasome to degrade oxidised proteins decreases with increasing amount of oxidative modification as proteins need to be unfolded in order to fit through the narrow catalytic core. When heavily oxidised aggregates or lipofuscin (oxidised fatty acids, protein, sugar and metal) are formed, they are not only resistant but also inhibitory to proteases (Jung et al., 2014).

4.1.2.2 Lysosomal degradation

The lysosome contains hydrolytic enzymes called cathepsins, involved in the degradation of extra and intracellular proteins, in addition to their role in the recycling of organelles such as proteasomes and mitochondria. Autophagy, which can be induced by starvation, involves nonspecific degradation of portions of the cytosol including proteins, mitochondria and proteasomes. The fusion of increasingly mature vacuoles form the autolysosome or autophagolysosome to degrade the components of the cargo (Kurz et al., 2008).

The proposed method of degradation for oxidised proteins is a cooperation between the proteasome and endosomal-lysosomal pathways, whereby the heavily modified proteins switch from the proteasomal to the lysosomal pathway of degradation (Rodgers et al., 2002). This was demonstrated through a study by Kaganovich *et al.* where misfolded and ubiquitinated proteins move to proteasome rich perinuclear sites and severely aggregated proteins are found in autophagic vacuoles (Kaganovich et al., 2008).

4.1.3 Aims

My aims at the outset were to investigate:

- The damage caused to RPA by ciprofloxacin, ofloxacin, 6-thioguanine (6-TG) and FICZ in combination with UVA, and the impact of RPA overexpression on cell survival and DNA damage repair,
- The removal of severely oxidised, cross-linked proteins formed by photosensitiser and UVA treatment.

The results presented in this chapter have been published in the Journal of Investigative Dermatology (Guven et al., 2015).

4.2 Results

4.2.1 The RPA overexpressing U2OS cell line, RPA21

To investigate whether damage to RPA has relevance in living cells, I used the U2OS-RPA21 cell line (RPA21) that overexpresses all three RPA subunits. In these U2OS derived cells (kindly provided by Drs. J. Lucas and L.Toledo (Toledo et al., 2013)), RPA is expressed using 2-A peptide technology, a schematic representation of which is shown in Figure 4.2 (Kim et al., 2011; Ryan et al., 1991). The proteins are translated from a single, in-frame cDNA that contains 2A-peptide sequences from P2A porcine viruses between the ORFs (open reading frames) encoding each RPA subunit. The RPA14 ORF is also in-frame with AcGFP (green fluorescent protein). During translation, ribosomes skip the synthesis of the peptide bond between glycine and proline at the C-terminus of the 2A sequence, resulting in cleavage and generating the separate subunits of RPA in stoichiometric amounts (Donnelly et al., 2001). Part of the 2A sequence is retained in each subunit resulting in a slight mobility shift on SDS-PAGE.

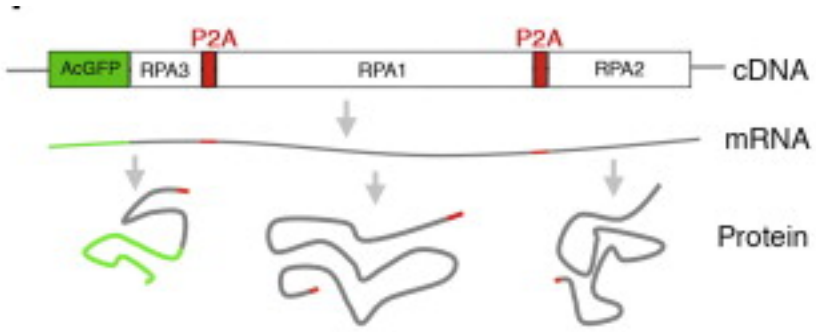

Figure 4.2: Schematic representation of the cDNA used for RPA overexpression in the RPA21 cell line
The three proteins are expressed from a single, in-frame cDNA. 2A-peptide sequences from P2A porcine viruses separate the ORFs encoding each of the subunits. The RPA14 ORF is also in-frame with AcGFP to generate a fusion protein. During translation, ribosomes skip the synthesis of the peptide bond between glycine and proline at the C-terminus of the 2A sequence, resulting in cleavage and generating the separate subunits of RPA in stoichiometric amounts (Toledo et al., 2013).

I carried out a western blot analysis to estimate the level of overexpression of the RPA subunits (Figure 4.3). This confirmed an approximately two-fold overexpression of RPA70 and RPA32. Expression of the endogenous U2OS RPA14 was unchanged and the presence of the RPA14-AcGFP fusion protein encoded by the construct was also confirmed. Longer exposure of the blots revealed a high molecular weight immunoreactive species of RPA32. The nature of this protein will be discussed in Section 4.2.6.

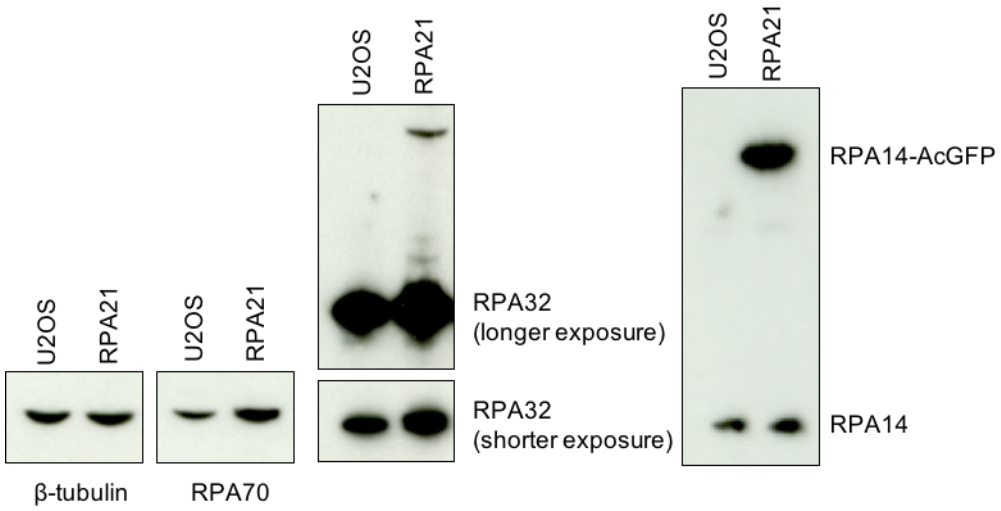

Figure 4.3: RPA overexpression in RPA21 cells
Extracts (20µg protein) from U2OS and RPA21 cells were analysed by western blots probed with antibodies against RPA70, 32, 14 and β-tubulin as indicated.

4.2.2 The effect of RPA overexpression on survival following photosensitised UVA treatment

Similar to ciprofloxacin, another fluoroquinolone, ofloxacin, also produces ROS when combined with UVA, detectable by the CM-H_2DCFDA assay. Ofloxacin appears to require double the dose of ciprofloxacin in combination with UVA to reach the same levels of ROS production as can be seen in Figure 4.4. Both drugs at this particular dosage produce lower levels of intracellular ROS than 6-TG+UVA.

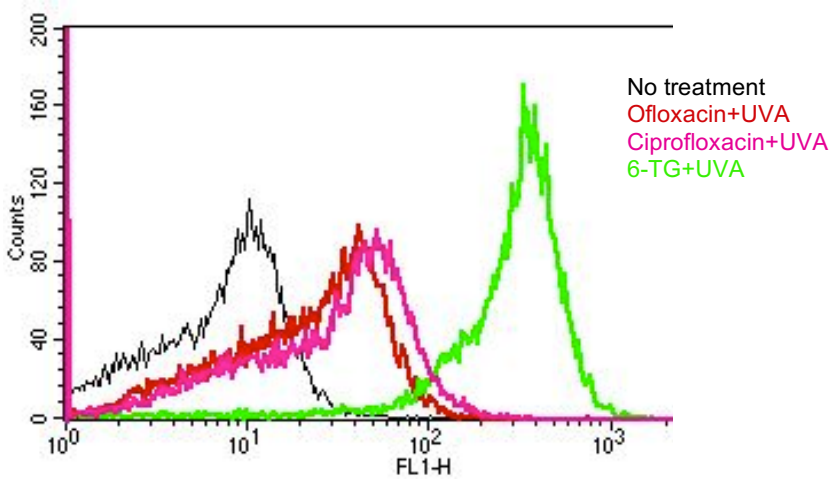

Figure 4.4: ROS production by ciprofloxacin, ofloxacin and 6-TG
U2OS cells were treated with ciprofloxacin (1 hour, 250μM), ofloxacin (1 hour, 500μM) or 6-TG (24 hours, 3μM) and incubated for 20 minutes with 7.5μM CM-H_2DCFDA. The cells were then irradiated with 20kJ/m^2 UVA and were washed and resuspended in PBS for subsequent FACS analysis. The fluorescence intensity (FL1-H log 10) vs frequency distribution (counts) is shown.

Initially, I tested whether RPA overexpression affected the survival of cells exposed to 6-TG, ciprofloxacin or ofloxacin in combination with UVA. MTT survival assays were performed to compare the survival of the RPA overexpressing RPA21 cells to that of the parental U2OS cells.

Figure 4.5 (A) shows the toxicity of ciprofloxacin+UVA (Cip+UVA) in the two cell lines. Individually, neither UVA nor ciprofloxacin caused a significant decrease in viability in either U2OS or RPA21 cells. In combination with UVA, however, ciprofloxacin induced a concentration-dependent decrease in viability in both cell lines. RPA21 cells were considerably more resistant to Cip+UVA than U2OS cells. At 200μM ciprofloxacin, less than 2% of UVA irradiated U2OS cells were viable whereas approximately 70% of RPA21 cells survived the same treatment ($p=0.007$, paired t-test).

As demonstrated in Figure 4.4, ofloxacin requires over double the dose of ciprofloxacin to generate similar levels of ROS. Therefore, relatively higher doses of ofloxacin were used to study its effect on survival. Ofloxacin+UVA (Oflx+UVA) treatment was also differentially toxic towards U2OS and RPA21 cells (Figure 4.5 (B)), although the difference between the two cell lines was more modest than that

for Cip+UVA. At 500μM ofloxacin, the viabilities of irradiated U2OS and RPA21 cells were 50% and 85% respectively (p=0.0165, paired t-test). As expected, ofloxacin alone was not detectably toxic in either cell line.

U2OS and RPA21 cells incorporate 6-TG into DNA at different rates. Accordingly, viability comparisons were carried out in cells treated with different 6-TG concentrations to compensate for this difference. HPLC analysis of DNA 6-TG was performed in each experiment to ensure similar levels of incorporation were achieved. RPA21 cells were more resistant to 6-TG+UVA than U2OS (Figure 4.5 (C)). Following treatment with a low 6-TG concentration and the highest UVA dose, U2OS cells exhibited approximately 50% viability, compared to 85% for RPA21 cells. At the higher concentration, this becomes approximately 30 and 70% for U2OS and RPA21 cells, respectively. These findings demonstrate that 6-TG+UVA is less toxic in RPA21 cells than in U2OS cells.

My findings reveal that RPA21 cells are more resistant to the three different photosensitiser+UVA combinations than their U2OS parent cells. They indicate that even a modest overexpression of RPA confers resistance to the toxicity of these treatments.

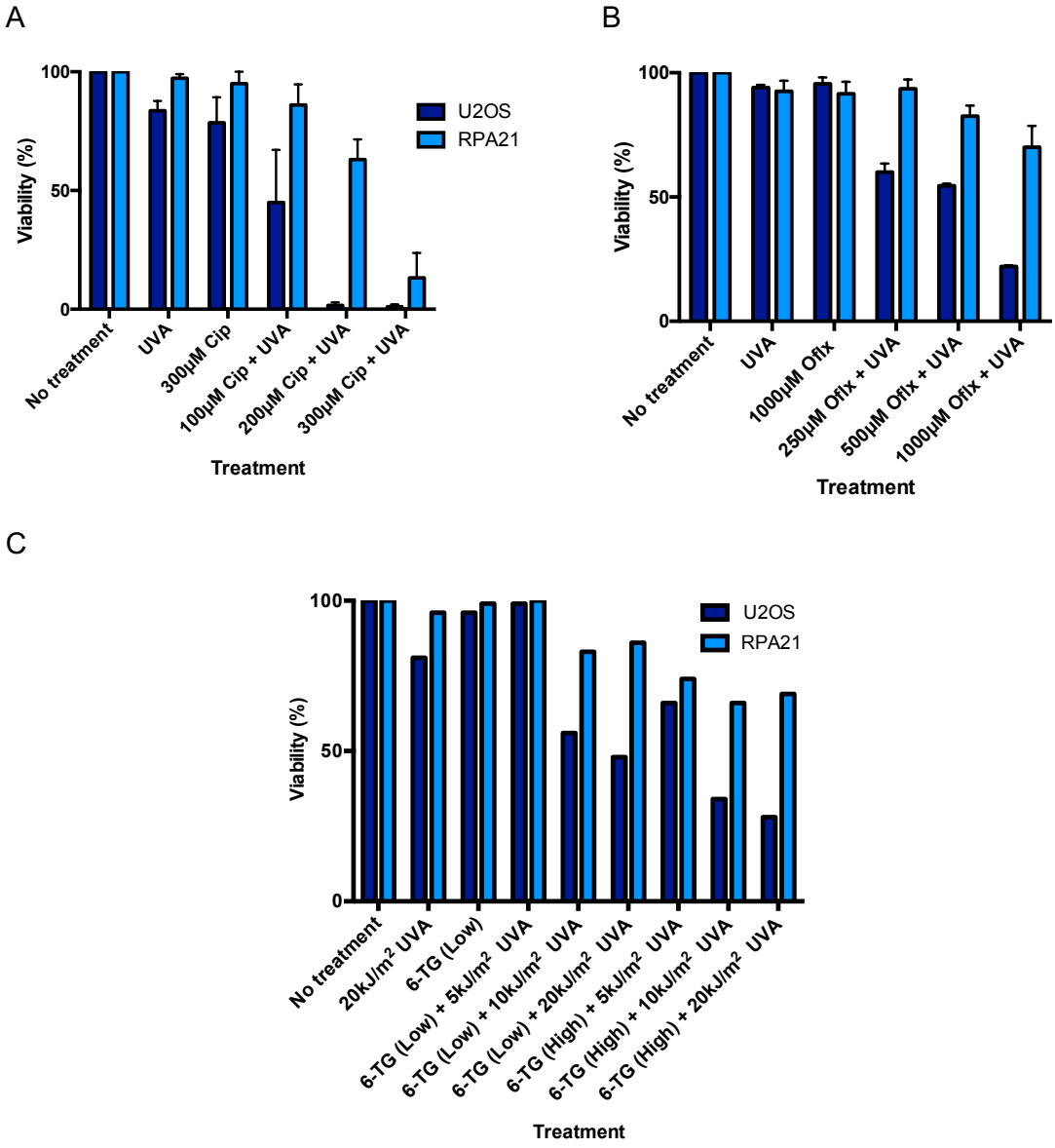

Figure 4.5: MTT survival assays for RPA21 and U2OS cells treated with UVA combined with ciprofloxacin, ofloxacin or 6-TG
(A) Viability of cells treated with ciprofloxacin (Cip) (1 hour) and UVA (20kJ/m^2). Mean values from 3 experiments. **(B)** Viability of cells treated with ofloxacin (Oflx) (1 hour) and UVA (20kJ/m^2). Mean values from 3 experiments. **(C)** Viability of cells treated with 6-TG (24 hours) and UVA (20kJ/m^2). Mean values from 2 experiments. Low concentration of 6-TG, 0.1μM (0.06% DNA 6-TG incorporation) and 0.2μM (0.07% incorporation), for U2OS and RPA21 respectively. High concentration of 6-TG, 0.25μM (0.12% incorporation) and 0.5μM (0.15% incorporation), for U2OS and RPA21 respectively.

4.2.3 The effect of RPA overexpression on photosensitiser+UVA induced inhibition of NER

Treatment of HeLa or CCRF-CEM cells with 6-TG+UVA inhibits NER (Gueranger et al., 2014; Peacock et al., 2014). I investigated NER inhibition by this treatment, and by the other photosensitiser+UVA combinations in U2OS and RPA21 cells.

U2OS and RPA21 cells were treated with 6-TG for 24 hours (3 and 9μM, respectively) to produce DNA incorporation that was determined by HPLC analysis to be 0.85% and 0.86%. They were irradiated with 20kJ/m^2 UVA and then immediately with 10 J/m^2 UVC to induce canonical NER substrates. Genomic DNA was isolated at different times after irradiation and the efficiency of NER was determined by measuring the remaining UVC-induced 6,4 pyrimidine-pyrimidone photoproducts (6,4 Py:Py) by ELISA.

Figure 4.6 (A) shows the effect of 6-TG+UVA on 6,4 Py:Py repair. Excision of 6,4 Py:Pys in untreated cells is rapid and they are removed with a half-life of 1-2 hours by both U2OS and RPA21 cells. Repair is effectively complete by 3 hours post-irradiation. As expected, 6-TG+UVA treatment inhibited NER by U2OS cells and they removed only approximately 15% of the initial 6,4 Py:Py, in 3 hours. RPA overexpression in RPA21 cells significantly improved NER efficiency and they repaired 55% of these lesions in 3 hours ($p=0.012$, paired t-test).

Figure 4.6 (B) confirms the inhibition of NER by Cip+UVA (Peacock et al., 2014). At 3 hours post irradiation, U2OS cells treated with 500μM Cip+UVA had repaired around 10% of their 6,4 Py:Py whereas for RPA21 cells, this figure was 45% ($p=0.027$, paired t-test).

Figure 4.6 (C) shows that treatment with Oflx+UVA also inhibited 6,4 Py:Py excision in U2OS cells and that this inhibition was partially reversed in RPA21 cells, ($p=0.026$, paired t-test).

These findings confirm the significant inhibition of NER by photosensitizer+UVA combinations. They indicate further that a modest overexpression of RPA can significantly reverse this inhibition.

A

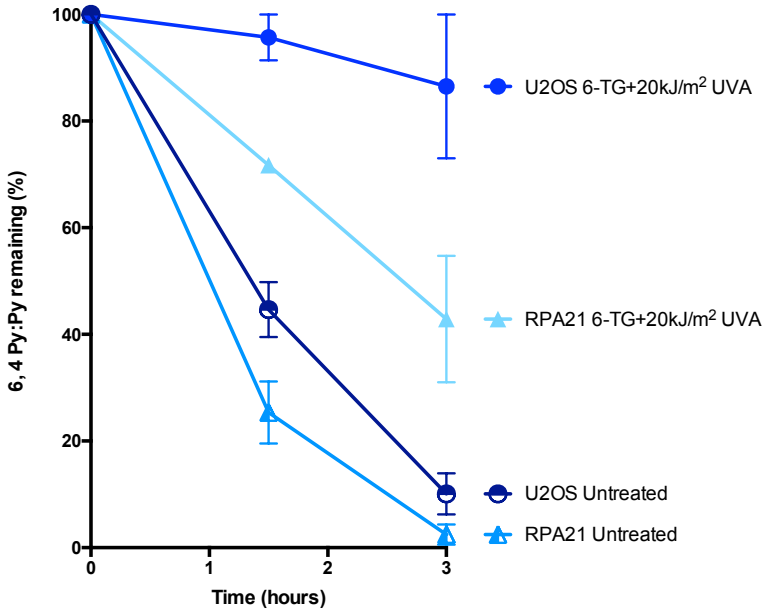

B

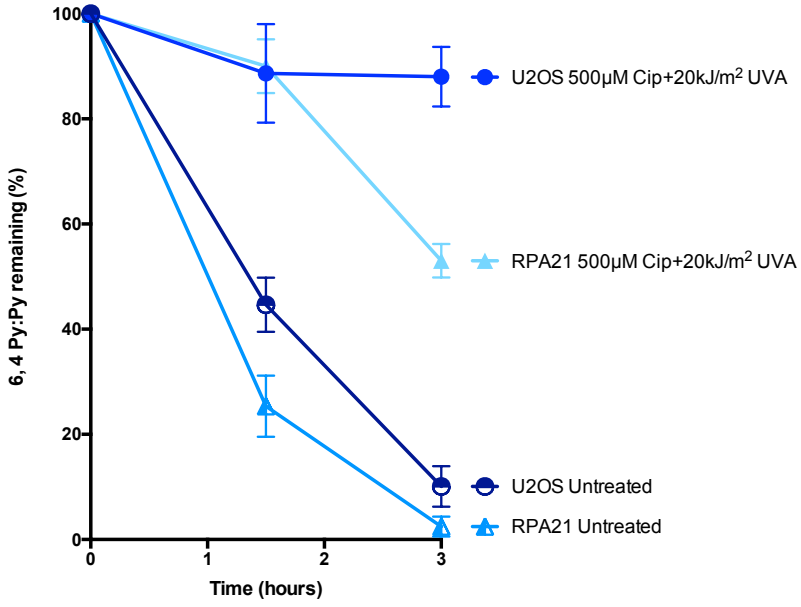

Continued…

C

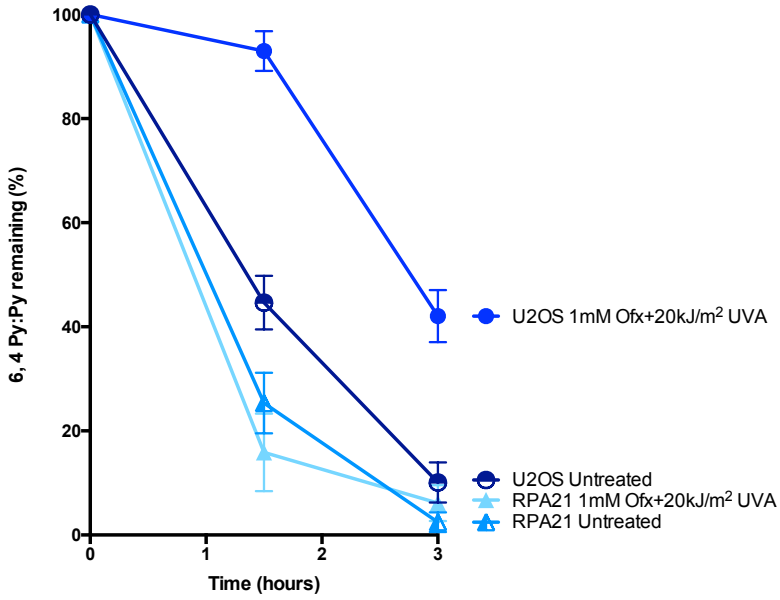

Figure 4.6: RPA overexpression and photosensitiser mediated inhibition of 6,4 Py:Py repair by NER
U2OS and RPA21 cells were treated with **(A)** 6-TG (24 hours, 3 and 9μM 6-TG for 0.85 and 0.86% incorporation, respectively), **(B)** ciprofloxacin (Cip, 500μM, 1 hour) and **(C)** ofloxacin (Oflx, 1mM, 1 hour). Cells were irradiated with 20kJ/m^2 UVA and then immediately with 10 J/m^2 UVC. Genomic DNA was extracted at the indicated times after irradiation and 6,4 Py:Pys were measured by ELISA. The 6,4 Py:Py levels recorded immediately after irradiation were set to 100%. Each treatment result is the mean of three independent experiments. The results for untreated U2OS and RPA21 are the mean of 11 independent experiments and were used in all three graphs.

4.2.4 The effect of RPA overexpression on UVA-mediated NER inhibition

While these experiments were being carried out, work in the laboratory established that high doses of UVA also inhibit NER in the absence of an exogenous photosensitiser (McAdam et al., 2016). I therefore examined the effect of RPA overexpression on UVA-mediated NER inhibition. U2OS and RPA21 cells were irradiated with 200 kJ/m^2 UVA, immediately followed by 10 J/m^2 UVC. Genomic DNA was isolated at different times after irradiation and the removal of 6,4 Py:Pys was measured by ELISA.

Figure 4.7 (A), confirms UVA-induced inhibition of NER in U2OS cells in which around 50% of the initial 6,4 Py:Pys remain at 3 hours post irradiation. In contrast

RPA21 cells repair around 80% at this time (p=0.038, paired t-test). Thus, RPA overexpression enables U2OS cells to partially overcome NER inhibition induced by high dose UVA.

Reviewing the historical control data for NER by U2OS and RPA21 cells exposed to UVC alone, I noticed that RPA21 cells generally repaired 6,4 Py:Pys more efficiently than U2OS. The composite data from 11 independent experiments are presented in Figure 4.7 (B). The difference was small but statistically significant (p=0.01, paired t-test). It appears from these data that a small increase in RPA expression can enhance the basal NER rate.

Figure 4.7 (C) analyses the difference between the two cell lines in a different format. It is a plot of the rate of 6,4 Py:Py removal as a function of initial 6,4 Py:Py load ($6.4x10^5$ 6,4 Py:Pys induced by a UVC dose of $20J/m^2$) (Perdiz et al., 2000). The Lineweaver-Burk plot has the reciprocal of the velocity of the reaction on the y-axis, which in this case is the rate of 6,4 Py:Py removal. On the x-axis it has the reciprocal of the substrate concentration, which in this case is the number of 6,4 Py:Pys. The y-intercept is $1/V_{max}$ (maximum velocity) of NER for 6,4 Py:Py removal, while the x-intercept is $-1/K_m$, which is the concentration of 6,4 Py:Pys at half the V_{max}. From the fitted equations it appears that a two-fold higher RPA level is associated with a three-fold increase in the efficiency of NER (V_{max}=3333 and 10000 for U2OS and RPA21 respectively). In agreement with this, NER in U2OS cells reaches half of its V_{max} at a third of the concentration of 6,4 Py:Py compared to RPA21 (K_m= $5.2x10^5$ and $1.5x10^6$ for U2OS and RPA21 respectively). This observation suggests that RPA levels are limiting for NER – at least in U2OS cells. This limitation becomes more important and potentially lethal under oxidative conditions.

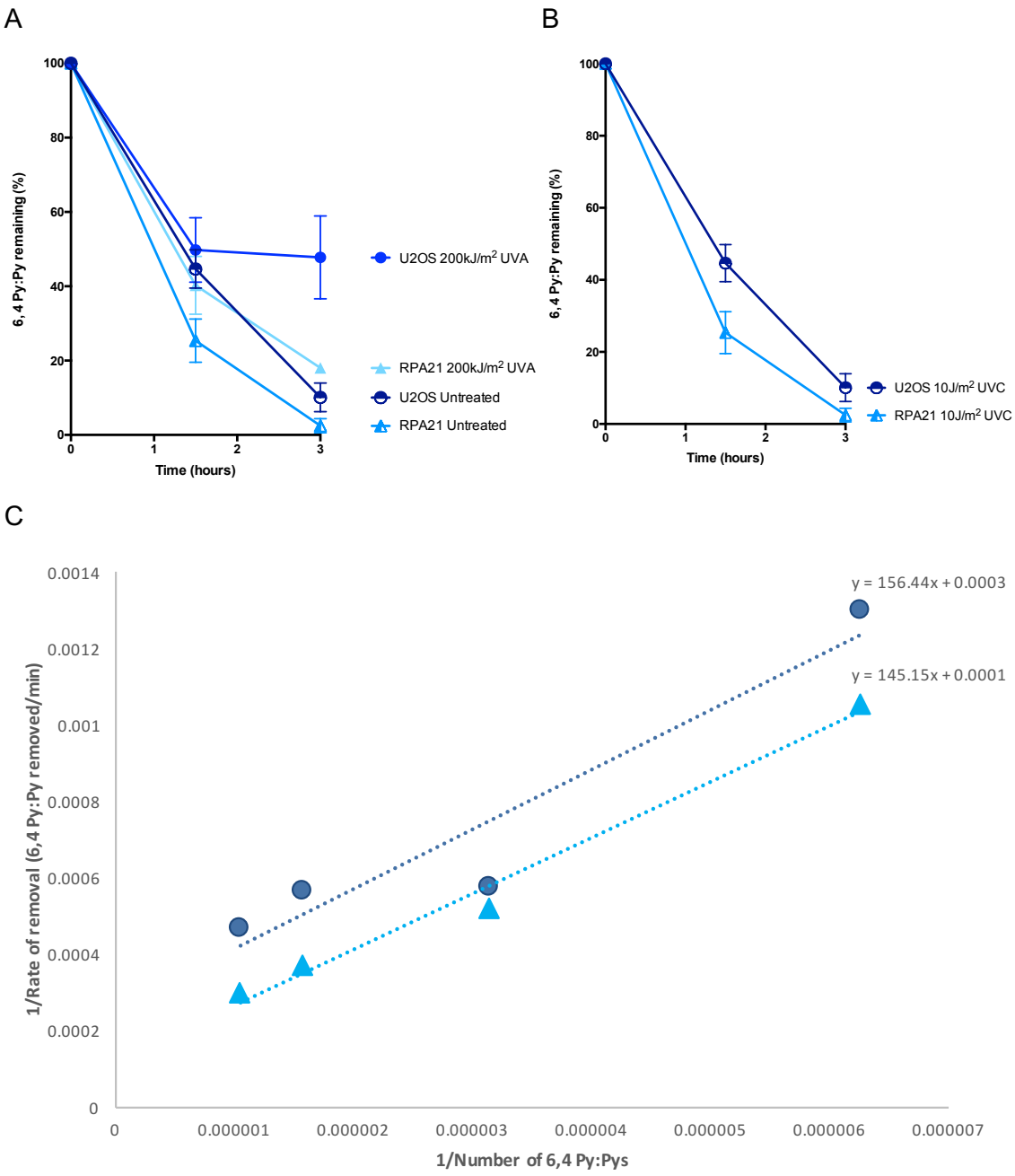

Figure 4.7: The effect of RPA overexpression on UVA-mediated inhibition of NER and NER efficiency
U2OS and RPA21 cells were treated with **(A)** 200kJ/m^2 UVA and 10 J/m^2 UVC, or **(B)** UVC only. Genomic DNA was extracted after the indicated times and 6,4 Py:Pys were measured by ELISA. The 6,4 Py:Py levels immediately after irradiation were set to 100%. Data are means of (A) 4 independent or (B) 11 independent experiments. **(C)** The rates of 6,4 Py:Py removal were determined for different amounts of 6,4 Py:Pys. The line of best fit was drawn to determine the K_m and V_{max} for the removal of 6,4 Py:Pys using a Lineweaver-Burk plot.

To investigate the effects of RPA expression on survival, I examined the viability of U2OS and RPA21 cells following irradiation by UVC, UVA or UVC+UVA. The results shown in Figure 4.8 indicate that the higher level of RPA in RPA21 cells does not confer a significantly increased protection against killing by UVC and there were no measurable differences in viability between U2OS and RPA21 cells irradiated with up to 8 J/m^2 UVC. On the other hand, RPA21 cells were generally more resistant to lethal UVA doses and their increased RPA expression protected against killing by UVA either alone or in combination with a low dose of UVC.

I conclude that although RPA is not limiting for survival of U2OS cells following UVC irradiation up to 8 J/m^2, when DNA damage is induced under more oxidative conditions, RPA levels are a major determinant of cell survival.

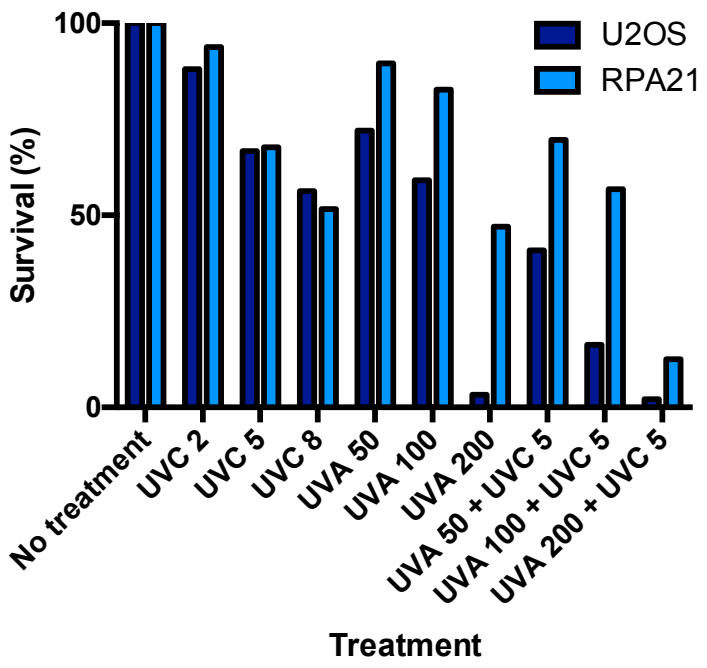

Figure 4.8: MTT survival assay for RPA21 and U2OS cells treated with UVA, UVC and UVA+UVC
Viability of UVA (doses in kJ/m^2) and UVC (doses in J/m^2) irradiated U2OS and RPA21 cells. Mean values from two experiments.

4.2.5 RPA chromatinisation by ciprofloxacin

In chapter 3, I explained that RPA is chromatinised due to exposed ssDNA caused by 6-TG+UVA mediated replication blocking lesions. When activated by UVA, ciprofloxacin can induce the formation of T<>T CPDs, that can also block replication, sequester RPA and impede NER (Lhiaubet-Vallet et al., 2009). Figure 4.9 (A) shows this chromatinisation with Cip+UVA treatment in U2OS and RPA21 cells. Since RPA21 has a larger quantity of RPA available in the cell, the proportion that is chromatinised is much smaller in comparison to the total.

On the other hand, Oflx+UVA is a very poor source of CPDs and therefore has no visible effect on RPA recovery from either cell line (Figure 4.9 (B)) (Peacock et al., 2014). The DDB2 component of DDB1:DDB2 (DNA damage binding 1: DNA damage binding 2) is another indicator of NER substrates. It is chromatinised with 6-TG+UVA and Cip+UVA, but not with Oflx+UVA (Guven et al., 2015). Therefore, Oflx+UVA is unlikely to result in NER substrates.

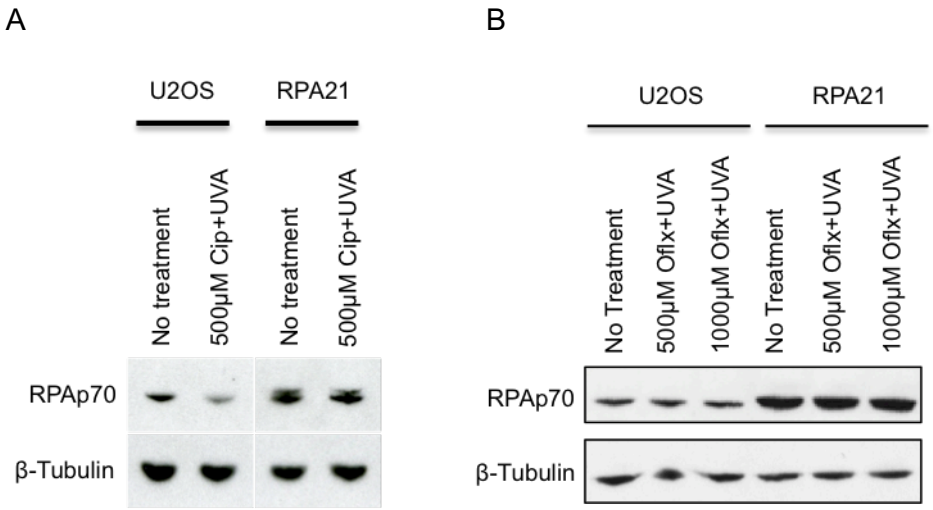

Figure 4.9: Chromatinisation of RPA70 with ciprofloxacin and ofloxacin
RIPA extracts were prepared from HeLa cells treated with **(A)** ciprofloxacin (Cip) or **(B)** ofloxacin (Oflx) for 1 hour and irradiated with 20kJ/m^2 UVA. The extracts were analysed by western blot (20µg) using antibodies against RPA70 and β-tubulin.

Oflx+UVA mediated NER inhibition and cell death are prevented by RPA overexpression. I have shown that this is not because RPA is chromatinised and is unavailable for NER. Therefore, I decided to investigate oxidative RPA damage.

4.2.6 RPA inter-subunit crosslinking in U2OS and RPA21 cells

I demonstrated in the previous chapter that a fraction of RPA32 in 6-TG+UVA-treated HeLa cells is converted to higher molecular weight forms that are consistent with the formation of inter-subunit crosslinks. I decided to investigate this crosslinking further in U2OS and RPA21 cells. In particular, I examined whether the other photosensitizers, ciprofloxacin and ofloxacin, damage RPA in a similar manner.

It is important to point out that the RPA32 antibody recognises several polypeptides in extracts of RPA21 cells. These species are not treatment-related. They can be most clearly seen in Figure 4.10 (A). The prominent band at around 100kDa, I believe is the product of incomplete cleavage at the P2A site between RPA70 and RPA32 (102kDa). There is also a low, but detectable level of what appears to be the full length, fusion polypeptide (AcGFP-RPA14-RPA70-RPA32) at 143 kDa. To distinguish these endogenous forms from the treatment-generated crosslinked RPA32, the latter are designated with *, ** and ***.

Western blotting of extracts from Cip+UVA treated U2OS and RPA21 cells (Figure 4.10 (A)) revealed a 100kDa RPA32-containing species that appeared to be identical to that previously observed in HeLa cells treated with 6-TG+UVA and Cip+UVA (Figure 3.7 (A) and Figure 3.8 (B), respectively). In this case, there is a second band between 70-100kDa (**), which is most likely a product of AcGFP-RPA14 crosslinking to RPA32. A third band (***) migrating between 40-50kDa may represent an additional crosslinked species comprising RPA32 and endogenous RPA14, as seen previously in Figure 3.8 (B).

Oflx+UVA also induced RPA32 crosslinking and the same products were observed in Figure 4.10 (B). The higher level of RPA in the RPA21 cells was reflected in the reproducibly more extensive crosslinking compared to U2OS cells.

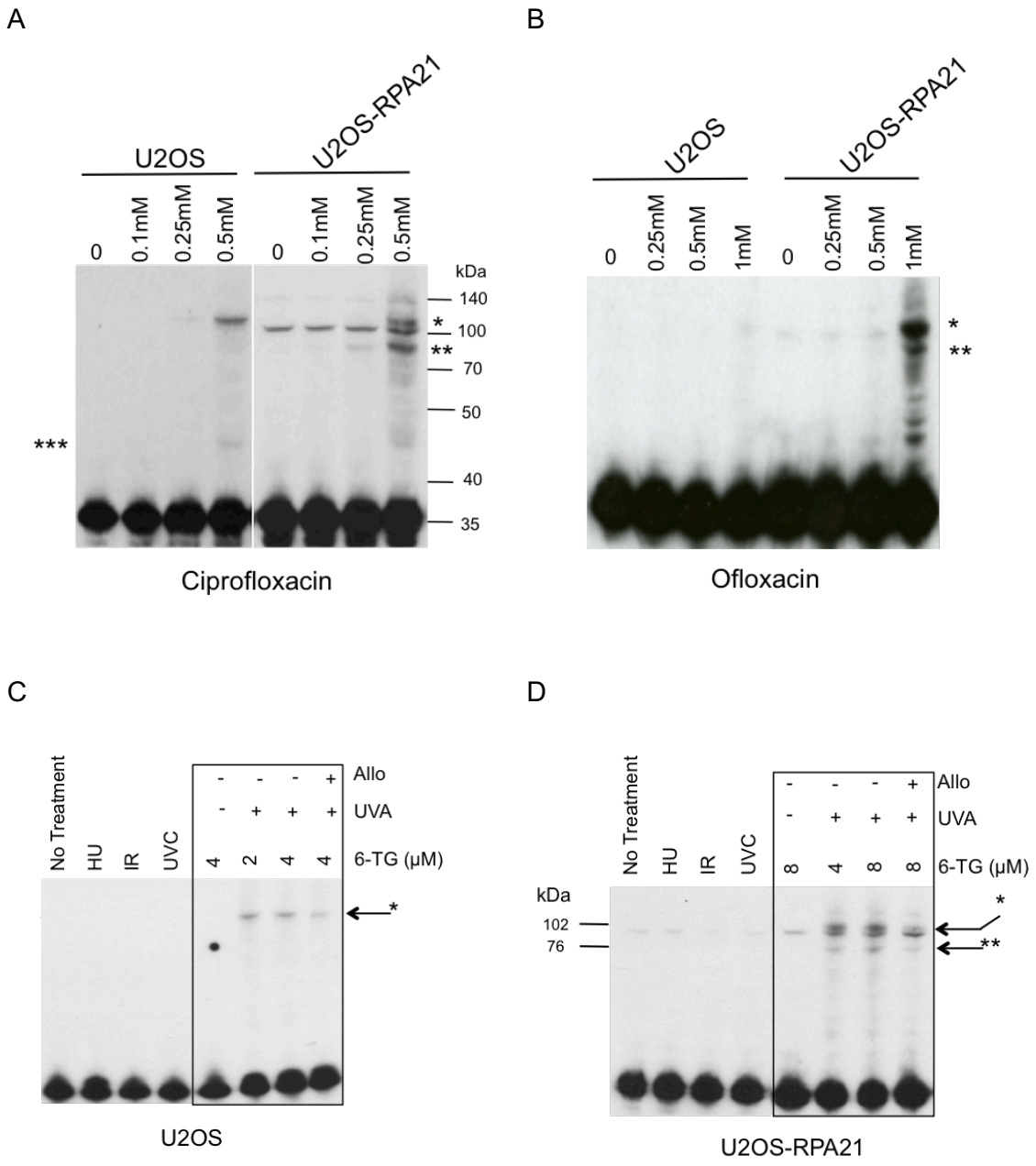

Figure 4.10: RPA32 complexes formed by Cip+UVA and Oflx+UVA treatments in U2OS and RPA21 cells

Cell extracts (20μg) were analysed by western blotting and probed with anti-RPA32 antibody. **(A)** Ciprofloxacin+20kJ/m^2 UVA **(B)** ofloxacin+20kJ/m^2 UVA. Extracts from **(C)** U2OS or **(D)** RPA21 cells treated with hydroxyurea (HU, 3mM, 3 hours), ionising radiation (IR, 20Gy), UVC (100J/m^2) or with 6-TG +/- 1mM allopurinol as indicated. DNA 6-TG substitution was 0.83 and 0.71% for U2OS and RPA21, respectively. RPA32 complexes are indicated with (*, ** and ***). Molecular weight markers are indicated. Unmodified RPA32 serves as the loading control.

Consistent with my findings with 6-TG+UVA treated HeLa cells, the crosslinked RPA32 complexes were not detected after exposure to hydroxyurea, or high dose

ionising radiation or UVC (Figure 4.10 (C and D)) confirming that their formation is not due to extensive DNA damage or replication arrest and is not cell type specific. In addition, allopurinol partially suppressed the formation of crosslinked RPA32 complexes (Figure 4.10 (C and D)) consistent with the involvement of ROS in their formation.

HeLa and U2OS are tumour-derived cell lines. To investigate whether RPA32 was crosslinked in non-tumour cells, I examined RPA in extracts of untransformed GM8339 human fibroblasts treated with Cip+UVA or Oflx+UVA. The results are shown in Figure 4.11. Western blot analysis confirmed RPA32 crosslinking is not specific to transformed cells. The same (*) designation as Figure 4.10 was used to mark the bands representing crosslinks.

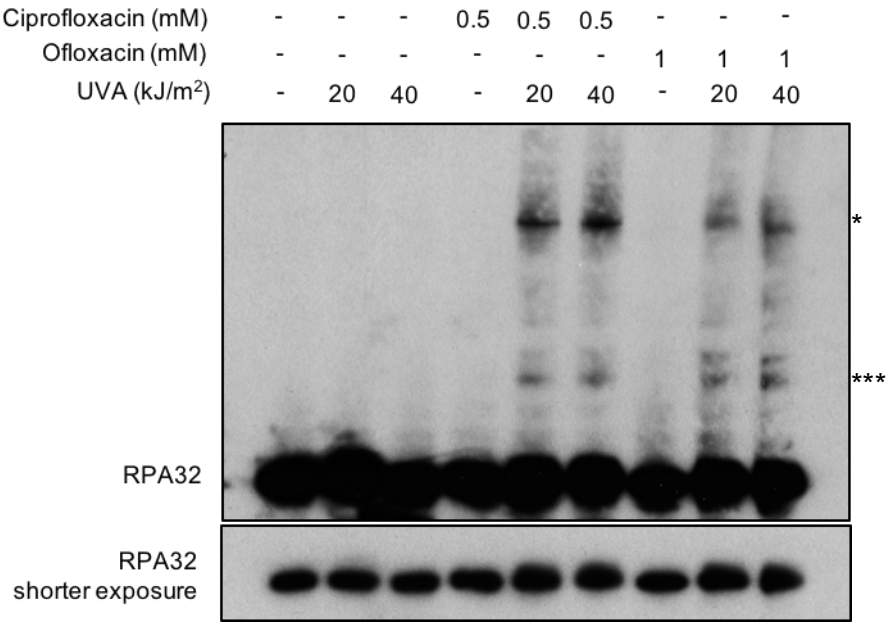

Figure 4.11: Formation of crosslinked RPA32 in untransformed GM8339 cells
Extracts (20µg) prepared from GM8339 cells treated with ciprofloxacin (1 hour), ofloxacin (1 hour) and UVA as indicated, were analysed by western blotting and probed with anti-RPA32 antibody. Unmodified RPA32 serves as the loading control. RPA32 complexes are indicated with (* and ***).

To investigate whether RPA32 is in fact crosslinked covalently to RPA70, I immunoprecipitated RPA from RPA21 extracts and analysed the precipitated

material by western blotting for RPA70. The RPA overexpressing cells were used for these experiments to increase the chances of detecting any crosslinked proteins. The results are shown in Figure 4.12. Input is simply the extract and the supernatant (sup) are the proteins that remain after RPA32 immunodepletion. The eluate should contain RPA32 plus any crosslinked complexes. Figure 4.12 (30-second exposure) shows that RPA70-immunoreactive material of approximately 100 kDa is immunoprecipitated along with RPA32, consistent with Cip+UVA induced RPA32:RPA70 crosslinking. It is also possible to see the RPA70-RPA32 unprocessed polypeptide in the eluate from untreated RPA21 cells. This is not resolved from the crosslinked species in treated cells.

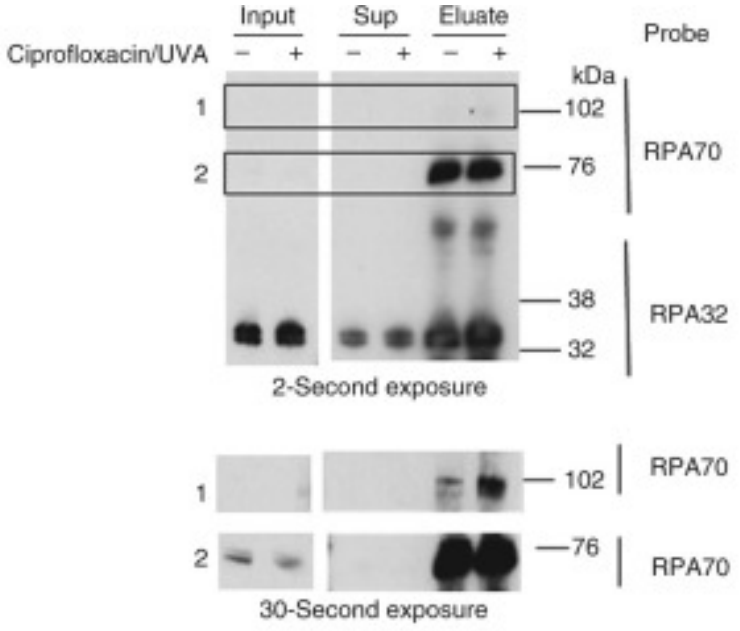

Figure 4.12: Immunoprecipitation of RPA32:RPA70 from ciprofloxacin+UVA treated RPA21 cells
Anti-RPA32 antibodies were used with protein A dynabeads to immunoprecipitate RPA from extracts of ciprofloxacin+UVA (0.5mM ciprofloxacin, 20kJ/m^2 UVA) treated RPA21 cells. The eluates from protein A beads were analysed by western blotting with an anti-RPA70 probe. The lower panels represent longer exposure of areas 1 and 2 above. Molecular weight markers are indicated.

4.2.7 The fate of inter-subunit crosslinked proteins

In addition to RPA crosslinking, 6-TG+UVA also causes crosslinking of the subunits of PCNA (proliferating cell nuclear antigen), DNA replication and repair trimer (Montaner et al., 2007). I investigated whether PCNA is also vulnerable to crosslinking by Oflx+UVA and Cip+UVA. I also addressed the subsequent fate of the crosslinked complexes. Figure 4.13 (A and B) shows that both Oflx+UVA and Cip+UVA cause PCNA crosslinking (PCNA*) in U2OS and RPA21 cells.

The levels of Cip+UVA-mediated PCNA and RPA protein-protein crosslinks were diminished three hours post-irradiation and disappeared almost completely from U2OS and RPA21 cells within 24 hours (Figure 4.13 (B)). To investigate a possible role for the proteasome in this disappearance, I pre-incubated cells with the proteasome inhibitors MG-132 and lactacystin for two hours before treatment with Cip+UVA.

Figure 4.13 (C), shows that MG-132 and lactacystin completely abrogated the removal of *PCNA indicating that that the proteasome is responsible for its degradation. On the other hand, although the degradation of crosslinked RPA was slowed, it was incompletely inhibited suggesting that its removal is partly proteasome-independent.

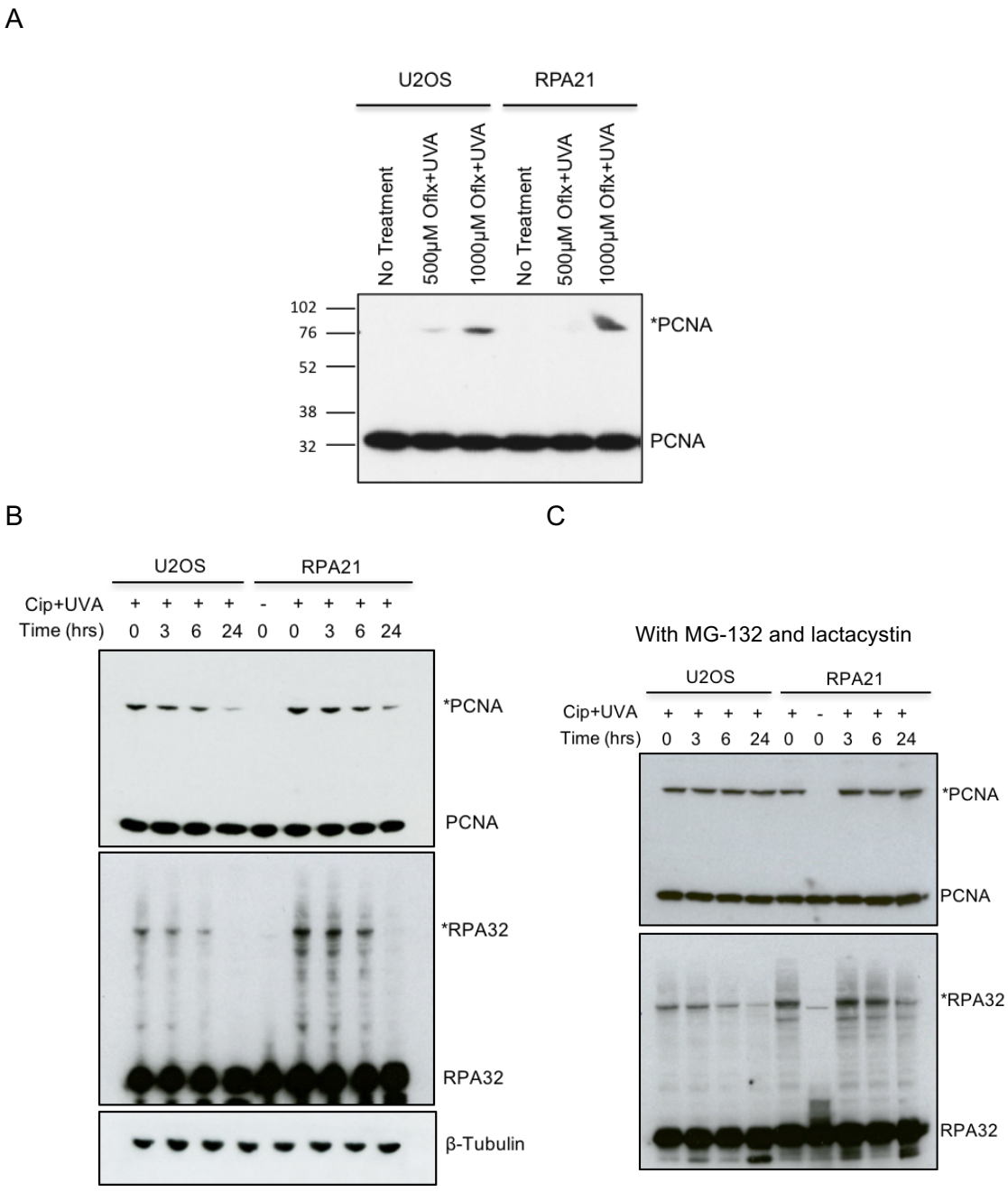

Figure 4.13: PCNA and RPA protein-protein crosslinking and removal of crosslinked proteins

Extracts (20μg) from U2OS and RPA21 cells were analysed by western blotting for RPA32, PCNA and β-tubulin**.** Molecular weight markers are indicated. **(A)** Cells were treated with ofloxacin (Oflx) for 1 hour and UVA (20kJ/m^2). **(B)** Cells were treated with 500μM ciprofloxacin (Cip) for 1 hour and irradiated with UVA (20kJ/m^2). **(C)** Cells were treated with proteasome inhibitors MG-132 (5μg/ml) and lactacystin (10μM) for 2 hours, followed by 500μM Cip for 1 hour and irradiated with UVA (20kJ/m^2). Crosslinked species are denoted by (*).

4.2.8 RPA cysteine sulfenates

In order to examine whether cysteine thiols (-SH) are oxidised to cysteine sulfenate (Cys-SOH), I selectively derivatised protein sulfenates in RPA21 extracts with a probe, BP-1 (biotin-1,3-cyclopentanedione). This probe contains a sulfenate-reactive group attached to biotin (Qian et al., 2011). The derivatised proteins are then recovered by affinity binding to streptavidin. I used the RPA21 cell line as higher levels of RPA facilitated detection of cysteine sulfenates.

Figure 4.14 (A and B) shows that oxidized forms of RPA32 that contain cysteine sulfenate are present in RPA21 cells treated with Oflx+UVA or Cip+UVA under conditions that induce RPA32:RPA70 crosslinking. A small amount of BP-1-derivatised RPA32 was reproducibly detected in untreated RPA21 cells and the level was increased by Oflx+UVA or Cip+UVA treatment. It appears that at least in the RPA overexpressing cells, there is a detectable steady state level of oxidized RPA under normal growth conditions. The oxidative stress induced by ciprofloxacin or ofloxacin in combination with UVA significantly increases RPA cysteine thiol oxidation.

.

Interestingly, the longer exposure western blot of the eluate from BP-1 derivatized Oflx+UVA treated cells revealed that along with oxidized uncomplexed RPA32, cysteine sulfenate is also detectable in the crosslinked RPA32:RPA70 complex (Figure 4.14 (B)). Since this complex accounts for a very small fraction of the total RPA32, detection of cysteine sulfenate suggests that the crosslinked RPA32 is heavily oxidized.

Thus, oxidation of cysteine residues to sulfenates is another potential contributor to RPA inactivation and NER inhibition in oxidative stress conditions.

A

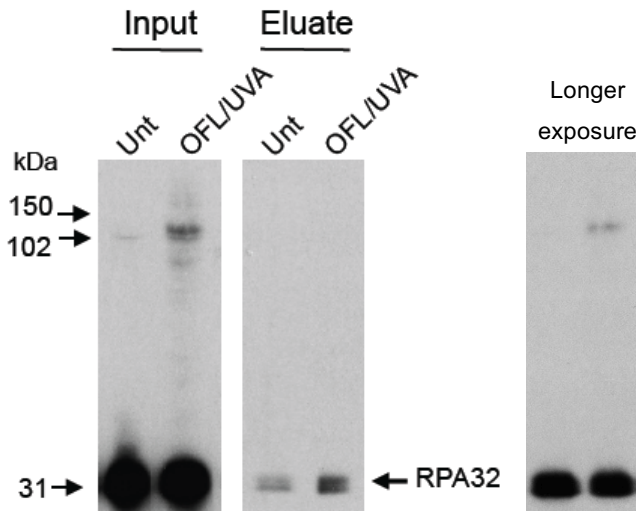

B

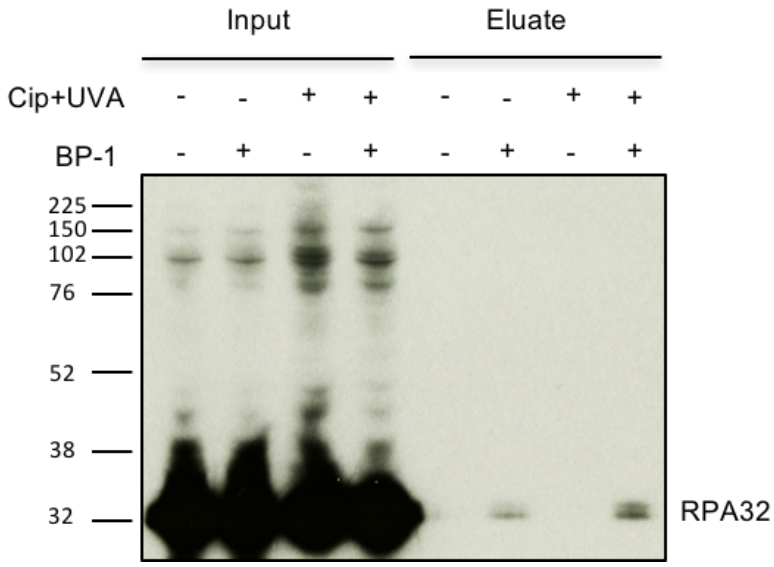

Figure 4.14: BP-1 derivatisation of RPA32 cysteine sulfenates
(A) RPA21 cells were treated with 500μM ofloxacin (Ofl) for 1 hour and UVA (20kJ/m^2). **(B)** RPA21 cells were treated with 250μM ciprofloxacin (Cip) for 1 hour and irradiated with UVA (20kJ/m^2). Extracts were prepared and cysteine sulfenates were derivatised with the BP-1 probe. Derivatised proteins were recovered by binding and elution from streptavidin beads (Eluate). Input = samples prior to streptavidin enrichment. Analysis was by western blotting for RPA32.

4.2.9 FICZ mediated RPA and PCNA crosslinking

During the final stages of my experimental work on RPA, it was reported that FICZ, a UVB photoproduct of the amino acid tryptophan, is an endogenous cellular UVA chromophore. FICZ, a UVA/visible photosensitiser, causes oxidative stress and oxidative damage to DNA at nanomolar concentrations (Park et al., 2015). I examined whether photoactivation of FICZ causes protein oxidation, specifically, inter-subunit crosslinking of PCNA and RPA.

Western blot analysis indicated that treatment of U2OS cells with FICZ induces UVA-dependent crosslinking of PCNA (Figure 4.15 (A)). A low level of RPA32 crosslinking was also apparent in the RPA overexpressing RPA21 cells (Figure 4.15 (B)). FICZ+UVA appeared to be less effective in RPA crosslinking in comparison to other photosensitising treatments.

These results show that UVA activation of a defined endogenous UVA chromophore also causes significant protein oxidation and damaging modifications to essential DNA repair/replication proteins.

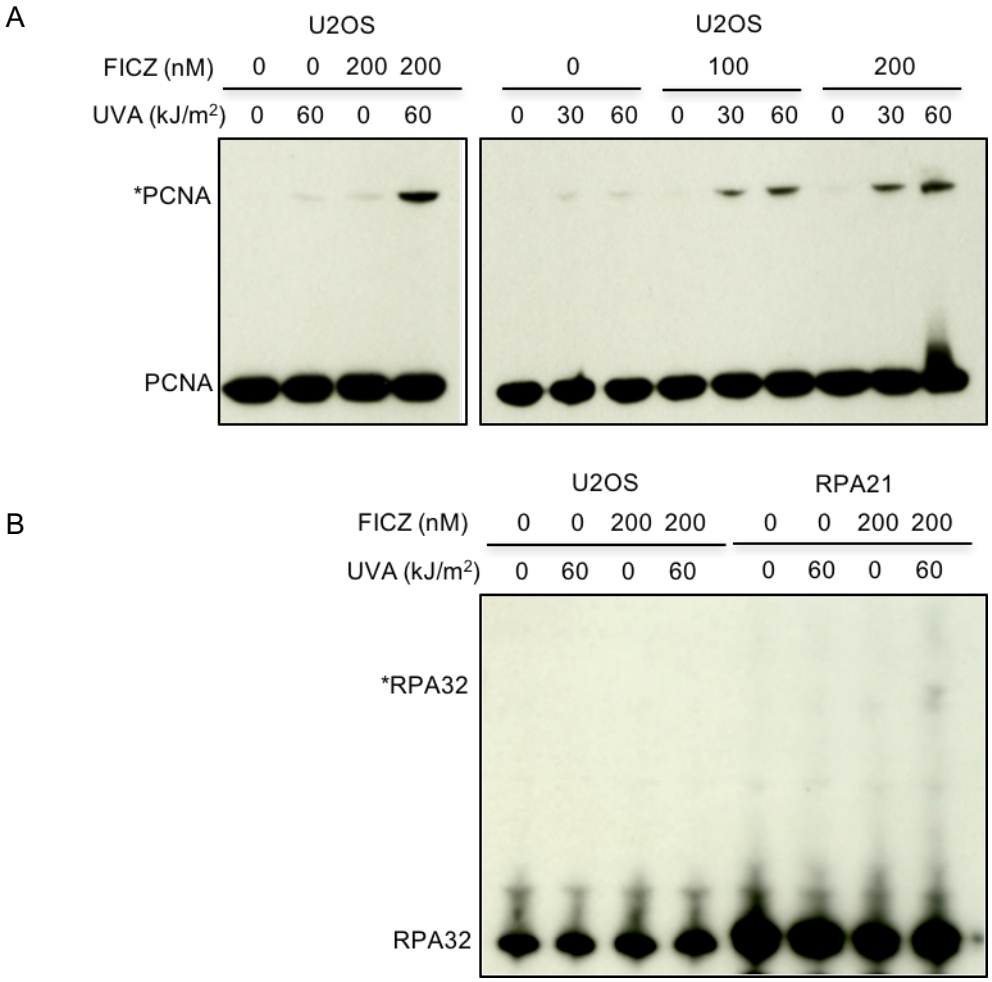

Figure 4.15: FICZ+UVA mediated crosslinking of PCNA and RPA
Extracts (20µg) from U2OS and RPA21 cells treated with FICZ (1 hour) and UVA were analysed by western blotting for **(A)** PCNA and **(B)** RPA32. Crosslinks are indicated with (*).

4.2.10 ROS levels and RPA overexpression

My findings presented so far suggest that RPA is particularly susceptible to oxidative damage. To investigate the possible source of oxidised RPA32 in untreated RPA21 cells, I measured their steady-state ROS levels using the CM-H_2DCFDA assay. These measurements reproducibly indicated a considerably higher constitutive ROS level compared to U2OS cells.

To examine further the relationship between RPA overexpression and increased ROS, I used a second cell line RPA16 (also provided by Drs. J. Lucas and L.Toledo, (Toledo et al., 2013)). RPA expression in the RPA16 cell line is intermediate between that of U2OS and RPA21. This was confirmed by western blotting (Figure 4.16 (A)).

Figure 4.16 (B) shows the CM-H_2DCFDA assays for the untreated cells. U2OS cells had the lowest ROS level and RPA21 cells had the highest. ROS levels in RPA16 cells were reproducibly intermediate between these two extremes. RPA16 appears to be more similar to RPA21 than to U2OS but this is exaggerated by the logarithmic scale. These differentials were maintained following UVA irradiation (Figure 4.16 (C)). This agrees with the hypothesis that levels of RPA expression influence intracellular ROS.

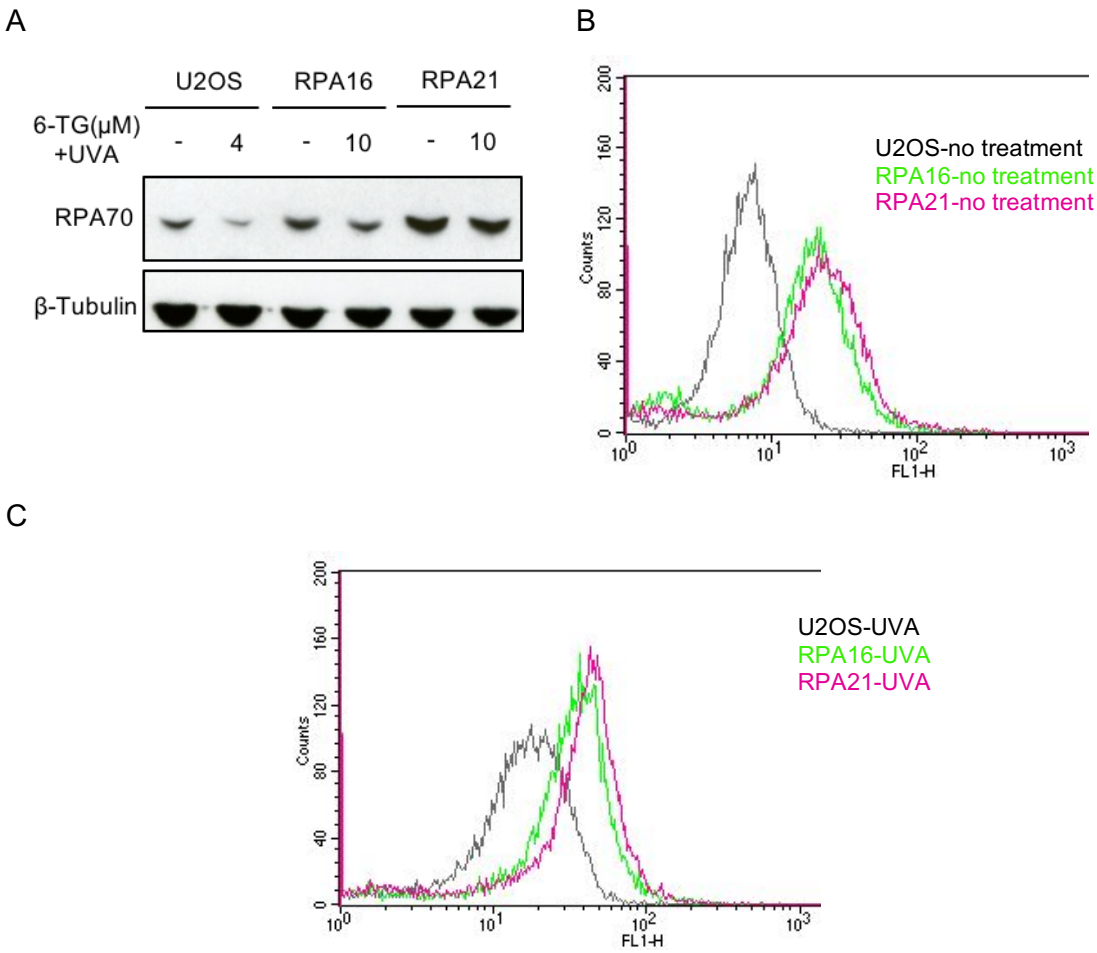

Figure 4.16: Comparison of ROS levels between U2OS, RPA16 and RPA21 cells
(A) RIPA extracts were prepared from U2OS, RPA16 and RPA21 cells (treated with 6-TG for 24 hours and 20kJ/m^2 UVA) and analysed by western blotting for RPA70 and β-tubulin**.** 6-TG incorporations were 1.424, 1.330 and 1.556% for U2OS, RPA16 and RPA21, respectively. For ROS measurements cells were **(B)** left untreated or **(C)** irradiated with UVA (20kJ/m^2). They were incubated for 20 minutes with 7.5μM CM-H_2DCFDA prior to UVA irradiation and were washed and resuspended in PBS for subsequent FACS analysis. The fluorescence intensity (FL1-H log 10) vs frequency distribution (counts) is shown.

Excess ROS reflects the saturation of the cell's antioxidant capacity. Glutathione (GSH) is a non-protein thiol that provides reducing equivalents to important antioxidant enzymes, as well as scavenging free radicals itself. It is central to cellular antioxidant defences. I measured GSH levels in U2OS, RPA16 and RPA21 cells using the Trevigen glutathione assay kit. The assay uses glutathione reductase to reduce oxidised glutathione (GSSG) present in cell extracts to GSH (Figure 4.17). GSH then reacts with DTNB (5,5'-dithiobis-2-nitrobenzoic acid), to produce 5-thio-2-nitrobenzoic acid (TNB), that can be detected by its absorbance at 405 or 414 nm.

The reaction also produces a mixed disulphide, GSTNB, that is also reduced by glutathione reductase to TNB and GSH. GSH levels are therefore proportional to TNB produced. An important additional feature of the assay is the specific measurement of GSSG. This involves an additional reaction with 4-vinylpyridine to selectively block all free SH groups, including that of GSH. Unfortunately, despite several attempts I was unable to measure GSSG as 4-vinylpyridine mediated blocking of free thiols appeared to be ineffective.

The total glutathione levels for U2OS, RPA16 and RPA21 were 4653, 3674 and 3429 pmol respectively (averages from four independent determinations). Interestingly, the increasing RPA levels exhibit a negative correlation with the amount of GSH in the cell.

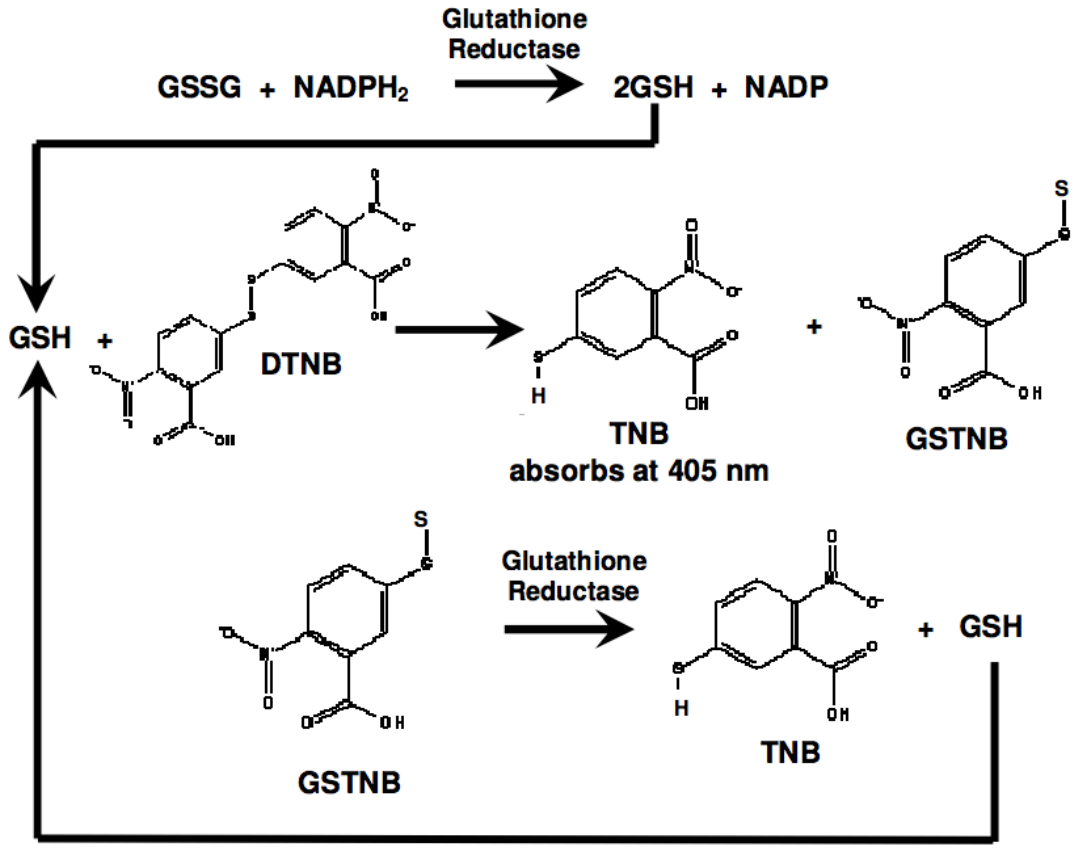

Figure 4.17: The Trevigen glutathione assay
The assay uses glutathione reductase to convert oxidised glutathione (GSSG) to its reduced form (GSH). GSH is then reacted with DTNB (5,5'-dithiobis-2-nitrobenzoic acid) to generate 5-thio-2-nitrobenzoic acid (TNB). The mixed disulphide reaction product (GSTNB) is reduced to TNB and GSH, also by glutathione reductase. TNB absorbs at 405 or 414 nm. Total glutathione levels are estimated by TNB production. (Trevigen)

In summary, increased RPA expression is associated with improved tolerance to toxicity and improved NER function under oxidising conditions. Although higher levels of RPA appear to be beneficial for the cell, they are also associated with higher steady state ROS and possibly lower cellular GSH levels.

Chapter 5. Proteomics based method for identifying DPCs

5.1 Introduction

DNA lesions are well-characterized and the specific mechanisms by which they are repaired are generally well understood. DNA-protein crosslinks (DPCs) are an exception in this regard and the identities of the cellular proteins that are particularly susceptible to crosslinking, the mechanisms of DPC formation and their repair have been less thoroughly investigated.

5.1.1 DNA-protein crosslinks

DPCs involve a covalent linkage between DNA and protein, resulting in a bulky lesion. Proteins are generally unreactive with DNA. However, exposure to a range of agents such as ultraviolet radiation (UV), ionising radiation, chemotherapeutic drugs and various aldehydes can result in DPC formation (reviewed in (Barker et al., 2005b)). These include crosslinking to DNA directly through free radical formation under oxidative stress, or *via* a chemical, drug or metal ion. Due to associated unpredictability of free radical reactions, there is an added level of complexity that a particular crosslinking agent can cause multiple types of chemical crosslinks between protein and DNA (Tretyakova et al., 2015).

DPCs are particularly detrimental to cells as they sequester and inactivate proteins in close proximity to DNA that are likely to be involved in essential DNA metabolic processes. In addition, the bulky nature of DPCs can impede DNA repair, block DNA replication fork progression *in vivo* and restrict RNA polymerase movement on the transcribed strand (Kuo et al., 2007; Nakano et al., 2012; Yeo et al., 2014). Failure to repair DPCs is likely to cause genomic instability.

DPCs can be formed through enzymatic reactions in the cell. The best examples are those involving topoisomerases (Chen et al., 2013). Topoisomerase 1 (TOP1)

relieves DNA supercoiling by introducing a single strand break and remaining covalently attached to DNA until re-ligation of the DNA is complete. TOP2 works by introducing double strand breaks. Both TOP1 and 2 can be trapped in this covalent reaction intermediate through chemotherapeutic drugs and, interestingly, through nearby DNA lesions (Pommier, 2006; Pourquier et al., 1997). Therefore, exposure of cells to DNA damaging agents can stabilize these normally transient covalent complexes as DPCs.

Non-enzymatic DPCs involve proteins in close proximity to DNA. One of the most potent and commonly used crosslinking agents is formaldehyde, as a part of chromatin immunoprecipitation assays for DNA-protein interaction studies. It works mainly by forming a covalent bond between guanine and nucleophilic amino acid residues lysine and cysteine (Lu et al., 2010; Solomon et al., 1988). Mice exposed to formaldehyde by inhalation exhibit DPCs, lowered glutathione and higher reactive oxygen species (ROS) and malondialdehyde in their bone marrow and other organs (Ye et al., 2013). It has even been proposed that number of DPCs can be used as a biomarker for occupational exposure to formaldehyde (Shaham et al., 1997).

Production of ROS through cellular redox reactions and oxidative stress conditions can result in various types of DNA and protein damage. This altered chemistry can result in reactions to occur between DNA and proteins. Oxidation of guanine, cytosine or thymine DNA bases, and lysine or tyrosine protein side chains by ROS can result in reactions that can cause DPC formation (Tretyakova et al., 2015). There are various proposed crosslinking mechanisms, such as hydroxyl radical (•OH) mediated abstraction of a methyl group from thymine and its subsequent reaction with tyrosine (Dizdaroglu et al., 1989; Tretyakova et al., 2015).

5.1.2 6-Thioguanine and UVA mediated DPCs

Heat and reducing agent-resistant DPCs are formed when oligopeptides are incubated with oligonucleotides containing G^{SO3}, an oxidized form of 6-thioguanine (6-TG). Crosslinking can involve free amino groups (arginine, asparagine, glutamine, lysine), which are often exposed on the protein surface due to their hydrophilic

nature (Gueranger et al., 2011). DPCs are detected when cells containing DNA 6-TG are exposed to UVA. Preliminary findings indicated that PCNA, MSH2 and XPA DNA replication/repair proteins were among those crosslinked by 6-TG+UVA. This work underlined the susceptibility of nuclear proteins in close proximity of DNA to DPC formation.

Ciprofloxacin, like 6-TG, is a Type II photosensitizer. Unlike 6-TG, it does not become covalently embedded in DNA. Prior to my starting this project, the ability of UV photoactivated ciprofloxacin to generate DPCs had not been examined.

5.1.3 Detection of DPCs

There are several methods by which DPCs generated in cells can be detected. In the alkaline elution assay, cell lysates are applied to filters that bind DNA (Fornace and Kohn, 1976). Under alkaline conditions, smaller DNA fragments unwind and pass through the membrane. Increased DNA elution following protease treatment reveals the presence of DPCs. DPCs may also be detected by the change in buoyant density in caesium chloride of DNA extracted from cells (Barker et al., 2005a; Gueranger et al., 2011; Lipinski, 2011; Subramanian and Furbee, 2001). In addition, the presence of DPCs decreases the yield of DNA from cells treated with a DPC inducing agent. Restoration of quantitative DNA recovery by the inclusion of a protease step indicates the presence of DPCs.

Crosslinked proteins can be identified from the DNA fraction by fluorescent labelling and mass spectrometry (MS) (Shoulkamy et al., 2012; Tretyakova et al., 2015). The involvement of specific proteins in DPCs can be revealed by immunoblotting in the rapid DNA adduct recovery (RADAR) approach, in which extracts from treated cells are applied to nitrocellulose or PVDF (polyvinylidene difluoride) membranes and probed with antibodies (Kiianitsa and Maizels, 2013). Each of these methods has drawbacks either in the ability to identify the crosslinked species or their quantitation. For this reason, I developed an improved and unbiased method for DPC analysis.

5.1.4 Mass spectrometry

In order to study proteins involved in DPCs, Gherezghiher *et al.* used 1,2,3,4-Diepoxybutane, a carcinogenic metabolite of 1,3-butadiene found in urban air and cigarette smoke, to generate DPCs in human fibrosarcoma cells (Gherezghiher et al., 2013). Their method of DPC isolation involved extracting DNA from treated cells and subjecting them to neutral thermal hydrolysis to release protein-guanine conjugates, which were separated by SDS-PAGE and analysed by MS (HPLC−ESI^+−MS/MS). They identified around 150 proteins that included histones, high mobility group proteins, transcription factors, splicing factors, and tubulins and identified the presence of crosslinks between protein cysteine thiols and N-7 guanine. The drawback of this approach is that it relies on a chemically modified DNA base as the DNA end of the DPCs.

Chromatin enrichment of proteins (ChEP) utilises formaldehyde to form crosslinks between DNA and protein and involves resuspending chromatin in sodium dodecyl sulphate and urea to remove non-specific interactions before detection by MS (Kustatscher et al., 2014). However, the authors recognise that not all contaminating proteins are removed in this approach.

The study by Kustatscher *et al.* involved stable isotope labelling by amino acids in cell culture (SILAC) (Kustatscher et al., 2014). SILAC involves growing two populations of cells that have been grown in medium supplemented with 'heavy' amino acid, which includes ^{2}H instead of ^{1}H, ^{13}C instead of ^{12}C, or ^{15}N instead of ^{14}N. This results in a mass shift for the proteins from cells grown in heavy medium compared to the light version without any other chemical changes. This metabolic labelling is stable and complete labelling occurs after five cell doublings, even for proteins that do not exhibit a significant turnover.

SILAC allows comparison of proteins from cells that have undergone different treatments (reviewed by (Mann, 2006)). An advantage is that cells can be pooled together after undergoing a variety of different treatments and any further processing can occur without introducing artefacts due to differential handling of samples. Upon extraction and analysis by MS, the peptides with the lower and higher masses can

be compared as a pair in the mass spectra. If they appear to be in a 1:1 ratio, there is no difference between the two proteomes. If there is a difference, due to the mass shift, it is possible to identify in which proteome the protein is more or less abundant. I therefore developed a SILAC-based approach that provides a more statistically rigorous and sensitive method of DPC analysis.

5.1.5 Aims

My aims at the outset were to:

- Develop a sensitive and statistically rigorous proteomic method to study DPCs following a variety of damaging treatments,
- Examine the types of proteins involved in DPC formation.

5.2 Results

5.2.1 UVA-mediated DPC formation in CCRF-CEM cells containing DNA 6-TG

I measured 6-TG incorporated into the DNA of CCRF-CEM cells grown in medium containing 6-TG. Incorporation was concentration dependent and non-linear (Table 5.1). Inhibition of DNA replication by pre-treatment with hydroxyurea (HU) for 6 hours prior to addition of 6-TG reduced incorporation to below detectable levels.

Table 5.1: Incorporated 6-TG as a percentage of DNA guanine in CCRF-CEM cells
Cells were incubated in medium containing 6-TG for 48 h. DNA was extracted and 6-TG and guanine measured by HPLC (see Section 2.3.8). Hydroxyurea (HU, 3mM) was added 6 hours prior to addition of 6-TG and was present throughout the subsequent incubation.

6-TG concentration (μM)	Incorporated 6-TG as a percentage of DNA guanine (%)
0	0
0.3	0.047
0.6	0.17
0.9	0.61
0.9 + HU	<0.001

Previous investigations had revealed that the yield of DNA extracted using the Wizard (Promega) extraction protocol was reduced if the cells had been treated with 6-TG and UVA (Gueranger et al., 2011). The Wizard protocol involves a protein precipitation step prior to harvesting the DNA. When cells have proteins covalently attached to their DNA, this step can result in the precipitation of these proteins and therefore loss of DNA and a decline in the final DNA concentration that is measured. Quantitative DNA recovery is restored by the inclusion of a proteinase K digestion step before DNA precipitation – implicating DPCs in the DNA losses.

An example of this behaviour is shown in Table 5.2, which reports the increase in DNA recovery achieved by including proteinase K digestion during purification of DNA from 6-TG+UVA treated CCRF-CEM cells. The modest dose of UVA (50 kJ/m^2) did not affect DNA recovery whereas 6-TG treatment resulted in significant DNA losses that were reversed by proteinase K digestion. The effects of 6-TG and UVA were synergistic and treatment with 0.9μM 6-TG+UVA resulted in complete loss of extractable DNA. Thus, 6-TG+UVA treatment, and to a lesser extent 6-TG alone, induce the formation of DPCs in CCRF-CEM cells.

The dependence of DPC formation on DNA-embedded 6-TG was investigated in two ways. Firstly, DNA recovery was measured in 6-TG-treated GM03467 Lesch-Nyhan fibroblasts. These cells do not express hypoxanthine-guanine phosphoribosyltransferase and cannot salvage 6-TG for DNA incorporation. DNA recovery was quantitative and was unaffected by proteinase K digestion in Lesch-Nyhan cells treated with 6-TG+UVA (Table 5.2). Secondly, CCRF-CEM cells were treated with HU prior to and during incubation with 6-TG to prevent DNA replication and 6-TG incorporation. The yield of DNA was again quantitative with or without proteinase K digestion. These findings indicate that 6-TG-induced DPC formation requires DNA-embedded 6-TG.

Table 5.2: Proteinase K induced increase in DNA recovery
Cells were treated with 6-TG for 24 hours. CCRF-CEM cells treated with hydroxyurea (HU) were incubated with HU for 6 hours prior to 6-TG addition. GM03467 Lesch-Nyhan cells are hypoxanthine-guanine phosphoribosyltransferase deficient and cannot scavenge 6-TG for DNA incorporation. DNA extracts were made with Wizard (Promega) extraction kit and measured by NanoDrop. Results of the paired t-tests comparing each treatment to the control sample are shown. ns, not significant ($p > 0.05$); * ($p < 0.05$), ** ($p < 0.01$). All values are mean of ≥ 2 independent determinations.

Treatment	CCRF-CEM	CCRF-CEM with 3mM HU	GM03467 Lesch-Nyhan cells
No treatment	1.00	1.00	1.01
50kJ/m^2 UVA	1.09 (NS)	1.03 (NS)	1.04 (NS)
0.3μM 6-TG	1.82*	1.03 (NS)	1.07 (NS)
0.9μM 6-TG	2.44*	1.04 (NS)	1.09 (NS)
0.3μM 6-TG + UVA	3.85**	1.01 (NS)	1.02 (NS)

DNA 6-TG generates ROS when cells are exposed to UVA. Unincorporated free 6-TG and its nucleot(s)ides are also a source of ROS upon UVA activation. To determine whether DNA 6-TG-derived ROS were required for DPC formation, I measured intracellular ROS in CCRF-CEM cells, CCRF-CEM cells treated with HU and GM03467 Lesch-Nyhan cells.

Figure 5.1 (A) shows that UVA induces ROS in 6-TG-treated GM03467 Lesch-Nyhan cells. Since these cells do not incorporate 6-TG, ROS production can be ascribed to free intracellular 6-TG. Consistent with this view, approximately similar ROS levels are generated in UVA-irradiated CCRF-CEM cells treated with 6-TG in the presence of HU (Figure 5.1 (B)). Since UVA does not induce detectable DPCs under these conditions, it appears that this level of ROS is insufficient for DPC formation in the absence of DNA-embedded 6-TG. Incorporated DNA 6-TG makes a major contribution to UVA-induced ROS (Figure 5.1 (B), orange line). There is significant DPC formation under these conditions, indicating that ROS generated from DNA 6-TG is a significant contributor to DPC formation. I note, however, that since 6-TG is more reactive than canonical DNA bases, the preferential formation of DPCs involving DNA 6-TG or its oxidation products is not excluded by these data.

A. GM03467 Lesch-Nyhan

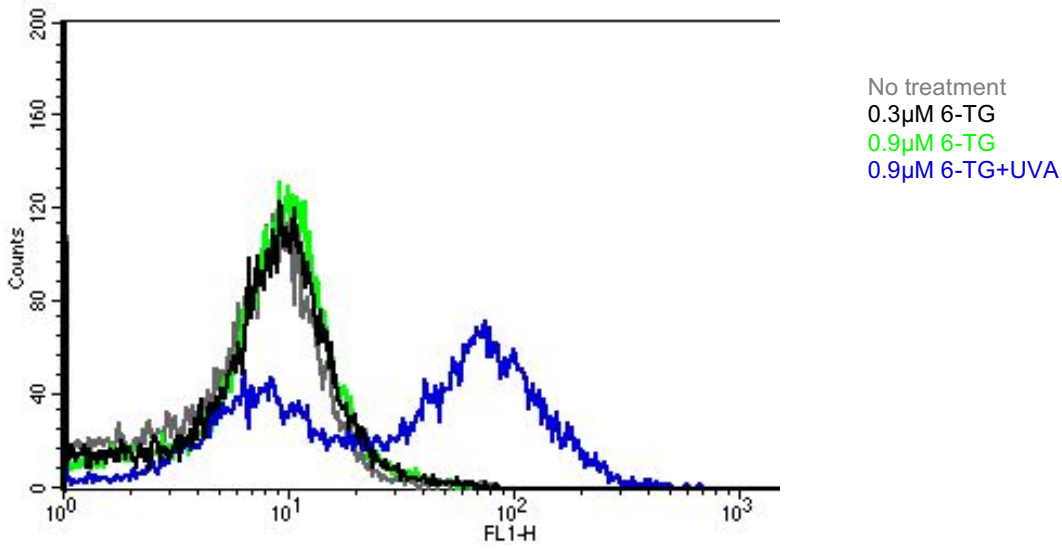

B. CCRF-CEM+HU

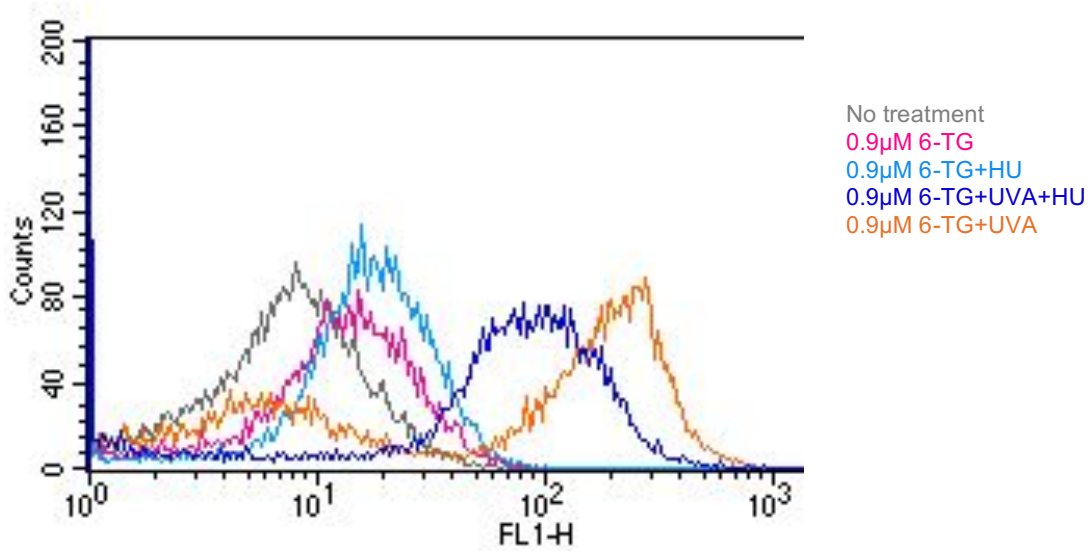

Figure 5.1: Intracellular ROS measurements with and without 6-TG incorporation
(A) GM03467 Lesch-Nyhan cells were treated with indicated doses of 6-TG for 24 hours and 50kJ/m^2 UVA. **(B)** CCRF-CEM cells were treated with hydroxyurea (HU) for 6 hours prior to 6-TG incubation and maintained in the medium along with 6-TG for 24 hours and irradiated with 50kJ/m^2 UVA. Cells were all incubated for 20 minutes with 7.5μM CM-H_2DCFDA prior to UVA irradiation and were washed and resuspended in PBS for subsequent FACS analysis. The fluorescence intensity (FL1-H log 10) vs frequency distribution (counts) is shown.

5.2.2 Optimising detection of individual proteins in DPCs

To investigate DPC formation in CCRF-CEM cells, I devised a method to enrich for DPCs. In order to do this, I needed to eliminate proteins that were non-covalently associated with DNA. I therefore prepared chromatin and depleted it of non-covalently associated proteins by high salt (500mM NaCl) washes. Sheared, salt-washed chromatin was then applied to a Hybond-N^+ membrane, which has high affinity for DNA. The DNA was crosslinked to the membrane by UVC irradiation (Stratalinker). Any remaining non-covalently associated proteins were further depleted by extensive washing with 8M urea. Figure 5.2 shows an example of a membrane to which chromatin from CCRF-CEM cells treated with 6-TG+UVA had been applied. It demonstrates the decrease in background protein levels (SyproRuby staining) achieved by the urea wash and shows further that this step did not affect the amount of bound DNA (SYBR Green staining).

DNA repair/replication proteins were detected on the urea-washed membranes by antibody probes. An example is shown in Figure 5.2. The presence of XPA, PCNA and MSH2 in DPCs was confirmed (Gueranger et al., 2011) and I additionally detected RPA70, which I focused on extensively in the previous two chapters.

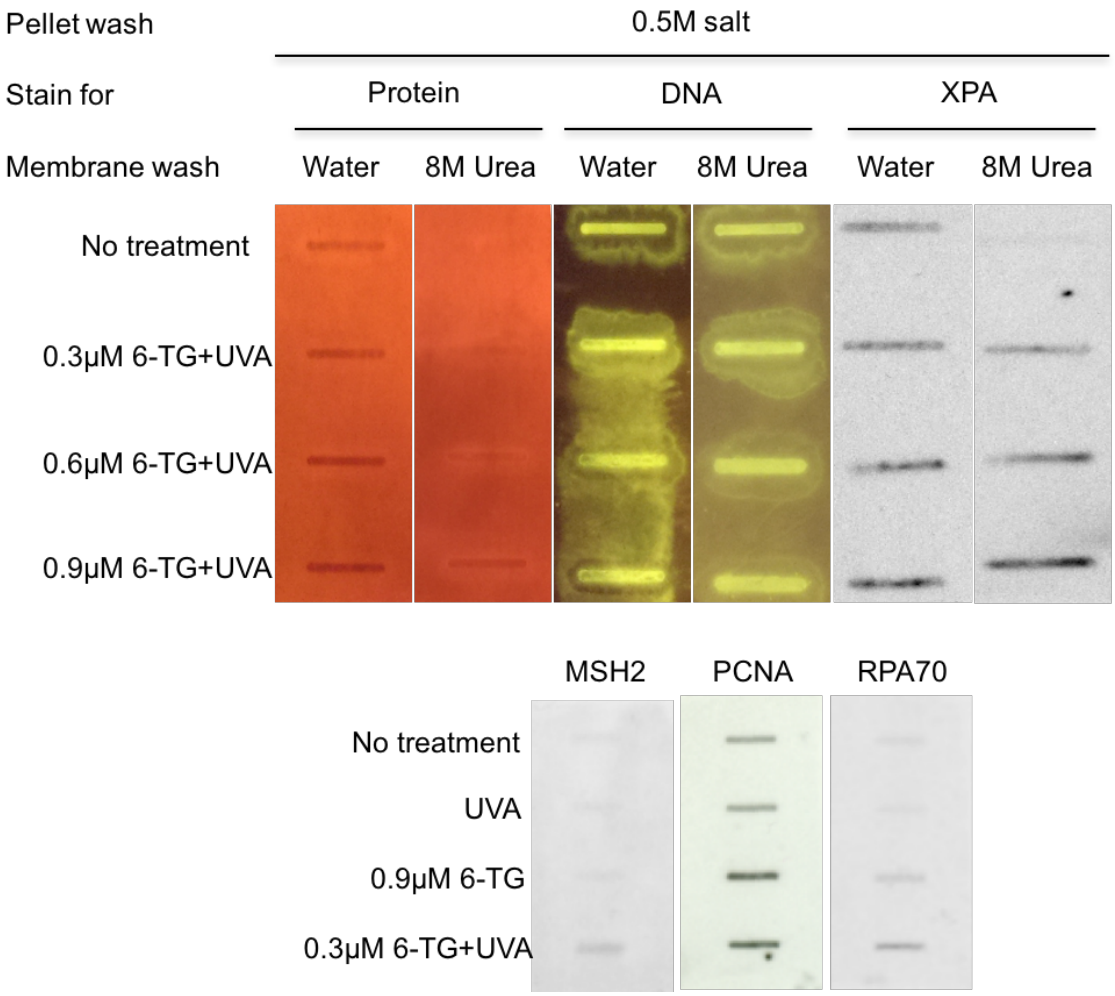

Figure 5.2: Detection of DNA-crosslinked proteins
CCRF-CEM cells were treated with 6-TG and 50 kJ/m^2 UVA as indicated. Chromatin was prepared, washed with 0.5M salt, extensively sheared and UVC-crosslinked to a HyBond-N$^+$ membrane. Membranes were washed with 8M urea that was removed by rinsing with water. Protein and DNA on the membrane were detected by staining with Sypro Ruby and SYBR Green, respectively. The membrane was probed with antibodies against MSH2, PCNA, RPA70 and XPA.

5.2.3 A proteomics method to study DPCs

Immunodetection of DNA crosslinked proteins on Hybond-N+ membranes is insensitive and depends absolutely on the availability of high quality antibodies that produce very little or no non-specific staining. These requirements severely limit its applicability. I therefore developed a proteomics-based method to identify proteins in

DPCs in a comprehensive, statistically rigorous and unbiased way. These experiments were carried out in collaboration with Drs. Karin Barnouin and Bram Snijders from the Protein Analysis and Proteomics Laboratory at Clare Hall.

The experimental scheme is presented in Figure 5.3. It utilises SILAC, which provides an internal control and enables a statistically rigorous comparison of samples. CCRF-CEM cells were grown for a week in medium containing heavy or light isotopes of arginine and lysine. Full isotopic labelling of proteins was confirmed by MS. Samples that have been exposed to exactly the same treatment can be labelled in the opposite way with light and heavy labels and compared. If the results of the two experiments match each other, it means that two independent experiments of the same treatment have resulted in the same outcome.

One half of each heavy and light culture was treated with 0.9μM 6-TG for 24 hours. The other half was untreated. Half of each of the resulting four cultures was irradiated with UVA (50 kJ/m^2) and the other half was unirradiated. Equal numbers of light and heavy-labelled cells were mixed (Figure 5.3, table) to generate 16 Mixes of heavy and light-labelled cells in 1:1 ratios. Each of these Mixes was then divided into two equal aliquots. One half of each was used to prepare salt-washed sheared chromatin that was applied to the HyBond-N^+ membrane. Following washing with 8M urea, membrane-associated proteins were digested with trypsin *in situ* and the digests analysed by MS. This procedure was designed to enrich for DPCs.

A DNA-free whole cell (RIPA) extract was prepared from the other half of each Mix. These were separated by SDS-PAGE and digested in-gel with trypsin for subsequent MS analysis. If certain proteins become crosslinked to DNA, there would be a selective loss of these proteins in the RIPA extract. This would not only give an indication of the impact of DPC formation, resulting in a noticeable decline in overall extractable protein, but also would act to validate the results of the chromatin experiment.

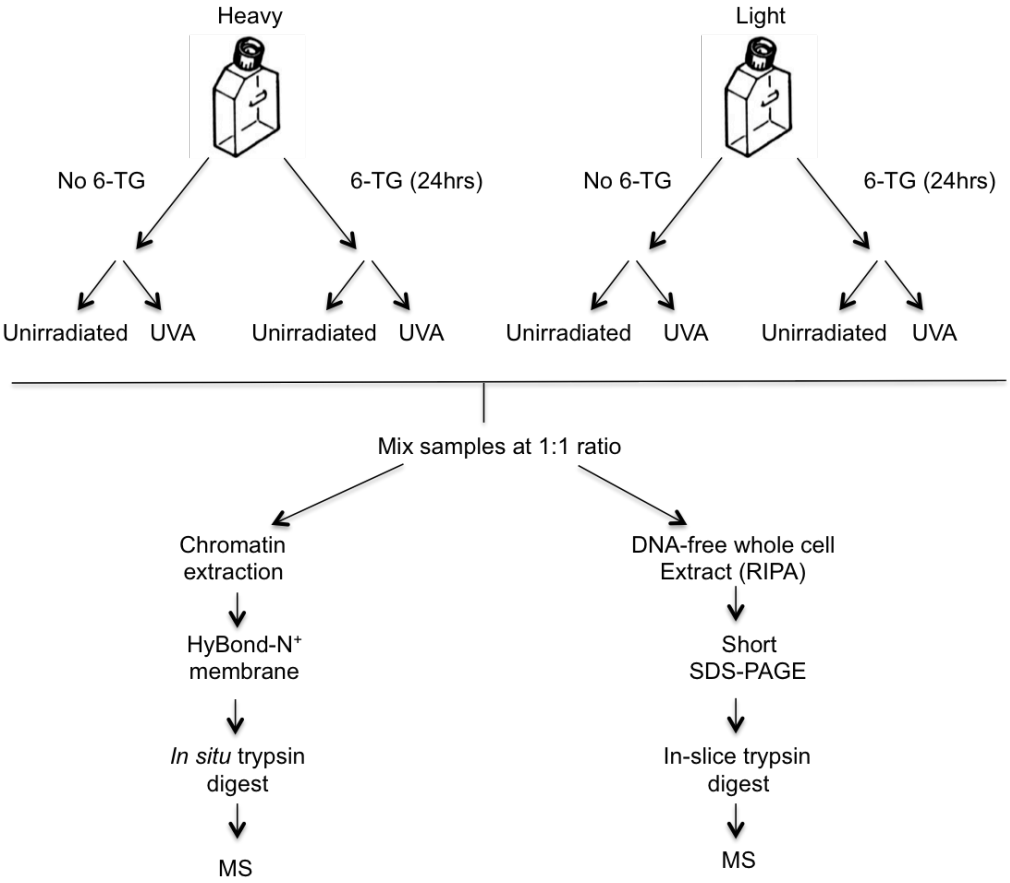

				Heavy			
				6-TG			
				-		+	
				No UVA	UVA	No UVA	UVA
Light	6-TG	-	No UVA	Mix 1	Mix 2	Mix 3	Mix 4
			UVA	Mix 5	Mix 6	Mix 7	Mix 8
		+	No UVA	Mix 9	Mix 10	Mix 11	Mix 12
			UVA	Mix 13	Mix 14	Mix 15	Mix 16

Figure 5.3: Outline of the SILAC analysis
CCRF-CEM cells were labelled with heavy or light arginine and lysine isotopes and half were treated with 0.9μM 6-TG for 24 hours. Half of the cells from each culture were irradiated with 50 kJ/m^2 UVA and the remaining cells were not irradiated. Cells from each of the 8 cultures were mixed in a 1:1 ratio as indicated in the table of mixes. The 16 mixed samples were then divided into two equal aliquots., From one aliquot, chromatin was prepared and applied to a HyBond-N$^+$ membrane for MS analysis. The other aliquot was used to prepare a DNA-free whole-cell (RIPA) extract for SDS-PAGE and MS analysis.

5.2.4 DPC formation by 6-TG+UVA

In two independent experiments of forward and reverse SILAC labelling, MS analysis identified 2611 proteins from Hybond-N^+ membrane-bound, DPC enriched samples. The analysis of each Mix provides a heavy/light (H/L) ratio. This is a ratio of the abundance of heavy and light-labelled proteins in that particular Mix. As an intrinsic quality control, mixes of cells that were labelled differently but were otherwise treated in exactly the same way were compared. The H/L ratio for these proteomes was expected to be 1.0. Deviations from 1.0 (expressed as log2 = 0) reflect the effects of treatments.

An example of this intrinsic SILAC control is shown in Figure 5.4. In the Table in Figure 5.3, it can be seen that Mixes 1, 6, 11 and 16 contain heavy and light-labelled cells that have received identical treatments. Figure 5.4 (A and B) present scatter and density plots for Mix 1. The protein abundance is represented as intensity or density, which refers to the statistical distribution of a variable. This is plotted as a function of H/L ratio. As expected, the H/L ratios for Mix 1 (combined untreated heavy and untreated light-labelled cells) cluster symmetrically around the log2 value of 0, indicating equal abundance of heavy and light isomers of the proteins and confirming that Mix 1 contains an accurate 1:1 ratio of heavy and light-labelled cells. More than 99.5% of the H/L ratios lie between log2 values of -1 and +1. In analysing the effects of treatments, I therefore considered values outside this range (>2 fold enrichment) to be a significant response to treatment and a result of DPC formation. As expected, the distributions for Mixes 6, 11 and 16 also cluster tightly around log2 values close to zero (Figure 5.4 (C-F)).

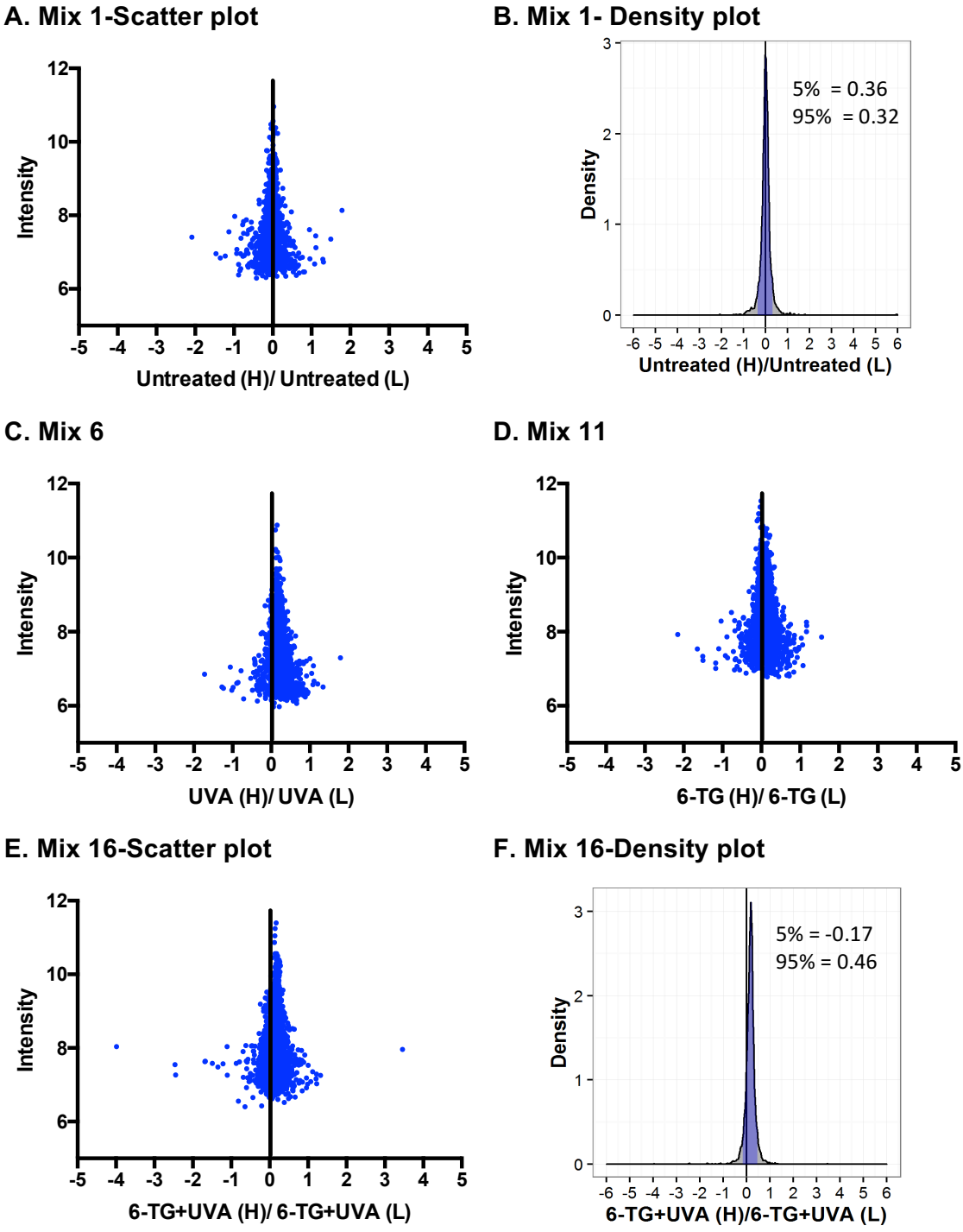

Figure 5.4: SILAC H/L ratios of the control samples
CCRF-CEM cells were labelled with heavy (H) or light (L) arginine and lysine isotopes and treated with 0.9μM 6-TG for 24 hours and irradiated with 50 kJ/m^2 UVA as indicated. Chromatin extracts were applied on HyBond-N$^+$ membranes, subject to *in situ* trypsin digestion and analysed by MS. Scatterplots of log2 SILAC H/L ratios of the detected proteins in each sample vs log10 Intensity **(A, C, D and E)** or Density **(B and F)** are presented. The H/L values at 5% and 95% of the density distribution are indicated.

An increase in H/L ratios indicates that the heavy-labelled cells contain more of a particular protein compared to the light-labelled cells. If 6-TG+UVA causes DPC formation, we would expect the heavy-labelled cells treated with 6-TG+UVA compared to untreated light-labelled cells to result in an increase in the SILAC H/L ratio. A decrease in H/L ratios would result from the reverse, if the light-labelled cells were treated with 6-TG+UVA and the heavy-labelled cells were left untreated.

Starting with UVA, Mix 2 is a mixture of heavy-labelled cells treated with UVA and untreated light-labelled cells. Mix 5 is the reverse-labelled version of Mix 2 that comprises UVA-treated light-labelled cells and untreated heavy-labelled cells. The distribution/scatter plots for these mixes are presented in Figure 5.5 (A and B for Mix 2; C and D for Mix 5) . In both cases, there are no changes in the H/L ratio, indicating a lack of DPC formation with UVA treatment at this particular dosage.

Mix 3 is a mixture of heavy-labelled cells treated with 6-TG and untreated light-labelled cells. Mix 9 is the reverse-labelled version of Mix 3 that comprises 6-TG-treated light-labelled cells and untreated heavy-labelled cells. The distribution/scatter plots for these mixes are presented in Figure 5.6 (A and B for Mix 3; C and D for Mix 9). In each case there is a shift in the H/L ratios, where the ratios increase when heavy-labelled cells are treated with 6-TG and decrease when light-labelled cells are treated. This is consistent with a 6-TG-mediated enrichment in DNA-associated proteins. The effect is small, however, and most of the values fall within -1 and +1 representing < 2-fold enrichment.

In contrast, 6-TG+UVA (Mixes 4 and 13) caused significant changes in the distribution of H/L ratios as seen in Figure 5.7 (A and B for Mix 4; C and D for Mix 13). In each case there is a highly significant shift in the H/L ratios, where the ratios increase when heavy-labelled cells are treated with 6-TG+UVA and decrease when light-labelled cells are treated. Most of the ratios fall outside the -1 to +1 range and confirm a significant increase in DPC formation. Since UVA on its own did not induce significant changes in H/L ratios, the effects of 6-TG and UVA on DPC formation are synergistic.

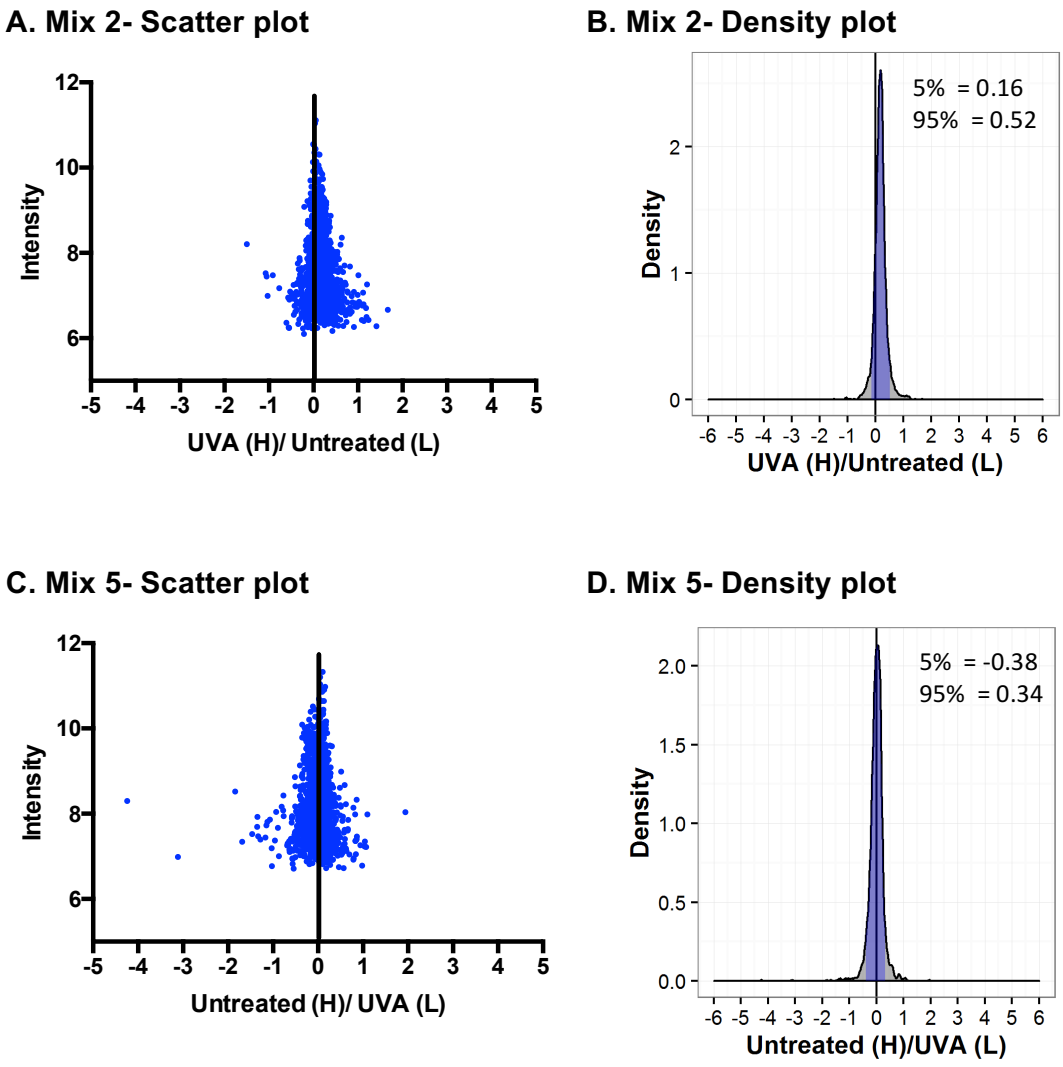

Figure 5.5: SILAC H/L ratios for UVA treatment
CCRF-CEM cells were labelled with heavy (H) or light (L) arginine and lysine isotopes and irradiated with 50 kJ/m^2 UVA as indicated. Chromatin extracts were applied on HyBond-N$^+$ membranes, subject to *in situ* trypsin digestion and analysed by MS. Scatterplots of log2 SILAC H/L ratios of the detected proteins in each sample vs log10 Intensity **(A and C)** or Density **(B and D)** are presented. The H/L values at 5% and 95% of the density distribution are indicated.

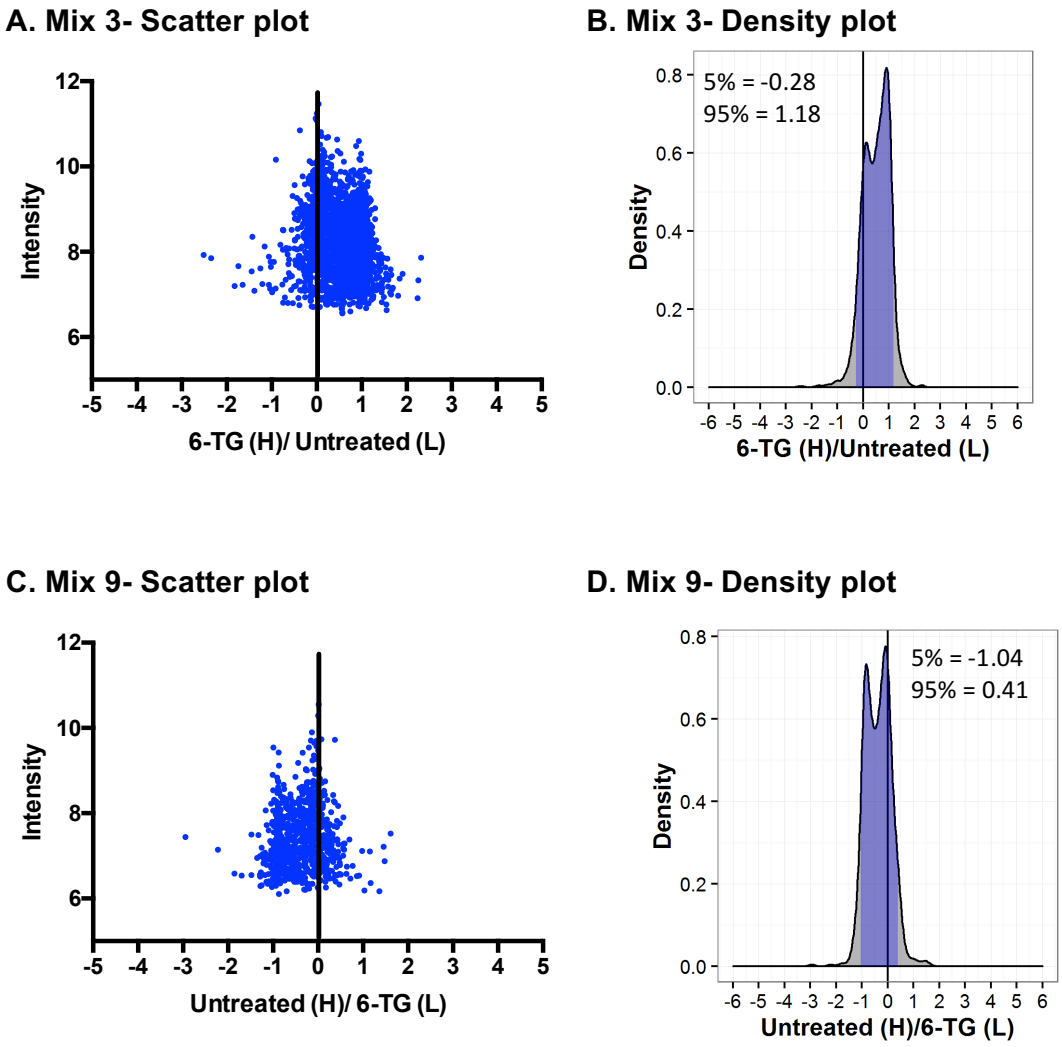

Figure 5.6: SILAC H/L ratios for 6-TG treatment
CCRF-CEM cells were labelled with heavy (H) or light (L) arginine and lysine isotopes and treated with 0.9μM 6-TG for 24 hours as indicated. Chromatin extracts were applied on HyBond-N^+ membranes, subject to *in situ* trypsin digestion and analysed by MS. Scatterplots of log2 SILAC H/L ratios of the detected proteins in each sample vs log10 Intensity **(A and C)** or Density **(B and D)** are presented. The H/L values at 5% and 95% of the density distribution are indicated.

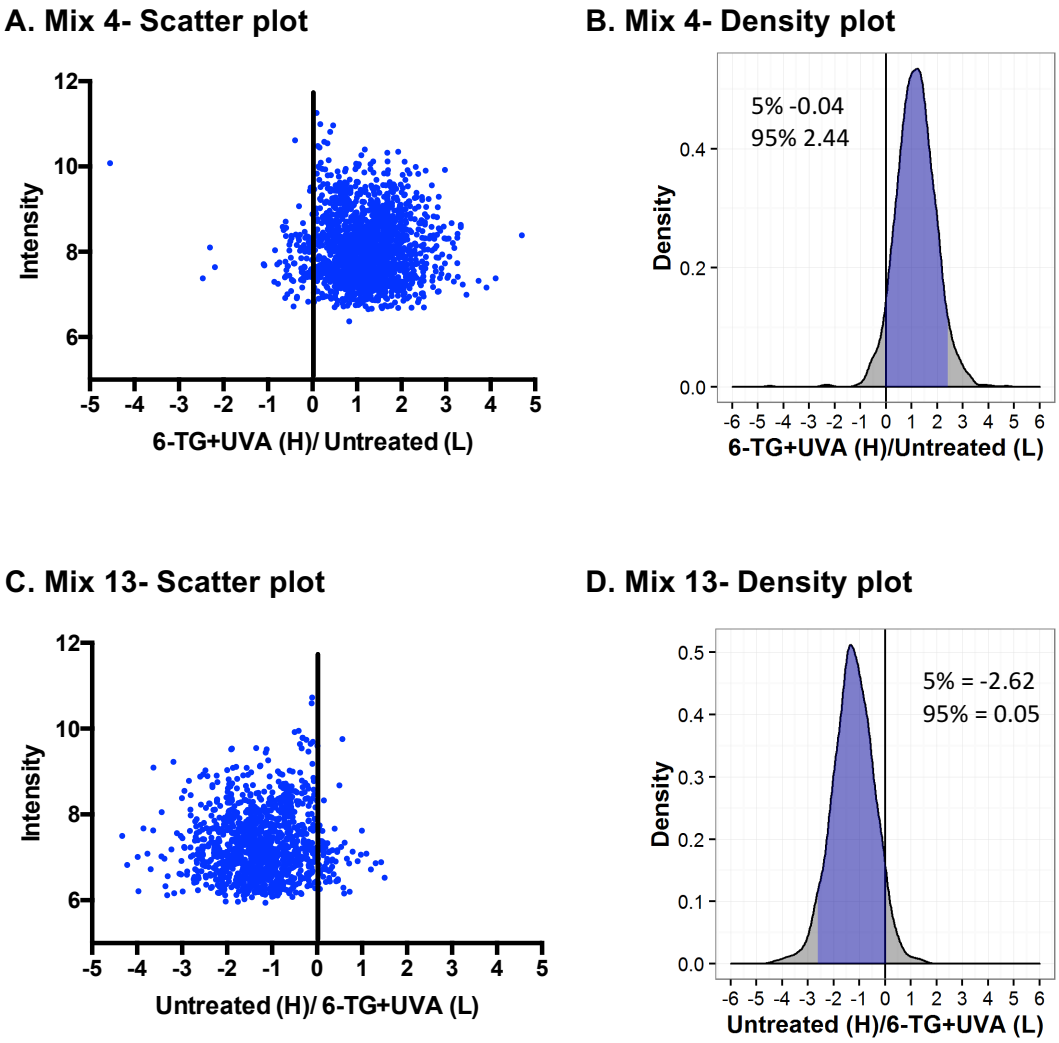

Figure 5.7: SILAC H/L ratios for 6-TG+UVA treatment
CCRF-CEM cells were labelled with heavy (H) or light (L) arginine and lysine isotopes and treated with 0.9μM 6-TG for 24 hours and irradiated with 50 kJ/m^2 UVA as indicated. Chromatin extracts were applied on HyBond-N$^+$ membranes, subject to *in situ* trypsin digestion and analysed by MS. Scatterplots of log2 SILAC H/L ratios of the detected proteins in each sample vs log10 Intensity **(A and C)** or Density **(B and D)** are presented. The H/L values at 5% and 95% of the density distribution are indicated.

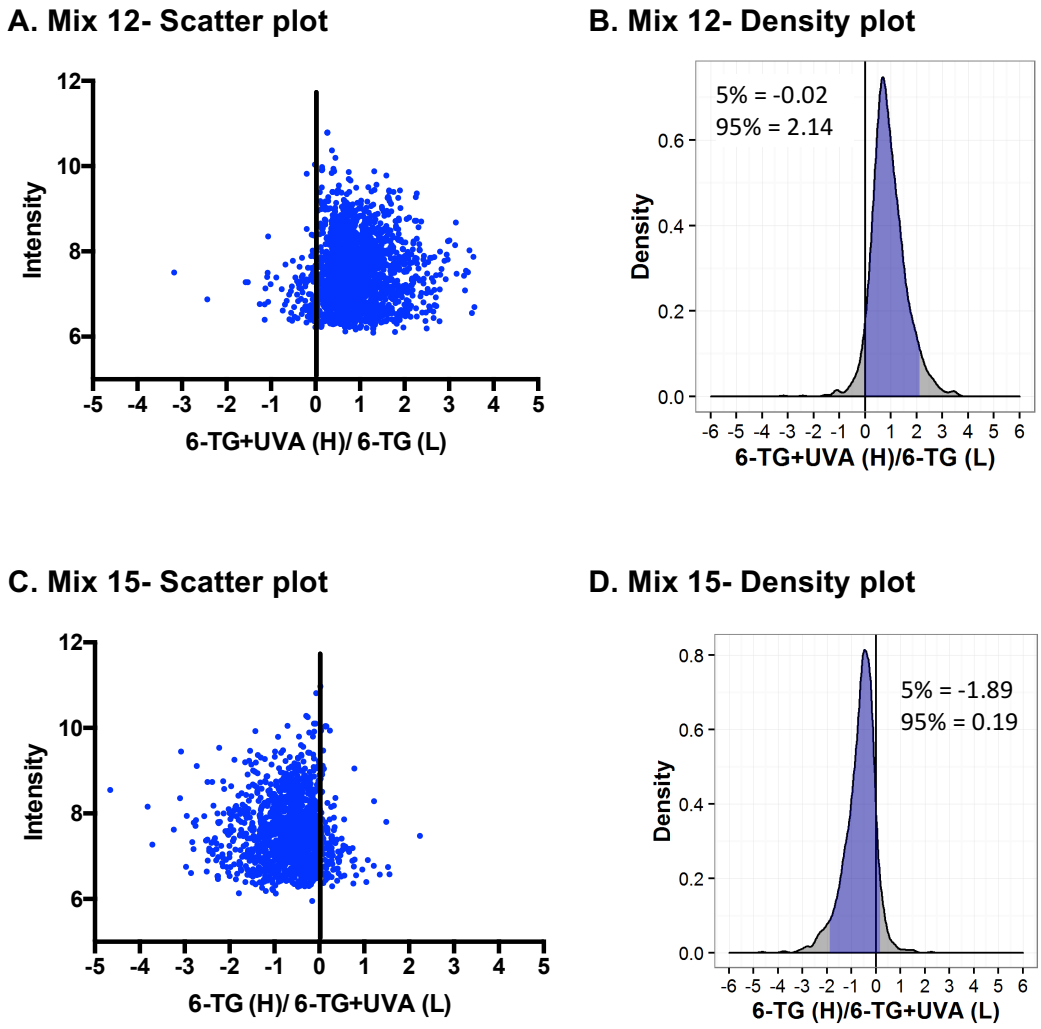

Figure 5.8: SILAC H/L ratios for 6-TG+UVA treatment vs. 6-TG only
CCRF-CEM cells were labelled with heavy (H) or light (L) arginine and lysine isotopes and treated with 0.9μM 6-TG for 24 hours and irradiated with 50 kJ/m^2 UVA as indicated. Chromatin extracts were applied on HyBond-N$^+$ membranes, subject to *in situ* trypsin digestion and analysed by MS. Scatterplots of log2 SILAC H/L ratios of the detected proteins in each sample vs log10 Intensity **(A and C)** or Density **(B and D)** are presented. The H/L values at 5% and 95% of the density distribution are indicated.

This synergy was confirmed in the analysis of Mixes 12 and 15 (Figure 5.8 A and B for Mix 12; C and D for Mix 15), which specifically addresses the effect of UVA on cells treated with 6-TG. Mix 12 is a mixture of heavy-labelled cells treated with 6-TG+UVA and light-labelled cells treated with 6-TG. Mix 15 is the reverse-labelled version of Mix 12 that comprises 6-TG+UVA treated light-labelled cells and 6-TG treated heavy-labelled cells. In the absence of synergy between 6-TG and UVA, the log2 H/L ratios when comparing 6-TG and 6-TG+UVA would fall within the -1 to +1 range, indicating no change. However, there is a highly significant shift in H/L ratios confirming that efficient DPC formation requires both 6-TG and UVA and their effects are synergistic.

H/L ratio density distributions and scatter plots for analysis of the other mixes are presented in the Appendix (Figure 7.1).

Figure 5.9 is an example of an alternative presentation of the SILAC data for DPC formation. In it, each treatment is compared to its equivalent reverse label treatment. By performing this comparison, I combine data from two completely independent experiments to analyse changes in the amount of specific proteins as a result of treatment in otherwise untreated cells. In other words, if the effect of a particular treatment is reproducible, a comparison of two reverse-labelled mixes should result in a correlation.

Figure 5.9 (A) addresses the impact of UVA on DPC formation. It compares the H/L ratios of Mix 2 and Mix 5, which represents UVA (H)/No treatment (L) and No treatment (H)/UVA (L), respectively. It shows that H/L ratios remain tightly clustered around the origin of the scatter plot. This is in agreement with the proteinase K data and confirms that 50kJ/m^2 UVA does not induce significant DPC formation.

On the other hand, comparison of Mixes 3 and 9 (Figure 5.9 (B)) results in a negative correlation, where a majority of the proteins shift to the lower right hand quadrant. This shows the effect of 6-TG treatment on membrane-associated protein. The fact that 6-TG (H)/ No treatment (L), shows an increase in protein ratios and the reverse label results in a decrease, indicates that 6-TG alters the association of proteins with DNA in two independent experiments. Even though this effect is reproducible, a

majority of the proteins (84 and 93% for Mixes 3 and 9, respectively) still lie within the -1 and 1 range. Therefore, we can conclude that 6-TG on its own induces a low level of DPC formation.

A similar analysis addressing the effects of 6-TG+UVA treatment is shown in Figure 5.9 (C). In this case, an increase in protein H/L ratios for 6-TG+UVA (H)/No treatment (L), and decrease in ratios for the reverse label results in the majority of proteins occupying the lower right hand quadrant of the scatter plot. Most of the ratios lie outside the -1 to 1 range of log2 values. In this way, data from two independent experiments combine to demonstrate significant DPC formation by 6-TG+UVA.

Synergy between 6-TG and UVA in DPC formation (Figure 5.9 (D)) was demonstrated by combining data from Mixes 12 and 15 to specifically address the effect of UVA on cells treated with 6-TG. The effect of UVA here clearly differs from its effect in non-6-TG treated cells, underlining the photosensitising effect of 6-TG and the synergy between 6-TG+UVA in DPC formation.

In conclusion, I have developed a proteomics-based analysis that uses SILAC to reveal extensive DPC formation by combined 6-TG+UVA treatment of CCRF-CEM cells. It confirms that 6-TG and UVA act synergistically in DPC induction. 6-TG treatment induces only a low level of DNA-protein crosslinking and DPCs are not detected following exposure to the relatively low dose of UVA used.

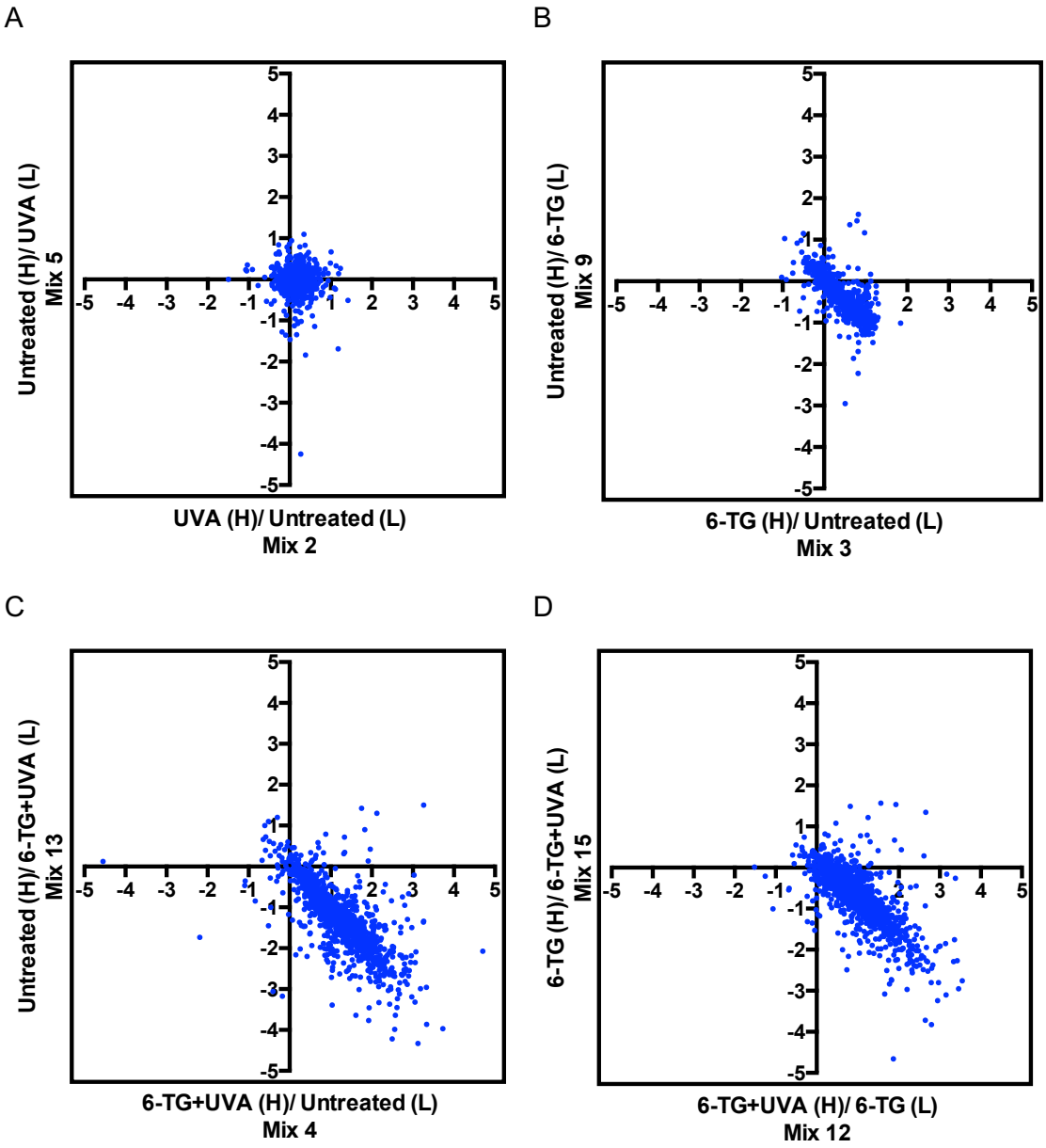

Figure 5.9: Comparison of protein SILAC H/L ratios
CCRF-CEM cells were labelled with heavy (H) or light (L) arginine and lysine isotopes and treated with 0.9μM 6-TG for 24 hours and irradiated with 50 kJ/m^2 UVA as indicated. Chromatin extracts were applied on HyBond-N$^+$ membranes, subject to *in situ* trypsin digestion and analysed by MS. Scatterplots of log2 SILAC H/L ratios of the detected proteins in each Mix is shown. **(A)** Mix 2 vs Mix 5, **(B)** Mix 3 vs Mix 9, **(C)** Mix 4 vs Mix 13, **(D)** Mix 12 vs Mix 15.

5.2.5 MS analysis of RIPA extracts and changes in protein abundance

Treatment with 6-TG affects cells in numerous ways. In particular, it significantly impairs transcription and possibly translation. Since the cells are treated for 24 hours in my experiments, I examined whether 6-TG-mediated impairment of transcription and translation might have led to significant decline in protein abundance and skewing of crosslinking analysis in 6-TG treated cells. Proteomic analysis of DNA-free whole cell (RIPA) extracts was carried out to address this possibility.

In Figure 5.10 (A), I compared the chromatin extract Mix 3, which is a mixture of heavy-labelled cells treated with 6-TG and light-labelled cells left untreated, with the RIPA extract Mix 3 treated in exactly the same way. I have shown that 6-TG results in a change in SILAC H/L ratios and in Mix 3 results in an increase in the ratio due to some DPC formation. Therefore, the protein density should be moving up along the y-axis away from the origin to indicate DPC formation. This is indeed what we see in this plot. If 6-TG treatment had an impact on overall protein levels in the cell this would show up in the RIPA extract results and cause a shift along the x-axis. In this case, there does seem to be a very minor shift left, towards lower ratios. This shift almost entirely lies within the -1 to 0 range and is therefore not considered significant. Figure 5.10 (B), is the reverse label version of Figure 5.10 (A), and as expected the effect of 6-TG is mirrored in this plot.

Figure 5.10 (C and D), show the effect of UVA, which results in protein ratios clustered around the origin of the graph. This indicates that UVA does not cause DPC formation, nor any change in protein abundance.

In Figure 5.10 (E), I investigated the impact of 6-TG+UVA on DPC formation and overall protein abundance. There was again an increase in H/L ratios for the chromatin extract to indicate DPC formation, as I have demonstrated previously. However, there was also a significant shift left to indicate a decrease in protein recovery with treatment. Figure 5.10 (F), is the reverse label version of Figure 5.10 (E), and as expected the effect of 6-TG+UVA is mirrored in this plot.

A 24-hour incubation of cells with 6-TG can inhibit transcription and/or translation and can therefore cause changes in protein abundance. If this were the case then we should see a similar dramatic shift in the 6-TG only treatment, which we do not.

The analysis did, however, reveal a significant decline in protein recovery when 6-TG and UVA were combined. Since cell extracts were prepared immediately after irradiation, these losses cannot reflect changes in transcription/translation. The formation of DPCs is probably a significant contributor to reduced protein recovery in this case. In addition, 6-TG+UVA causes widespread protein oxidation that negatively impacts protein solubility. Losses through precipitation most likely also contribute to diminished protein yields.

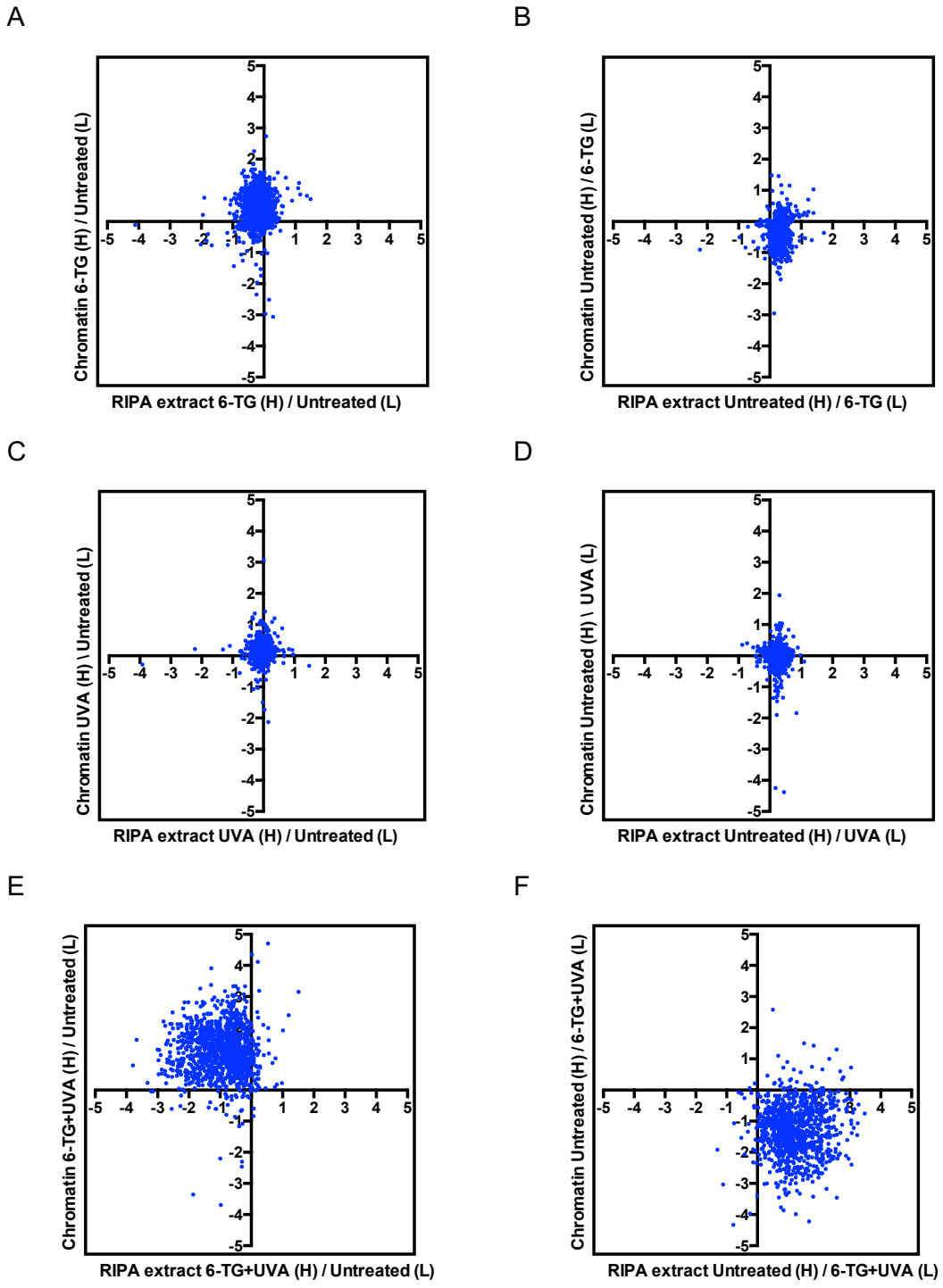

Figure 5.10: Comparison of SILAC H/L ratios of chromatin and RIPA extracts
CCRF-CEM cells were labelled with heavy (H) or light (L) arginine and lysine isotopes and treated with 0.9μM 6-TG for 24 hours and irradiated with 50 kJ/m^2 UVA as indicated. Chromatin extracts were applied on HyBond-N$^+$ membranes, subject to *in situ* trypsin digestion and analysed by MS. DNA-free whole-cell (RIPA) extracts were separated by SDS-PAGE, trypsin digested in gel and analysed by MS. Scatterplots of log2 SILAC H/L ratios of the detected proteins in chromatin and RIPA extracts of identically treated cells are shown.

5.2.6 Proteins involved in DPCs

MS analysis identifies which proteins are crosslinked to DNA. To analyse the proteins that are most vulnerable to crosslinking, I compiled the H/L ratio values of the upper 95th percentile (5th percentile if the light-labelled cells are treated) to define the most extreme shifts in H/L ratio caused by each treatment. These values were obtained by K. Barnouin using density distributions and the ggplot2 data visualization package for the statistical programming language, R. The control samples were set to 0. The values are summarised in the table in Figure 5.11 (A).

Using these figures, I generated an ideal protein profile plot (Figure 5.11 (A)), that represents the expected behaviour of the proteins most vulnerable to crosslinking by each treatment. Using Perseus, the software with which the data were analysed, I then determined the proteins with the closest match to the ideal profile. In Figure 5.11 (B), the top 200 closest matches are superimposed in red on the profiles of all 2611 proteins displayed in grey.

I used Uniprot and Gene Cards to determine protein functions and classify them as nuclear/non-nuclear (Figure 5.11 (C)). Among the 200 best fits, 192 are predominantly nuclear proteins or can be detected in the nucleus. The three largest functional categories are gene expression (31%) and DNA replication/repair (16%), followed by cell cycle (11%).

Interestingly, DNA- or RNA- binding proteins were equally represented and together accounted for around half of the 200 best fit proteins (Figure 5.11 (D)). Since 6-TG can also be incorporated into RNA and photoreactive purine analogues can crosslink proteins to RNA when exposed to UVA, it is possible that RNA-protein crosslinks contribute to overall nucleic acid-protein crosslinking (Costas et al., 2000). To examine this possibility, I measured the RNA content of the chromatin extracts applied to the HyBond N+ membrane. Since RNA comprises <2% of the total nucleic acids in these extracts, I conclude that RNA-protein crosslinks are unlikely to contribute significantly to overall crosslinking. The presence of RNA processing proteins most likely represents their presence in DPCs.

A

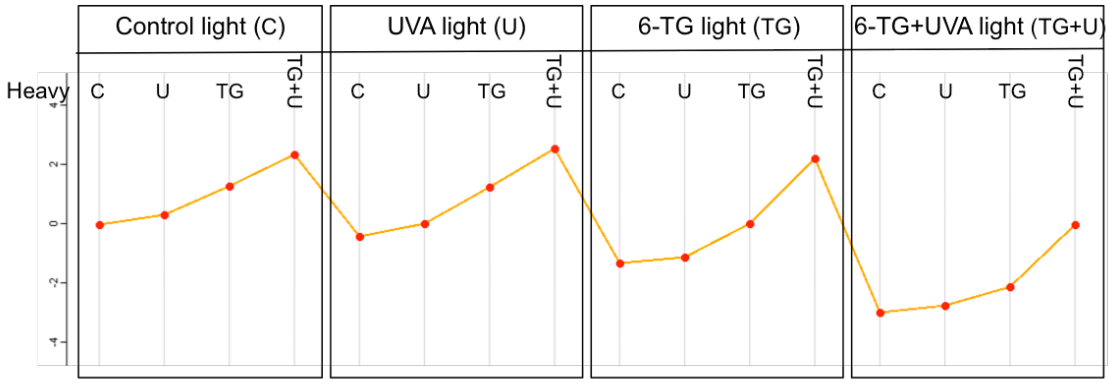

Mix	1	2	3	4	5	6	7	8	9	10	11	12	13	14	15	16
95th or 5th percentile ratio	0.00	0.52	1.18	2.44	-0.38	0.00	1.20	2.45	-1.04	-0.67	0.00	2.14	-2.62	-2.33	-1.89	0.00

B

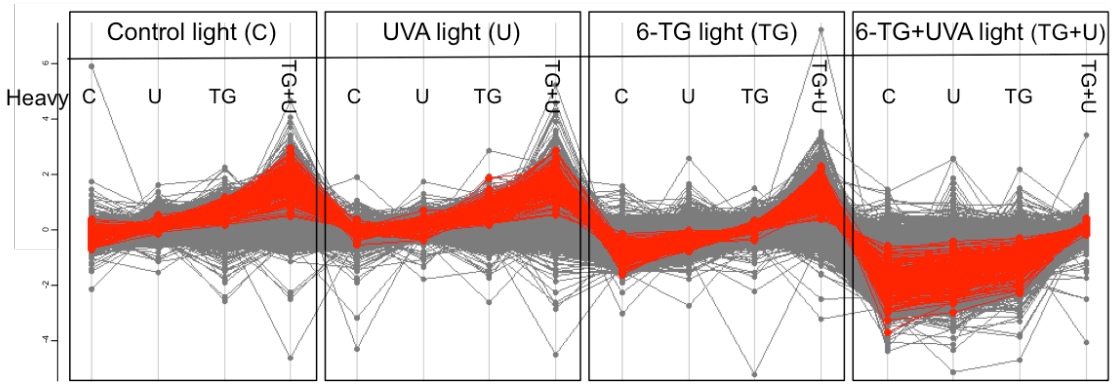

C

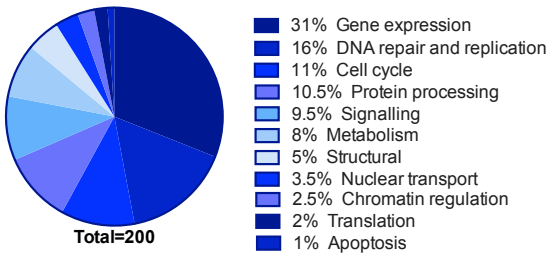

D

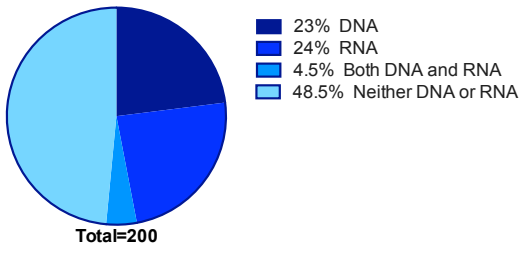

Figure 5.11: Analysis of proteins most vulnerable to DPC formation
(A) 95th or 5th percentile heavy/light (H/L) ratios for each treatment are presented in the table and plotted in Perseus to form a hypothetical crosslinking profile. **(B)** The crosslinking profile of 200 proteins (red) that most closely match the hypothetical profile are superimposed on the profile of all identified proteins (grey). **(C)** Functional categories of the 200 proteins as specified by UniProt. **(D)** RNA and DNA binding by the 200 proteins.

5.2.7 DNA crosslinking of DNA repair proteins

The close proximity of DNA repair proteins to DNA may increase their vulnerability to crosslinking. My analysis identified 52 members of a list of 179 DNA repair proteins (http://sciencepark.mdanderson.org/labs/wood/dna_repair_genes.html). Figure 5.12 (A) shows the profiles of these 52 DNA repair proteins. Most, but not all of them follow a similar pattern to the hypothetical crosslinking profile in Figure 5.11 (A). I selected the proteins that closely matched this profile and found that 30 of the 52 were a good fit (Figure 5.12 (B)). Some others followed a similar pattern but deviated from the ideal profile in one or two of the treatment conditions. In addition, other DNA repair proteins were identified that did not change in a treatment-dependent manner.

Consistent with their involvement in DPCs, analysis of RIPA extracts confirmed that the majority of the 30 DNA repair proteins were less abundant in cells treated with 6-TG+UVA (Figure 5.12 (C)).

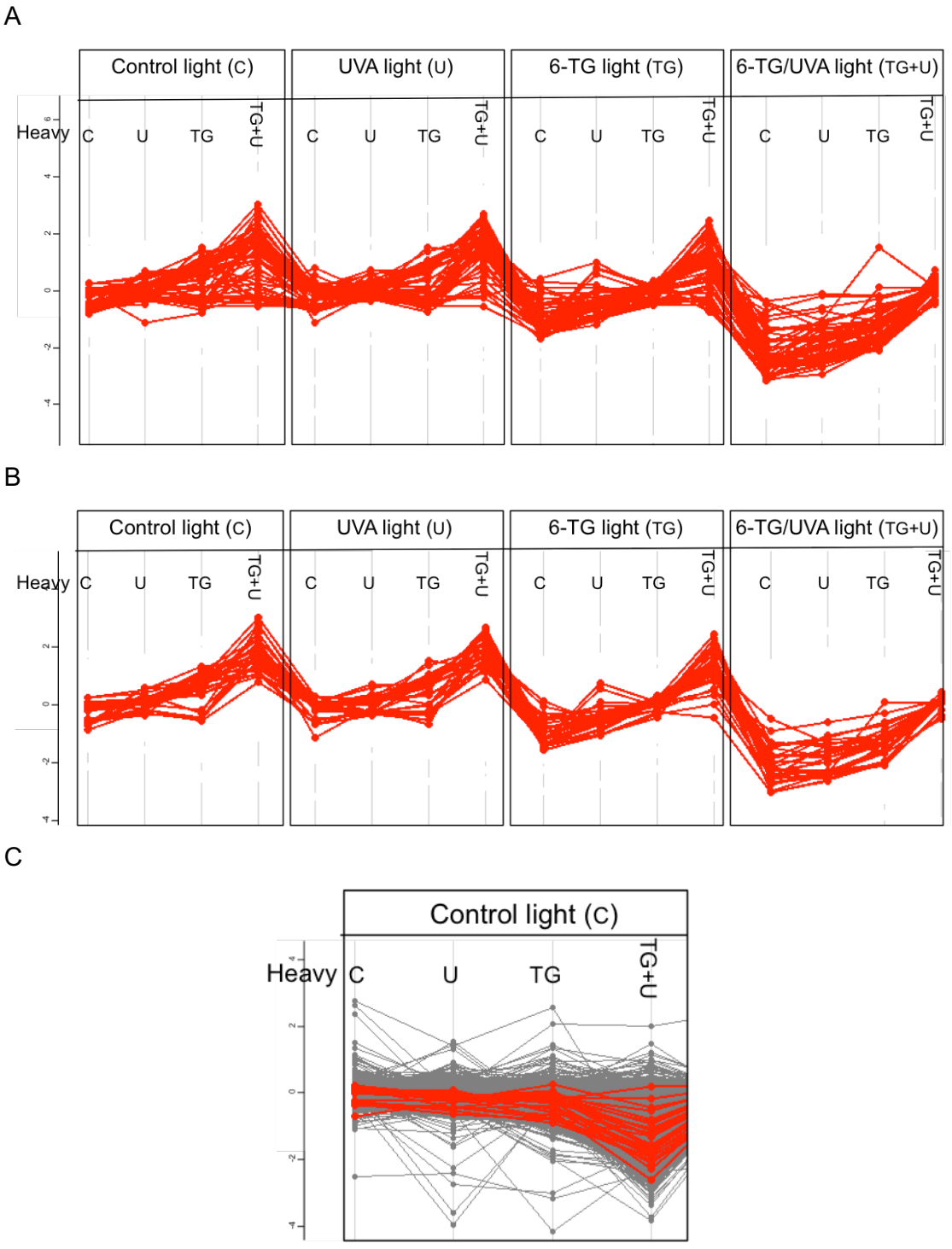

Figure 5.12: Crosslinking of DNA repair proteins
(A) Log2 SILAC Heavy/Light (H/L) ratio profiles of 52 designated DNA repair proteins detected in the analysis. **(B)** Log2 SILAC H/L ratio profiles of 30 proteins among the 52 repair proteins that were detected, which closely match the hypothetical crosslinking profile. **(C)** Log2 SILAC H/L ratio profiles for the 30 DNA repair proteins (in red) most vulnerable to crosslinking to DNA, superimposed on all identified proteins (grey) from DNA-free whole cell (RIPA) extracts.

5.2.8 Analysis of individual DNA repair and replication proteins

I investigated the crosslinking characteristics of individual DNA repair and replication proteins.

DNA polymerase δ (POLD) is a tetramer, required for DNA repair and replication. Three of the subunits, POLD1 (125kDa catalytic), POLD2 (66kDa) and POLD3 (50kDa), were identified among the 2611 proteins but the smaller 12kDa subunit was not. The SILAC H/L ratio profiles of these three proteins is presented in Figure 5.13 (A-C). POLD1 is almost an exact match to the generic crosslinking profile defined in Figure 5.11 (A), confirming its vulnerability to crosslinking. As defined by the profile, POLD1 exhibits an altered H/L ratio following 6-TG treatment and a significant additional shift after 6-TG+UVA. POLD3 on the other hand appears to be predominantly vulnerable to photochemical crosslinking through 6-TG+UVA treatment. POLD2 is not a good fit to the expected crosslinking profile and may be less susceptible to crosslinking.

The hexameric MCM complex (MCM2-7) is an essential component of DNA replication initiation. SILAC H/L ratio profiles of all six of the subunits match the expected crosslink profile and are almost perfectly superimposable (Figure 5.13 (D)). This suggests that the MCM complex is vulnerable to DPC formation by both 6-TG and 6-TG+UVA.

Topoisomerases (TOPs) relieve supercoiling by introducing breaks in the DNA during replication and transcription. TOP1, TOP2A and 2B were among the proteins identified by the analysis. SILAC H/L profiles of these three proteins appear almost identical. They resemble the profile of POLD3 and it appears that TOPs are predominantly susceptible to photochemical crosslinking by 6-TG+UVA (Figure 5.13 (E)).

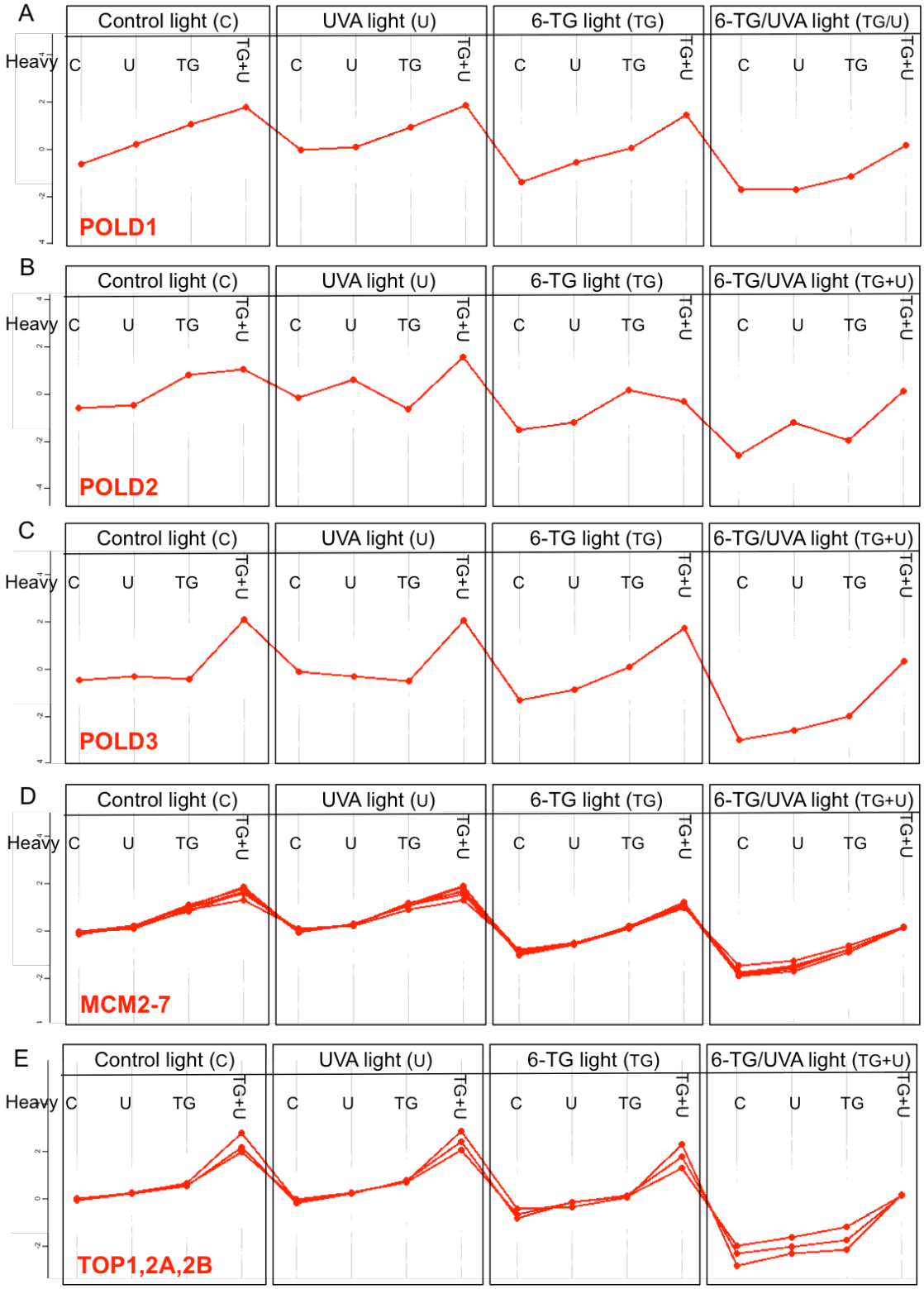

Figure 5.13: DNA crosslinking of individual DNA repair/replication proteins
Log2 SILAC heavy/light (H/L) ratio profiles of **(A)** POLD1, **(B)** POLD2, **(C)** POLD3, **(D)** MCM2-7 and **(E)** TOP1, 2A and 2B, in chromatin DPC extracts.

Analysis of RIPA extracts confirmed that the three POLD proteins (A), all six MCM proteins (B) and the three TOP proteins (C), were present at reduced levels following 6-TG+UVA treatment (Figure 5.14). This is consistent with selective loss of these proteins due to DPC formation.

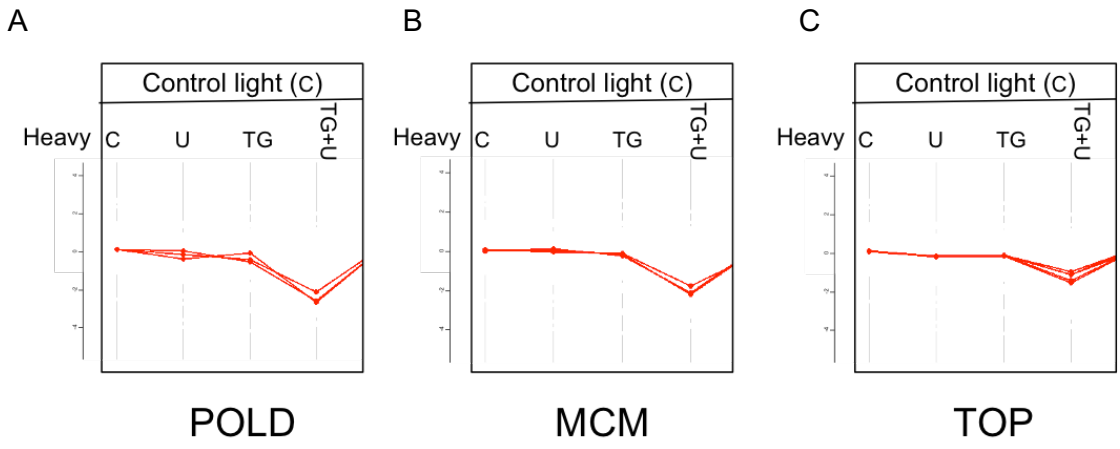

Figure 5.14: Loss of DNA replication/repair proteins in RIPA extracts
Log2 SILAC heavy/light (H/L) ratio profiles of **(A)** POLD1, POLD2, POLD3, **(B)** MCM2-7 and **(C)** TOP1, 2A and 2B, in RIPA extracts.

5.2.9 DPC formation by ciprofloxacin+UVA

I also used the SILAC/HyBond-N^+ analysis to investigate DPC formation by ciprofloxacin+UVA (Cip+UVA). Unlike 6-TG, ciprofloxacin is not covalently incorporated into DNA and Cip+UVA-induced DPC formation must therefore involve canonical DNA constituents. Thus, Cip+UVA represents a proof of principle for the general detection of DPCs by this method.

Heavy and light-labelled CCRF-CEM cells were treated with 500μM ciprofloxacin and 50 kJ/m^2 UVA. The combination of treatments and the Mixes I prepared are presented in Figure 5.15 (A). Subsequent steps in the analysis were identical to those described for 6-TG+UVA.

Figure 5.15 (B) shows the changes in H/L ratios induced by Cip+UVA. The clustering of a majority of the proteins in the lower right hand quadrant of the scatter plot is similar to the distribution shift induced by 6-TG+UVA (Figure 5.9 (C)) and indicates extensive DPC formation. A total of 2269 crosslinked proteins were detected. The number of total DNA and RNA binding proteins in both the ciprofloxacin and 6-TG experiments were very similar, indicating that they have similar vulnerabilities to crosslinking under both treatment conditions (Figure 5.15 (C)).

I identified 41 DNA repair proteins in the ciprofloxacin experiment compared to 52 with 6-TG (http://sciencepark.mdanderson.org/labs/wood/dna_repair_genes.html). Among these, 29 of them fit the expected profile for DPC induction (no change for control Mixes 1 and 4, significant shift for Mixes 2 and 3). The SILAC H/L profile of these 29 proteins are presented in green in Figure 5.15 (D), superimposed on all of the proteins identified in the experiment in grey.

I compared the types of DNA repair proteins that were crosslinked by 6-TG+UVA and with Cip+UVA. The Venn diagram in Figure 5.15 (E) reveals the significant overlap in the DNA repair proteins identified in the two experiments ($p= 1.125879e^{-11}$, calculated in R). The DNA repair proteins identified by both approaches are listed in Table 5.3.

A

		Heavy	
		Untreated	Cip+UVA
Light	Untreated	Mix 1	Mix 2
	Cip+UVA	Mix 3	Mix 4

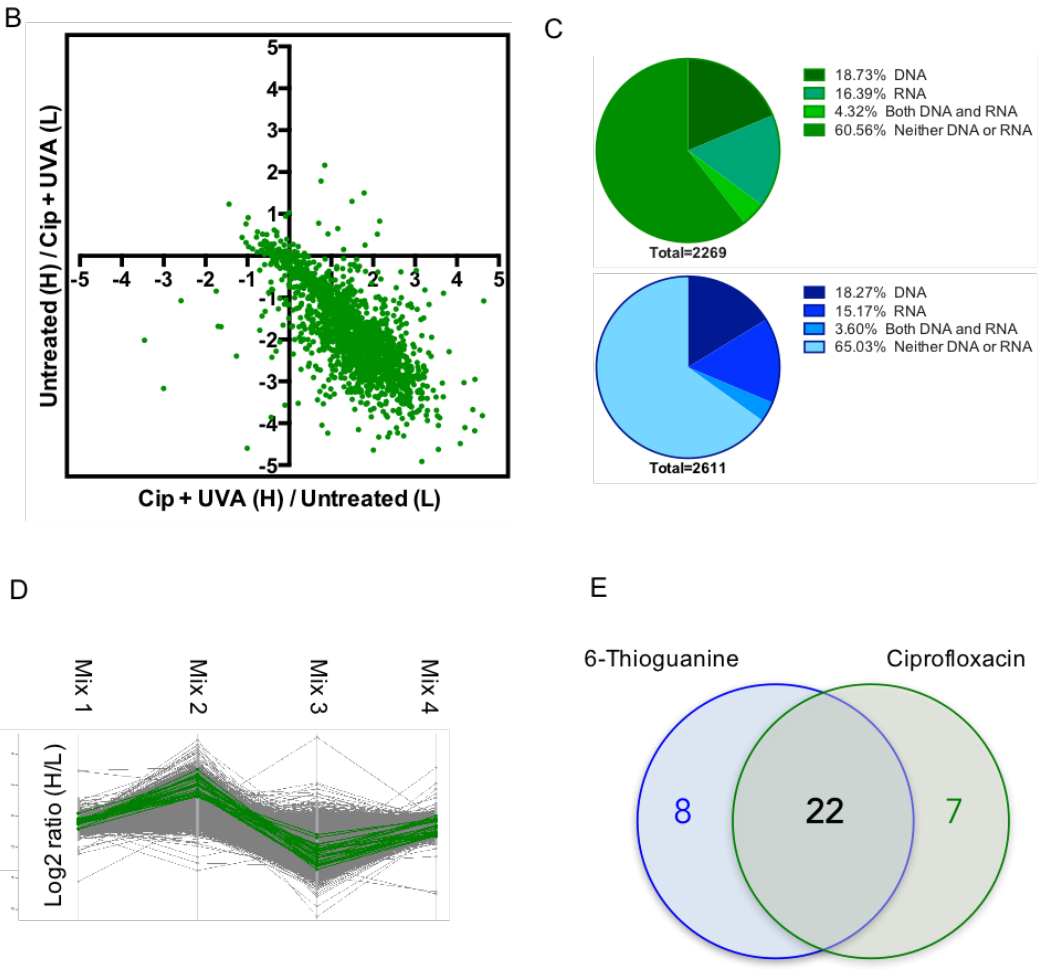

Figure 5.15: Ciprofloxacin+UVA mediated DPC formation
(A) Heavy (H) and light-labelled (L) CCRF-CEM cells were treated with 500μM ciprofloxacin (Cip) for 1 hour and UVA (50 kJ/m^2) as indicated. Cells were counted and mixed at 1:1 ratio as indicated in the table. High salt-washed chromatin extracts were applied to a HyBond-N$^+$ membrane. The membrane was washed with 8M Urea and water before membrane-associated proteins were digested *in situ* with trypsin and analysed by MS. **(B)** Scatterplot comparing log2 SILAC H/L ratios of proteins in Mix 2 and Mix 3. **(C)** DNA and RNA binding proteins identified in Cip+UVA (green) and 6-TG+UVA (blue) experiments. **(D)** Log2 SILAC H/L ratio profile plots of all identified proteins (grey) and 29 DNA repair proteins that are most vulnerable to crosslinking (green). **(E)** Overlap of the 29 DNA repair proteins most vulnerable to crosslinking by Cip+UVA and the 30 proteins by 6-TG+UVA.

Table 5.3: DNA repair proteins identified in DPCs
DNA repair proteins identified to be most vulnerable to crosslinking by 6-Thioguanine+UVA and Ciprofloxacin+UVA. (+) indicates crosslinking by the specified treatment.

Protein	6-Thioguanine+UVA	Ciprofloxacin+UVA
APEX1 (APE1)	+	+
BLM	+	+
DDB1	+	+
DUT	+	+
FEN1 (DNase IV)	+	+
LIG1	+	+
LIG3	+	+
MRE11A	+	+
MSH2	+	+
MSH6	+	+
PARP1 (ADPRT)	+	+
PCNA	+	+
POLD1	+	+
POLD3	+	+
POLE3	+	+
PRPF19 (PSO4)	+	+
RAD50	+	+
RECQL (RECQ1)	+	+
RPA1	+	+
XRCC1	+	+
XRCC5 (Ku80)	+	+
XRCC6 (Ku70)	+	+
MGMT	+	-
MMS19	+	-
MPG	+	-
NBN (NBS1)	+	-
NUDT MTH1	+	-
POLE1	+	-
PRKDC	+	-
UBE2N (UBC13)	+	-
CHAF1A (CAF1)	-	+
FANCD2	-	+
FANCI	-	+
MSH3	-	+
TP53	-	+
TP53BP1 (53BP1)	-	+
WRN	-	+

5.2.10 Hierarchical clustering and identifying false positives

Hierarchical clustering was used to identify proteins with similar behaviours. I found that it was a useful way to summarise all the data as a conclusion to this chapter. This method of analysis also identifies false positives.

The hierarchical clusters for both 6-TG+UVA (A) and Cip+UVA (B) experiments are presented in Figure 5.16. By inspection, the majority of the proteins follow the crosslinking profile that I described earlier in the chapter. I placed this profile below the 6-TG+UVA cluster for reference. For treatments where we anticipate an increase in SILAC H/L ratios, for example where heavy-labelled cells are treated with 6-TG+UVA, those columns in the clusters are mostly red (increase). For treatments were we anticipate a decrease in SILAC H/L ratios, for example where light-labelled cells are treated with 6-TG+UVA, those columns in the clusters are mostly green (decrease).

Some groups of proteins exhibit hardly any change in response to treatment. These generate black sections in the heat map (example arrowed in Figure 5.16). I concluded that these are false positive proteins and analysed the members of this family in 6-TG+UVA treated cells.

The crosslinking profiles of the 114 potential false positive proteins are shown in Figure 5.17 (A). They are largely unaffected by treatment and this confirms their false positive status. Gene expression is the largest functional group of these false positives. There are also numerous factors involved in ribosome biogenesis and chromatin regulation (eg. histones) in this group (Figure 5.17 (B)). There is no significant difference in the number of DNA and RNA binding proteins identified as false positives (Figure 5.17 (C)), compared to the proteins vulnerable to DPC formation (Figure 5.11 (D)).

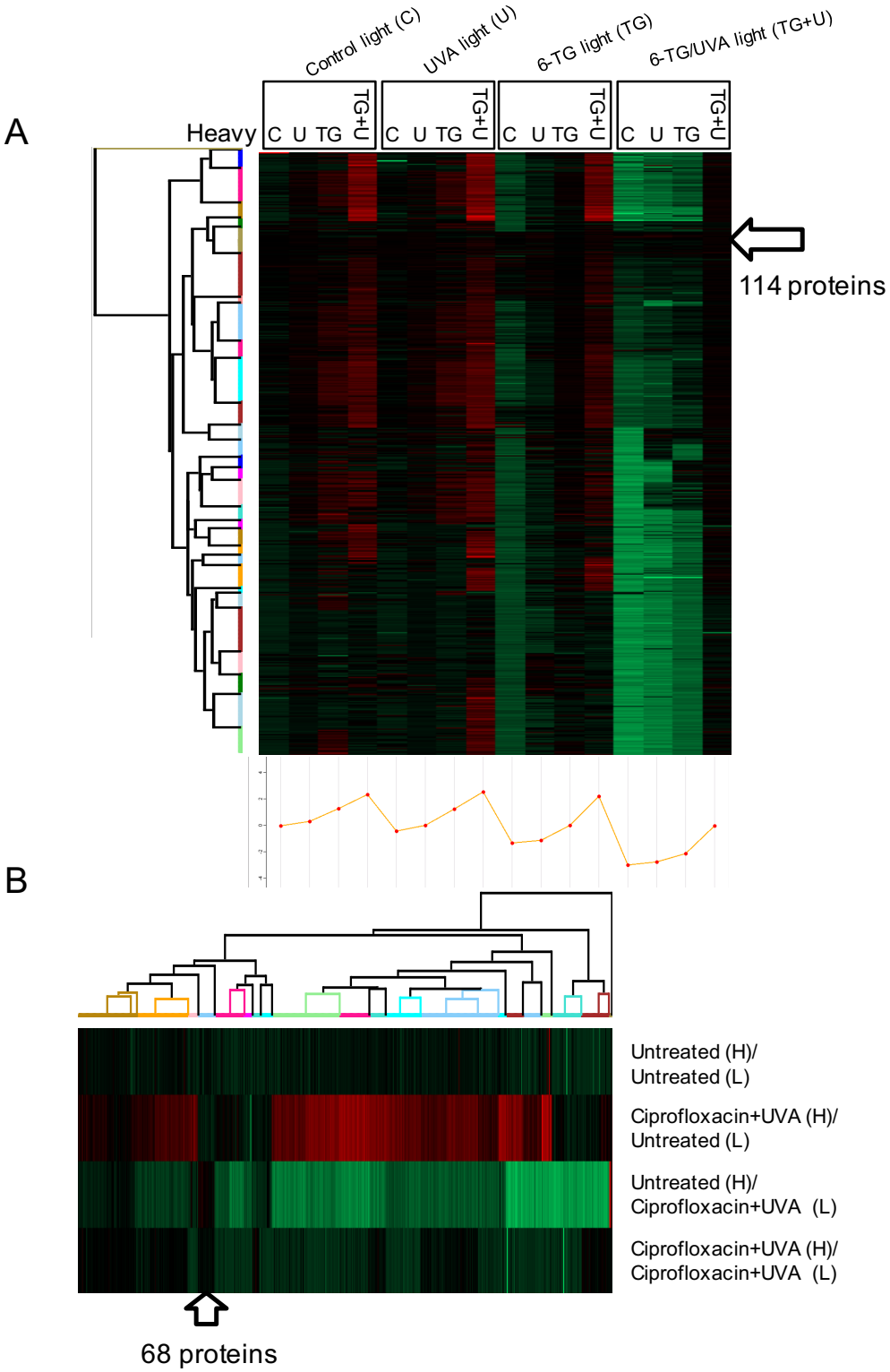

Figure 5.16: Heat map of DPC formation
Hierarchical clustering analysis of SILAC heavy/light (H/L) ratios of **(A)** 6-TG and **(B)** ciprofloxacin experiments. The general crosslinking profile is under the 6-TG heat map. Red indicates an increase and green indicates a decrease in SILAC H/L ratios. Arrow indicates family of potential false positive proteins. All clustering was Euclidean.

False positives may appear in the analysis because they are particularly high abundance proteins and have particularly strong affinity for DNA or for the HyBond-N^+ membrane. These reasons are not mutually exclusive. Among the 114 proteins, I identified the highly abundant intermediate filament protein, Vimentin. Histones were also present. These proteins are not only highly abundant, but also interact strongly with DNA.

The Cip+UVA hierarchical clustering also revealed a family of 68 proteins that were unaffected by treatment (Figure 5.16 (B)). This family contained a large group of histone proteins. The histones identified are listed in Table 5.4. There is a significant overlap between the false positives from the 6-TG+UVA and Cip+UVA analyses.

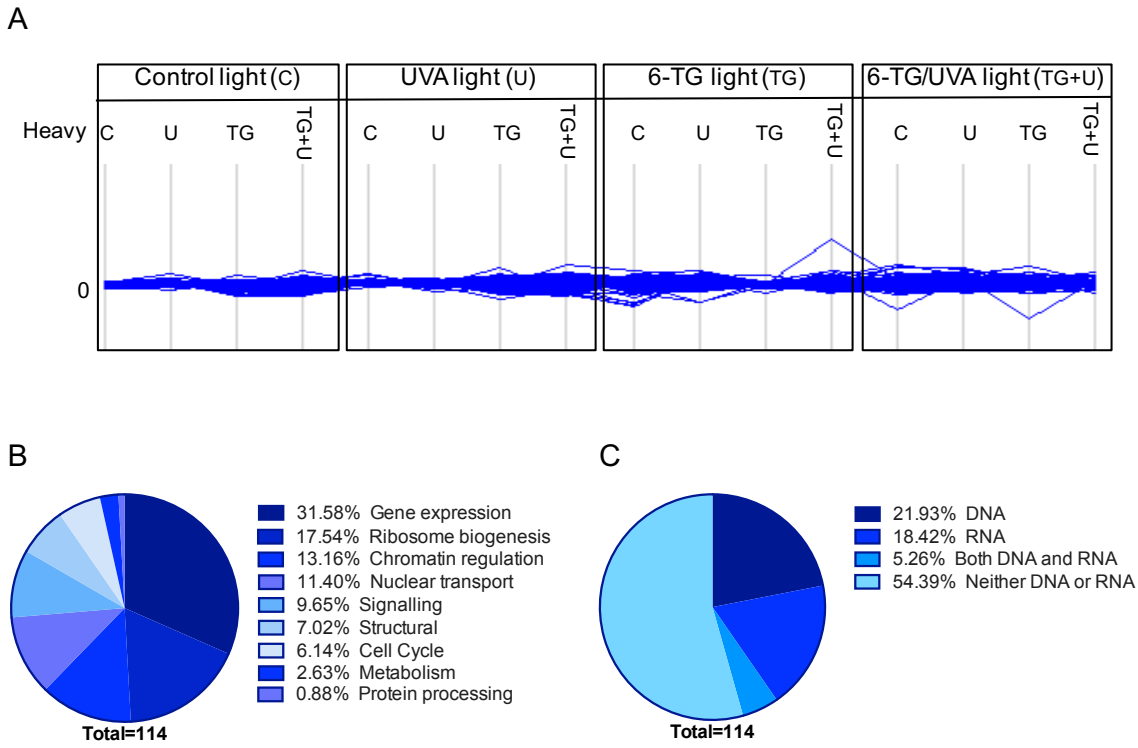

Figure 5.17: Analysis of false positives
(A) Log2 SILAC heavy/light (H/L) ratio crosslinking profiles of 114 potential false positive proteins. **(B)** Functional characterization of the 114 proteins using UniProt. **(C)** DNA and RNA binding ability of the proteins.

Table 5.4: Histones identified in the false positive group
The gene names and protein names of histones identified in the false positives group of both the 6-thioguanine and ciprofloxacin experiments. The overlapping proteins between the two experiments are in bold.

Treatment	Protein names	Gene names
6-Thioguanine+UVA	**Histone H2A.x**	**H2AFX**
	Histone H2A.Z;Histone H2A.V;Histone H2A	**H2AFZ;H2AFV**
	Histone H2A type 1-B/E;Histone H2A;Histone H2A type 3	HIST1H2AB;HIST3H2A
	Histone H2A type 1-D;Histone H2A	HIST1H2AD
	Histone H2A;Histone H2A type 1;Histone H2A type 1-H;Histone H2A type 2-A;Histone H2A type 1-J;Histone H2A.J;Histone H2A type 2-C	HIST1H2AK;HIST1H2AG;HIST1H2AH;HIST2H2AA3;HIST1H2AJ;H2AFJ;HIST2H2AC
	Histone H2B type 1-D;Histone H2B	HIST1H2BD
	Histone H2B;Histone H2B type 1-C/E/F/G/I	HIST1H2BF;HIST1H2BC
	Histone H2B type 1-K	**HIST1H2BK**
	Histone H2B type 1-L	**HIST1H2BL**
	Histone H2B type 1-M	**HIST1H2BM**
	Histone H2B type 1-N	**HIST1H2BN**
	Histone H2B type 1-O	HIST1H2BO
	Histone H2A type 2-B	**HIST2H2AB**
	Histone H2B type 2-F;Histone H2B type 1-H;Histone H2B	**HIST2H2BF;HIST1H2BH**
Ciprofloxacin+UVA	**Histone H2A.x**	**H2AFX**
	Core histone macro-H2A.1;Histone H2A	H2AFY
	Histone H2A.Z;Histone H2A.V;Histone H2A	**H2AFZ;H2AFV**
	Histone deacetylase 3	HDAC3
	HIG1 domain family member 1A	HIGD1A
	Histone H2A type 1-C	HIST1H2AC
	Histone H2B type 1-B	HIST1H2BB
	Histone H2B type 1-D;Histone H2B	**HIST1H2BD**
	Histone H2B type 1-K	**HIST1H2BK**
	Histone H2B type 1-L	**HIST1H2BL**
	Histone H2B type 1-M	**HIST1H2BM**
	Histone H2B type 1-N	**HIST1H2BN**
	Histone H3.1;Histone H3;Histone H3.1t;Histone H3.3C	HIST1H3A;HIST3H3;H3F3C;H3F3A
	Histone H4	HIST1H4L;HIST1H4A;HIST1H4H
	Histone H2A type 2-A;Histone H2A type 2-C	HIST2H2AA3;HIST2H2AC
	Histone H2A type 2-B	**HIST2H2AB**
	Histone H2B type 2-F;Histone H2B type 1-H;Histone H2B	**HIST2H2BF;HIST1H2BH**
	Histone H3.2	HIST2H3A

In summary, I have devised a SILAC and proteomics method to investigate DPC formation in human cells treated with UVA photosensitisers. The method identified over 2000 proteins that were crosslinked by a DNA incorporated photosensitiser (6-TG) and a DNA embedded/intercalated photosensitiser (ciprofloxacin), underlining the versatility of the technique and the different ways by which DPCs can form. The proteins most susceptible to DNA crosslinking were those involved in gene expression and DNA repair and replication, including RPA.

Chapter 6. Discussion

6.1 Oxidative damage to proteins caused by 6-TG+UVA

The initial aim of this thesis was to investigate the oxidative damage caused by 6-thioguanine (6-TG) and UVA (ultraviolet radiation) on proteins involved in DNA repair, in particular to study the possible functional impairment of RPA. As the project developed, I also examined whether antioxidant allopurinol is able to lower ROS levels generated by 6-TG+UVA and alleviate protein damage.

At the outset, it had been shown that 6-TG+UVA generates intracellular ROS, particularly singlet oxygen ($^1O_2$) (O'Donovan et al., 2005). These findings were confirmed, and I was able to show in addition that allopurinol inhibited $^1O_2$ production by 6-TG+UVA or UVA treatment. Protection by allopurinol was, however, only partial and it was unable to restore untreated steady state ROS levels.

It had previously been shown that allopurinol alleviates DNA damage and improves cell survival following antioxidant depletion by 6-TG treatment (Brem and Karran, 2012). Protection was ascribed to the antioxidant effects of allopurinol rather than its ability to inhibit xanthine oxidase (XO), because an alternative XO inhibitor (febuxostat) was unable to protect 6-TG-treated cells (Brem and Karran, 2012). Only allopurinol was able to scavenge UVA mediated ROS.

The inability of allopurinol to reinstate steady state levels might reflect the different reactive oxygen species (ROS) generated by UVA and 6-TG+UVA. Both produce not only $^1O_2$ but also superoxide, hydrogen peroxide and, in the presence of a metal cation, hydroxyl radicals (See Section 1.2.2). The scavenging ability of allopurinol may differ among the different types of ROS. In the case of 6-TG+UVA, it is clear from the magnitude of the signal (the x-axis is a logarithmic scale) that substantially high levels of ROS are produced that may overwhelm the allopurinol present.

The short half-lives and diffusion distances of ROS make it likely that proteins in close proximity to DNA are more vulnerable to oxidation by UVA-activated DNA-

embedded 6-TG. I found that 6-TG+UVA treatment decreased the recovery in cell extracts of three proteins involved in nucleotide excision repair (NER): XPD (xeroderma pigmentosum group D), XPA and RPA (replication protein A, RPA70). In the case of XPA and RPA70, the protein recovery was restored to apparently normal levels by the inclusion of allopurinol.

The decrease in extractable protein is most likely due to protein oxidation. Structural changes including protein carbonylation, thiol oxidation or protein-protein crosslinking may expose hydrophobic regions that can result in aggregation, precipitation and loss during protein extraction. The improved recovery in the presence of allopurinol is consistent with an antioxidant effect.

Normal levels of XPD were not recovered by allopurinol inclusion. It is noteworthy that XPD contains an iron-sulphur cluster which may make it particularly vulnerable to oxidative damage and precipitation. Alternatively, XPD may be vulnerable to a particular type of ROS that allopurinol is unable to scavenge (Liu and Huang, 2015).

I also considered chromatinisation as a possible contributor to the lower recovery of RPA. 6-TG+UVA induces numerous different DNA lesions and causes replication arrest. Photoproducts induced by high doses of UVC also cause double strand breaks (DSBs) and stalled replication forks. These lesions recruit RPA to exposed single-stranded DNA (ssDNA) regions. My results show that RPA70 recovery decreases with time following 6-TG+UVA and UVC treatment and is improved by benzonase digestion. By digesting DNA, benzonase releases DNA-bound proteins. These results indicate that some RPA70 is most likely recruited to DNA following 6-TG+UVA (and UVC) treatment and is lost to extraction under relatively low-salt conditions. They do not, however, discount the possibility that RPA is also oxidatively damaged. Benzonase treatment also releases protein covalently bound to DNA. Therefore, these findings do not exclude possible depletion of RPA by DNA-protein crosslinking.

6-TG+UVA treatment resulted in a significant loss of ssDNA binding activity. This was not observed following UVC treatments that induced similar levels of

chromatinisation. These functional assays provide additional support for the conclusion that RPA suffers oxidative damage that impairs its function.

An interaction between XPA and RPA is imperative for NER (Jiang et al., 2012; Saijo et al., 2011; Tsodikov et al., 2007). 6-TG+UVA treatment abolished this interaction. At the lower concentration of 6-TG tested (0.5μM), the chromatinisation is very low, suggesting that the complete loss of detectable binding is unlikely to be solely due to RPA chromatinisation. The absence of detectable RPA and XPA interaction is consistent with damage to RPA, XPA or to both proteins and is also consistent with the lower recovery of XPA from 6-TG+UVA treated cells.

One important finding from my work is the formation of higher molecular weight RPA species of around 100 and 45-50kDa in cells treated with 6-TG+UVA. This modification does not occur in cells treated with 6-TG or with UVA alone. The modification is not due to severe DNA damage, stalled replication forks or fork collapse as it was not observed in cells treated with high doses of ionising radiation, hydroxyurea (HU) or UVC.

The size of the higher molecular weight complexes suggests that they may be products of covalent crosslinking between RPA70 and RPA32 (102kDa), and RPA14 and RPA32 (46kDa). The two prominent bands in the 45-50kDa region are consistent with RPA32 and RPA14 crosslinking in two different ways, perhaps through different residues, that result in slightly different migrations. Crosslinking is not *via* disulphide links as the complexes were resistant to denaturing conditions in the presence of DTT and β-mercaptoethanol. None of the complexes are detected with the RPA70 and RPA14 antibodies, which may reflect the loss of the epitopes recognised by these antibodies through crosslinking or may simply be a result of the quality of the antibodies. It is also possible that the crosslinked RPA complexes involve other close interacting partners such as PCNA (proliferating cell nuclear antigen) or XPA.

The protein-protein crosslinking appears to be mediated by ROS and was partially inhibited by allopurinol. However, the widely-used antioxidants N-acetyl cysteine (NAC) and ascorbic acid (AA) were not protective. Depending on the concentration and uptake by cells, antioxidants may also act as pro-oxidants. It is possible that

NAC and AA were not at the optimal concentration for antioxidant effects. Because these antioxidant experiments were equivocal, I sought confirmation of ROS involvement by using a different photosensitiser+UVA combination.

Ciprofloxacin is also a UVA photosensitiser that generates ROS. Ciprofloxacin+UVA (Cip+UVA) generated modified RPA32 species that were similar to those formed by 6-TG+UVA. This confirms that ROS are most likely responsible for these RPA32 modifications. In addition, this indicates that protein-protein crosslink formation does not require the photosensitiser to be incorporated into DNA. Ciprofloxacin is not incorporated but maintains a close interaction with DNA through DNA intercalation (Vilfan et al., 2003).

In summary, upon UVC and 6-TG+UVA treatment, RPA undergoes chromatinisation due to the formation of photoproducts and stalled replication forks. In addition to chromatinisation, RPA is also damaged, partially by inter-subunit crosslinking of RPA32. Impaired ssDNA and XPA binding by RPA can contribute towards loss of NER function in cells under oxidizing conditions. RPA is particularly susceptible to oxidation and this crosslinking is only one example of the oxidized RPA forms. In the next chapter, I investigated this crosslinking further and will discuss other types of RPA damage. In addition, I will be describing the impact of RPA overexpression in cells under oxidative stress.

6.2 Photosensitiser+UVA mediated damage to RPA

In this chapter, I describe my investigation into the nature and consequences of the damage caused to RPA by UVA photosensitising treatments. The photosensitisers were: 6-TG, ciprofloxacin, ofloxacin and FICZ (6-formylindolo[3,2-*b*]carbazole). This chapter addressed the impact of RPA overexpression on cell survival and DNA damage repair. An essential tool for this investigation was the RPA21 cell line in which RPA is modestly (two-fold) overexpressed.

RPA21 cells were more resistant than their parental U2OS cells to the toxic effect of the three photosensitisers. This indicates that a modest two-fold overexpression of RPA confers resistance to the toxicity caused by UVA photosensitising treatments. The cytotoxic effect of ofloxacin is more modest compared to ciprofloxacin or 6-TG in combination with UVA. All three photosensitiser+UVA combinations inhibited NER in U2OS cells. RPA overexpression in RPA21 cells prevented this inhibition.

Both Cip+UVA and 6-TG+UVA can produce replication arresting lesions. Cip+UVA can result in the formation of T<>T cyclobutane pyrimidine dimers (CPDs) (Lhiaubet-Vallet et al., 2009) and cause the chromatinisation of both RPA70 and DDB2 confirming the presence of NER substrates (DDB2 data in (Guven et al., 2015)). 6-TG+UVA causes the production of guanine sulfinate (G^{SO2}) and guanine sulfonate (G^{SO3}), single-strand and double-strand breaks, DNA-protein crosslinks (DPCs) and interstrand crosslinks (ICLs). It is therefore possible that depletion of RPA at stalled replication forks caused by 6-TG or ciprofloxacin and UVA can cause replication fork collapse and cell death. Exposure to UVC in addition to this damage, imposes conflicting demands on the RPA pool (Tsaalbi-Shtylik et al., 2014). In this case, not only is RPA demanded primarily at stalled replication forks but it is also taken up by regions of NER repair, resulting in depletion of RPA. Therefore, having more functional RPA in the cell can alleviate this competition between stalled replication forks and photolesions and allow NER to function.

I consider it unlikely that chromatinisation is the only explanation for the effects on RPA for the following reasons: Firstly, replication fork collapse occurs exclusively in S phase. The almost complete inhibition of NER activity in photosensitiser+UVA treated U2OS cells indicate that the NER inhibition cannot be confined to S phase. Secondly, the CPDs that are generated by 6-TG+UVA and Cip+UVA are removed much less efficiently than the UVC-induced 6,4 Py:Pys (6,4 pyrimidine-pyrimidone photoproducts) that were monitored in the NER ELISA. They would not provide sufficient competition to inhibit NER (Hwang et al., 1999). In addition, Ofloxacin+UVA (Oflx+UVA) is a very weak source of replication blocking photolesions (T<>T CPDs) and does not result in RPA chromatinisation (Lhiaubet-Vallet et al., 2009; Peacock et al., 2014). Yet, Oflx+UVA is cytotoxic and inhibits NER. Finally, nuclear extracts used in the NER assays have a higher level of salt and do not exhibit a decrease in

RPA recovery with treatment, yet NER inhibition still occurs in 6-TG+UVA, Cip+UVA and Oflx+UVA treated cells (Gueranger et al., 2014; Guven et al., 2015; Peacock et al., 2014). This strongly suggests that RPA chromatinisation cannot fully account for NER inhibition in photosensitiser+UVA treated cells.

UVA can result in the formation of CPDs, as well as causing ROS production and extensive protein oxidation. It has previously been shown that this oxidation damages NER proteins and inhibits NER (McAdam et al., 2016). In addition to photosensitisers, RPA overexpression also enables U2OS cells to partially overcome NER inhibition induced by high dose UVA. Oxidative damage to RPA is most likely responsible for this UVA-mediated inhibition of NER. Overexpression of RPA means that more undamaged RPA is available for NER.

Higher levels of RPA also appear to increase baseline NER efficiency when cells are exposed only to UVC. The two-fold increase in RPA expression resulted in a significant increase in the rate of NER. This indicates that RPA levels may be limiting in NER at least in U2OS cells and that this limitation is more pronounced when cells are exposed to oxidative stress conditions.

Data presented in Chapter 3 established that RPA undergoes oxidative damage to form a higher molecular weight complex. These photoproducts were also formed by Cip+UVA, as well as Oflx+UVA. This modification is not specific to tumour derived cell lines HeLa and U2OS, but is also formed in untransformed human fibroblasts.

The availability of the RPA overexpressing cell line allowed me to investigate the nature of the crosslinked RPA products. Immunoprecipitation (IP) confirmed that the higher molecular weight species in the treated cells is crosslinked RPA32 and RPA70. Considering that RPA70 and RPA32 contain the ssDNA binding sites, crosslinking involving these two subunits is predicted to have a detrimental effect on ssDNA binding.

According to the crystal structure of the RPA trimerisation core by Bochkareva *et al.*, the interaction between the three subunits occurs through DBD-C/DBD-D/RPA14(Bochkareva et al., 2002). There is a metal cation, zinc, coordinated by four

cysteines in the RPA DBD-C domain, which can lower the oxidation potential of RPA70 and result in oxidation and crosslinking. However, the structure places the Zn away from the trimerisation core, diminishing the possibility of its involvement in the crosslinking. The trimerisation is stabilised by amino acids, Tyr599, Tyr602, Leu606, Val607, Ile610 and Ala614 of RPA70; Met152, Phe155, Ile159, Leu160, Ile163 and Met167 of RPA32; and Leu98, Ala102, Ile105, Phe109 and Phe112 of RPA14. The crosslink between RPA70 and RPA32 can therefore be between a tyrosine and a methionine. The proposed mechanism for RPA binding suggests that when binding short length ssDNA (8-10nt) only DBD-A and B of RPA70 is engaged, while long length DNA binding (23-27nt) requires DBD-C and D for tight binding. This binding of DBD-C and D requires a conformational adjustment, which may be prohibited by the crosslinking and contribute towards the impaired NER in photosensitiser+UVA treated cells.

As mentioned previously, the crosslinked portion is a very small fraction of the overall RPA32. Interestingly, assays for NER function show that this crosslinked form is present in all NER-negative extracts and is not detected in NER-functional extracts (NER assay results in (Guven et al., 2015)). It is possible that this crosslinked form exerts a dominant negative effect, however, it is more plausible that the crosslinking is an indication of widespread RPA damage.

It is also important to address the clearance of heavily oxidised and crosslinked proteins from the cell. The proposed mechanism of clearance for proteins that experience low levels of oxidation is through the proteasome and for those that are heavily oxidised, it is through lysosomal pathways (Kaganovich et al., 2008; Rodgers et al., 2002). Crosslinking of proteins may make it difficult for them to fit through the channel of the proteasome and therefore deviate to the lysosomal pathway. In order to investigate whether crosslinked RPA and PCNA were processed by the proteasome, I used two proteasome inhibitors in combination, MG-132 and lactacystin. MG-132 is a peptide aldehyde that selectively and reversibly inhibits the activity of the 26S proteasome. Lactacystin works by irreversibly modifying specific catalytic subunits of the proteasome. Proteasome inhibition prevented the removal of PCNA crosslinks, indicating that they are removed through the proteasome. RPA

removal appeared to be partially prevented by proteasome inhibition, but a substantial proportion of crosslinked RPA was still removed after 24 hours.

PCNA crosslinking can be detected at relatively low UVA doses. My prediction is that photosensitising treatments would further exacerbate this damage, resulting in a heavily oxidised protein. If this is the case, it is surprising that the crosslinked form of PCNA is mainly removed by the proteasome, considering the difficulty of unfolding heavily oxidised proteins. It is possible that other than crosslinking PCNA is not as heavily oxidised as RPA, which suffers further damage as described below.

RPA is sensitive to oxidation and was identified in a screen for protein carbonyls (Peacock et al., 2014). The redox sensitivity of RPA also leaves it vulnerable to thiol oxidation (Men et al., 2007; Park et al., 1999). RPA contains 15 cysteines and four of them coordinate the zinc finger in DBD-C. This zinc finger is essential for RPA's role in replication but not repair (Lin et al., 1998). These cysteines involved in zinc coordination are susceptible to disulphide bond formation, while the remaining 11 cysteines were shown to be unaffected (Men et al., 2007). In my experiments, untreated RPA21 cells exhibited low but detectable levels of Cys-SOH, which is formed through cysteine oxidation. This type of modification can work as a redox switch to provide allosteric changes within the protein to alter its function, and can be reduced to a thiolate anion ($Cys\text{-}S^-$) by thioredoxin and glutaredoxin to restore the protein to its original state (Groitl and Jakob, 2014; Hall et al., 2009; Winterbourn and Hampton, 2008). However, these can also be further and irreversibly oxidised to sulfinic and sulfonic acids and can react with other amino groups to generate sulfenamide crosslinks. Following Cip+UVA or Oflx+UVA treatments the level of oxidised cysteines were considerably higher, indicating significant oxidation of RPA32.

In addition to RPA32 oxidation there was also detectable levels of cysteine sulfenate at around 100kDa, which may correspond to crosslinked RPA32:RPA70. This crosslinked product is a small fraction of the overall RPA32. Therefore, the fact that this product was detected in this assay indicates heavy cysteine oxidation of the crosslinked complex. This heavy oxidation of cysteines highlights the possibility for the oxidation of methionines at the interface of RPA32 and 70, which may contribute

to crosslinking, RPA inactivation and NER inhibition. Cysteines that are oxidised beyond sulfenate are not actually detected by the BP-1 probe. Therefore, it is likely that the cysteine oxidation of proteins following photosensitiser+UVA treatment are underestimated. Irreversible thiol oxidations are difficult to study with selective tagging due to their chemical inertness. Both sulfinate and sulfonate can be detected by mass spectrometry (MS). However, their analysis is complex due to inefficient ionisation as a result of their high negative charge and difficulty in distinguishing their fragmentation patterns from other post-translational modifications (Murray and Van Eyk, 2012).

After studying the oxidising effect of photosensitising drugs, I also investigated whether an endogenous photosensitiser (FICZ) was able to cause PCNA and RPA crosslinking. FICZ is a UVB photoproduct of tryptophan and absorbs in the UVA region of the spectrum. These characteristics make it physiologically very important, as tryptophan in human skin cells would be exposed to UVB and UVA at the same time from sunlight. FICZ results in the production of intracellular ROS upon UVA irradiation and can cause DNA damage (Park et al., 2015). PCNA was oxidised and formed inter-subunit crosslinking in a FICZ+UVA concentration dependent manner. RPA was not as significantly oxidised and a crosslinked product was only detected in the RPA21 cells due to the higher levels of RPA. This indicates that at nanomolar concentrations of this endogenous photoproduct, an essential protein involved in DNA repair and replication is oxidised and damaged, impeding its function. This can contribute to the detrimental effects of physiological exposure to sunlight.

The previous results show that higher expression of RPA seems to have a protective response against toxicity and DNA damage under oxidising conditions. It then raises the question as to why cells do not generally express higher levels of RPA. It is possible that RPA needs to be maintained at a particular concentration to be the regulatory factor in DNA replication and repair, as discussed previously (see Section 3.1.1). However, there may be an additional reason. RPA is particularly susceptible to oxidative damage even under steady state conditions. It is possible that having higher levels of RPA can result in accumulation of oxidised RPA and put pressure on the cell's antioxidant defences, such as glutathione. This can lower the amount of

reduced glutathione in the cell and result in higher overall ROS levels. The sensitivity of RPA to oxidation may be the reason why cells do not express higher levels of RPA.

Interestingly, I noted that the steady state ROS levels of RPA21 cells were substantially higher than those of U2OS. This stable increase in ROS is unlikely to be the result of the construction of RPA21 cells, as transient increases of ROS should not persist long after transfection. I considered the possibility that higher levels of RPA is permissive for higher ROS levels. RPA16 has an intermediate amount of RPA between RPA21 and U2OS (about 1.5-fold higher that U2OS). Its steady state ROS levels were intermediate between U2OS and RPA21, and closer to the latter. Although this is a very limited comparison, it would be interesting to explore in more detail the relationships between RPA expression and endogenous ROS.

This oxidative stress is a reflection of the insufficiency of the cell's antioxidant defences. GSH levels provide an indication of the depletion of antioxidant resources as GSH provides reducing equivalents to antioxidant enzymes and is very important in the cell's antioxidant defence. Unfortunately, I was only able to measure the total GSH present in the cell and not the oxidised GSSG levels, which limits the conclusions that can be drawn from this data. It is interesting that total GSH appears to be inversely correlated to ROS and RPA levels in U2OS, RPA16 and RPA21 cells. It is possible that some of the oxidised glutathione in RPA16 and RPA21 cells is in a form that is not reducible by glutathione reductase and would therefore escape detection in this assay. I regard this as an interesting but preliminary observation that suggests that accurate determination of reduced:oxidized glutathione ratios in these cells might yield important information.

To summarise, increased RPA expression has a protective effect. It improves cell survival after DNA damaging treatments as well as under conditions of oxidative stress. RPA also appears to be the limiting factor in NER under steady state conditions. This raises the question as to why RPA is limiting. I propose that a contributing factor to this limitation is the vulnerability of RPA to oxidative damage, including thiol oxidation and protein-protein crosslinking. This susceptibility may result in higher steady-state utilisation of antioxidant defences and therefore result in higher levels of steady state ROS.

6.3 Proteomics based method for identifying DPCs

The aim of this chapter was to develop a statistically rigorous technique to investigate the identity of the proteins involved in DPCs.

Initially, confirmation of the synergistic formation of DPCs with 6-TG+UVA was obtained through the Wizard (Promega) DNA extraction protocol with an additional proteinase K digestion step. This process revealed that 6-TG+UVA and, to a lesser extent, 6-TG result in DPC formation. No DPCs were detected after cells were exposed to 50kJ/m^2 UVA alone. This underlines the synergistic effect of 6-TG+UVA.

The incorporation of 6-TG into DNA was essential for DPC formation. Lesch-Nyhan fibroblasts and CCRC-CEM cells that were treated with HU to prevent 6-TG incorporation were not susceptive to DPC formation. In terms of ROS production, unincorporated 6-TG did not result in any ROS production in GM03467 Lesch-Nyhan fibroblasts, while in HU treated CCRF-CEM cells it did. This could be because the Lesch-Nyhan cells are HPRT deficient and do not phosphorylate 6-TG to retain it in the cell. 6-TG most likely establishes an equilibrium concentration between the extracellular and intracellular environment. On the other hand, CCRF-CEM cells treated with HU, still phosphorylate and retain 6-TG in the cell, which can generate more intracellular ROS. When Lesch-Nyhan cells, and CCRF-CEM cells treated with HU, are treated with 6-TG+UVA it results in ROS levels higher than 6-TG on its own but lower than incorporated 6-TG+UVA. However, this ROS is insufficient in causing crosslinks. Even though there is intracellular ROS detected with unincorporated 6-TG, it does not mean the ROS is generated in the right location to cause DPCs.

Crosslinks between oligonucleotides containing 6-TG and oligopeptides can occur between peptide SH or NH_2 and G^{SO3}, which is a good leaving group for nucleophilic substitution reactions (Gueranger et al., 2011). In addition, crosslinks can also form through a free protein NH_2 group and a 6-TG radical cation or a 6-TG thiyl radical formed by oxidation of DNA 6-TG (Perrier et al., 2006). These radicals can result in a significant number of propagating reactions and damage to nearby DNA and

proteins resulting in more DPCs. This data also suggests that reactions between protein nucleophiles and oxidised guanine are not contributors to DPC formation by 6-TG and a majority of the crosslinking occurs through incorporated 6-TG.

I decided to analyse DPC formation by MS. An acknowledged issue with identifying proteins involved in DPCs is contamination by non-covalently bound proteins. Therefore, the method development aimed at maximising the removal of free DNA and free protein to enrich the DNA:protein crosslink fraction. The removal of free protein was maximized by performing high salt washes of the chromatin fraction. After DNA was immobilized on a filter, extensive washing with urea further depleted any proteins not covalently attached to DNA. The analysis of tryptic digests effectively excluded any contribution from DNA.

I identified over 2000 cellular proteins that were crosslinked by 6-TG and 6-TG+UVA. Using SILAC (stable isotope labelling by amino acids in cell culture), the analysis confirmed that the modest UVA dose I used does not cause significant DPC formation. As the significance level was set to a conservative log2 value of 1 (2-fold enrichment), 6-TG treatment alone was a relatively inefficient crosslinker. On the other hand, 6-TG+UVA resulted in a very significant increase in the association of proteins with DNA following treatment, highlighting both the contribution of 6-TG+UVA to DPC formation as well as the synergistic relationship between 6-TG and UVA. The formation of ICLs has been demonstrated to require both 6-TG incorporation and ROS production (Brem and Karran, 2012). These results suggest that it is also a requirement for DPC formation. SILAC reverse labelling provided a statistically rigorous and highly reproducible approach to viewing the effects of 6-TG and 6-TG+UVA treatments.

I analysed DNA-free total lysate data to examine whether 6-TG had an overall effect on protein recovery. Because 6-TG impairs transcription (and possibly translation) during the 24-hour incubation period, underrepresentation of proteins due to expression changes might have skewed the crosslinking data. The results show that 6-TG treatment was not associated with significant changes in protein abundance in RIPA extracts, indicating that changes in transcription and translation caused by 6-TG over the 24-hour incubation did not have a substantial impact on overall protein

levels. There was evidence of a decline in protein recovery from 6-TG+UVA cells. This cannot be related to changes in transcription or translation as proteins were extracted immediately after irradiation. These changes most likely represent the effects of DPC formation and protein oxidation. The resulting protein unfolding, aggregation and precipitation can decrease overall protein recovery as well as possibly impeding the detection of some proteins that are recovered due to heavy oxidation. This may explain why the data presents itself as a scatter rather than a clear correlation.

The MS analysis revealed that the proteins most vulnerable to crosslinking were predominantly nuclear proteins involved in gene expression, DNA replication/repair and cell cycle. The proteins involved in these cellular functions are anticipated to exist in close proximity to DNA.

Among 179 DNA repair proteins, 52 were detected and 30 of these appeared to be crosslinked to DNA. An advantage of this method is that it recognises proteins that do not change in a treatment-dependent manner. This facilitates the identification of false positives. The information from the RIPA extracts also confirms this depletion of DNA repair proteins through either DPC formation or protein oxidation. This can contribute towards reduced protein recovery that was identified with DNA repair proteins in Chapter 3. In fact, RPA70 was among the 30 proteins that display a crosslinking profile. RPA32 and RPA14 were detected but did not appear to be crosslinked. This may be because RPA70 is the subunit with the most intimate association with DNA.

Investigating individual proteins involved in replication and repair revealed different susceptibilities to crosslinking. While POLD1 subunit of DNA polymerase δ and the MCM proteins were efficiently crosslinked by both 6-TG and 6-TG+UVA, the smaller POLD3 and the topoisomerases exhibit mainly photochemical crosslinking dependent on 6-TG+UVA. The vulnerability to crosslinking with 6-TG on its own may be due to oxidation susceptibilities or the way in which the proteins interact with DNA. The MCM complex proteins exhibit almost perfect overlap in their DPC formation. This can be a result of the subunits having equal susceptibilities to DPC formation or through one subunit crosslinking to DNA and the other subunits forming inter-subunit

protein-protein crosslinks. In agreement with the crosslinking data, the whole-cell protein abundance of POLD, MCM and TOP proteins were visibly reduced in 6-TG+UVA treated cells.

After applying this method to studying 6-TG+UVA mediated DPC formation, I investigated Cip+UVA mediated crosslinking. DPCs with 6-TG and 6-TG+UVA can occur through proteins reacting with 6-TG itself. Ciprofloxacin can be DNA-intercalated, but because of its lack of incorporation, covalent protein crosslinking must occur through canonical DNA constituents (Vilfan et al., 2003). Both DNA 6-TG and ciprofloxacin are Type II photosensitisers. $^1O_2$ is most likely a significant contributor to DPC formation by both Cip+UVA and 6-TG+UVA.

As a proof of principle, I wanted to test whether this DPC detection method can be applied to treatments that result in a reactive centre in DNA, such as 6-TG, as well as crosslinking without a DNA incorporated target, such as ciprofloxacin. DPC formation by Cip+UVA was extensive and over 2000 DNA-crosslinked proteins were identified. This confirms that the method can be applied to different crosslinking treatments. The particular DNA repair proteins that were crosslinked by Cip+UVA and 6-TG+UVA exhibited significant overlap. This suggests that some DNA repair proteins are highly vulnerable to DNA crosslinking and indicates that crosslinking under both conditions may be by a similar mechanism.

The analysis clearly identified some false positives. Most of these were gene expression, ribosome biosynthesis and chromatin regulation proteins. There was a large family of histones in the false positive groups from both 6-TG+UVA and Cip+UVA treated cells. Histones and structural proteins like vimentin, which was also among the false positives, are highly abundant proteins and this high abundance can make them difficult to remove fully from the samples and cause its detection by MS. Initially, I anticipated that histones may be particularly prone to crosslinking by photosensitising treatments due to their intimate association with DNA. However, it appears that histone levels are unchanged with treatment. It may be possible that some histone crosslinking is masked by the high abundance and high propensity for contamination by histones.

There are various proposed ways by which DPCs are repaired including NER, homologous recombination (HR), the proteasome and more recently the DPC-specific protease SPRTN (Barker et al., 2005b; Quievryn and Zhitkovich, 2000; Ridpath et al., 2007; Stingele et al., 2015). The difficulty in fully determining which pathway is responsible for DPC repair is that most treatments that result in DPC formation also result in other forms of DNA damage. In these experiments, I have not only identified proteins from NER, HR and Fanconi anaemia pathways forming DPCs but it was also previously shown by our lab that NER is inhibited by both 6-TG+UVA and ciprofloxacin+UVA treatments (Gueranger et al., 2014; Peacock et al., 2014). Therefore, potential repair by these pathways may be impeded by DPC formation and by the other damaging effects of these oxidizing treatments. It would be interesting to use the method described here to investigate changes in protein composition of DPCs over time and examine their repair.

There have been other methods used to identify proteins involved in DPCs. Formaldehyde induced DPCs have been investigated by chromatin enrichment of proteins (ChEP) (Kliszczak et al., 2011). Biotinylated oligonucleotides have been used to investigate crosslinking by a specific subsets of proteins (Mittler et al., 2009). In addition, *in vivo* labelling of DNA by DNA polymerases, on-bead digestion of immunoprecipitated crosslinked proteins and immunoprecipitation of tri-methylated histone 3 to investigate the heterochromatin proteome are other methods that have been developed (Byrum et al., 2012; Mohammed et al., 2016; Soldi and Bonaldi, 2014). Most of these methods have a labelling step to quantify the crosslinking. However, to my knowledge, enrichment of DPCs using a Hybond-N^+ membrane and analysis of these proteins by SILAC-LC-MS/MS is a new, statistically rigorous and versatile method in the identification of DPCs.

In summary, I have devised a sensitive and highly informative proteomics based method to investigate DPC formation in human cells treated with UVA photosensitisers. The method identified over 2000 proteins many involved in essential processes such as gene expression, DNA repair and replication that can become crosslinked to DNA under acute oxidative stress conditions.

6.4 Conclusions

ROS production by UVA photosensitisers can lead to protein losses through oxidation and precipitation. RPA is particularly susceptible to oxidation by inter-subunit protein crosslinking, thiol oxidation and crosslinking to DNA. RPA has a crucial role in all aspects of DNA metabolism that involves a ssDNA intermediate, including DNA replication, recombination, repair, telomere maintenance and DNA damage response. RPA was identified as the limiting factor for NER and is the key target for inactivation in cells treated with 6-TG+UVA. Oxidation of RPA results in impaired ssDNA and XPA binding. This can contribute towards loss of NER function in cells under oxidizing conditions. Increased RPA expression improves cell survival and NER function after DNA damaging treatments as well as under conditions of oxidative stress.

I have also devised a SILAC and proteomics based method to investigate DPC formation in human cells treated with UVA photosensitisers. The method identified over 2000 proteins crosslinked to DNA by 6-TG and 6-TG+UVA or Cip+UVA treatment-mediated photochemical production of ROS. The proteins most vulnerable to crosslinking were those involved in gene expression, DNA repair and replication. RPA70 was among this group of susceptible proteins.

The experiments described in this thesis were aimed to reflect an amplified version of the clinical impact of photosensitising medications and potentially mimic long term effects. As the source of genetic information, DNA has received a majority of the attention as a target of damage by ROS compared to protein oxidation, due to the ease of replacement of oxidised proteins by protein turnover. However, oxidation of DNA repair proteins and the resulting impaired removal of DNA damage connects these two fields. This thesis has contributed some evidence to support the detrimental impact of protein oxidation to cellular viability and genomic integrity.

Chapter 7. Appendix

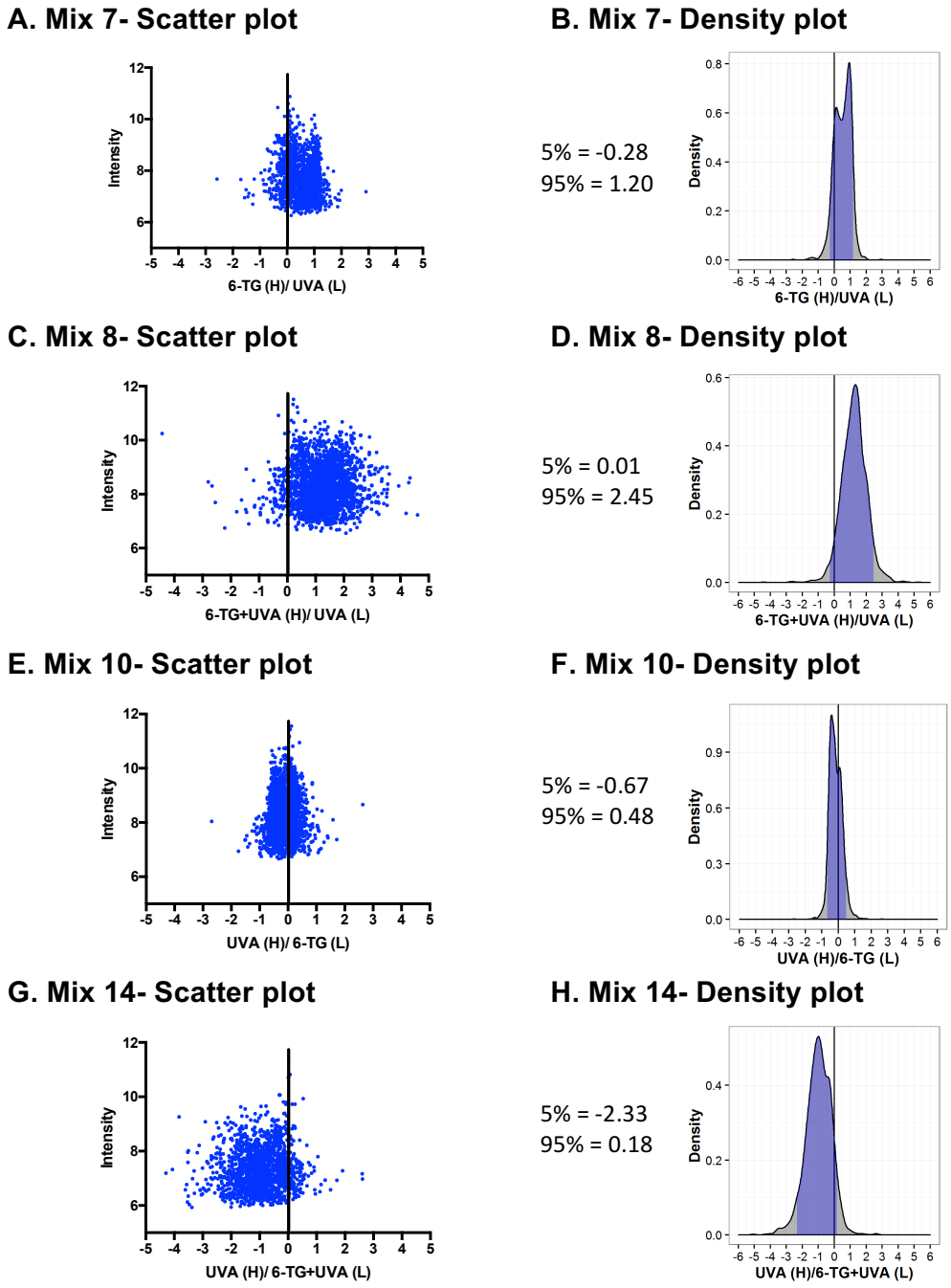

Figure 7.1: The effects of the different treatments on DPC formation
CCRF-CEM cells were labelled with heavy (H) or light (L) arginine and lysine isotopes and treated with 0.9μM 6-TG for 24 hours and irradiated with 50 kJ/m^2 UVA as indicated. Chromatin extracts were applied on HyBond-N$^+$ membranes, subject to *in situ* trypsin digestion and analysed by MS. Scatterplots of log2 SILAC H/L ratios of the detected proteins in each sample vs log10 Intensity **(A, C, E and G)** or Density **(B, D, F and H)** are presented. The H/L values at 5% and 95% of the density distribution are indicated.

Reference List

Abel, J., and Haarmann-Stemmann, T. (2010). An introduction to the molecular basics of aryl hydrocarbon receptor biology. Biol. Chem. *391*, 1235–1248.

Agostinis, P., Garmyn, M., and Van Laethem, A. (2007). The Aryl hydrocarbon receptor: an illuminating effector of the UVB response. Sci. STKE *2007*, pe49.

Agrawal, N., Ray, R.S., Farooq, M., Pant, A.B., and Hans, R.K. (2007). Photosensitizing potential of ciprofloxacin at ambient level of UV radiation. Photochemistry and Photobiology *83*, 1226–1236.

Ahnesorg, P., Smith, P., and Jackson, S.P. (2006). XLF interacts with the XRCC4-DNA ligase IV complex to promote DNA nonhomologous end-joining. Cell *124*, 301–313.

Amstad, P., Moret, R., and Cerutti, P. (1994). Glutathione peroxidase compensates for the hypersensitivity of Cu,Zn-superoxide dismutase overproducers to oxidant stress. J. Biol. Chem. *269*, 1606–1609.

Ando, W., and Takata, T. (1986). Photooxidation of sulfur compounds (Chemischer Informationsdienst).

Atkar, R., Ocampo, M., Euvrard, S., McGregor, J., Kanitakis, J., and Harwood, C. (2013). Ultraviolet radiation exposure through window glass may be associated with localization of nonmelanoma skin cancer in organ transplant recipients: a study in France and the UK. Br. J. Dermatol. *169*, 484–485.

Attard, N.R., and Karran, P. (2012). UVA photosensitization of thiopurines and skin cancer in organ transplant recipients. Photochem. Photobiol. Sci. *11*, 62–68.

Bakhmutova-Albert, E.V., Yao, H., Denevan, D.E., and Richardson, D.E. (2010). Kinetics and mechanism of peroxymonocarbonate formation. Inorg Chem *49*, 11287–11296.

Bandyopadhyay, U., Das, D., and Banerjee, R.K. (1999). Reactive oxygen species: oxidative damage and pathogenesis. Curr. Sci. *77*, 658–666.

Barker, S., Murray, D., Zheng, J., Li, L., and Weinfeld, M. (2005a). A method for the isolation of covalent DNA-protein crosslinks suitable for proteomics analysis. Anal. Biochem. *344*, 204–215.

Barker, S., Weinfeld, M., and Murray, D. (2005b). DNA-protein crosslinks: their induction, repair, and biological consequences. Mutat. Res. *589*, 111–135.

Bartek, J., and Lukas, J. (2007). DNA damage checkpoints: from initiation to recovery or adaptation. Curr. Opin. Cell Biol. *19*, 238–245.

Bastin-Shanower, S.A., and Brill, S.J. (2001). Functional analysis of the four DNA binding domains of replication protein A. The role of RPA2 in ssDNA binding. J.

Biol. Chem. *276*, 36446–36453.

Beard, W.A., and Wilson, S.H. (2006). Structure and mechanism of DNA polymerase Beta. Chem. Rev. *106*, 361–382.

Beersma, D.G.M., and Gordijn, M.C.M. (2007). Circadian control of the sleep–wake cycle. Physiol Behav *90*, 190–195.

Berlett, B.S., and Stadtman, E.R. (1997). Protein oxidation in aging, disease, and oxidative stress. J. Biol. Chem. *272*, 20313–20316.

Besaratinia, A., Synold, T.W., Xi, B., and Pfeifer, G.P. (2004). G-to-T transversions and small tandem base deletions are the hallmark of mutations induced by ultraviolet A radiation in mammalian cells. Biochemistry *43*, 8169–8177.

Bickers, D.R., and Athar, M. (2006). Oxidative stress in the pathogenesis of skin disease. J Invest Dermatol *126*, 2565–2575.

Bielski, B., Cabelli, D.E., Arudi, R.L., and Ross, A.B. (1985). Reactivity of HO2/O−2 radicals in aqueous solution. J. Phys. Chem. Ref. Data *14*, 1041–1100.

Biemond, P., van Eijk, H.G., Swaak, A.J., and Koster, J.F. (1984). Iron mobilization from ferritin by superoxide derived from stimulated polymorphonuclear leukocytes. Possible mechanism in inflammation diseases. J. Clin. Invest. *73*, 1576–1579.

Bienert, G.P., Møller, A.L.B., Kristiansen, K.A., Schulz, A., Møller, I.M., Schjoerring, J.K., and Jahn, T.P. (2007). Specific aquaporins facilitate the diffusion of hydrogen peroxide across membranes. J. Biol. Chem. *282*, 1183–1192.

Bigelow, D.J., and Squier, T.C. (2011). Thioredoxin-dependent redox regulation of cellular signaling and stress response through reversible oxidation of methionines. Mol Biosyst *7*, 2101–2109.

Binz, S.K., Sheehan, A.M., and Wold, M.S. (2004). Replication protein A phosphorylation and the cellular response to DNA damage. DNA Repair (Amst.) *3*, 1015–1024.

Bochkarev, A., Bochkareva, E., Frappier, L., and Edwards, A.M. (1999). The crystal structure of the complex of replication protein A subunits RPA32 and RPA14 reveals a mechanism for single-stranded DNA binding. Embo J. *18*, 4498–4504.

Bochkareva, E., Korolev, S., Lees-Miller, S.P., and Bochkarev, A. (2002). Structure of the RPA trimerization core and its role in the multistep DNA-binding mechanism of RPA. Embo J. *21*, 1855–1863.

Borovanský, J., and Elleder, M. (2003). Melanosome degradation: fact or fiction. Pigment Cell Res. *16*, 280–286.

Bökkerink, J.P., Stet, E.H., De Abreu, R.A., Damen, F.J., Hulscher, T.W., Bakker, M.A., and van Baal, J.A. (1993). 6-Mercaptopurine: cytotoxicity and biochemical pharmacology in human malignant T-lymphoblasts. Biochem. Pharmacol. *45*, 1455–1463.

Brash, D.E. (1988). UV mutagenic photoproducts in Escherichia coli and human cells: a molecular genetics perspective on human skin cancer. Photochemistry and Photobiology *48*, 59–66.

Brem, R., Li, F., Montaner, B., Reelfs, O., and Karran, P. (2010). DNA breakage and cell cycle checkpoint abrogation induced by a therapeutic thiopurine and UVA radiation. Oncogene *29*, 3953–3963.

Brem, R., and Karran, P. (2012). Oxidation-mediated DNA cross-linking contributes to the toxicity of 6-thioguanine in human cells. Cancer Res. *72*, 4787–4795.

Brem, R., Li, F., and Karran, P. (2009). Reactive oxygen species generated by thiopurine/UVA cause irreparable transcription-blocking DNA lesions. Nucleic Acids Res. *37*, 1951–1961.

Brenner, M., and Hearing, V.J. (2008). Modifying skin pigmentation – approaches through intrinsic biochemistry and exogenous agents. Drug Discov Today Dis Mech *5*, e189–e199.

Bridges, B.A. (2005). Error-prone DNA repair and translesion synthesis: focus on the replication fork. DNA Repair (Amst.) *4*, 618–9–634.

Brill, S.J., and Bastin-Shanower, S. (1998). Identification and characterization of the fourth single-stranded-DNA binding domain of replication protein A. Mol. Cell. Biol. *18*, 7225–7234.

Brooks, P.J. (2013). Blinded by the UV light: how the focus on transcription-coupled NER has distracted from understanding the mechanisms of Cockayne syndrome neurologic disease. DNA Repair (Amst.) *12*, 656–671.

Brosey, C.A., Soss, S.E., Brooks, S., Yan, C., Ivanov, I., Dorai, K., and Chazin, W.J. (2015). Functional dynamics in replication protein A DNA binding and protein recruitment domains. Structure *23*, 1028–1038.

Bustami, R.T., Ojo, A.O., Wolfe, R.A., Merion, R.M., Bennett, W.M., McDiarmid, S.V., Leichtman, A.B., Held, P.J., and Port, F.K. (2004). Immunosuppression and the risk of post-transplant malignancy among cadaveric first kidney transplant recipients. Am. J. Transplant. *4*, 87–93.

Byrum, S.D., Raman, A., Taverna, S.D., and Tackett, A.J. (2012). ChAP-MS: a method for identification of proteins and histone posttranslational modifications at a single genomic locus. Cell Rep *2*, 198–205.

Cadet, J., Mouret, S., Ravanat, J.-L., and Douki, T. (2012). Photoinduced damage to cellular DNA: direct and photosensitized reactions. Photochemistry and Photobiology *88*, 1048–1065.

Cadet, J., Sage, E., and Douki, T. (2005). Ultraviolet radiation-mediated damage to cellular DNA. Mutat. Res. *571*, 3–17.

Camenisch, U., Dip, R., Schumacher, S.B., Schuler, B., and Naegeli, H. (2006). Recognition of helical kinks by xeroderma pigmentosum group A protein triggers

DNA excision repair. Nat. Struct. Mol. Biol. *13*, 278–284.

Cavarra, E., Fimiani, M., Lungarella, G., Andreassi, L., de Santi, M., Mazzatenta, C., and Ciccoli, L. (2002). UVA light stimulates the production of cathepsin G and elastase-like enzymes by dermal fibroblasts: a possible contribution to the remodeling of elastotic areas in sun-damaged skin. Biol. Chem. *383*, 199–206.

Ceccaldi, R., Sarangi, P., and D'Andrea, A.D. (2016). The Fanconi anaemia pathway: new players and new functions. Nat. Rev. Mol. Cell Biol. *17*, 337–349.

Chance, B., Sies, H., and Boveris, A. (1979). Hydroperoxide metabolism in mammalian organs. Physiol Rev.

Chappell, C., Hanakahi, L.A., Karimi-Busheri, F., Weinfeld, M., and West, S.C. (2002). Involvement of human polynucleotide kinase in double-strand break repair by non-homologous end joining. Embo J. *21*, 2827–2832.

Chen, R., and Wold, M.S. (2014). Replication protein A: single-stranded DNA's first responder: dynamic DNA-interactions allow replication protein A to direct single-strand DNA intermediates into different pathways for synthesis or repair. Bioessays *36*, 1156–1161.

Chen, S.H., Chan, N.-L., and Hsieh, T.-S. (2013). New mechanistic and functional insights into DNA topoisomerases. Annu. Rev. Biochem. *82*, 139–170.

Clydesdale, G.J., Dandie, G.W., and Muller, H.K. (2001). Ultraviolet light induced injury: immunological and inflammatory effects. Immunol Cell Biol *79*, 547–568.

Coin, F., Oksenych, V., and Egly, J.M. (2007). Distinct roles for the XPB/p52 and XPD/p44 subcomplexes of TFIIH in damaged DNA opening during nucleotide excision repair. Mol. Cell *26*, 245–256.

Coin, F., Oksenych, V., Mocquet, V., Groh, S., Blattner, C., and Egly, J.M. (2008). Nucleotide excision repair driven by the dissociation of CAK from TFIIH. Mol. Cell *31*, 9–20.

Cooke, M.S., Duarte, T.L., Cooper, D., Chen, J., Nandagopal, S., and Evans, M.D. (2008). Combination of azathioprine and UVA irradiation is a major source of cellular 8-oxo-7,8-dihydro-2'-deoxyguanosine. DNA Repair (Amst.) *7*, 1982–1989.

Costas, C., Yuriev, E., Meyer, K.L., Guion, T.S., and Hanna, M.M. (2000). RNA-protein crosslinking to AMP residues at internal positions in RNA with a new photocrosslinking ATP analog. Nucleic Acids Res. *28*, 1849–1858.

Courdavault, S., Baudouin, C., Charveron, M., Favier, A., Cadet, J., and Douki, T. (2004). Larger yield of cyclobutane dimers than 8-oxo-7,8-dihydroguanine in the DNA of UVA-irradiated human skin cells. Mutat. Res. *556*, 135–142.

Cox, J., and Mann, M. (2008). MaxQuant enables high peptide identification rates, individualized p.p.b.-range mass accuracies and proteome-wide protein quantification. Nat. Biotechnol. *26*, 1367–1372.

Cuffari, C., Li, D.Y., Mahoney, J., Barnes, Y., and Bayless, T.M. (2004). Peripheral blood mononuclear cell DNA 6-thioguanine metabolite levels correlate with decreased interferon-gamma production in patients with Crohn's disease on AZA therapy. Dig. Dis. Sci. *49*, 133–137.

Dalle-Donne, I., Rossi, R., Giustarini, D., Colombo, R., and Milzani, A. (2007). S-glutathionylation in protein redox regulation. Free Radic. Biol. Med. *43*, 883–898.

Dalle-Donne, I., Rossi, R., Giustarini, D., Milzani, A., and Colombo, R. (2003). Protein carbonyl groups as biomarkers of oxidative stress. Clin. Chim. Acta *329*, 23–38.

Damian, D.L., Matthews, Y.J., Phan, T.A., and Halliday, G.M. (2011). An action spectrum for ultraviolet radiation-induced immunosuppression in humans. Br. J. Dermatol. *164*, 657–659.

Darvin, M.E., Fluhr, J.W., Meinke, M.C., Zastrow, L., Sterry, W., and Lademann, J. (2011). Topical beta-carotene protects against infra-red-light-induced free radicals. Exp. Dermatol. *20*, 125–129.

Das, D.K., Engelman, R.M., Clement, R., Otani, H., Prasad, M.R., and Rao, P.S. (1987). Role of xanthine oxidase inhibitor as free radical scavenger: a novel mechanism of action of allopurinol and oxypurinol in myocardial salvage. Biochem. Biophys. Res. Commun. *148*, 314–319.

Daughdrill, G.W., Buchko, G.W., Botuyan, M.V., Arrowsmith, C., Wold, M.S., Kennedy, M.A., and Lowry, D.F. (2003). Chemical shift changes provide evidence for overlapping single-stranded DNA- and XPA-binding sites on the 70 kDa subunit of human replication protein A. Nucleic Acids Res. *31*, 4176–4183.

Davies, K.J. (2001). Degradation of oxidized proteins by the 20S proteasome. Biochimie *83*, 301–310.

Davies, M.J. (2003). Singlet oxygen-mediated damage to proteins and its consequences. Biochem. Biophys. Res. Commun. *305*, 761–770.

de Gruijl, F.R., and van der Leun, J.C. (2000). Environment and health: 3. Ozone depletion and ultraviolet radiation. Cmaj *163*, 851–855.

de Laat, W.L., Appeldoorn, E., Sugasawa, K., Weterings, E., Jaspers, N.G., and Hoeijmakers, J.H. (1998). DNA-binding polarity of human replication protein A positions nucleases in nucleotide excision repair. Genes Dev. *12*, 2598–2609.

Deans, A.J., and West, S.C. (2011). DNA interstrand crosslink repair and cancer. Nat. Rev. Cancer *11*, 467–480.

DeFazio, L.G., Stansel, R.M., Griffith, J.D., and Chu, G. (2002). Synapsis of DNA ends by DNA-dependent protein kinase. Embo J. *21*, 3192–3200.

DeMott, M.S., Zigman, S., and Bambara, R.A. (1998). Replication protein A stimulates long patch DNA base excision repair. J. Biol. Chem. *273*, 27492–27498.

Deng, X., Prakash, A., Dhar, K., Baia, G.S., Kolar, C., Oakley, G.G., and Borgstahl, G.E.O. (2009). Human replication protein A-Rad52-single-stranded DNA complex: stoichiometry and evidence for strand transfer regulation by phosphorylation. Biochemistry *48*, 6633–6643.

Deponte, M. (2013). Glutathione catalysis and the reaction mechanisms of glutathione-dependent enzymes. Biochim. Biophys. Acta *1830*, 3217–3266.

Dexheimer, T.S. (2013). DNA repair pathways and mechanisms. In DNA Repair of Cancer Stem Cells, L.A. Mathews, S.M. Cabarcas, and E.M. Hurt, eds. (Springer), pp. 19–32.

Di Mascio, P., Bechara, E.J., Medeiros, M.H., Briviba, K., and Sies, H. (1994). Singlet molecular oxygen production in the reaction of peroxynitrite with hydrogen peroxide. FEBS Lett. *355*, 287–289.

Diffey, B.L. (2002). Human exposure to solar ultraviolet radiation. J Cosmet Dermatol *1*, 124–130.

Dizdaroglu, M., Gajewski, E., Reddy, P., and Margolis, S.A. (1989). Structure of a hydroxyl radical induced DNA-protein cross-link involving thymine and tyrosine in nucleohistone. Biochemistry *28*, 3625–3628.

Domagala, J.M. (1994). Structure-activity and structure-side-effect relationships for the quinolone antibacterials. J. Antimicrob. Chemother. *33*, 685–706.

Donnelly, M.L., Luke, G., Mehrotra, A., Li, X., Hughes, L.E., Gani, D., and Ryan, M.D. (2001). Analysis of the aphthovirus 2A/2B polyprotein 'cleavage' mechanism indicates not a proteolytic reaction, but a novel translational effect: a putative ribosomal 'skip'. J. Gen. Virol. *82*, 1013–1025.

Douki, T., and Cadet, J. (2001). Individual determination of the yield of the main UV-induced dimeric pyrimidine photoproducts in DNA suggests a high mutagenicity of CC photolesions. Biochemistry *40*, 2495–2501.

Douki, T., Laporte, G., and Cadet, J. (2003a). Inter-strand photoproducts are produced in high yield within A-DNA exposed to UVC radiation. Nucleic Acids Res. *31*, 3134–3142.

Douki, T., Reynaud-Angelin, A., Cadet, J., and Sage, E. (2003b). Bipyrimidine photoproducts rather than oxidative lesions are the main type of DNA damage involved in the genotoxic effect of solar UVA radiation. Biochemistry *42*, 9221–9226.

Dunlop, R.A., Brunk, U.T., and Rodgers, K.J. (2009). Oxidized proteins: mechanisms of removal and consequences of accumulation. IUBMB Life *61*, 522–527.

Dupont, E., Gomez, J., and Bilodeau, D. (2013). Beyond UV radiation: a skin under challenge. Int J Cosmet Sci *35*, 224–232.

Dwivedi, A., Mujtaba, S.F., Yadav, N., Kushwaha, H.N., Amar, S.K., Singh, S.K., Pant, M.C., and Ray, R.S. (2014). Cellular and molecular mechanism of ofloxacin induced apoptotic cell death under ambient UV-A and sunlight exposure. Free Radic. Res. *48*, 333–346.

Dwivedi, A., Mujtaba, S.F., Kushwaha, H.N., Ali, D., Yadav, N., Singh, S.K., and Ray, R.S. (2012). Photosensitizing mechanism and identification of levofloxacin photoproducts at ambient UV radiation. Photochemistry and Photobiology *88*, 344–355.

Easton, C.J. (1997). Free-Radical Reactions in the Synthesis of alpha-Amino Acids and Derivatives. Chem. Rev. *97*, 53–82.

Elion, G.B. (1989). The purine path to chemotherapy. Science *244*, 41–47.

Elion, G.B., Kovensky, A., and Hitchings, G.H. (1966). Metabolic studies of allopurinol, an inhibitor of xanthine oxidase. Biochem. Pharmacol. *15*, 863–880.

England, M.D., Cavarocchi, N.C., O'Brien, J.F., Solis, E., Pluth, J.R., Orszulak, T.A., Kaye, M.P., and Schaff, H.V. (1986). Influence of antioxidants (mannitol and allopurinol) on oxygen free radical generation during and after cardiopulmonary bypass. Circulation *74*, III134–III137.

Euvrard, S., Kanitakis, J., and Claudy, A. (2003). Skin cancers after organ transplantation. N. Engl. J. Med. *348*, 1681–1691.

Fagbemi, A.F., Orelli, B., and Schärer, O.D. (2011). Regulation of endonuclease activity in human nucleotide excision repair. DNA Repair (Amst.) *10*, 722–729.

Fan, J., and Pavletich, N.P. (2012). Structure and conformational change of a replication protein A heterotrimer bound to ssDNA. Genes Dev. *26*, 2337–2347.

Finkel, T. (2000). Redox-dependent signal transduction. FEBS Lett. *476*, 52–54.

Finkel, T. (2011). Signal transduction by reactive oxygen species. J. Cell Biol. *194*, 7–15.

Flynn, R.L., and Zou, L. (2010). Oligonucleotide/oligosaccharide-binding fold proteins: a growing family of genome guardians. Crit. Rev. Biochem. Mol. Biol. *45*, 266–275.

Foote, C.S., and Wexler, S. (1964). Olefin oxidations with excited singlet molecular oxygen. J. Am. Chem. Soc. *86*, 3879–3880.

Fornace, A.J., Jr, and Kohn, K.W. (1976). DNA-protein cross-linking by ultraviolet radiation in normal human and xeroderma pigmentosum fibroblasts. Biochim. Biophys. Acta *435*, 95–103.

Frei, B. (1994). Reactive oxygen species and antioxidant vitamins: mechanisms of action. Am. J. Med. *97*, S5–S13.

Fridovich, I. (1983). Superoxide radical: an endogenous toxicant. Annu. Rev.

Pharmacol. Toxicol *23*, 239–257.

Friedhoff, P., Li, P., and Gotthardt, J. (2016). Protein-protein interactions in DNA mismatch repair. DNA Repair (Amst.) *38*, 50–57.

Fritsche, E., Schäfer, C., Calles, C., Bernsmann, T., Bernshausen, T., Wurm, M., Hübenthal, U., Cline, J.E., Hajimiragha, H., Schroeder, P., et al. (2007). Lightening up the UV response by identification of the arylhydrocarbon receptor as a cytoplasmatic target for ultraviolet B radiation. Proc. Natl. Acad. Sci. U.S.a. *104*, 8851–8856.

Gallogly, M.M., and Mieyal, J.J. (2007). Mechanisms of reversible protein glutathionylation in redox signaling and oxidative stress. Curr Opin Pharmacol *7*, 381–391.

Genschel, J., and Modrich, P. (2003). Mechanism of 5'-directed excision in human mismatch repair. Mol. Cell *12*, 1077–1086.

Gey, K.F., Brubacher, G.B., and Stähelin, H.B. (1987). Plasma levels of antioxidant vitamins in relation to ischemic heart disease and cancer. Am. J. Clin. Nutr. *45*, 1368–1377.

Gherezghiher, T.B., Ming, X., Villalta, P.W., Campbell, C., and Tretyakova, N.Y. (2013). 1,2,3,4-Diepoxybutane-induced DNA-protein cross-linking in human fibrosarcoma (HT1080) cells. J. Proteome Res. *12*, 2151–2164.

Gibb, B., Ye, L.F., Gergoudis, S.C., Kwon, Y., Niu, H., Sung, P., and Greene, E.C. (2014). Concentration-dependent exchange of replication protein A on single-stranded DNA revealed by single-molecule imaging. PLoS ONE *9*, e87922.

Giorgio, M., Trinei, M., Migliaccio, E., and Pelicci, P.G. (2007). Hydrogen peroxide: a metabolic by-product or a common mediator of ageing signals? Nat. Rev. Mol. Cell Biol. *8*, 722–728.

Gourdin, A.M., van Cuijk, L., Tresini, M., Luijsterburg, M.S., Nigg, A.L., Giglia-Mari, G., Houtsmuller, A.B., Vermeulen, W., and Marteijn, J.A. (2014). Differential binding kinetics of replication protein A during replication and the pre- and post-incision steps of nucleotide excision repair. DNA Repair (Amst.) *24*, 46–56.

Green, H., Rahamimov, R., Gafter, U., Leibovitci, L., and Paul, M. (2011). Antibiotic prophylaxis for urinary tract infections in renal transplant recipients: a systematic review and meta-analysis. Transpl Infect Dis *13*, 441–447.

Groitl, B., and Jakob, U. (2014). Thiol-based redox switches. Biochim. Biophys. Acta *1844*, 1335–1343.

Grulich, A.E., van Leeuwen, M.T., Falster, M.O., and Vajdic, C.M. (2007). Incidence of cancers in people with HIV/AIDS compared with immunosuppressed transplant recipients: a meta-analysis. Lancet *370*, 59–67.

Gueranger, Q., Kia, A., Frith, D., and Karran, P. (2011). Crosslinking of DNA repair and replication proteins to DNA in cells treated with 6-thioguanine and UVA.

Nucleic Acids Res. *39*, 5057–5066.

Gueranger, Q., Li, F., Peacock, M., Larnicol-Fery, A., Brem, R., Macpherson, P., Egly, J.M., and Karran, P. (2014). Protein oxidation and DNA repair inhibition by 6-thioguanine and UVA radiation. J Invest Dermatol *134*, 1408–1417.

Gutteridge, J.M. (1986). Iron promoters of the Fenton reaction and lipid peroxidation can be released from haemoglobin by peroxides. FEBS Lett. *201*, 291–295.

Guven, M., Brem, R., Macpherson, P., Peacock, M., and Karran, P. (2015). Oxidative Damage to RPA Limits the Nucleotide Excision Repair Capacity of Human Cells. J Invest Dermatol *135*, 2834–2841.

Hall, A., Karplus, P.A., and Poole, L.B. (2009). Typical 2-Cys peroxiredoxins–structures, mechanisms and functions. Febs J. *276*, 2469–2477.

Halliday, G.M., Byrne, S.N., and Damian, D.L. (2011). Ultraviolet A radiation: its role in immunosuppression and carcinogenesis. Semin Cutan Med Surg *30*, 214–221.

Halliwell, B. (1991). Reactive oxygen species in living systems: source, biochemistry, and role in human disease. Am. J. Med. *91*, 14S–22S.

Halliwell, B. (1998). Free radicals and human disease- trick or treat? In Oxygen Radicals and the Disease Process, C. Thomas, and B. Kalyanaraman, eds. (Netherlands: Harwood academic publishers), pp. 1–14.

Halliwell, B., and Gutteridge, J.M. (1984). Oxygen toxicity, oxygen radicals, transition metals and disease. Biochem. J. *219*, 1–14.

Halliwell, B., Zantella, A., and Gomez, E.O. (1997). Antioxidants and human disease: a general introduction. Nutr. Rev. *55*, S44–S52.

Halliwell, B., and Gutteridge, J.M.C. (2007). Free Radicals in Biology and Medicine (New York: Oxford University Press).

Hampton, M.B., Morgan, P.E., and Davies, M.J. (2002). Inactivation of cellular caspases by peptide-derived tryptophan and tyrosine peroxides. FEBS Lett. *527*, 289–292.

Haring, S.J., Humphreys, T.D., and Wold, M.S. (2010). A naturally occurring human RPA subunit homolog does not support DNA replication or cell-cycle progression. Nucleic Acids Res. *38*, 846–858.

Hartevelt, M.M., Bavinck, J.N., Kootte, A.M., Vermeer, B.J., and Vandenbroucke, J.P. (1990). Incidence of skin cancer after renal transplantation in The Netherlands. Transplantation *49*, 506–509.

Hass, C.S., Gakhar, L., and Wold, M.S. (2010). Functional characterization of a cancer causing mutation in human replication protein A. Mol. Cancer Res. *8*, 1017–1026.

Helfrich, Y.R., Sachs, D.L., and Voorhees, J.J. (2008). Overview of skin aging and photoaging. Dermatol. Nurs. *20*, 177–183.

Hemmens, V.J., and Moore, D.E. (1986). Photochemical sensitization by azathioprine and its metabolites--I. 6-Mercaptopurine. Photochemistry and Photobiology *43*, 247–255.

Higgins, P.G., Fluit, A.C., and Schmitz, F.J. (2003). Fluoroquinolones: structure and target sites. Curr Drug Targets *4*, 181–190.

Hitomi, K., Iwai, S., and Tainer, J.A. (2007). The intricate structural chemistry of base excision repair machinery: implications for DNA damage recognition, removal, and repair. DNA Repair (Amst.) *6*, 410–428.

Hofbauer, G.F.L., Attard, N.R., Harwood, C.A., McGregor, J.M., Dziunycz, P., Iotzova-Weiss, G., Straub, G., Meyer, R., Kamenisch, Y., Berneburg, M., et al. (2012). Reversal of UVA skin photosensitivity and DNA damage in kidney transplant recipients by replacing azathioprine. Am. J. Transplant. *12*, 218–225.

Holman, C.D., and Armstrong, B.K. (1984). Cutaneous malignant melanoma and indicators of total accumulated exposure to the sun: an analysis separating histogenetic types. J. Natl. Cancer Inst. *73*, 75–82.

Holmgren, A. (1989). Thioredoxin and glutaredoxin systems. J. Biol. Chem. *264*, 13963–13966.

Hooper, D.C., and Wolfson, J.S. (1985). The fluoroquinolones: pharmacology, clinical uses, and toxicities in humans. Antimicrob. Agents Chemother. *28*, 716–721.

Huang, T.T., Nijman, S.M.B., Mirchandani, K.D., Galardy, P.J., Cohn, M.A., Haas, W., Gygi, S.P., Ploegh, H.L., Bernards, R., and D'Andrea, A.D. (2006). Regulation of monoubiquitinated PCNA by DUB autocleavage. Nat. Cell Biol. *8*, 339–347.

Huffman, J.L., Sundheim, O., and Tainer, J.A. (2005). DNA base damage recognition and removal: new twists and grooves. Mutat. Res. *577*, 55–76.

Hussein, M.R. (2005). Ultraviolet radiation and skin cancer: molecular mechanisms. J. Cutan. Pathol *32*, 191–205.

Hwang, B.J., Ford, J.M., Hanawalt, P.C., and Chu, G. (1999). Expression of the p48 xeroderma pigmentosum gene is p53-dependent and is involved in global genomic repair. Proc. Natl. Acad. Sci. U.S.a. *96*, 424–428.

Ichihashi, M., Ando, H., Yoshida, M., Niki, Y., and Matsui, M. (2009). Photoaging of the skin. Anti-Aging Medicine *6*, 46–59.

Ignarro, L.J. (1990). Haem-dependent activation of guanylate cyclase and cyclic GMP formation by endogenous nitric oxide: a unique transduction mechanism for transcellular signaling. Pharmacol. Toxicol. *67*, 1–7.

Ikehata, H., Kawai, K., Komura, J.-I., Sakatsume, K., Wang, L., Imai, M., Higashi,

S., Nikaido, O., Yamamoto, K., Hieda, K., et al. (2008). UVA1 genotoxicity is mediated not by oxidative damage but by cyclobutane pyrimidine dimers in normal mouse skin. J Invest Dermatol *128*, 2289–2296.

Ikehata, H., Kudo, H., Masuda, T., and Ono, T. (2003). UVA induces C-->T transitions at methyl-CpG-associated dipyrimidine sites in mouse skin epidermis more frequently than UVB. Mutagenesis *18*, 511–519.

Ip, S.C.Y., Rass, U., Blanco, M.G., Flynn, H.R., Skehel, J.M., and West, S.C. (2008). Identification of Holliday junction resolvases from humans and yeast. Nature *456*, 357–361.

Jackson, S.P., and Bartek, J. (2009). The DNA-damage response in human biology and disease. Nature *461*, 1071–1078.

Jacobs, A.L., and Schär, P. (2012). DNA glycosylases: in DNA repair and beyond. Chromosoma *121*, 1–20.

Jang, S.-W., Jung, J.K., and Kim, J.M. (2016). Replication Protein A (RPA) deficiency activates the Fanconi anemia DNA repair pathway. Cell Cycle 1–10.

Jansen, J.G., Tsaalbi-Shtylik, A., Hendriks, G., Gali, H., Hendel, A., Johansson, F., Erixon, K., Livneh, Z., Mullenders, L.H.F., Haracska, L., et al. (2009). Separate domains of Rev1 mediate two modes of DNA damage bypass in mammalian cells. Mol. Cell. Biol. *29*, 3113–3123.

Jariel-Encontre, I., Bossis, G., and Piechaczyk, M. (2008). Ubiquitin-independent degradation of proteins by the proteasome. Biochim. Biophys. Acta *1786*, 153–177.

Jaspers, N.G.J., Raams, A., Silengo, M.C., Wijgers, N., Niedernhofer, L.J., Robinson, A.R., Giglia-Mari, G., Hoogstraten, D., Kleijer, W.J., Hoeijmakers, J.H.J., et al. (2007). First reported patient with human ERCC1 deficiency has cerebro-oculo-facio-skeletal syndrome with a mild defect in nucleotide excision repair and severe developmental failure. Am. J. Hum. Genet. *80*, 457–466.

Jeggo, P.A., and Löbrich, M. (2007). DNA double-strand breaks: their cellular and clinical impact? Oncogene *26*, 7717–7719.

Jeggo, P., and O'Neill, P. (2002). The Greek Goddess, Artemis, reveals the secrets of her cleavage. DNA Repair (Amst.) *1*, 771–777.

Jiang, G., Zou, Y., and Wu, X. (2012). Replication-mediated disassociation of replication protein A-XPA complex upon DNA damage: implications for RPA handing off. Cell Biol. Int. *36*, 713–720.

Jiménez-Banzo, A., Sagristà, M.L., Mora, M., and Nonell, S. (2008). Kinetics of singlet oxygen photosensitization in human skin fibroblasts. Free Radic. Biol. Med. *44*, 1926–1934.

Johnson, R.E., Washington, M.T., Haracska, L., Prakash, S., and Prakash, L. (2000). Eukaryotic polymerases iota and zeta act sequentially to bypass DNA lesions. Nature *406*, 1015–1019.

Jun, T., Liancai, Z., and Bochu, W. (2007). Effects of Quercetin on DNA Damage Induced by Copper Ion. International Journal of Pharmacology *3*, 19–26.

Jung, T., Höhn, A., and Grune, T. (2014). The proteasome and the degradation of oxidized proteins: Part II - protein oxidation and proteasomal degradation. Redox Biol *2*, 99–104.

Jux, B., Kadow, S., Luecke, S., Rannug, A., Krutmann, J., and Esser, C. (2011). The Aryl Hydrocarbon Receptor Mediates UVB Radiation–Induced Skin Tanning. Journal of Investigative Dermatology *131*, 203–210.

Kadyrov, F.A., Dzantiev, L., Constantin, N., and Modrich, P. (2006). Endonucleolytic function of MutLalpha in human mismatch repair. Cell *126*, 297–308.

Kaganovich, D., Kopito, R., and Frydman, J. (2008). Misfolded proteins partition between two distinct quality control compartments. Nature *454*, 1088–1095.

Kanofsky, J.R., and Sima, P. (1991). Singlet oxygen production from the reactions of ozone with biological molecules. J. Biol. Chem. *266*, 9039–9042.

Kanofsky, J.R., Hoogland, H., Wever, R., and Weiss, S.J. (1988). Singlet oxygen production by human eosinophils. J. Biol. Chem. *263*, 9692–9696.

Kansanen, E., Kuosmanen, S.M., Leinonen, H., and Levonen, A.-L. (2013). The Keap1-Nrf2 pathway: Mechanisms of activation and dysregulation in cancer. Redox Biol *1*, 45–49.

Kappes, U.P., Luo, D., Potter, M., Schulmeister, K., and Rünger, T.M. (2006). Short- and long-wave UV light (UVB and UVA) induce similar mutations in human skin cells. J Invest Dermatol *126*, 667–675.

Karran, P. (2001). Mechanisms of tolerance to DNA damaging therapeutic drugs. Carcinogenesis *22*, 1931–1937.

Karran, P. (2006). Thiopurines, DNA damage, DNA repair and therapy-related cancer. Br. Med. Bull. *79-80*, 153–170.

Karran, P., Offman, J., and Bignami, M. (2003). Human mismatch repair, drug-induced DNA damage, and secondary cancer. Biochimie *85*, 1149–1160.

Kashiyama, K., Nakazawa, Y., Pilz, D.T., Guo, C., Shimada, M., Sasaki, K., Fawcett, H., Wing, J.F., Lewin, S.O., Carr, L., et al. (2013). Malfunction of nuclease ERCC1-XPF results in diverse clinical manifestations and causes Cockayne syndrome, xeroderma pigmentosum, and Fanconi anemia. Am. J. Hum. Genet. *92*, 807–819.

Kielbassa, C., Roza, L., and Epe, B. (1997). Wavelength dependence of oxidative DNA damage induced by UV and visible light. Carcinogenesis *18*, 811–816.

Kiianitsa, K., and Maizels, N. (2013). A rapid and sensitive assay for DNA-protein covalent complexes in living cells. Nucleic Acids Res. *41*, e104.

Kim, C., Paulus, B.F., and Wold, M.S. (1994). Interactions of human replication protein A with oligonucleotides. Biochemistry *33*, 14197–14206.

Kim, J.K., Kim, Y.J., Fillmore, J.J., Chen, Y., Moore, I., Lee, J., Yuan, M., Li, Z.W., Karin, M., Perret, P., et al. (2001). Prevention of fat-induced insulin resistance by salicylate. J. Clin. Invest. *108*, 437–446.

Kim, J.H., Lee, S.-R., Li, L.-H., Park, H.-J., Park, J.-H., Lee, K.Y., Kim, M.-K., Shin, B.A., and Choi, S.-Y. (2011). High cleavage efficiency of a 2A peptide derived from porcine teschovirus-1 in human cell lines, zebrafish and mice. PLoS ONE *6*, e18556.

Kirkman, H.N., Rolfo, M., Ferraris, A.M., and Gaetani, G.F. (1999). Mechanisms of protection of catalase by NADPH. Kinetics and stoichiometry. J. Biol. Chem. *274*, 13908–13914.

Kliszczak, A.E., Rainey, M.D., Harhen, B., Boisvert, F.M., and Santocanale, C. (2011). DNA mediated chromatin pull-down for the study of chromatin replication. Sci Rep *1*, 95–95.

Korichneva, I. (2005). Redox regulation of cardiac protein kinase C. Exp Clin Cardiol *10*, 256–261.

Kow, Y.W. (2002). Repair of deaminated bases in DNA. Free Radic. Biol. Med. *33*, 886–893.

Kraemer, K.H., Patronas, N.J., Schiffmann, R., Brooks, B.P., Tamura, D., and DiGiovanna, J.J. (2007). Xeroderma pigmentosum, trichothiodystrophy and Cockayne syndrome: a complex genotype-phenotype relationship. Neuroscience *145*, 1388–1396.

Kricker, A., Armstrong, B.K., English, D.R., and Heenan, P.J. (1995). Does intermittent sun exposure cause basal cell carcinoma? a case-control study in Western Australia. Int. J. Cancer *60*, 489–494.

Krisko, A., and Radman, M. (2010). Protein damage and death by radiation in Escherichia coli and Deinococcus radiodurans. Proc. Natl. Acad. Sci. U.S.a. *107*, 14373–14377.

Krisko, A., and Radman, M. (2013). Phenotypic and genetic consequences of protein damage. PLoS Genet. *9*, e1003810.

Krokan, H.E., Drablos, F., and Slupphaug, G. (2002). Uracil in DNA-occurrence, consequences and repair. Oncogene *21*, 8935–8948.

Krokan, H.E., and Bjørås, M. (2013). Base excision repair. Cold Spring Harb Perspect Biol *5*, a012583.

Kroutil, L.C., Register, K., Bebenek, K., and Kunkel, T.A. (1996). Exonucleolytic proofreading during replication of repetitive DNA. Biochemistry *35*, 1046–1053.

Krutmann, J., and Schroeder, P. (2009). Role of mitochondria in photoaging of

human skin: the defective powerhouse model. J. Investig. Dermatol. Symp. Proc. *14*, 44–49.

Kuchel, J.M., Barnetson, R.S.C., and Halliday, G.M. (2002). Ultraviolet a augments solar-simulated ultraviolet radiation-induced local suppression of recall responses in humans. J Invest Dermatol *118*, 1032–1037.

Kunkel, T.A., and Erie, D.A. (2015). Eukaryotic Mismatch Repair in Relation to DNA Replication. Annu. Rev. Genet. *49*, 291–313.

Kuo, H.K., Griffith, J.D., and Kreuzer, K.N. (2007). 5-Azacytidine induced methyltransferase-DNA adducts block DNA replication in vivo. Cancer Res. *67*, 8248–8254.

Kurz, T., Terman, A., Gustafsson, B., and Brunk, U.T. (2008). Lysosomes and oxidative stress in aging and apoptosis. Biochim. Biophys. Acta *1780*, 1291–1303.

Kustatscher, G., Wills, K.L.H., Furlan, C., and Rappsilber, J. (2014). Chromatin enrichment for proteomics. Nat Protoc *9*, 2090–2099.

Lainé, J.P., Mocquet, V., and Egly, J.M. (2006). TFIIH enzymatic activities in transcription and nucleotide excision repair. Meth. Enzymol. *408*, 246–263.

Lamore, S.D., Azimian, S., Horn, D., Anglin, B.L., Uchida, K., Cabello, C.M., and Wondrak, G.T. (2010). The malondialdehyde-derived fluorophore DHP-lysine is a potent sensitizer of UVA-induced photooxidative stress in human skin cells. J. Photochem. Photobiol. B, Biol. *101*, 251–264.

Langlots, R., Ali, H., Brasseur, N., Wagner, J.R., and van Lier, J.E. (1986). Biological activities of phthalocyanines- IV. type II sensitized photooxidation of L-tryptophan and cholesterol by sulfonated metallo phthalocyanines. Photochemistry and Photobiology *44*, 117–123.

Lasch, P., Petras, T., Ullrich, O., Backmann, J., Naumann, D., and Grune, T. (2001). Hydrogen peroxide-induced structural alterations of RNAse A. J. Biol. Chem. *276*, 9492–9502.

Leonard, S.E., Reddie, K.G., and Carroll, K.S. (2009). Mining the thiol proteome for sulfenic acid modifications reveals new targets for oxidation in cells. ACS Chem. Biol. *4*, 783–799.

Lhiaubet-Vallet, V., Sarabia, Z., Hernández, D., Castell, J.V., and Miranda, M.A. (2003). In vitro studies on DNA-photosensitization by different drug stereoisomers. Toxicol in Vitro *17*, 651–656.

Lhiaubet-Vallet, V., Bosca, F., and Miranda, M.A. (2009). Photosensitized DNA damage: the case of fluoroquinolones. Photochemistry and Photobiology *85*, 861–868.

Lhiaubet-Vallet, V., Cuquerella, M.C., Castell, J.V., Bosca, F., and Miranda, M.A. (2007). Triplet excited fluoroquinolones as mediators for thymine cyclobutane dimer formation in DNA. J Phys Chem B *111*, 7409–7414.

Lieber, M.R., Lu, H., Gu, J., and Schwarz, K. (2008). Flexibility in the order of action and in the enzymology of the nuclease, polymerases, and ligase of vertebrate non-homologous DNA end joining: relevance to cancer, aging, and the immune system. Cell Res. *18*, 125–133.

Limoli, C.L., Giedzinski, E., Bonner, W.M., and Cleaver, J.E. (2002). UV-induced replication arrest in the xeroderma pigmentosum variant leads to DNA double-strand breaks, gamma -H2AX formation, and Mre11 relocalization. Proc. Natl. Acad. Sci. U.S.a. *99*, 233–238.

Lin, Y.L., Shivji, M.K., Chen, C., Kolodner, R., Wood, R.D., and Dutta, A. (1998). The evolutionarily conserved zinc finger motif in the largest subunit of human replication protein A is required for DNA replication and mismatch repair but not for nucleotide excision repair. J. Biol. Chem. *273*, 1453–1461.

Lindahl, T. (1974). An N-glycosidase from Escherichia coli that releases free uracil from DNA containing deaminated cytosine residues. Proc. Natl. Acad. Sci. U.S.a. *71*, 3649–3653.

Lindahl, T. (1993). Instability and decay of the primary structure of DNA. Nature *362*, 709–715.

Lindahl, T., and Nyberg, B. (1972). Rate of depurination of native deoxyribonucleic acid. Biochemistry *11*, 3610–3618.

Lipinski, B. (2011). Hydroxyl radical and its scavengers in health and disease. Oxid Med Cell Longev *2011*, 809696.

Liu, L., and Huang, M. (2015). Essential role of the iron-sulfur cluster binding domain of the primase regulatory subunit Pri2 in DNA replication initiation. Protein Cell *6*, 194–210.

Liu, T., and Huang, J. (2016). Replication protein A and more: single-stranded DNA-binding proteins in eukaryotic cells. Acta Biochim. Biophys. Sin. (Shanghai) *48*, 665–670.

Long, M.D., Herfarth, H.H., Pipkin, C.A., Porter, C.Q., Sandler, R.S., and Kappelman, M.D. (2010). Increased risk for non-melanoma skin cancer in patients with inflammatory bowel disease. Clin. Gastroenterol. Hepatol. *8*, 268–274.

Lu, K., Ye, W., Zhou, L., Collins, L.B., Chen, X., Gold, A., Ball, L.M., and Swenberg, J.A. (2010). Structural characterization of formaldehyde-induced cross-links between amino acids and deoxynucleosides and their oligomers. J. Am. Chem. Soc. *132*, 3388–3399.

Lukas, J., Lukas, C., and Bartek, J. (2011). More than just a focus: The chromatin response to DNA damage and its role in genome integrity maintenance. Nat. Cell Biol. *13*, 1161–1169.

MacDougall, C.A., Byun, T.S., Van, C., Yee, M.-C., and Cimprich, K.A. (2007). The structural determinants of checkpoint activation. Genes Dev. *21*, 898–903.

Mahmoud, B.H., Hexsel, C.L., and Hamzavi, I.H. (2008). Effects of visible light on the skin. Photochemistry and Photobiology *84*, 450–462.

Malayappan, B., Garrett, T.J., Segal, M., and Leeuwenburgh, C. (2007). Urinary analysis of 8-oxoguanine, 8-oxoguanosine, fapy-guanine and 8-oxo-2'-deoxyguanosine by high-performance liquid chromatography-electrospray tandem mass spectrometry as a measure of oxidative stress. J Chromatogr A *1167*, 54–62.

Mann, M. (2006). Functional and quantitative proteomics using SILAC. Nat. Rev. Mol. Cell Biol. *7*, 952–958.

Marteijn, J.A., Lans, H., Vermeulen, W., and Hoeijmakers, J.H.J. (2014). Understanding nucleotide excision repair and its roles in cancer and ageing. Nat. Rev. Mol. Cell Biol. *15*, 465–481.

Masutani, C., Araki, M., Yamada, A., Kusumoto, R., Nogimori, T., Maekawa, T., Iwai, S., and Hanaoka, F. (1999). Xeroderma pigmentosum variant (XP-V) correcting protein from HeLa cells has a thymine dimer bypass DNA polymerase activity. Embo J. *18*, 3491–3501.

Mathieu, N., Kaczmarek, N., Rüthemann, P., Luch, A., and Naegeli, H. (2013). DNA quality control by a lesion sensor pocket of the xeroderma pigmentosum group D helicase subunit of TFIIH. Curr. Biol. *23*, 204–212.

Matsumura, Y., and Ananthaswamy, H.N. (2004). Toxic effects of ultraviolet radiation on the skin. Toxicol. Appl. Pharmacol. *195*, 298–308.

Maxwell, A. (1992). The molecular basis of quinolone action. J. Antimicrob. Chemother. *30*, 409–414.

Mäkinen, M., Forbes, P.D., and Stenbäck, F. (1997). Quinolone antibacterials: a new class of photochemical carcinogens. J. Photochem. Photobiol. B, Biol. *37*, 182–187.

McAdam, E., Brem, R., and Karran, P. (2016). Oxidative Stress-Induced Protein Damage Inhibits DNA Repair and Determines Mutation Risk and Therapeutic Efficacy. Mol. Cancer Res. *14*, 612–622.

McClendon, A.K., and Osheroff, N. (2007). DNA topoisomerase II, genotoxicity, and cancer. Mutat. Res. *623*, 83–97.

McCulloch, S.D., and Kunkel, T.A. (2008). The fidelity of DNA synthesis by eukaryotic replicative and translesion synthesis polymerases. Cell Res. *18*, 148–161.

McIlwraith, M.J., McIlwraith, M.J., Vaisman, A., Liu, Y., Fanning, E., Woodgate, R., and West, S.C. (2005). Human DNA polymerase eta promotes DNA synthesis from strand invasion intermediates of homologous recombination. Mol. Cell *20*, 783–792.

Melnikova, V.O., and Ananthaswamy, H.N. (2005). Cellular and molecular events leading to the development of skin cancer. Mutat. Res. *571*, 91–106.

Melov, S., Schneider, J.A., Day, B.J., Hinerfeld, D., Coskun, P., Mirra, S.S., Crapo, J.D., and Wallace, D.C. (1998). A novel neurological phenotype in mice lacking mitochondrial manganese superoxide dismutase. Nat. Genet. *18*, 159–163.

Men, L., Roginskaya, M., Zou, Y., and Wang, Y. (2007). Redox-dependent formation of disulfide bonds in human replication protein A. Rapid Commun. Mass Spectrom. *21*, 2743–2749.

Mer, G., Bochkarev, A., Gupta, R., Bochkareva, E., Frappier, L., Ingles, C.J., Edwards, A.M., and Chazin, W.J. (2000). Structural basis for the recognition of DNA repair proteins UNG2, XPA, and RAD52 by replication factor RPA. Cell *103*, 449–456.

Mimitou, E.P., and Symington, L.S. (2009). Nucleases and helicases take center stage in homologous recombination. Trends Biochem. Sci. *34*, 264–272.

Min, J.-H., and Pavletich, N.P. (2007). Recognition of DNA damage by the Rad4 nucleotide excision repair protein. Nature *449*, 570–575.

Mirzaei, H., and Regnier, F. (2008). Protein:protein aggregation induced by protein oxidation. J. Chromatogr. B Analyt. Technol. Biomed. Life Sci. *873*, 8–14.

Mittler, G., Butter, F., and Mann, M. (2009). A SILAC-based DNA protein interaction screen that identifies candidate binding proteins to functional DNA elements. Genome Res *19*, 284–293.

Moan, J., Nielsen, K.P., and Juzeniene, A. (2012). Immediate pigment darkening: its evolutionary roles may include protection against folate photosensitization. Faseb J. *26*, 971–975.

Mocquet, V., Lainé, J.P., Riedl, T., Yajin, Z., Lee, M.Y., and Egly, J.M. (2008). Sequential recruitment of the repair factors during NER: the role of XPG in initiating the resynthesis step. Embo J. *27*, 155–167.

Mohammed, H., Taylor, C., Brown, G.D., Papachristou, E.K., Carroll, J.S., and D'Santos, C.S. (2016). Rapid immunoprecipitation mass spectrometry of endogenous proteins (RIME) for analysis of chromatin complexes. Nat Protoc *11*, 316–326.

Montaner, B., O'Donovan, P., Reelfs, O., Perrett, C.M., Zhang, X., Xu, Y.-Z., Ren, X., Macpherson, P., Frith, D., and Karran, P. (2007). Reactive oxygen-mediated damage to a human DNA replication and repair protein. EMBO Rep. *8*, 1074–1079.

Moorhouse, P.C., Grootveld, M., Halliwell, B., Quinlan, J.G., and Gutteridge, J.M. (1987). Allopurinol and oxypurinol are hydroxyl radical scavengers. FEBS Lett. *213*, 23–28.

Morgan, P.E., Dean, R.T., and Davies, M.J. (2002). Inhibition of glyceraldehyde-3-phosphate dehydrogenase by peptide and protein peroxides generated by singlet oxygen attack. Eur. J. Biochem. *269*, 1916–1925.

Moser, J., Kool, H., Giakzidis, I., Caldecott, K., Mullenders, L.H.F., and Fousteri,

M.I. (2007). Sealing of chromosomal DNA nicks during nucleotide excision repair requires XRCC1 and DNA ligase III alpha in a cell-cycle-specific manner. Mol. Cell *27*, 311–323.

Mouret, S., Baudouin, C., Charveron, M., Favier, A., Cadet, J., and Douki, T. (2006). Cyclobutane pyrimidine dimers are predominant DNA lesions in whole human skin exposed to UVA radiation. Proc. Natl. Acad. Sci. U.S.a. *103*, 13765–13770.

Murray, C.I., and Van Eyk, J.E. (2012). Chasing cysteine oxidative modifications: proteomic tools for characterizing cysteine redox status. Circ Cardiovasc Genet *5*, 591.

Nagelhus, T.A., Haug, T., Singh, K.K., Keshav, K.F., Skorpen, F., Otterlei, M., Bharati, S., Lindmo, T., Benichou, S., Benarous, R., et al. (1997). A sequence in the N-terminal region of human uracil-DNA glycosylase with homology to XPA interacts with the C-terminal part of the 34-kDa subunit of replication protein A. J. Biol. Chem. *272*, 6561–6566.

Nakano, T., Ouchi, R., Kawazoe, J., Pack, S.P., Makino, K., and Ide, H. (2012). T7 RNA polymerases backed up by covalently trapped proteins catalyze highly error prone transcription. J. Biol. Chem. *287*, 6562–6572.

Natarajan, V.T., Ganju, P., Ramkumar, A., Grover, R., and Gokhale, R.S. (2014a). Multifaceted pathways protect human skin from UV radiation. Nat. Chem. Biol. *10*, 542–551.

Natarajan, V.T., Ganju, P., Singh, A., Vijayan, V., Kirty, K., Yadav, S., Puntambekar, S., Bajaj, S., Dani, P.P., Kar, H.K., et al. (2014b). IFN-γ signaling maintains skin pigmentation homeostasis through regulation of melanosome maturation. Proc. Natl. Acad. Sci. U.S.a. *111*, 2301–2306.

Neuzil, J., Gebicki, J.M., and Stocker, R. (1993). Radical-induced chain oxidation of proteins and its inhibition by chain-breaking antioxidants. Biochem. J. *293 (Pt 3)*, 601–606.

Niedernhofer, L.J. (2007). The Fanconi anemia signalosome anchor. Mol. Cell *25*, 487–490.

Nimse, S.B., and Pal, D. (2015). Free radicals, natural antioxidants, and their reaction mechanisms. RSC Advances *5*, 27986–28006.

Nishi, R., Okuda, Y., Watanabe, E., Mori, T., Iwai, S., Masutani, C., Sugasawa, K., and Hanaoka, F. (2005). Centrin 2 stimulates nucleotide excision repair by interacting with xeroderma pigmentosum group C protein. Mol. Cell. Biol. *25*, 5664–5674.

Nordberg, J., and Arner, E. (2001). Reactive oxygen species, antioxidants, and the mammalian thioredoxin system. Free Radic. Biol. Med. *31*, 1287–1312.

Norval, M. (2006). The mechanisms and consequences of ultraviolet-induced

immunosuppression. Prog. Biophys. Mol. Biol. *92*, 108–118.

O'Donovan, P., Perrett, C.M., Zhang, X., Montaner, B., Xu, Y.-Z., Harwood, C.A., McGregor, J.M., Walker, S.L., Hanaoka, F., and Karran, P. (2005). Azathioprine and UVA light generate mutagenic oxidative DNA damage. Science *309*, 1871–1874.

Oakley, G.G., and Patrick, S.M. (2010). Replication protein A: directing traffic at the intersection of replication and repair. Front Biosci (Landmark Ed) *15*, 883–900.

Oberg, M., Bergander, L., Håkansson, H., Rannug, U., and Rannug, A. (2005). Identification of the tryptophan photoproduct 6-formylindolo[3,2-b]carbazole, in cell culture medium, as a factor that controls the background aryl hydrocarbon receptor activity. Toxicol. Sci. *85*, 935–943.

Ogi, T., Limsirichaikul, S., Overmeer, R.M., Volker, M., Takenaka, K., Cloney, R., Nakazawa, Y., Niimi, A., Miki, Y., Jaspers, N.G., et al. (2010). Three DNA polymerases, recruited by different mechanisms, carry out NER repair synthesis in human cells. Mol. Cell *37*, 714–727.

Ogilby, P.R. (2010). Singlet oxygen: there is indeed something new under the sun. Chem Soc Rev *39*, 3181–3209.

Oleinick, N.L., Kim, J., Rodriguez, M.E., Xue, L.-Y., Kenney, M.E., and Anderson, V.E. (2009). Identifying initial molecular targets of PDT: protein and lipid oxidation products. 12th World Congress of the

International Photodynamic Association *7380*.

Olson, J.A., and Krinsky, N.I. (1995). Introduction: the colorful, fascinating world of the carotenoids: important physiologic modulators. Faseb J. *9*, 1547–1550.

Ouédraogo, G., Morlière, P., Bazin, M., Santus, R., Kratzer, B., Miranda, M.A., and Castell, J.V. (1999). Lysosomes are sites of fluoroquinolone photosensitization in human skin fibroblasts: a microspectrofluorometric approach. Photochemistry and Photobiology *70*, 123–129.

Overmeer, R.M., Moser, J., Volker, M., Kool, H., Tomkinson, A.E., van Zeeland, A.A., Mullenders, L.H.F., and Fousteri, M. (2011). Replication protein A safeguards genome integrity by controlling NER incision events. J. Cell Biol. *192*, 401–415.

Park, J.S., Wang, M., Park, S.J., and Lee, S.H. (1999). Zinc finger of replication protein A, a non-DNA binding element, regulates its DNA binding activity through redox. J. Biol. Chem. *274*, 29075–29080.

Park, S.L., Justiniano, R., Williams, J.D., Cabello, C.M., Qiao, S., and Wondrak, G.T. (2015). The Tryptophan-Derived Endogenous Aryl Hydrocarbon Receptor Ligand 6-Formylindolo[3,2-b]Carbazole Is a Nanomolar UVA Photosensitizer in Epidermal Keratinocytes. J Invest Dermatol *135*, 1649–1658.

Pattison, D.I., and Davies, M.J. (2006). Actions of ultraviolet light on cellular structures. Exs 131–157.

Pavlovic, R., and Santaniello, E. (2007). Peroxynitrite and nitrosoperoxycarbonate, a tightly connected oxidizing-nitrating couple in the reactive nitrogen-oxygen species family: new perspectives for protection from radical-promoted injury by flavonoids. J. Pharm. Pharmacol. *59*, 1687–1695.

Peacock, M., Brem, R., Macpherson, P., and Karran, P. (2014). DNA repair inhibition by UVA photoactivated fluoroquinolones and vemurafenib. Nucleic Acids Res. *42*, 13714–13722.

Perdiz, D., Grof, P., Mezzina, M., Nikaido, O., Moustacchi, E., and Sage, E. (2000). Distribution and repair of bipyrimidine photoproducts in solar UV-irradiated mammalian cells. Possible role of Dewar photoproducts in solar mutagenesis. J. Biol. Chem. *275*, 26732–26742.

Perrett, C.M., Walker, S.L., O'Donovan, P., Warwick, J., Harwood, C.A., Karran, P., and McGregor, J.M. (2008). Azathioprine treatment photosensitizes human skin to ultraviolet A radiation. Br. J. Dermatol. *159*, 198–204.

Perrier, S., Hau, J., Gasparutto, D., Cadet, J., Favier, A., and Ravanat, J.-L. (2006). Characterization of lysine-guanine cross-links upon one-electron oxidation of a guanine-containing oligonucleotide in the presence of a trilysine peptide. J. Am. Chem. Soc. *128*, 5703–5710.

Perry, J.J.P., Yannone, S.M., Holden, L.G., Hitomi, C., Asaithamby, A., Han, S., Cooper, P.K., Chen, D.J., and Tainer, J.A. (2006). WRN exonuclease structure and molecular mechanism imply an editing role in DNA end processing. Nat. Struct. Mol. Biol. *13*, 414–422.

Peyrin-Biroulet, L., Khosrotehrani, K., Carrat, F., Bouvier, A.-M., Chevaux, J.-B., Simon, T., Carbonnel, F., Colombel, J.-F., Dupas, J.-L., Godeberge, P., et al. (2011). Increased risk for nonmelanoma skin cancers in patients who receive thiopurines for inflammatory bowel disease. Gastroenterology *141*, 1621–28.e1–5.

Pileni, M.P., Giraud, M., and Santus, R. (1979). Kynurenic acid-II. photosensitising properties. Photochemistry and Photobiology *30*, 257–261.

Pileni, M.P., Santus, R., and Land, E.J. (1978). On the photosensitizing properties of N-formylkynurenine and related compounds. Photochemistry and Photobiology *28*, 525–529.

Polefka, T.G., Meyer, T.A., Agin, P.P., and Bianchini, R.J. (2012). Effects of solar radiation on the skin. J Cosmet Dermatol *11*, 134–143.

Pommier, Y. (2006). Topoisomerase I inhibitors: camptothecins and beyond. Nat. Rev. Cancer *6*, 789–802.

Pourquier, P., and Pommier, Y. (2001). Topoisomerase I-mediated DNA damage. Adv. Cancer Res. *80*, 189–216.

Pourquier, P., Ueng, L.M., Kohlhagen, G., Mazumder, A., Gupta, M., Kohn, K.W., and Pommier, Y. (1997). Effects of uracil incorporation, DNA mismatches, and

abasic sites on cleavage and religation activities of mammalian topoisomerase I. J. Biol. Chem. *272*, 7792–7796.

Prinsze, C., Dubbelman, T.M., and Van Steveninck, J. (1990). Protein damage, induced by small amounts of photodynamically generated singlet oxygen or hydroxyl radicals. Biochim. Biophys. Acta *1038*, 152–157.

Proietti-De-Santis, L., Drané, P., and Egly, J.M. (2006). Cockayne syndrome B protein regulates the transcriptional program after UV irradiation. Embo J. *25*, 1915–1923.

Pryor, W.A., and Porter, N.A. (1990). Suggested mechanisms for the production of 4-hydroxy-2-nonenal from the autoxidation of polyunsaturated fatty acids. Free Radic. Biol. Med. *8*, 541–543.

Qian, J., Klomsiri, C., Wright, M.W., King, S.B., Tsang, A.W., Poole, L.B., and Furdui, C.M. (2011). Simple synthesis of 1,3-cyclopentanedione derived probes for labeling sulfenic acid proteins. Chem. Commun. (Camb.) *47*, 9203–9205.

Quievryn, G., and Zhitkovich, A. (2000). Loss of DNA-protein crosslinks from formaldehyde-exposed cells occurs through spontaneous hydrolysis and an active repair process linked to proteosome function. Carcinogenesis *21*, 1573–1580.

Ramsay, H.M., Fryer, A.A., Hawley, C.M., Smith, A.G., and Harden, P.N. (2002). Non-melanoma skin cancer risk in the Queensland renal transplant population. Br. J. Dermatol. *147*, 950–956.

Ray, R.S., Agrawal, N., Misra, R.B., Farooq, M., and Hans, R.K. (2006). Radiation-induced in vitro phototoxic potential of some fluoroquinolones. Drug Chem Toxicol *29*, 25–38.

Raynard, S., Niu, H., and Sung, P. (2008). DNA double-strand break processing: the beginning of the end. Genes Dev. *22*, 2903–2907.

Räschle, M., Knipscheer, P., Knipsheer, P., Enoiu, M., Angelov, T., Sun, J., Griffith, J.D., Ellenberger, T.E., Schärer, O.D., and Walter, J.C. (2008). Mechanism of replication-coupled DNA interstrand crosslink repair. Cell *134*, 969–980.

Reardon, J.T., and Sancar, A. (2003). Recognition and repair of the cyclobutane thymine dimer, a major cause of skin cancers, by the human excision nuclease. Genes Dev. *17*, 2539–2551.

Regensburger, J., Knak, A., Maisch, T., Landthaler, M., and Bäumler, W. (2012). Fatty acids and vitamins generate singlet oxygen under UVB irradiation. Exp. Dermatol. *21*, 135–139.

Reid, T.M., and Loeb, L.A. (1993). Tandem double CC-->TT mutations are produced by reactive oxygen species. Proc. Natl. Acad. Sci. U.S.a. *90*, 3904–3907.

Reimann, V., Krämer, U., Sugiri, D., Schroeder, P., Hoffmann, B., Medve-Koenigs, K., Jöckel, K.-H., Ranft, U., and Krutmann, J. (2008). Sunbed use induces the photoaging-associated mitochondrial common deletion. J Invest Dermatol *128*,

1294–1297.

Reinheckel, T., Sitte, N., Ullrich, O., Kuckelkorn, U., Davies, K.J., and Grune, T. (1998). Comparative resistance of the 20S and 26S proteasome to oxidative stress. Biochem. J. *335 (Pt 3)*, 637–642.

Reits, E., Neijssen, J., Herberts, C., Benckhuijsen, W., Janssen, L., Drijfhout, J.W., and Neefjes, J. (2004). A major role for TPPII in trimming proteasomal degradation products for MHC class I antigen presentation. Immunity *20*, 495–506.

Requena, J.R., Chao, C.C., Levine, R.L., and Stadtman, E.R. (2001). Glutamic and aminoadipic semialdehydes are the main carbonyl products of metal-catalyzed oxidation of proteins. Proc. Natl. Acad. Sci. U.S.a. *98*, 69–74.

Rhee, S.G., Chang, T.S., Bae, Y.S., Lee, S.R., and Kang, S.W. (2003). Cellular regulation by hydrogen peroxide (J. Am. Soc. Nephrol.).

Ridpath, J.R., Nakamura, A., Tano, K., Luke, A.M., Sonoda, E., Arakawa, H., Buerstedde, J.-M., Gillespie, D.A.F., Sale, J.E., Yamazoe, M., et al. (2007). Cells deficient in the FANC/BRCA pathway are hypersensitive to plasma levels of formaldehyde. Cancer Res. *67*, 11117–11122.

Rigel, D.S. (2008). Cutaneous ultraviolet exposure and its relationship to the development of skin cancer. J. Am. Acad. Dermatol. *58*, S129–S132.

Rodgers, K.J., Wang, H., Fu, S., and Dean, R.T. (2002). Biosynthetic incorporation of oxidized amino acids into proteins and their cellular proteolysis. Free Radic. Biol. Med. *32*, 766–775.

Rosen, J.E., Prahalad, A.K., Schlüter, G., Chen, D., and Williams, G.M. (1997). Quinolone antibiotic photodynamic production of 8-oxo-7, 8-dihydro-2'-deoxyguanosine in cultured liver epithelial cells. Photochemistry and Photobiology *65*, 990–996.

Rubbo, H., Radi, R., Anselmi, D., Kirk, M., Barnes, S., Butler, J., Eiserich, J.P., and Freeman, B.A. (2000). Nitric oxide reaction with lipid peroxyl radicals spares alpha-tocopherol during lipid peroxidation. Greater oxidant protection from the pair nitric oxide/alpha-tocopherol than alpha-tocopherol/ascorbate. J. Biol. Chem. *275*, 10812–10818.

Russo, A., Acquaviva, R., Campisi, A., Sorrenti, V., Di Giacomo, C., Virgata, G., Barcellona, M.L., and Vanella, A. (2000). Bioflavonoids as antiradicals, antioxidants and DNA cleavage protectors. Cell Biol. Toxicol. *16*, 91–98.

Ryan, M.D., King, A.M., and Thomas, G.P. (1991). Cleavage of foot-and-mouth disease virus polyprotein is mediated by residues located within a 19 amino acid sequence. J. Gen. Virol. *72 (Pt 11)*, 2727–2732.

Saijo, M., Kuraoka, I., Masutani, C., Hanaoka, F., and Tanaka, K. (1996). Sequential binding of DNA repair proteins RPA and ERCC1 to XPA in vitro. Nucleic Acids Res. *24*, 4719–4724.

Saijo, M., Takedachi, A., and Tanaka, K. (2011). Nucleotide excision repair by mutant xeroderma pigmentosum group A (XPA) proteins with deficiency in interaction with RPA. J. Biol. Chem. *286*, 5476–5483.

Saito, I., Matsuura, T., and Nakagawa, M. (1977). Peroxidic intermediates in photosensitized oxygenation of tryptophan derivatives. Acc. Chem. Res. *10*, 346–352.

San Filippo, J., Sung, P., and Klein, H. (2008). Mechanism of eukaryotic homologous recombination. Annu. Rev. Biochem. *77*, 229–257.

Santocanale, C., Neecke, H., Longhese, M.P., Lucchini, G., and Plevani, P. (1995). Mutations in the gene encoding the 34 kDa subunit of yeast replication protein A cause defective S phase progression. J. Mol. Biol. *254*, 595–607.

Santus, P., Corsico, A., Solidoro, P., Braido, F., Di Marco, F., and Scichilone, N. (2014). Oxidative stress and respiratory system: pharmacological and clinical reappraisal of N-acetylcysteine. Copd *11*, 705–717.

Sauvaigo, S., Douki, T., Odin, F., Caillat, S., Ravanat, J.L., and Cadet, J. (2001). Analysis of fluoroquinolone-mediated photosensitization of 2'-deoxyguanosine, calf thymus and cellular DNA: determination of type-I, type-II and triplet-triplet energy transfer mechanism contribution. Photochemistry and Photobiology *73*, 230–237.

Schäfer, M., Schmitz, C., and Horneck, G. (1998). High sensitivity of Deinococcus radiodurans to photodynamically-produced singlet oxygen. Int. J. Radiat. Biol. *74*, 249–253.

Schärer, O.D. (2013). Nucleotide excision repair in eukaryotes. Cold Spring Harb Perspect Biol *5*, a012609.

Schieber, M., and Chandel, N.S. (2014). ROS function in redox signaling and oxidative stress. Curr. Biol. *24*, R453–R462.

Schmitt, M.W., Matsumoto, Y., and Loeb, L.A. (2009). High fidelity and lesion bypass capability of human DNA polymerase delta. Biochimie *91*, 1163–1172.

Schrader, M., and Fahimi, H.D. (2006). Peroxisomes and oxidative stress. Biochim. Biophys. Acta *1763*, 1755–1766.

Schroeder, P., and Krutmann, J. (2010). Infrared A-induced Skin Aging. In Textbook of Aging Skin, M.A. Farage, K.W. Miller, and H.I. Mailbach, eds. (Springer), pp. 421–425.

Schroeder, P., Haendeler, J., and Krutmann, J. (2008). The role of near infrared radiation in photoaging of the skin. Exp. Gerontol. *43*, 629–632.

Scrima, A., Konícková, R., Czyzewski, B.K., Kawasaki, Y., Jeffrey, P.D., Groisman, R., Nakatani, Y., Iwai, S., Pavletich, N.P., and Thomä, N.H. (2008). Structural basis of UV DNA-damage recognition by the DDB1-DDB2 complex. Cell *135*, 1213–1223.

Seki, M., Nakagawa, T., Seki, T., Kato, G., Tada, S., Takahashi, Y., Yoshimura, A., Kobayashi, T., Aoki, A., Otsuki, M., et al. (2006). Bloom helicase and DNA topoisomerase IIIalpha are involved in the dissolution of sister chromatids. Mol. Cell. Biol. *26*, 6299–6307.

Sertic, S., Pizzi, S., Cloney, R., Lehmann, A.R., Marini, F., Plevani, P., and Muzi-Falconi, M. (2011). Human exonuclease 1 connects nucleotide excision repair (NER) processing with checkpoint activation in response to UV irradiation. Proc. Natl. Acad. Sci. U.S.a. *108*, 13647–13652.

Setshedi, M., Epstein, D., Winter, T.A., Myer, L., Watermeyer, G., and Hift, R. (2012). Use of thiopurines in the treatment of inflammatory bowel disease is associated with an increased risk of non-melanoma skin cancer in an at-risk population: a cohort study. J. Gastroenterol. Hepatol. *27*, 385–389.

Shaham, J., Bomstein, Y., Melzer, A., and Ribak, J. (1997). DNA-Protein Crosslinks and Sister Chromatid Exchanges as Biomarkers of Exposure to Formaldehyde. Int J Occup Environ Health *3*, 95–104.

Shang, F., and Taylor, A. (1995). Oxidative stress and recovery from oxidative stress are associated with altered ubiquitin conjugating and proteolytic activities in bovine lens epithelial cells. Biochem. J. *307 (Pt 1)*, 297–303.

Shen, H.R., Spikes, J.D., and Kopečeková, P. (1996). Photodynamic crosslinking of proteins. I. Model studies using histidine-and lysine-containing N-(2-hydroxypropyl) methacrylamide copolymers. J. Photochem. Photobiol. B, Biol. *34*, 203–210.

Shen, H.R., Spikes, J.D., Smith, C.J., and Kopeček, J. (2000). Photodynamic cross-linking of proteins: IV. Nature of the His–His bond (s) formed in the rose bengal-photosensitized cross-linking of N-benzoyl-L-histidine. J. Photochem. Photobiol. a, Chem. *130*, 1–6.

Sheng, Y., Abreu, I.A., Cabelli, D.E., Maroney, M.J., Miller, A.-F., Teixeira, M., and Valentine, J.S. (2014). Superoxide dismutases and superoxide reductases. Chem. Rev. *114*, 3854–3918.

Shi, W., Feng, Z., Zhang, J., Gonzalez-Suarez, I., Vanderwaal, R.P., Wu, X., Powell, S.N., Roti Roti, J.L., Gonzalo, S., and Zhang, J. (2010). The role of RPA2 phosphorylation in homologous recombination in response to replication arrest. Carcinogenesis *31*, 994–1002.

Shimizu, M., Gruz, P., Kamiya, H., Kim, S.-R., Pisani, F.M., Masutani, C., Kanke, Y., Harashima, H., Hanaoka, F., and Nohmi, T. (2003). Erroneous incorporation of oxidized DNA precursors by Y-family DNA polymerases. EMBO Rep. *4*, 269–273.

Shoulkamy, M.I., Nakano, T., Ohshima, M., Hirayama, R., Uzawa, A., Furusawa, Y., and Ide, H. (2012). Detection of DNA-protein crosslinks (DPCs) by novel direct fluorescence labeling methods: distinct stabilities of aldehyde and radiation-induced DPCs. Nucleic Acids Res. *40*, e143–e143.

Silverstein, T.D., Johnson, R.E., Jain, R., Prakash, L., Prakash, S., and Aggarwal, A.K. (2010). Structural basis for the suppression of skin cancers by DNA polymerase eta. Nature *465*, 1039–1043.

Silvester, J.A., Timmins, G.S., and Davies, M.J. (1998). Protein hydroperoxides and carbonyl groups generated by porphyrin-induced photo-oxidation of bovine serum albumin. Arch. Biochem. Biophys. *350*, 249–258.

Singh, J., Dwivedi, A., Mujtaba, S.F., Singh, K.P., Pal, M.K., Chopra, D., Goyal, S., Srivastav, A.K., Dubey, D., Gupta, S.K., et al. (2016). Ambient UV-B exposure reduces the binding of ofloxacin with bacterial DNA gyrase and induces DNA damage mediated apoptosis. Int. J. Biochem. Cell Biol. *73*, 111–126.

Skinner, A.M., and Turker, M.S. (2008). High frequency induction of CC to TT tandem mutations in DNA repair-proficient mammalian cells. Photochemistry and Photobiology *84*, 222–227.

Smerdon, M.J. (1991). DNA repair and the role of chromatin structure. Curr. Opin. Cell Biol. *3*, 422–428.

Smerdon, M.J., and Lieberman, M.W. (1978). Nucleosome rearrangement in human chromatin during UV-induced DNA- reapir synthesis. Proc. Natl. Acad. Sci. U.S.a. *75*, 4238–4241.

Soldi, M., and Bonaldi, T. (2014). The ChroP approach combines ChIP and mass spectrometry to dissect locus-specific proteomic landscapes of chromatin. J Vis Exp.

Solomon, M.J., Larsen, P.L., and Varshavsky, A. (1988). Mapping protein-DNA interactions in vivo with formaldehyde: evidence that histone H4 is retained on a highly transcribed gene. Cell *53*, 937–947.

Souza, J.M., Giasson, B.I., Chen, Q., Lee, V.M., and Ischiropoulos, H. (2000). Dityrosine cross-linking promotes formation of stable alpha -synuclein polymers. Implication of nitrative and oxidative stress in the pathogenesis of neurodegenerative synucleinopathies. J. Biol. Chem. *275*, 18344–18349.

Spratt, T.E., Schultz, S.S., Levy, D.E., Chen, D., Schlüter, G., and Williams, G.M. (1999). Different mechanisms for the photoinduced production of oxidative DNA damage by fluoroquinolones differing in photostability. Chem. Res. Toxicol. *12*, 809–815.

Stadtman, E.R., and Levine, R.L. (2000). Protein oxidation. Ann. N. Y. Acad. Sci. *899*, 191–208.

Steinbeck, M.J., Khan, A.U., and Karnovsky, M.J. (1993). Extracellular production of singlet oxygen by stimulated macrophages quantified using 9,10-diphenylanthracene and perylene in a polystyrene film. J. Biol. Chem. *268*, 15649–15654.

Steinberg, D. (1997). Low density lipoprotein oxidation and its pathobiological

significance. J. Biol. Chem. *272*, 20963–20966.

Stingele, J., Habermann, B., and Jentsch, S. (2015). DNA-protein crosslink repair: proteases as DNA repair enzymes. Trends Biochem. Sci. *40*, 67–71.

Stockfleth, E., and Ulrich, C. (2009). Skin Cancer after Organ Transplantation (New York: Springer Science & Business Media).

Strickland, E., Hakala, K., Thomas, P.J., and DeMartino, G.N. (2000). Recognition of misfolding proteins by PA700, the regulatory subcomplex of the 26 S proteasome. J. Biol. Chem. *275*, 5565–5572.

Subramanian, D., and Furbee, C.S. (2001). ICE Bioassay: Isolating in vivo complexes of enzyme to DNA. In DNA Topoisomerase Protocols: Enzymology and Drugs, N. Osheroff, and M.-A. Bjornsti, eds. (Humana Press), pp. 137–147.

Sugasawa, K., Akagi, J.-I., Nishi, R., Iwai, S., and Hanaoka, F. (2009). Two-step recognition of DNA damage for mammalian nucleotide excision repair: Directional binding of the XPC complex and DNA strand scanning. Mol. Cell *36*, 642–653.

Sugiyama, H., Fujiwara, T., Ura, A., Tashiro, T., Yamamoto, K., Kawanishi, S., and Saito, I. (1994). Chemistry of thermal degradation of abasic sites in DNA. Mechanistic investigation on thermal DNA strand cleavage of alkylated DNA. Chem. Res. Toxicol. *7*, 673–683.

Sun, Y.W., Heo, E.P., Cho, Y.H., Bark, K.M., Yoon, T.J., and Kim, T.H. (2001). Pefloxacin and ciprofloxacin increase UVA-induced edema and immune suppression. Photodermatol Photoimmunol Photomed *17*, 172–177.

Svilar, D., Goellner, E.M., Almeida, K.H., and Sobol, R.W. (2011). Base excision repair and lesion-dependent subpathways for repair of oxidative DNA damage. Antioxid. Redox Signal. *14*, 2491–2507.

Svobodova, A., and Vostalova, J. (2010). Solar radiation induced skin damage: review of protective and preventive options. Int. J. Radiat. Biol. *86*, 999–1030.

Svobodova, A., Walterova, D., and Vostalova, J. (2006). Ultraviolet light induced alteration to the skin. Biomed Pap Med Fac Univ Palacky Olomouc Czech Repub *150*, 25–38.

Swann, P.F., Waters, T.R., Moulton, D.C., Xu, Y.-Z., Zheng, Q., Edwards, M., and Mace, R. (1996). Role of postreplicative DNA mismatch repair in the cytotoxic action of thioguanine. Science *273*, 1109–1111.

Sysak, P.K., Foote, C.S., and Ching, T.Y. (1977). Chemistry of singlet oxygen—XXV. Photooxygenation of methionine. Photochemistry and Photobiology *26*, 19–27.

Szüts, D., Marcus, A.P., Himoto, M., Iwai, S., and Sale, J.E. (2008). REV1 restrains DNA polymerase zeta to ensure frame fidelity during translesion synthesis of UV photoproducts in vivo. Nucleic Acids Res. *36*, 6767–6780.

Toledo, L.I., Altmeyer, M., Rask, M.-B., Lukas, C., Larsen, D.H., Povlsen, L.K., Bekker-Jensen, S., Mailand, N., Bartek, J., and Lukas, J. (2013). ATR prohibits replication catastrophe by preventing global exhaustion of RPA. Cell *155*, 1088–1103.

Tran, P.T., Erdeniz, N., Symington, L.S., and Liskay, R.M. (2004). EXO1-A multi-tasking eukaryotic nuclease. DNA Repair (Amst.) *3*, 1549–1559.

Tretyakova, N.Y., Groehler, A., and Ji, S. (2015). DNA-Protein Cross-Links: Formation, Structural Identities, and Biological Outcomes. Acc. Chem. Res. *48*, 1631–1644.

Trujillo, M., Ferrer-Sueta, G., Thomson, L., Flohé, L., and Radi, R. (2007). Kinetics of peroxiredoxins and their role in the decomposition of peroxynitrite. Subcellular Biochemistry *44*, 83–113.

Tsaalbi-Shtylik, A., Moser, J., Mullenders, L.H.F., Jansen, J.G., and de Wind, N. (2014). Persistently stalled replication forks inhibit nucleotide excision repair in trans by sequestering Replication protein A. Nucleic Acids Res. *42*, 4406–4413.

Tsodikov, O.V., Ivanov, D., Orelli, B., Staresincic, L., Shoshani, I., Oberman, R., Schärer, O.D., Wagner, G., and Ellenberger, T. (2007). Structural basis for the recruitment of ERCC1-XPF to nucleotide excision repair complexes by XPA. Embo J. *26*, 4768–4776.

Tyrrell, R.M. (1973). Induction of pyrimidine dimers in bacterial DNA by 365 nm radiation. Photochemistry and Photobiology *17*, 69–73.

Tyrrell, R.M., Werfelli, P., and Moraes, E.C. (1984). Lethal action of ultraviolet and visible (blue-violet) radiations at defined wavelengths on human lymphoblastoid cells: action spectra and interaction sites. Photochemistry and Photobiology *39*, 183–189.

Urabe, K., Aroca, P., Tsukamoto, K., Mascagna, D., Palumbo, A., Prota, G., and Hearing, V.J. (1994). The inherent cytotoxicity of melanin precursors: a revision. Biochim. Biophys. Acta *1221*, 272–278.

Valko, M., Rhodes, C.J., Moncol, J., and Izakovic, M.M. (2006). Free radicals, metals and antioxidants in oxidative stress-induced cancer. Chemico-Biological Interactions *160*, 1–40.

Verschooten, L., Claerhout, S., Van Laethem, A., Agostinis, P., and Garmyn, M. (2006). New strategies of photoprotection. Photochemistry and Photobiology *82*, 1016–1023.

Vilfan, I.D., Drevenšek, P., Turel, I., and Ulrih, N.P. (2003). Characterization of ciprofloxacin binding to the linear single-and double-stranded DNA. Biochim. Biophys. Acta *1628*, 111–122.

Viola, G., Facciolo, L., Canton, M., Vedaldi, D., Dall'Acqua, F., Aloisi, G.G., Amelia, M., Barbafina, A., Elisei, F., and Latterini, L. (2004). Photophysical and phototoxic

properties of the antibacterial fluoroquinolones levofloxacin and moxifloxacin. Chem. Biodivers. *1*, 782–801.

Vitasa, B.C., Taylor, H.R., Strickland, P.T., Rosenthal, F.S., West, S., Abbey, H., Ng, S.K., Munoz, B., and Emmett, E.A. (1990). Association of nonmelanoma skin cancer and actinic keratosis with cumulative solar ultraviolet exposure in Maryland watermen. Cancer *65*, 2811–2817.

Wagai, N., and Tawara, K. (1991). Important role of oxygen metabolites in quinolone antibacterial agent-induced cutaneous phototoxicity in mice. Arch. Toxicol. *65*, 495–499.

Walker, J.R., Corpina, R.A., and Goldberg, J. (2001). Structure of the Ku heterodimer bound to DNA and its implications for double-strand break repair. Nature *412*, 607–614.

Wang, Y., Jones-Tabah, J., Chakravarty, P., Stewart, A., Muotri, A., Laposa, R.R., and Svejstrup, J.Q. (2016). Pharmacological Bypass of Cockayne Syndrome B Function in Neuronal Differentiation. Cell Rep *14*, 2554–2561.

Wang, Y., Putnam, C.D., Kane, M.F., Zhang, W., Edelmann, L., Russell, R., Carrión, D.V., Chin, L., Kucherlapati, R., Kolodner, R.D., et al. (2005). Mutation in Rpa1 results in defective DNA double-strand break repair, chromosomal instability and cancer in mice. Nat. Genet. *37*, 750–755.

Waters, L.S., Minesinger, B.K., Wiltrout, M.E., D'Souza, S., Woodruff, R.V., and Walker, G.C. (2009). Eukaryotic translesion polymerases and their roles and regulation in DNA damage tolerance. Microbiol. Mol. Biol. Rev. *73*, 134–154.

Wefers, H., and Sies, H. (1988). The protection by ascorbate and glutathione against microsomal lipid peroxidation is dependent on vitamin E. Eur. J. Biochem. *174*, 353–357.

Wickham, H. (2009). ggplot2: elegant graphics for data analysis.

Wicks, N.L., Chan, J.W., Najera, J.A., Ciriello, J.M., and Oancea, E. (2011). UVA phototransduction drives early melanin synthesis in human melanocytes. Curr. Biol. *21*, 1906–1911.

Wilkinson, F., Helman, W.P., and Ross, A.B. (1995). Rate constants for the decay and reactions of the lowest electronically excited singlet state of molecular oxygen in solution. An expanded and revised compilation. J. Phys. Chem. Ref. Data *24*, 113–262.

Wink, D.A., and Mitchell, J.B. (1998). Chemical biology of nitric oxide: Insights into regulatory, cytotoxic, and cytoprotective mechanisms of nitric oxide. Free Radic. Biol. Med. *25*, 434–456.

Winterbourn, C.C., Vissers, M.C., and Kettle, A.J. (2000). Myeloperoxidase. Curr. Opin. Hematol. *7*, 53–58.

Winterbourn, C.C. (2013). The biological chemistry of hydrogen peroxide. Meth.

Enzymol. *528*, 3–25.

Winterbourn, C.C., and Hampton, M.B. (2008). Thiol chemistry and specificity in redox signaling. Free Radic. Biol. Med. *45*, 549–561.

Wold, M.S. (1997). Replication protein A: a heterotrimeric, single-stranded DNA-binding protein required for eukaryotic DNA metabolism. Annu. Rev. Biochem. *66*, 61–92.

Wondrak, G.T., Roberts, M.J., Cervantes-Laurean, D., Jacobson, M.K., and Jacobson, E.L. (2003). Proteins of the extracellular matrix are sensitizers of photo-oxidative stress in human skin cells. J Invest Dermatol *121*, 578–586.

Wright, A., Bubb, W.A., Hawkins, C.L., and Davies, M.J. (2002). Singlet oxygen-mediated protein oxidation: evidence for the formation of reactive side chain peroxides on tyrosine residues. Photochemistry and Photobiology *76*, 35–46.

Wu, X., Yang, Z., Liu, Y., and Zou, Y. (2005). Preferential localization of hyperphosphorylated replication protein A to double-strand break repair and checkpoint complexes upon DNA damage. Biochem. J. *391*, 473–480.

Xu, G., and Chance, M.R. (2007). Hydroxyl radical-mediated modification of proteins as probes for structural proteomics. Chem. Rev. *107*, 3514–3543.

Yamaguchi, Y., Brenner, M., and Hearing, V.J. (2007). The regulation of skin pigmentation. J. Biol. Chem. *282*, 27557–27561.

Yan, T., Berry, S.E., Desai, A.B., and Kinsella, T.J. (2003). DNA mismatch repair (MMR) mediates 6-thioguanine genotoxicity by introducing single-strand breaks to signal a G2-M arrest in MMR-proficient RKO cells. Clin. Cancer Res. *9*, 2327–2334.

Ye, X., Ji, Z., Wei, C., McHale, C.M., Ding, S., Thomas, R., Yang, X., and Zhang, L. (2013). Inhaled formaldehyde induces DNA-protein crosslinks and oxidative stress in bone marrow and other distant organs of exposed mice. Environ. Mol. Mutagen. *54*, 705–718.

Yeo, J.E., Wickramaratne, S., Khatwani, S., Wang, Y.-C., Vervacke, J., Distefano, M.D., and Tretyakova, N.Y. (2014). Synthesis of site-specific DNA-protein conjugates and their effects on DNA replication. ACS Chem. Biol. *9*, 1860–1868.

Zaidi, M.R., Davis, S., Noonan, F.P., Graff-Cherry, C., Hawley, T.S., Walker, R.L., Feigenbaum, L., Fuchs, E., Lyakh, L., Young, H.A., et al. (2011). Interferon-γ links ultraviolet radiation to melanomagenesis in mice. Nature *469*, 548–553.

Zastrow, L., Groth, N., Klein, F., Kockott, D., Lademann, J., Renneberg, R., and Ferrero, L. (2009). The missing link--light-induced (280-1,600 nm) free radical formation in human skin. Skin Pharmacol Physiol *22*, 31–44.

Zhang, X., Jeffs, G., Ren, X., O'Donovan, P., Montaner, B., Perrett, C.M., Karran, P., and Xu, Y.-Z. (2007). Novel DNA lesions generated by the interaction between therapeutic thiopurines and UVA light. DNA Repair (Amst.) *6*, 344–354.

Zhao, B., Chignell, C.F., Rammal, M., Smith, F., Hamilton, M.G., Andley, U.P., and Roberts, J.E. (2010). Detection and prevention of ocular phototoxicity of ciprofloxacin and other fluoroquinolone antibiotics. Photochemistry and Photobiology *86*, 798–805.

Zhao, Q., Wang, Q.-E., Ray, A., Wani, G., Han, C., Milum, K., and Wani, A.A. (2009). Modulation of nucleotide excision repair by mammalian SWI/SNF chromatin-remodeling complex. J. Biol. Chem. *284*, 30424–30432.

Zhuang, Z., Johnson, R.E., Haracska, L., Prakash, L., Prakash, S., and Benkovic, S.J. (2008). Regulation of polymerase exchange between Poleta and Poldelta by monoubiquitination of PCNA and the movement of DNA polymerase holoenzyme. Proc. Natl. Acad. Sci. U.S.a. *105*, 5361–5366.